TR-147-2

ANALYSIS OF STRAPDOWN SENSOR TESTING

Phase II Final Report

June 30, 1970

TASC

THE ANALYTIC SCIENCES CORPORATION

6 JACOB WAY/READING, MASSACHUSETTS 01867 (617) 944-6850

TR-147-2

ANALYSIS OF STRAPDOWN SENSOR TESTING

Phase II Final Report

June 30, 1970

Prepared Under:

Contract Number NAS 12-678

for

NATIONAL AERONAUTICS AND SPACE ADMINISTRATION
Electronics Research Center
Cambridge, Massachusetts

Prepared by:

Bard S. Crawford

Approved by:

Arthur A. Sutherland, Jr.
Arthur Gelb

THE ANALYTIC SCIENCES CORPORATION
6 Jacob Way
Reading, Massachusetts 01867

Mr. Edward Spitzer
and
Mr. Maurice Lanman
Technical Monitors
NAS 12-678
Electronics Research Center
575 Technology Square
Cambridge, Massachusetts 02139

FOREWORD

This document describes the results of a study begun in 1968 for the NASA Electronics Research Center. The underlying objective was to help in choosing laboratory test equipment and procedures, especially in the light of the increasing interest in strapdown technology. This report is an expanded version of Reference 10. New material includes analysis of tests performed on pulse rebalanced sensors, a new treatment of input-dependent oscillations in ternary and binary pulse rebalance loops (Appendix F) and some illustrative nomographs relating desired test accuracy to required test equipment performance.

ABSTRACT

Some topics related to dynamic testing of strapdown sensors are analyzed, with emphasis on measuring parameters which give rise to motion-induced error torques in single-degree-of-freedom inertial sensors. The objective is to determine the dynamic inputs, test equipment characteristics and data processing procedures best suited for measuring these parameters. Single-axis, low frequency vibration tests and constant rate tests are studied in detail. Methods for analyzing the effects of test motion errors and measurement errors are developed and illustrated by examples. They are shown to be useful in predicting achievable test accuracies and required test times. Candidate test data processing methods are compared and recommendations concerning test equipment and data processing are made.

TABLE OF CONTENTS

		Page No.
FOREWORD		v
ABSTRACT		vii
List of Tables		xii
List of Figures		xv
1.	INTRODUCTION	1
1.1	Objectives of Study	2
1.2	Organization of the Report	7
2.	ERROR MODELS AND BASIC PARAMETER GROUPS	11
2.1	Single-Degree-of-Freedom Inertial Sensors	11
2.2	Test Objectives	15
2.3	Motion-Induced Error Torques	20
2.3.1	Single-Degree-of-Freedom Gyros: Angular Motion	22
2.3.2	Single-Degree-of-Freedom Gyros: Linear Motion	23
2.3.3	Single-Degree-of-Freedom Accelerometers: Angular Motion	24
2.3.4	Single-Degree-of-Freedom Accelerometers: Linear Motion	25
2.4	Basic Parameter Groups	26
2.4.1	Analog Rebalancing	26
2.4.2	Pulse-Rebalancing	34
2.5	Test Motion Possibilities	36
3.	SINGLE-AXIS, LOW-FREQUENCY TESTING	41
3.1	Observable Quantities	41
3.1.1	Vibration Testing	42
3.1.2	Constant Angular Rate Testing	51
3.1.3	Summary:Angular Motion Test Observables	52

TABLE OF CONTENTS (Continued)

		Page No.
3.2	Single-Axis Test Accuracy	55
3.2.1	Overview and Comparison	55
3.2.2	Bias Test Motion Errors	65
3.2.3	Cyclic Test Motion Errors	70
3.2.4	Errors Due to Quantization	79
3.2.5	Errors Due to Pulse Rebalancing	85
3.2.6	Random High Frequency Errors	100
3.2.7	Rebalance Loop Errors	105
3.2.8	Errors Due to Parameter Changes	113
3.3	Test Duration	115
3.3.1	Choice of Sample Interval	117
3.3.2	Effects of Quantization: Examples	118
3.3.3	Time to Reach Equilibrium	126
3.4	Test Data Processing	129
3.4.1	Fourier Analysis	130
3.4.2	Least Squares Estimation	135
3.4.3	Kalman Filtering	137
3.5	Example Calculations	140
3.5.1	Torque Levels	140
3.5.2	Test Errors	144
4.	IMPLICATIONS FOR TEST LABORATORY EQUIPMENT	163
4.1	Test Motion Machinery	163
4.2	Data Processing Equipment	171
5.	CONCLUSION	175
5.1	Summary of Findings	175
5.2	Recommendations	177

TABLE OF CONTENTS (Continued)

		Page No.
APPENDICES		
Appendix A	Derivation of Trigonometric Series Coefficients: Vibration Testing of Single-Degree-of-Freedom Sensors	181
Appendix B	Test Motion Bias Error Analysis: Angular Vibration Testing of Single-Degree-of-Freedom Gyro	187
Appendix C	Kalman Filtering Formulation	201
Appendix D	Fourier Analysis Equations for Pulse Rebalanced Testing	223
Appendix E	Survey of Strapdown Sensor Test Methods, 1968	233
Appendix F	Analysis of Oscillations in Ternary and and Binary Rebalance Loops	237
REFERENCES		267

LIST OF TABLES

Table No.		Page No.
2.3-1	Gyro Notation	21
2.3-2	Accelerometer Notation	21
2.4-1	Basic Parameter Groups	28
3.1-1	Fourier Coefficients: Gyro Angular Vibration Tests	46
3.1-2	Fourier Coefficients: Accelerometer Angular Vibration Tests	47
3.1-3	Fourier Coefficients: Gyro and Accelerometer Linear Vibration Tests	50
3.1-4	Applied Torque Expressions: Constant Rate Testing	52
3.1-5	Determinable Gyro Parameter Groups: Angular Motion Testing	53
3.2-1	Test Error Influences	56
3.2-2	Error Analysis Summary	60
3.2-3	Summary Comparison of Single-Axis Test Methods	63
3.2-4	Normalized Error Coefficients: Bias Test Motion Errors	69 69
3.2-5	Significant Cyclic Errors	71
3.2-6	Characteristic Frequency and Amplitude and Test Measurement Error in Pulse Rebalance Loops	95
3.2-7	Nonlinearity Effects on Sinusoid	109
3.3-1	Example Errors Due to Quantization: Analog Rebalancing	120
3.3-2	Example Errors Due to Quantization: Pulse Rebalancing	125

LIST OF TABLES (Continued)

Table No.		Page No.
3.5-1	Assumed Gyro Parameter Values	141
3.5-2	Illustrative Torque Levels	142
3.5-3	Assumed Error Source Values	147
3.5-4	Example Error Summary: o Test Axis	148
3.5-5	Example Error Summary: s Test Axis	149
3.5-6	Example Error Summary: i Test Axis	150
3.5-7	Example Error Summary: o/s Test Axis	151
3.5-8	Example Error Summary: i/o Test Axis	152
3.5-9	Example Error Summary: i/s Test Axis	153
3.5-10	Example Errors: Summary Comparison	155
B-1	Specialization to Six Cases of Interest	197

LIST OF FIGURES

Figure No.		Page No.
1.1-1	Test Sequence Flow Diagram	4
1.1-2	Dynamic Testing and Data Processing	5
1.1-3	The Strapdown Sensor Test Problem	6
2.1-1	Single Degree of Freedom Gyro	12
2.1-2	Single Degree of Freedom Pendulous Accelerometer	15
2.1-3	Rebalance Loop Configurations	16
2.2-1	General Test of a Single-Degree-of-Freedom Sensor	17
3.1-1	General Single-Axis Angular Vibration Test	44
3.1-2	Six Candidate Test Orientations	45
3.1-3	Data Processing Phases: Single-Axis Vibration Testing	49
3.2-1	Distorted Test Motion Sinusoids	72
3.2-2	Euler Angles Relating Base Axes to Table Axes	75
3.2-3	Pulse Sequence	80
3.2-4	Distribution of Error Due to Quantization	80
3.2-5	Block Diagram of a Generalized Rebalanced Loop	88
3.2-6	RMS Change in α' with a Fixed Phase Difference	92
3.2-7	Frequency of Oscillation versus Input Level for Ternary and Binary Rebalance Loops	96
3.2-8	Final Accuracy and Test Time: Random Errors	104
3.2-9	Torquer Nonlinearities	107
3.2-10	Linear Sensor Loop with Disturbance Function Added	110

LIST OF FIGURES (Continued)

Figure No.		Page No.
3.3-1	Time-Dependent Test Errors	117
3.3-2	Effective Drift Rate Due to Quantization	122
3.3-3	Estimation Error Variance Time History	127
3.5-1	Variation of Torque Levels with Test Motion Amplitude and Frequency: o and s Test Axes	145
3.5-2	Variation of Torque Levels with Test Motion Amplitude and Frequency: i, o/s, i/o and i/s Test Axes	146
4.1-1	Nomograph for Distortion Effect - Small Signal Cases	166
4.1-2	Nomograph for Quantization Effect - Constant Rate Testing	166
4.1-3	Nomograph for Quantization Effect - Sinusoidal Averaging	167
B-1	Test Axis Misalignment Angles	192
C-1	Numerical Integration Results	216
C-2	Improvement in Small Term Estimate Due to Correlation	217
D-1	Binary Pulse Rebalancing Waveforms	224
F.1-1	Ternary Rebalance Loop	239
F.1-2	Float Angle Time History Segments	239
F.1-3	Example Periodic Time Histories	245
F.1-4	Solution for Normalized Period	252
F.1-5	Normalized Period Versus Normalized Input	256
F.1-6	Normalized Amplitude Versus Normalized Input	261
F.1-7	Summary of Results - Ternary Loop	262
F.2-1	Summary of Results - Binary Loop	265

1. INTRODUCTION

The potential advantages of strapdown or gimballess inertial systems over conventional, gimballed systems have been recognized for some time (Ref. 1). These include flexible packaging, low power consumption, weight and volume, easy assembly and maintenance and convenient use of navigation sensors in autopilot functions. Continuing advances in the development of smaller, faster and more compact digital computers have led to increased interest in strapdown systems. It is clear that these devices will perform acceptably for certain missions and will be, in some cases, superior in overall cost and reliability.

With the advent of strapdown inertial systems, new problems in achieving high sensor accuracies have arisen. Platform systems isolate the inertial sensors from most rotational motion. However, when the instruments are rigidly attached to the vehicle, they can be subjected to a severe angular motion environment, resulting in errors which can be rectified both in the instrument and in the attitude transformation calculation. For example, Ref. 2 shows that the magnitudes of vibration-induced errors can be considerably greater than gyro drift rates which are usually acceptable for navigation applications. Errors of this kind are not observed during static tests. Thus, in order to measure their effects accurately enough to assure adequate compensation during operation, strapdown sensors must be subjected to dynamic testing.

Torque rebalance loops, which are a common feature of strapdown sensors, lead to additional errors, as well as creating problems in testing for motion-induced disturbance torques. While they provide data in a form suitable for digital navigation computers, pulse rebalance loops

in particular introduce essential nonlinearities which complicate the dynamic testing problem.

1.1 OBJECTIVES OF STUDY

The objectives of this study are summarized briefly as follows:

- Determine the input dynamical forcing functions best suited for testing for all significant error coefficients.
- Determine necessary test durations and the nature and accuracies required of the essential test equipment.
- Compare alternative methods of test data processing, considering the possibilities for both on-line and off-line computation.
- Suggest alternative test procedures which may substitute sophisticated test data processing for complex test motion machinery.
- Devise test procedures which will establish an understanding of statistical predictability in the stability of sensor parameters.

Substantial progress has been made regarding the first four objectives in the above list.

The investigation concerns testing for certain parameters which cause errors in single-degree-of-freedom sensors, especially those factors associated with angular motion, and therefore uniquely important for strapdown sensors. These parameters correspond to a set of fixed mechanical properties, such as products of inertia of various elements of an instrument and the alignment of sensor components with respect to

one another. Rebalance loop errors such as fixed scale factor error and torquer nonlinearity are also considered. The study has not been concerned with such items as torquer scale factor changes, friction, thermal gradients and electromagnetic effects, all of which may combine with angular motion to cause errors. Problems associated with rebalance loop dynamics are not treated (except in the treatment of test errors due to pulse rebalancing), but will be the subject of future work related to high frequency testing.

The ultimate goal of this effort is to help formulate complete test sequences, such as that pictured in Fig. 1.1-1. The illustrated sequence begins with a set of physical measurements on the basic sensor components, moves to a set of conventional static and low-rate tests which produce estimates of the quantities normally sought for platform applications, and concludes with a set of dynamic tests designed to extract the parameters uniquely important in strapdown applications. The requirements of a particular test sequence depend of course on the underlying reasons for the test. Are they, for example, related to a research program aimed at developing new sensors, or are they part of a mission-oriented program involving a series of qualification and calibration tests? The development presented herein is general enough to cover both situations.

The report describes an analysis of dynamic testing of single-degree-of-freedom sensors, emphasizing single-axis testing. This type of testing involves the hardware elements pictured in Fig. 1.1-2, connected together as indicated. The sensor outputs and test table outputs feed data into a computer, either directly for real-time processing, or by way of a data storage medium for subsequent processing. Elements of the strapdown sensor test problem are illustrated in Fig. 1.1-3. The main test objectives are to determine the magnitude and stability of

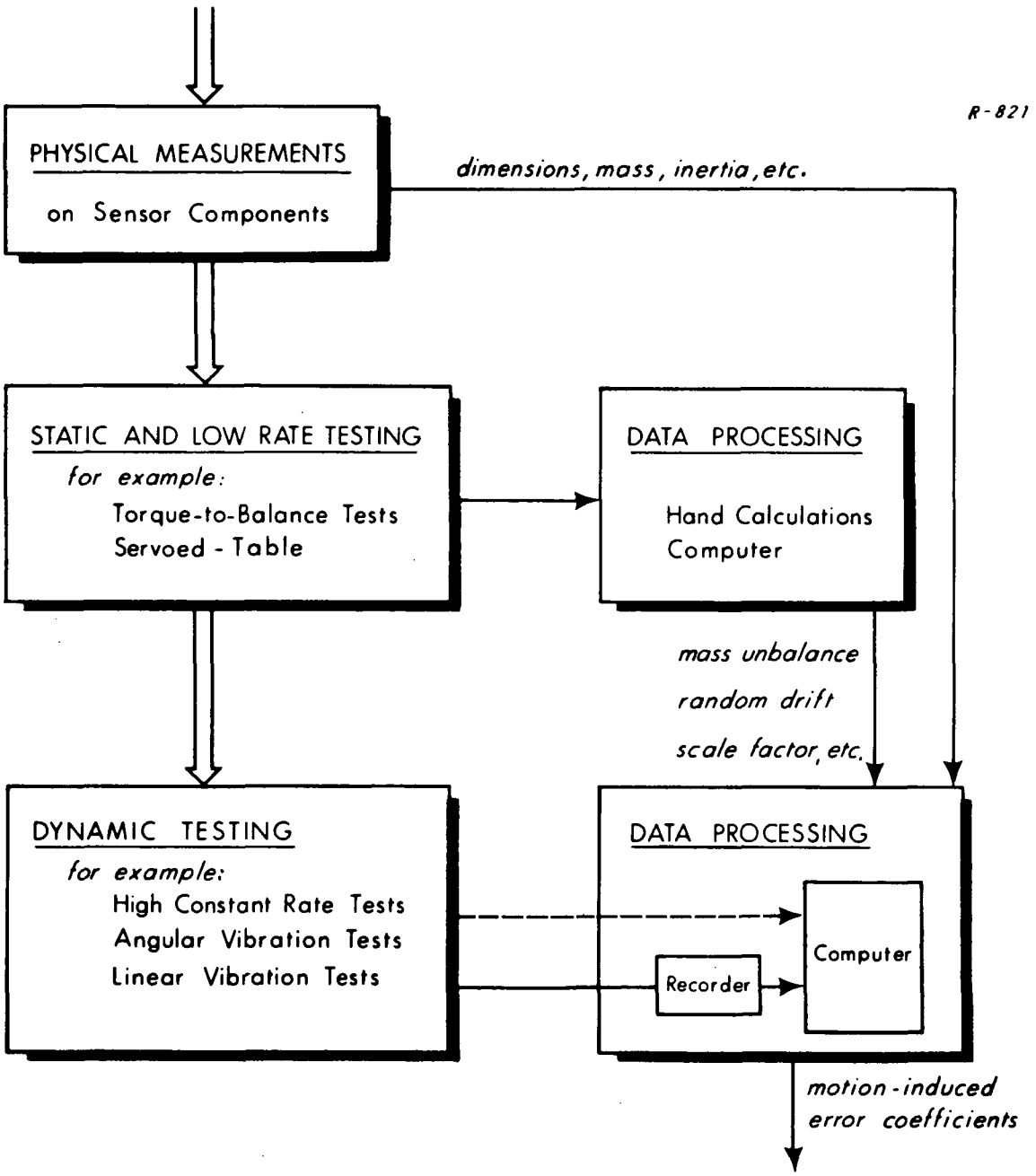

Figure 1.1-1 Test Sequence Flow Diagram

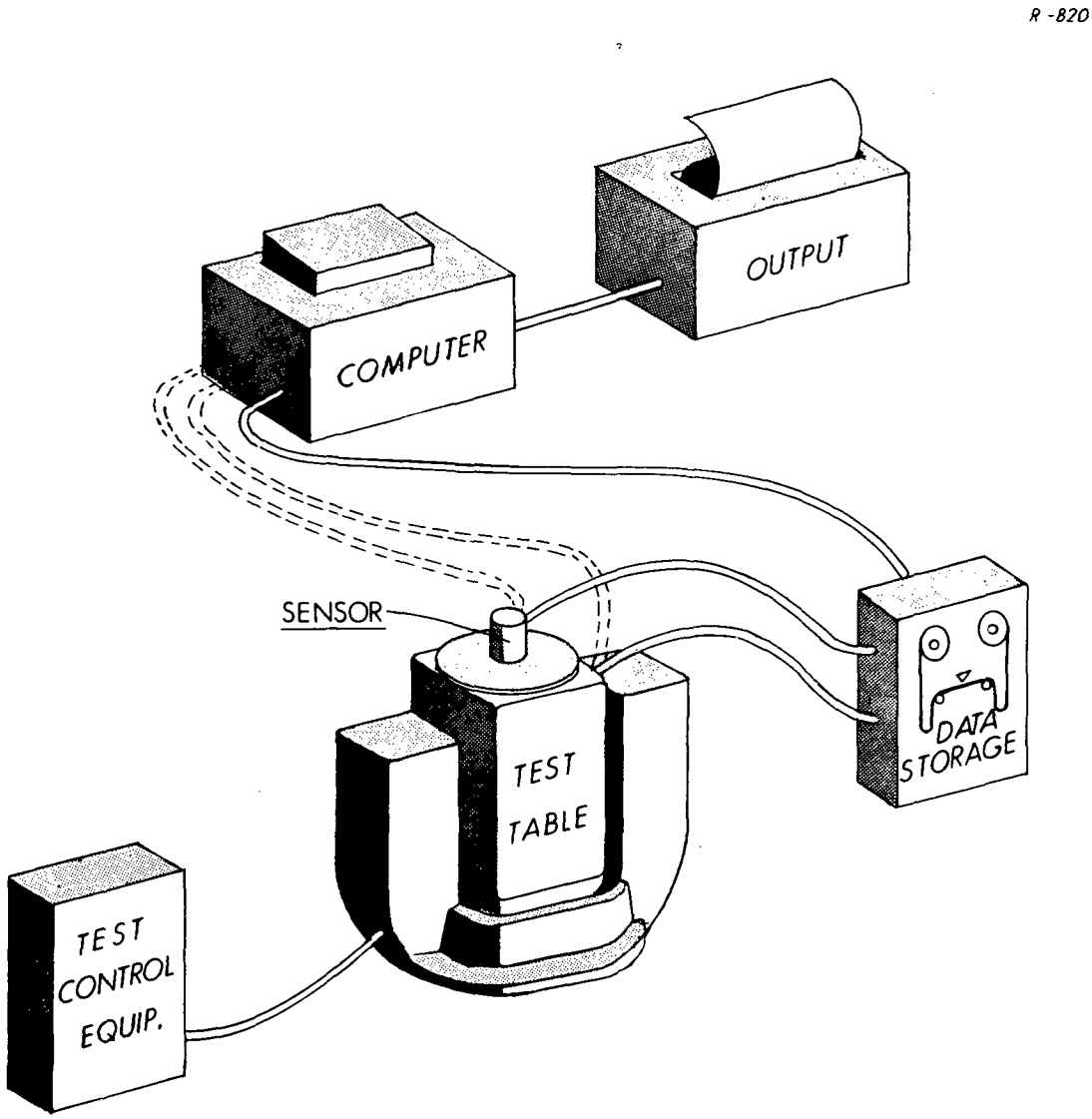

Figure 1.1-2 Dynamic Testing and Data Processing

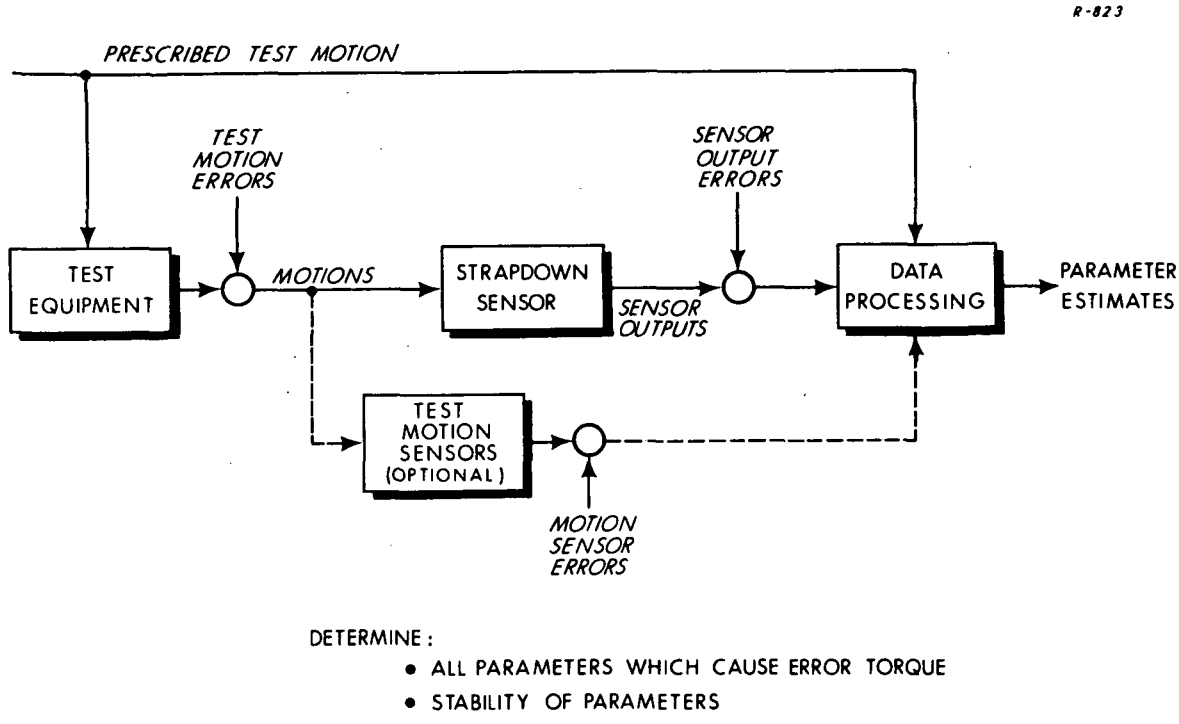

Figure 1.1-3 The Strapdown Sensor Test Problem

parameters which cause error torques. Test errors are associated with imperfections in the motion-supplying equipment, the (optional) sensors which may be used to measure the applied motion and those parts of the strapdown sensor itself which are used as a measuring instrument (such as torque rebalance electronics). The immediate goal of the study is to recommend input motions and data processing procedures and to analyze the effects of test errors on overall test accuracy and duration.

1.2 ORGANIZATION OF THE REPORT

In Chapter 2 the overall test objective is defined as the identification and measurement of the causes of sensor errors. These are grouped into three categories: motion-induced errors (such as those caused by angular motion about the spin and/or output axes of a gyro), residual errors (such as those caused by thermal and friction effects) and rebalance-loop errors. Models for certain important motion-induced errors in single-degree-of-freedom (SDF) gyros and accelerometers are presented, and specialized in a way which is valid for testing SDF sensors in the closed-loop (rebalanced) configuration, using low-frequency test motion inputs. (In this context "low frequency" means considerably less than $1/\tau_f$, where τ_f is the time constant associated with the sensor float dynamics. For typical inertial sensors a low frequency is therefore 20 Hz or less.) This development leads to a two-stage testing concept: A set of basic parameter groups is measured directly from a sequence of applied test motions, and individual parameters are subsequently determined, algebraically, from the values of the basic parameter groups. Chapter 2 concludes with a general discussion of possible test motions and introduces some of the reasoning behind the decision to emphasize single-axis testing.

In Chapter 3 single-axis, low-frequency testing is studied in detail. A particular sequence of sensor orientations with respect to the test motion axis is recommended. The observable quantities from each vibration test are a set of Fourier coefficients which define a periodic function representing the applied torque. A set of six angular vibration tests and a set of six linear vibration tests provide an array of observable quantities which theoretically permit determination of a complete set of basic parameter groups. The observable quantities generated by constant

rate tests and vibration tests, in which only the average torque is measured, are also presented. Three classes of test error sources are considered: test motion errors, measurement errors and changes in the sensor parameters. Motion errors and measurement errors have bias, cyclic and high-frequency noise components. Measurement errors also include the effects of quantization. Methods for analyzing all of these error sources are developed. The first phase of the data processing problem, that of estimating the Fourier coefficients, is formulated as a problem in linear estimation, for which the Kalman filter is an optimal solution. This formulation is useful in studying the combined effect of random high frequency fluctuations in test motion errors and measurement errors and in determining the useful test duration. The analysis of quantization effects also lends insight into the problems of choosing test time and the number of data samples per cycle of test motion. Three candidates for this data processing function -- Fourier analysis, least squares estimation and Kalman filtering -- are compared. Chapter 3 concludes by summarizing the results of example calculations for a sequence of constant rate and vibration tests on a SDF gyro. Illustrative values for the observable quantities as well as test error effects are included.

Tentative conclusions and recommendations concerning the choice of laboratory equipment are summarized in Chapter 4. Some illustrative nomographs relating desired test accuracy to required test equipment performance are included. Overall conclusions and a discussion of the recommended continuation of effort are presented in Chapter 5. A significant recommendation stemming from the study to date is that great stress should be placed on the appropriate use of conventional single-axis test devices, in a combined program of vibration testing and constant rate

testing of strapdown inertial sensors. In order to obtain the maximum usefulness from the test data, careful attention should be given to the means for controlling and/or measuring the supplied motion and to techniques for recording and/or processing the sensor output data produced during the tests. These points are explored in the body of the report.

Appendices A through D and F contain detailed technical material in support of the discussions contained in the main body of the report. Appendix E summarizes a brief survey of contemporary strapdown sensor testing and test equipment.

2. ERROR MODELS AND BASIC PARAMETER GROUPS

This chapter provides a general discussion of single-degree-of-freedom (SDF) sensors and sensor test objectives and develops a set of equations for motion-induced error torques. Based on these relations a set of basic parameter groups is defined. These groups in turn help clarify the problem of selecting appropriate linear and angular motions to be applied during tests. The possibilities for test motions are examined at the end of the chapter.

2.1 SINGLE-DEGREE-OF-FREEDOM INERTIAL SENSORS

Gyroscopes are angular motion sensors. They are commonly based on the use of a spinning member, the rotor, as the sensing element.* All gyroscopes which use a spinning rotor can be classified under two major groups: single-degree-of-freedom gyros and two-degree-of-freedom gyros. The two-degree-of-freedom gyro senses angular motion directly, by measuring the displacement of the rotor spin axis relative to the case. The rotor may be mounted in mechanical gimbals, or may be supported by electric or magnetic fields as in the electrostatically suspended vacuum gyro and cryogenic gyro.

In the case of the single-degree-of-freedom (SDF) gyro the spinning rotor is mounted in a gimbal which allows only one degree-of-freedom relative to the case (see Fig. 2.1-1). The equation of motion of an ideal single-degree-of-freedom gyro can be determined by equating reaction torques about the output axis to the "applied" gyroscopic

*Notable exceptions are the laser gyro and tuning fork gyro.

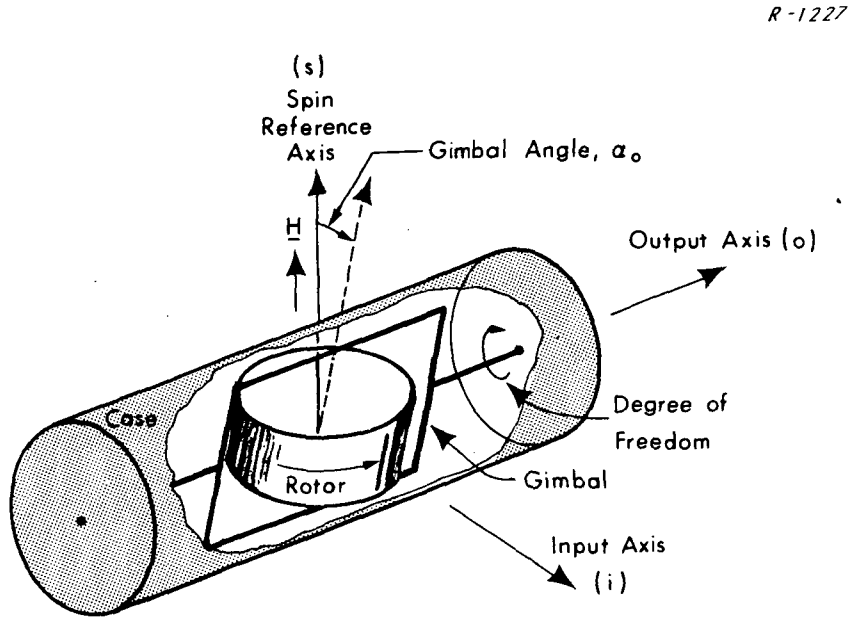

Figure 2.1-1 Single Degree of Freedom Gyro

precession torque which results from case motion about the input axis, viz:

$$I_{oo}\ddot{\alpha}_o + C\dot{\alpha}_o + K\alpha_o = H\omega_i \qquad (2.1\text{-}1)$$

where

α_o = gimbal-to-case-angle about the output axis

I_{oo} = rotor plus gimbal moment of inertia

C = viscous damping coefficient

K = spring constant

H = rotor angular momentum

ω_i = angular rate of the case about input axis

As indicated by Eq. (2.1-1), a constant value of ω_i results in the following steady-state value of α_o:

$$\alpha_o = \frac{H}{K} \omega_i$$

Hence, this gyro is referred to as a rate gyro, as the gimbal angle is a direct measure of case rate. In the situation where K = 0, we get a steady-state gimbal angle rate,

$$\dot{\alpha}_o = \frac{H}{C} \omega_i$$

Thus, gimbal angle is related directly to the integral of the input rate, and this gyro is therefore called a rate integrating gyro. By mounting the gyro rotor in an enclosure which serves as the gimbal and floating the whole assembly in a fluid of appropriate density, the gyro output axis bearings are unloaded, reducing some unwanted torques. This configuration, called the floated rate integrating gyro, is extensively used for very high accuracy applications such as inertial navigation.

In gimballed platform applications, the gyro float angle, α_o, is continuously nulled by platform gimbal servo action. In strapdown system applications, the gyro float angle is nulled by the application of a torque generated by passing an electric current through the windings of an output axis torquer. The current, which may be continuous (analog) or a series of pulses (digital), is derived from a measurement of the float angle. The closed loop comprised of float dynamics, float angle pick-off, torquing electronics and output axis torquer is called the rebalance loop. The rebalance current is taken as a measure of input rate (for continuous

torqued gyros) or incremental input angle (for pulse torqued gyros). Figure 2.1-3 shows a general schematic diagram of a strapdown gyro rebalance loop, including the following three types of torquing electronics: linear analog-rebalancing, binary pulse-rebalancing and ternary pulse-rebalancing.

The single-degree-of-freedom pendulous accelerometer is illustrated in Fig. 2.1-2. Two major differences between this representation of the instrument and that presented for the SDF gyro are obvious. The direction perpendicular to the output and input axes is called the pendulum (p) axis rather than the spin(s) axis. Also, the instrument is assumed to consist of only two basic parts: a case and a combination gimbal and pendulum. The equation of motion of an "ideal" single-degree-of-freedom accelerometer is:

$$I_{oo} \ddot{\alpha}_o + C\dot{\alpha}_o + K\alpha_o = -m\, \delta_p\, f_i \qquad (2.1\text{-}2)$$

where the quantities not previously defined are:

m = gimbal plus pendulum mass

δ_p = displacement of the center of mass

f_i = specific force on the case, along the input axis

Strapdown accelerometers use the same kinds of rebalance torquing schemes as those illustrated above for strapdown gyros. The rebalance current in this case is a measure of input specific force (for continuous torqued accelerometers) or incremental changes in the integral of the input specific force (for pulse torqued accelerometers).

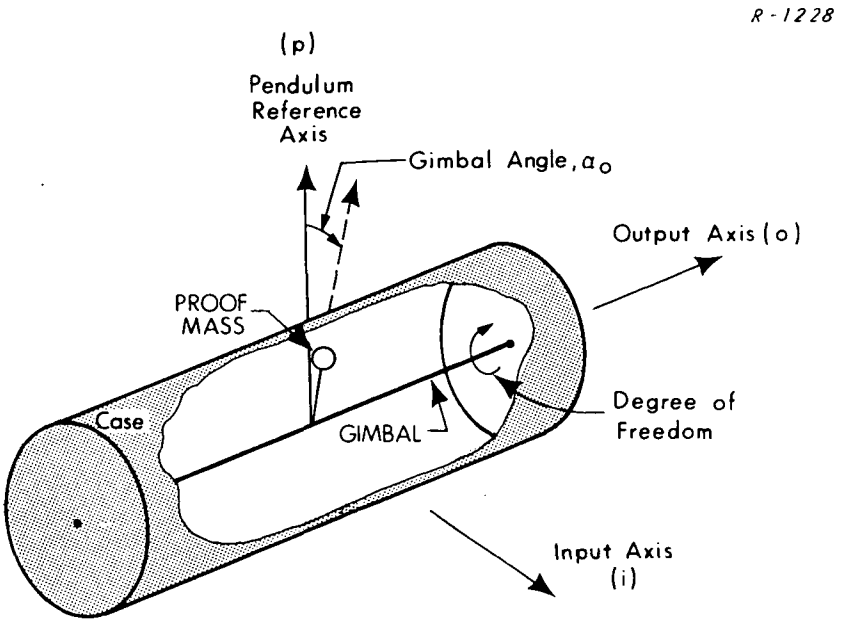

Figure 2.1-2 Single Degree of Freedom Pendulous Accelerometer

2.2 TEST OBJECTIVES

A block diagram representation of a general test of a SDF floated sensor in the torque-rebalancing configuration is shown in Fig. 2.2-1. The diagram illustrates the sensor's nature as a device which sums torques acting on the floated member. The "applied" torque, M_a, consisting of the input (gyroscopic or pendulous) torque and disturbance torque, M_d, is opposed by the torque-generator torque, M_{tg}. The latter is fed back through the rebalance loop, in a manner which tends to null the net torque about the gimbal output axis, M_o.

The controlled test environment includes all quantities (motion, orientation, temperature, etc.) which cause input torques or disturbance torques to be applied. By carefully controlling and/or measuring these

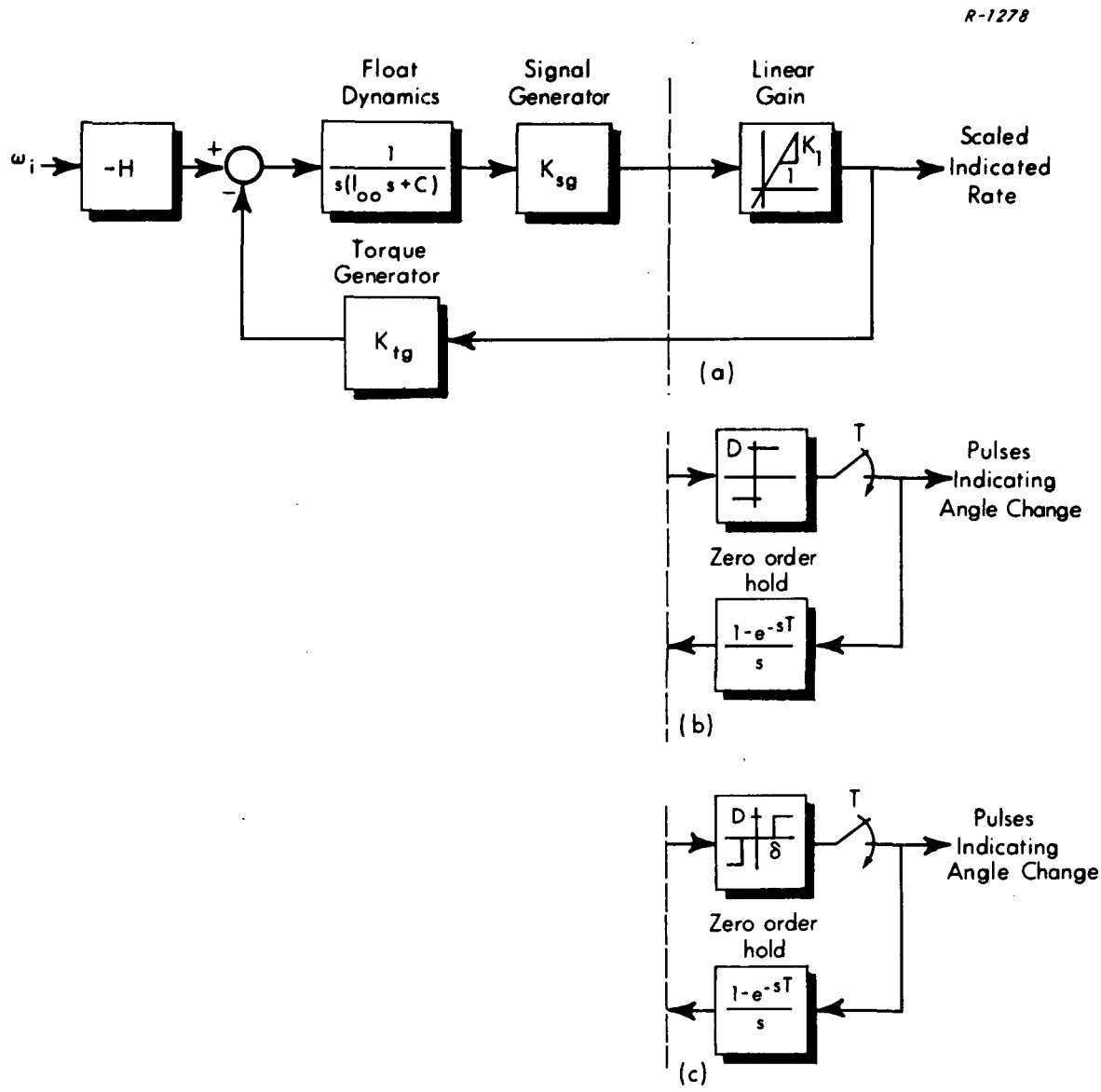

Figure 2.1-3 Rebalance Loop Configurations

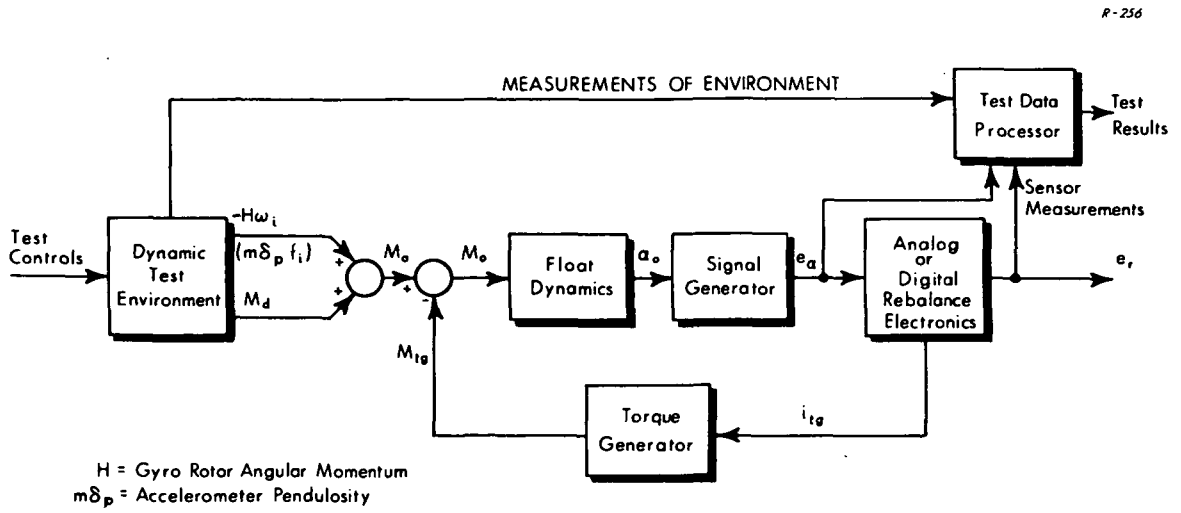

Figure 2.2-1 General Test of a Single-Degree-of-Freedom Sensor

quantities the test operator seeks to isolate and calibrate various sources of disturbance torque. From the gyro itself the only quantities available as inputs to the data processor are the voltages, e_α and e_r. The signal-generator output, e_α, is a voltage which is proportional to the float angle α_o. The output, e_r, of the block labeled "rebalance electronics" is an analog or digital indication of the rebalance torque M_{tg}. In the analog-rebalance case the function of the rebalance electronics is to generate a continuous current, i_{tg}, which is proportional to the voltage, e_α. In this case there is only one available output ($e_\alpha = e_r$) which is a measure of both the float angle time history and the rebalance torque. In the pulse-rebalance case e_r is the sampled output of a nonlinear element; it is used to determine the sign of a fixed-magnitude torque applied to the sensor.

The overall test objective can be defined as the identification and measurement of the causes of sensor errors; that is, all causes for a discrepancy between the output of the sensor and the quantity which that

output is supposed to represent. The output of a strapdown gyro is either a continuous indication of the input-axis angular rate, ω_i, or a digital indication of incremental changes in the integral of ω_i. Similarly, the output of an accelerometer is a continuous or digital indication of the input-axis specific force, f_i, or incremental changes in the integral of f_i.

Sensor error sources may be grouped as follows:

- Motion-Induced Error Torques

  Error torques are the various components of the disturbance torque, M_d, shown in Fig. 2.2-1. Motion-induced error torques are those directly associated with case motions, either angular or linear. They are sometimes referred to as "dynamic errors."

- Residual Error Torques

  Residual error torques are all components of M_d not associated with case motions. For example:

  Torques due to temperature gradients or non-standard temperatures.

  Torques associated with the orientation of the sensor. These could include mass unbalance effects during an angular motion test. (The same parameters lead to motion-induced torques during a linear vibration test).

  Undesired friction torques

  Undesired elastic restraint torques

  Undesired electromagnetic effects

  Torques of unknown origin

  Any of these may of course change with time. However, during the relatively short test durations required for the dynamic tests proposed the above torques are expected to exhibit very little variation.

- Rebalance-Loop Errors

  Two broad types of rebalance-loop errors exist, as follows:

  > The causes of discrepancies between the rebalance torque and the value indicated by the sensor output. Examples are torquer scale-factor error and torquer nonlinearity.
  >
  > Errors associated with sensor loop dynamics which are not fast enough to follow the input motion. In such a case the rebalance torque time history is not a perfect replica of the applied torque time history.

The main emphasis in this report is on testing for motion-induced errors, with some attention paid to torquer errors. Residual errors are not treated, except in the recognition that a "bias" error torque is always present during a test involving applied motions. Errors associated with the dynamics of the rebalance loop are not treated, but will be the subject of future work related to high-frequency testing.

One approach to testing for motion-induced errors is to assume no prior knowledge of the physical causes of such errors and to design a procedure which seeks to discover the functional relationship between M_d and various motions. Another approach is to start with a physically-derived error model which defines such a functional relationship in terms of unspecified parameters, and to design a testing procedure which seeks to determine those parameters. The latter method is followed below. However, if all the effects in the first technique are accounted for by one or more parameters in the second approach, the two are equivalent and the kind of testing described in Chapter 3 has considerable merit in either case. (This point is discussed further in Section 2.4.)

2.3 MOTION-INDUCED ERROR TORQUES

This section presents a set of physically-derived error models for motion-induced error torques in SDF gyros and accelerometers. These error models are taken from equations derived in Refs. 2 and 3. A general expression for the total "applied" output-axis torque is:

$$M_a = M_{bias} + M_{ang} + M_{lin} \qquad (2.3\text{-}1)$$

where

$M_{bias} \triangleq$ a random bias error torque not associated with motion

$M_{ang} \triangleq$ the torque induced by angular motions

$M_{lin} \triangleq$ the torque induced by linear motions

The error models presented below are given as expressions for M_{ang} and M_{lin} for the two types of sensors. The notation used is summarized in Tables 2.3-1 and 2.3-2. For any particular test situation the total applied torque as given in Eq. (2.3-1) must be considered.

TABLE 2.3-1

GYRO NOTATION

f_o, f_i, f_s	=	case linear specific force
$\omega_o, \omega_i, \omega_s$	=	case angular rates
$\dot{\omega}_o, \dot{\omega}_i, \dot{\omega}_s$	=	case angular accelerations
$\alpha_o, \alpha_i, \alpha_s$	=	gimbal-to-case angular misalignments
β_o, β_i	=	rotor-to-gimbal angular misalignments
I_{oo}, I_{ii}, I_{ss}	=	float moments of inertia (including gimbal and rotor components)
$I_{oo_r}, I_{ii_r}, I_{ss_r}$	=	rotor moments of inertia
$I_{os_g}, I_{oi_g}, I_{si_g}$	=	gimbal products of inertia
Ω_s	=	rotor spin rate relative to the gimbal
H	=	$I_{ss_r} \Omega_s$
$\delta_o, \delta_i, \delta_s$	=	float center of mass displacements
m	=	float mass
K_{ii}, K_{ss}	=	direct compliances
$K_{is}, K_{si}, K_{so}, K_{io}$	=	cross compliances

*The subscripts, o, i, s refer to output, input and spin axes, respectively.

TABLE 2.3-2

ACCELEROMETER NOTATION

f_o, f_i, f_p	=	case linear specific force resolved into case-fixed axes
$\omega_o, \omega_i, \omega_p$	=	case angular rates resolved into case-fixed axes
$\alpha_o, \alpha_i, \alpha_p$	=	gimbal-to-case angular misalignments
I_{oo}, I_{ii}, I_{pp}	=	float moments of inertia
I_{oi}, I_{op}, I_{pi}	=	float products of inertia
δ_p, δ_i	=	float center of mass displacements (in the absence of acceleration)
m	=	float mass
K_{ii}, K_{ss}	=	direct compliances
$K_{ip}, K_{pi}, K_{po}, K_{io}$	=	cross compliances

*The subscripts o, i, p refer to output, input and pendulum axes, respectively.

2.3.1 Single-Degree-of-Freedom Gyros: Angular Motion

In Ref. 2 a comprehensive expression is derived for inertial reaction torques associated with angular motion of the case of a SDF gyro. One term, $I_{oo}\ddot{\alpha}_o$, of that expression combines with the float viscous damping torque, $C\dot{\alpha}_o$, to provide the linear "float dynamics" block appearing in Fig. 2.1-3 and 2.2-1. Transferring all other terms to the applied torque side of the equation, we can write:

$$
\begin{aligned}
M_{ang} = -\Big\{ & I_{oo}\dot{\omega}_o + \left(I_{ii} - I_{ss}\right)\omega_s\omega_i - H\omega_i \\
& + I_{os_g}\left[\dot{\omega}_s - \omega_o\omega_i\right] + I_{oi_g}\left[\dot{\omega}_i + \omega_o\omega_s\right] \\
& + I_{si_g}\left[\omega_s^2 - \omega_i^2\right] + Q\left[\omega_o^2\right] \\
& + \alpha_o\left[\left(I_{ss} - I_{ii}\right)\left(\omega_s^2 - \omega_i^2\right) + H\omega_s\right] \\
& + \alpha_s\left[-\left(I_{ss} - I_{ii}\right)\omega_o\omega_s - H\omega_o - I_{oo}\dot{\omega}_i\right] \\
& + \alpha_i\left[\left(I_{ss} - I_{ii}\right)\omega_o\omega_i + I_{oo}\dot{\omega}_s\right] \\
& + \beta_o\left[\left(I_{ss_r} - I_{ii_r}\right)\omega_s^2 - \omega_i^2 + H\omega_s\right] \\
& + \beta_i\left[\left(I_{ss_r} - I_{oo_r}\right)\left(-\dot{\omega}_s + \omega_o\omega_i\right) - I_{ss_r}\dot{\Omega}_s\right]\Big\} \qquad (2.3\text{-}2)
\end{aligned}
$$

where the term, $Q\omega_o^2$, has been added to account for the experimentally-observed effect reported in Ref. 4. We regard the gyroscopic term, $-H\omega_i$, as the desired input torque. Thus, terms other than $-H\omega_i$ on the right hand side of Eq. (2.3-2) must be regarded as error torques. The term $I_{oo}\dot{\omega}_o$ is an error caused by the gimbal output axis inertia and can

lead to significant "pseudo-coning" errors in systems applications. The other term in the first line, $(I_{ii} - I_{ss})\ \omega_s\ \omega_i$, is an anisoinertia error torque which can lead to large rectification errors during angular vibrations. The product-of-inertia terms in the second and third lines are probably less important, but can also generate large constant torques. The terms involving α_o are coupling error torques (since α_o is the float angle which results from all applied torques, principally $H\omega_i$) and can also lead to large errors. The terms involving α_s, α_i, β_o and β_i represent the interaction of various component misalignments with angular motions; the most significant are the $-\alpha_s H\omega_o$ and $\beta_o H\omega_s$ terms which result when the sensitive axis of the gyro does not lie exactly parallel to the input axis fixed in the case.

2.3.2 Single-Degree-of-Freedom Gyros: Linear Motion

Ref. 2 provides an equation for torques about the output axis of an SDF gyro generated by linear motion. Based on it we can write:

$$M_{lin} = -\left\{m\left(\delta_o f_o + \delta_s f_i - \delta_i f_s\right) + m^2\left[K_{so} f_o f_i + K_{si} f_i^2 + \left(K_{ss} - K_{ii}\right) f_i f_s - K_{io} f_o f_s - K_{is} f_s^2\right]\right\} \qquad (2.3\text{-}3)$$

Since the only desired torque is the angular motion term, $H\omega_i$, appearing in Eq. (2.3-2), all of the terms in Eq. (2.3-3) must be considered error torques. The terms multiplying m have the form of mass unbalance torques, although the first one, $m\delta_o f_o$, is thought to be due to thermal convection effects. The terms multiplying m^2 are linear compliance effects.

2.3.3 Single-Degree-of-Freedom Accelerometers: Angular Motion

Ref. 3 provides an equation for torques about the output axis of an SDF accelerometer generated by angular motion. Based on it we can write:

$$
\begin{aligned}
M_{ang} = -\Big\{ & I_{oo}\,\omega_o + \left(I_{ii} - I_{pp}\right)\omega_p\,\omega_i + I_{op}\left(\dot{\omega}_p - \omega_o\,\omega_i\right) \\
& + I_{oi}\left(\dot{\omega}_i + \omega_o\,\omega_p\right) + I_{pi}\left(\omega_p^2 - \omega_i^2\right) \\
& + \alpha_o\left(I_{pp} - I_{ii}\right)\left(\omega_p^2 - \omega_i^2\right) \\
& - \alpha_p\left[\left(I_{pp} - I_{ii}\right)\omega_o\,\omega_p + I_{oo}\,\dot{\omega}_i\right] \\
& + \alpha_i\left[\left(I_{pp} - I_{ii}\right)\omega_o\,\omega_i + I_{oo}\,\dot{\omega}_p\right]\Big\}
\end{aligned}
\qquad (2.3\text{-}4)
$$

Since the ideal accelerometer is insensitive to angular motion, all of the terms in Eq. (2.3-4) must be considered as error torques in the SDF pendulous accelerometer. The error terms can be divided into several broad categories similar to many exhibited by the gyro. Sensitivity to angular accelerations is present. The principal contribution, that caused by angular acceleration about the sensor output axis, is unavoidable because of the nature of the pendulous acceleration sensing instrument. Several anisoinertia terms and product of inertia terms also appear.

2.3.4 Single-Degree-of-Freedom Accelerometers: Linear Motion

Ref. 3 provides an equation for torques about the output axis of an SDF accelerometer generated by linear motion. Based on it we can write:

$$M_{lin} = -\left\{m\delta_p\left(f_i + \alpha_o f_p - \alpha_p f_o\right) - m\delta_i\left(f_p + \alpha_i f_o - \alpha_o f_i\right)\right.$$

$$\left. + m^2\left[K_{pi}f_i^2 + K_{po}f_i f_o + \left(K_{pp} - K_{ii}\right)f_i f_p - K_{io}f_o f_p - K_{ip}f_p^2\right]\right\} \quad (2.3\text{-}5)$$

The first term of Eq. (2.3-5), $m\delta_p f_i$, measures linear acceleration along the input axis. This is the only output axis torque in the ideal pendulous accelerometer. The pendulosity $m\delta_p$ is designed into the instrument with care. All the remaining terms in this equation contribute errors to the accelerometer. The term $m\delta_p\alpha_o f_p$ is basically a cross-coupling error arising from rotation about the single axis of freedom and $m\delta_p\alpha_p f_o$ results from gimbal-to-case misalignment. Since accelerations along the input axis will cause considerable excursions of the gimbal angle, α_o, from null, sizeable rectification errors can be produced in this instrument by properly phased linear vibrations with components along the input and pendulum axes. The second term of Eq. (2.3-5) illustrates error torque contributions from unwanted mass unbalance and the last line expresses compliance error terms. It can be seen that linear compliance effects can produce constant error torques. The error in indicating linear accelerations along the case fixed input axis of an SDF pendulous accelerometer is simply the sum of all error torques, divided by the pendulosity, $m\delta_p$.

2.4 BASIC PARAMETER GROUPS

In this section the error models given above are specialized and extended slightly. This development is based on approximations which are valid for the closed-loop sensor configuration with low-frequency test motion inputs. The motivation for this development is to obtain useful relationships in which the disturbance torque is expressed as a function of motion components and sensor parameters which remain essentially constant over a given period of testing.

The motion-induced error models given above are general in that they apply to both the open-loop and closed-loop configurations, but they do not have the desired functional form because of the presence of time-varying terms α_o, $\ddot{\alpha}_o$, $\dot{\Omega}_s$ and H. The symbol α_o represents float angle which varies in response to all applied torques. The symbol $\dot{\Omega}_s$ represents the rate of change of rotor speed with respect to the gimbal which depends on the rate of change of case angular velocity about the spin axis, ω_s, and the rotor speed control loop dynamics.

When the gyro is torque rebalanced and can be viewed as a closed loop system, we can write approximate expressions for α_o as a function of certain motion quantities. These can then be substituted into the above equations to provide the kind of useful functional relationships mentioned above.

2.4.1 Analog Rebalancing

Consider, first, an analog-rebalanced SDF gyro experiencing angular motion. For the purpose of computing the float angle, the dominant applied torques can be represented by:

$$M_a \cong - I_{oo} \dot{\omega}_o + H\omega_i \qquad (2.4\text{-}1)$$

The rebalance torque is given by

$$M_{tg} = K\alpha_o \tag{2.4-2}$$

We restrict our attention to low frequency test motions, so that M_o is kept very small at all times and M_{tg} remains an accurate replica of M_a. Consequently,

$$M_o = M_a - M_{tg} \cong -I_{oo}\dot{\omega}_o + H\omega_i + K\alpha_o \cong 0 \tag{2.4-3}$$

Therefore,

$$\alpha_o \cong +\frac{H}{K}\,\omega_i - \frac{I_{oo}}{K}\,\dot{\omega}_o \tag{2.4-4}$$

We substitute Eq. (2.4-4) into Eq. (2.3-2) and drop the term $\beta_i I_{ss_r}\dot{\Omega}_s$ which is extremely small in practice. The result, after rearranging terms, is:

$$\begin{aligned} M_{ang} = {} & k_1\dot{\omega}_i + k_2\dot{\omega}_o + k_3\dot{\omega}_s + k_4\omega_i + k_5\omega_o + k_6\omega_s + k_7\omega_i^2 \\ & + k_8\omega_o^2 - k_7\omega_s^2 + k_9\omega_i\omega_o + k_{10}\omega_i\omega_s + k_{11}\omega_o\omega_s \\ & + k_{12}\omega_i^3 - k_{12}\omega_i\omega_s^2 + k_{13}\dot{\omega}_o\omega_s + k_{14}\dot{\omega}_o\omega_i^2 - k_{14}\dot{\omega}_o\omega_s^2 \end{aligned} \tag{2.4-5}$$

where k_1 through k_{14} are defined in Table 2.4-1(a). We shall call these coefficients basic parameter groups. Table 2.4-1 divides them into four types, μ, λ, γ and ρ, according to whether they multiply functions involving angular accelerations or functions which are linear, quadratic or cubic in angular rate, respectively. These classifications are useful in organizing both the analysis and the display of results concerning observable quantities and testing errors (see Chapter 3).

TABLE 2.4-1

BASIC PARAMETER GROUPS

Angular Motion		Type
a) Gyro	b) Accelerometer	
$k_1 = \alpha_s I_{oo} - I_{oi_g}$	$k_1 = \alpha_p I_{oo} - I_{oi}$	
$k_2 = - I_{oo}$	$k_2 = - I_{oo}$	μ
$k_3 = - \alpha_i I_{oo} - I_{os_g}$	$k_3 = - \alpha_i I_{oo} - I_{op}$	
$k_4 = H$		
$k_5 = \alpha_s H$		λ
$k_6 = - \beta_o H$		
$k_7 = I_{si_g} + \beta_o \left(I_{ss_r} - I_{ii_r} \right)$	$k_4 = I_{pi}$	
$k_8 = -Q$		
$k_9 = I_{os_g} - \alpha_i \left(I_{ss} - I_{ii} \right) - \beta_i \left(I_{ss_r} - I_{oo_r} \right)$	$k_5 = I_{op} - \alpha_j \left(I_{pp} - I_{ii} \right)$	γ
$k_{10} = -H^2/K + \left(I_{ss} - I_{ii} \right)$	$k_6 = \left(I_{pp} - I_{ii} \right)$	
$k_{11} = \alpha_s \left(I_{ss} - I_{ii} \right) - I_{oi_g}$	$k_7 = \alpha_p \left(I_{pp} - I_{ii} \right) - I_{oi}$	
$k_{12} = \left(H/K \right) \left(I_{ss} - I_{ii} \right)$		ρ
$k_{13} = I_{oo} H/K$		μ
$k_{14} = - \left(I_{oo}/K \right) \left(I_{ss} - I_{ii} \right)$	$k_8 = - \left(I_{oo}/K \right) \left(I_{pp} - I_{ii} \right)$	
Linear Motion		
c) Gyro	d) Accelerometer	
$k_1 = -m\delta_s$	$k_1 = -m\delta_p$	
$k_2 = -m\delta_o$	$k_2 = \alpha_p m\delta_p + \alpha_i m\delta_i$	λ
$k_3 = m\delta_i$	$k_3 = m\delta_i$	
$k_4 = -m^2 K_{si}$	$k_4 = - \left(m^2/K \right) \delta_p \delta_i - m^2 K_{pi}$	
$k_5 = m^2 K_{is}$	$k_5 = m^2 K_{ip}$	
$k_6 = -m^2 K_{so}$	$k_6 = -m^2 K_{po}$	γ
$k_7 = -m^2 \left(K_{ss} - K_{ii} \right)$	$k_7 = - \left(m^2/K \right) \delta_p^2 - m^2 \left(K_{pp} - K_{ii} \right)$	
$k_8 = m^2 K_{io}$	$k_8 = m^2 K_{io}$	

Except for the fact that H appears in several of them, all of the groups defined in Table 2.4-1 are functions of sensor parameters which remain essentially constant* over a given period of testing. We can write:

$$\begin{aligned} H &= I_{ss_r}\,\Omega_s \\ &= I_{ss_r}\left(\Omega_{s_{nom}} + \Delta\Omega_s\right) \\ &= H_{nom} + I_{ss_r}\,\Delta\Omega_s \end{aligned} \qquad (2.4\text{-}6)$$

where $\Delta\Omega_s$ represents the deviation of rotor speed with respect to the gimbal due to a dynamic lag in the action of the rotor speed control loop. The resulting variations in k_5, k_6, k_{10}, k_{12} and k_{13} will cause extremely small variations in the corresponding torque components appearing in Eq. (2.4-5). These can also be dropped, permitting us to treat most of the basic parameter groups as constants. The exception is the gyroscopic term, $H\omega_i$, which becomes:

$$H\omega_i = H_{nom}\omega_i + I_{ss_r}\,\Delta\Omega_s\omega_i \qquad (2.4\text{-}7)$$

*We have assumed here that float axis misalignments (α_i, α_s and α_p) and rotor axis misalignments (β_i and β_o) are constant. If future results indicate that these quantities significantly vary due to case motions, the only changes in this development which are likely to be significant involve the k_5 and k_6 terms in Eq. (2.4-5) and the k_2 term in Eq. (2.4-15). The affects on k_1, k_3, k_7, k_9 and k_{11} in Table 2.4-1(a) and on k_1, k_3, k_5 and k_7 in Table 2.4-1(b) will be very small if the misalignments are of the order of arc seconds.

The second term in Eq. (2.4-7) is zero except when the applied test motion involves both ω_i and a rapidly varying ω_s. Therefore, most of the time the parameter groups defined in Table 2.4-1(a) can be considered constants with $H = H_{nom}$. For example, with a vibratory angular motion about the spin axes, if the frequency of vibration is low compared to the wheel hunt frequency (typically a few cycles per second), $\Delta\Omega_s \cong 0$ and $H\omega_i = H_{nom}\omega_i$. If, on the other hand, the frequency of oscillation is considerably above the wheel hunt frequency, the rotor speed variation will become:

$$\Delta\Omega_s \cong -\omega_s \tag{2.4-8}$$

That is, ω_s is varying so rapidly that the speed control loop cannot follow it at all (see the more extensive discussion in Ref. 2). Consequently,

$$H\omega_i \cong H_{nom}\omega_i - I_{ss_r}\omega_i\omega_s \tag{2.4-9}$$

and the "extra" term can be added to the $k_{10}\omega_i\omega_s$ term in Eq. (2.4-5). In summary, all of the parameter groups defined in Table 2.4-1(a) can be considered independent of test motion frequency except k_{10}, which varies from:

$$k_{10} = \left(\frac{H_{nom}^2}{K}\right) + \left(I_{ss} - I_{ii}\right) \tag{2.4-10}$$

for angular oscillations about the spin axis which are well below the wheel hunt frequency, to:

$$k_{10} = \left(\frac{H_{nom}^2}{K}\right) + \left(I_{ss} - I_{ss_r} - I_{ii}\right) \qquad (2.4\text{-}11)$$

for oscillations well above the wheel hunt frequency.

The expression of the applied torque in the form of Eq. (2.4-5) leads to a testing concept in which the data processing portion of the test procedure is divided into two parts. In the first part the gyro output data from a sequence of tests is processed so as to determine values of the basic parameter groups. The second part is a purely algebraic problem in which the basic parameter groups are provided and the individual parameters appearing in the expressions in Table 2.4-1 are to be extracted.

The first phase is crucial because it bears on the choice of test motions and determines test accuracy and useful test duration. Note, for example, that some basic parameter groups appearing in Eq. (2.4-5) cannot possibly be found by applying a constant rotation rate since they multiply angular acceleration terms ($\dot{\omega}_i$, $\dot{\omega}_o$, $\dot{\omega}_s$). This indicates that if all parameter groups are to be determined, the testing program must include some motions more complex than constant rates.

In the second phase some of the parameters can be found algebraically and some cannot, but there is no way in which unusual test motions can be used to separate the effects of individual parameters which

appear in a given group. For example, consider the single term from Eq. (2.4-5) involving the product, $\omega_o\omega_s$.

$$k_{11}\omega_o\omega_s = -I_{oi_g}\omega_o\omega_s + \alpha_s\left(I_{ss} - I_{ii}\right)\omega_o\omega_s \qquad (2.4\text{-}12)$$

No matter what time history of ω_o and ω_s is applied to the gyro case, the term involving I_{oi_g} and the term involving α_s will both remain proportional to the product, $\omega_o\omega_s$, and their separate effects cannot be distinguished. However, if values for both k_1 and k_{11} (see Table 2.4-1(a)) have been determined, and if I_{oo} and $(I_{ss} - I_{ii})$ are considered known, then values for I_{oi_g} and α_s can be determined algebraically.

It should be noted that we could have started with an expression like that of Eq. (2.4-5), without assuming any knowledge of the physical causes of error torques, and simply set out to design a testing procedure which would determine values of the coefficients of the various motion functions. This corresponds to the first approach mentioned in Section 2.2.

For an SDF accelerometer basic parameter groups defined in Table 2.4-1(b) correspond to the following expression for torque due to an angular motion:

$$M_{ang} = k_1\dot{\omega}_i + k_2\dot{\omega}_o + k_3\dot{\omega}_p + k_4\omega_i^2 - k_4\omega_p^2$$
$$+ k_5\omega_i\omega_o + k_6\omega_i\omega_p + k_7\omega_o\omega_p + k_8\dot{\omega}_o\omega_i^2 - k_8\dot{\omega}_o\omega_p^2 \qquad (2.4\text{-}13)$$

where we have made use of the approximation:

$$\alpha_o \cong - \frac{I_{oo}}{K} \dot{\omega}_o \qquad (2.4\text{-}14)$$

which is analogous to Eq. (2.4-4) in the SDF gyro case. For the SDF gyro undergoing linear motion:

$$M_{lin} = k_1 f_i + k_2 f_o + k_3 f_s + k_4 f_i^2 + k_5 f_s^2 + k_6 f_i f_o + k_7 f_i f_s + k_8 f_o f_s \qquad (2.4\text{-}15)$$

where the corresponding basic parameter groups are defined in Table 2.4-1(c). For the SDF accelerometer undergoing linear motion:

$$M_{lin} = k_1 f_i + k_2 f_i + k_3 f_p + k_4 f_i^2 + k_5 f_p^2 + k_6 f_i f_o + k_7 f_i f_p + k_8 f_o f_p \qquad (2.4\text{-}16)$$

where we have used:

$$\alpha_o \cong -m \frac{\delta_p}{K} f_i \qquad (2.4\text{-}17)$$

and the corresponding basic parameter groups are defined in Table 2.4-1(d).

2.4.2 Pulse-Rebalancing

The basic parameter groups defined in Table 2.4-1 may be valid for some pulse-rebalanced sensors as well, even though Eq. (2.4-2) is no longer true. In some cases the float angle, α_o, experiences a high-frequency limit cycle* superimposed on a slowly changing "signal" value which follows quite closely the applied test motion. According to dual-input, describing-function theory (Ref. 5) the nonlinear torquing logic operates on these low frequency signals, which occur in the presence of the limit cycle, almost as though it were a linear gain. Therefore, we can write:

$$M_a = -\overline{M}_{tg} = -K_{sg} N_B K_{tg} \overline{\alpha}_o \qquad (2.4\text{-}18)$$

where:

K_{sg} = the signal generator gain

K_{tg} = the torque generator gain

N_B = the effective gain of the nonlinearity as seen by the "signal".

and the overbars indicate time-averages taken over intervals which are long compared to the limit cycle period but short compared to

*This is usually true in the binary-torquing case and for gyros with time-modulated torquing; it is usually not true in the ternary-torquing case. See Ref. 2.

test motion variations. It follows that, for the SDF gyro experiencing angular motion:

$$\bar{\alpha}_o = + \frac{H}{K_p} \omega_i - \frac{I_{oo}}{K_p} \dot{\omega}_o \qquad (2.4\text{-}19)$$

where K_p is the effective pulse-rebalance loop gain:

$$K_p = K_{sg} N_B K_{tg} \qquad (2.4\text{-}20)$$

For the SDF accelerometer experiencing only angular motion:

$$\bar{\alpha}_o = - \frac{I_{oo}}{K_p} \dot{\omega}_o \qquad (2.4\text{-}21)$$

For the SDF accelerometer undergoing linear motion alone:

$$\bar{\alpha}_o = - \frac{m\delta_p}{K_p} f_i \qquad (2.4\text{-}22)$$

Equations (2.4-19), (2.4-21) and (2.4-22) can be substituted into Eqs. (2.3-3), (2.3-4) and (2.3-5). When this is done we obtain the same error torque equations and basic parameter groups as in Section 2.4.1. These equations ignore certain high frequency, zero-average cross-coupling torques associated with float angle motion caused by the limit cycle.

2.5 TEST MOTION POSSIBILITIES

In order to determine values for all basic parameter groups appearing in Eqs. (2.4-5), (2.4-13), (2.4-15) and (2.4-16) it is necessary to choose a sequence of test motions which excite the various terms in these equations in such a way that their individual effects can be separated and measured. An important consideration in this choice is the desirability of keeping the test motion equipment as simple and accurately controllable as possible. For the angular motion-induced terms of Eqs. (2.4-5) and (2.4-13) it is necessary to specify a set of time histories of angular velocity components (ω_i, ω_o, ω_s). These cannot be confined to constant-rate tests alone since there are a number of terms involving angular accelerations ($\dot{\omega}_i$, $\dot{\omega}_o$, $\dot{\omega}_s$) which must be excited. For the linear motion-induced torques of Eqs. (2.3-15) and (2.3-16) it is necessary to specify a sequence of specific force (f_i, f_o, f_s) time histories.

Consider the following list of possible motion functions which are discussed, in turn, below:

- Step functions (constant angular rates and constant specific force components)
- Ramp functions (constant angular accelerations)
- Sinusoidal oscillations (angular and linear vibrations)
  - (a) motion about or along a single case-fixed axis
  - (b) oscillations about two axes with arbitrary phase
  - (c) oscillations about three axes with arbitrary phases
- Combinations and special functions

Note that two- and three-axis in-phase oscillations are actually single-axis oscillations where the axis is chosen to produce a specified ratio between principal axis components. (For example, angular oscillation

about a line midway between the input and spin axes of a gyro with rate W sin ωt, produces the principal axis in-phase oscillations, $\omega_i = \omega_s = (W/\sqrt{2}) \sin \omega t$.

Constant angular rates may be applied to inertial sensors by conventional laboratory test tables. Special mounting fixtures are required for various "combined-rate" tests. For example, if equal input-axis and spin-axis rates (ω_i and ω_s) are desired simultaneously, the gyro must be mounted with the line midway between these two axes coincident with the test table axis. Constant specific force components may be obtained simply by placing the sensor in a given orientation in the earth's gravitational field. Alternatively, it may be centrifuge tested at a higher g-level. (This produces a combination of constant angular rate about the centrifuge axis and a constant specific force, somewhat complicating matters.) These tests are all useful and are commonly performed in testing inertial sensors. Their major limitation is that, in testing for angular-motion-induced errors, they cannot excite all of the terms appearing in the error model equations. It is clear, therefore, that some test motions from the last three items in the above list should be included in a complete testing program.

Angular-rate ramp functions, involving constant angular accelerations, could be used to excite the terms which are not excited in constant rate testing. Supplying such motions would require the operation of standard test tables in an unconventional way, and it would be difficult to maintain a significant acceleration level for a long period of time because of the high rates which would be reached. There would also be serious data processing problems because of the continuously increasing torque levels associated with various parameter groups. For example, a constant angular acceleration about a gyro output axis would cause a

constant torque, $k_2\dot{\omega}_0$ [See Eq. (2.4-5).], and a linearly increasing torque, $k_5\omega_0$, and a parabolically increasing torque, $k_8\omega_0^2$.

Angular and linear single-axis sinusoidal oscillations are standard test motions which may be obtained using conventional techniques. Since first and higher derivatives automatically occur as sinusoids, all terms in the error models can be excited by a sequence of sinusoidal oscillations about various axes. As with ramp functions the torque levels during sinusoidal motion are continuously changing. However, they are cyclically repeating, affording the opportunity to average data over many cycles. The data processing procedures required to separate and measure the effects of various parameter groups during such testing are developed in some detail in Chapter 3. (They represent a considerable increase over those usually employed in test procedures which seek only to measure average effects.) It is demonstrated that a particular sequence of six single-axis vibration tests, each using a different test motion axis fixed in case coordinates can theoretically be used to isolate and measure all terms which appear in the error models we have adopted. (Some effects, such as torques associated with k_{12} and k_{14}, are extremely small and probably cannot be measured in practice in low frequency testing. But if they are too small to be measured, they are also likely to produce insignificant errors in operational systems. On the other hand these effects should be reviewed in later considerations of high frequency testing.)

Because a program of single-axis testing which includes constant angular rates and oscillatory motion has the capability mentioned above, multi-axis out-of-phase testing and angular rate histories which are combinations and special functions of time have not been studied in detail. Multi-axis test tables capable of supplying out-of-phase angular motions

are available and these should, of course, be used to check against predictions based on single-axis testing. However, a major conclusion of this study is that for strapdown inertial sensors considerable emphasis should be given to single-axis low-frequency testing.

The ultimate simplicity and usefulness of single-axis low-frequency testing will depend on the extent to which:

- all motion-affected error torques, including those not covered in the error models presented here, are frequency independent.
- It is valid to treat pulse rebalancing electronics as linear components in the fashion outlined in Section 2.4.2.
- it is possible to predict the significant system errors from the results of single-axis low-frequency tests.

A combination of experimental evidence and further analysis is needed in order to properly guage these matters.

Chapter Summary — Error equations for single-degree-of-freedom (SDF) gyros and accelerometers are developed for the special case of closed-loop low-frequency testing. The resulting expressions for torques applied to the instrument output axes are linear in a set of "basic parameter groups" defined herein. The expressions for angular-motion-induced error torques include fourteen such parameter groups for SDF gyros and eight groups for SDF accelerometers. The expressions for linear-motion-induced error torques include eight groups for both SDF gyros and accelerometers. The parameter groups are further divided into four categories, according to whether they generate error torques proportional to angular acceleration or linear, quadratic or cubic,

respectively, in angular rate or specific force. These classifications are useful in organizing both the analysis and the display of results developed in the following chapter.

Potential test motions are reviewed and qualitatively compared in light of the applied torque expressions mentioned above. A major conclusion is that theoretically the effects of all parameter groups can be observed separately using test motions which involve angular accelerations; it is not necessary to resort to multi-axis, out-of-phase test motions.

3. SINGLE-AXIS, LOW-FREQUENCY TESTING

This chapter presents a detailed study of single-axis, low-frequency testing, including sinusoidal vibration testing and constant angular rate testing. A particular set of sensor orientations with respect to the motion axis are recommended and the information which may be extracted from each test is outlined for angular and linear vibration tests as well as constant rate tests. Test accuracy, useful test duration and test data processing are investigated, with emphasis on the angular motion case. Example calculations are given at the end of the chapter.

3.1 OBSERVABLE QUANTITIES

This section identifies the quantities which may be observed as a result of single axis tests and the basic parameter groups which may be determined from the quantities observed during particular types of test sequences and combinations thereof. The following types of tests are considered:

- Constant Rate Testing
- Sinusoidal Testing, Averaging
- Sinusoidal Testing, Harmonic Extraction

The last two involve the same test motions, but are distinguished by the data processing performed. In sinusoidal averaging the only measurement is of the average torque over many cycles, yielding information about constant

torque only, part of which is due to rectification of dynamic effects. In sinusoidal harmonic testing the time-varying output signal is processed to yield additional information. Results are summarized in Section 3.1.3.

3.1.1 Vibration Testing

A general single-axis angular vibration of amplitude W and frequency ω can be represented by the following three equations:

$$\omega_i = c_i W \sin \omega t \tag{3.1-1}$$

$$\omega_o = c_o W \sin \omega t \tag{3.1-2}$$

$$\omega_s = c_s W \sin \omega t \tag{3.1-3}$$

where c_i, c_o and c_s are the direction cosines relating the vibration axis to the input, output and spin axes of the gyro being tested. It is shown in Appendix A that when Eqs. (3.1-1), (3.1-2) and (3.1-3) are substituted into Eq. (2.3-5), the resulting expression for applied torque is a periodic function represented by a 7-term trigonometric series of the form:

$$\begin{aligned} M_{ang} = {} & B + S_1 \sin \omega t + C_1 \cos \omega t \\ & + S_2 \sin 2\omega t + C_2 \cos 2\omega t \\ & + S_3 \sin 3\omega t + C_3 \cos 3\omega t \end{aligned} \tag{3.1-4}$$

When three similar equations representing accelerometer case motion (involving ω_p and c_p rather than ω_s and c_s) are substituted into Eq. (2.3-5), a similar periodic function of the form of Eq. (3.1-4) is found. This result is also developed in Appendix A. In both cases, expressions for the coefficients, B, S_1, C_1, etc., in terms of the basic parameter groups and the quantities defining the test motion have been derived.

Figure 3.1-1 illustrates the general situation for a single-axis angular vibration test. The first block represents the motion-induced torque model developed in Section 2.4; its output, M_{ang}, can be viewed as a 7-term periodic function of the form of Eq. (3.1-4). Added to this is a constant torque, M_c, which exists in the absence of the applied angular vibration. It consists of the terms, M_{bias} and M_{lin}, defined in Eq. (2.3-1) and a small additional torque due to the angular rotation rate of the earth. Since the only applied test motion is an angular oscillation, the linear-motion-induced torque is determined by the sensor's orientation in the earth's gravitational field. This torque can be held constant by orienting the vibration axis or "test axis" in the vertical direction. The complete applied torque, M_a, is, therefore, also represented by a 7-term function of the form of Eq. (3.1-4) in which the bias coefficient, B, includes the constant, M_c, as well as the average (rectification) torque resulting from the applied sinusoidal angular motion. Since the test motion frequency has been assumed to be low compared to gyro loop dynamics, the torque generator output is represented by the same 7-term function. The gyro output e_r is a scalar function which is proportional (ideally) to the torque M_{tg}. Therefore, a harmonic analysis of the output data should produce the seven Fourier coefficients which define the input periodic function $M_a(t)$. For any given choice of sensor orientation with respect to the test axis there is a set of seven such coefficients which are the observable quantities

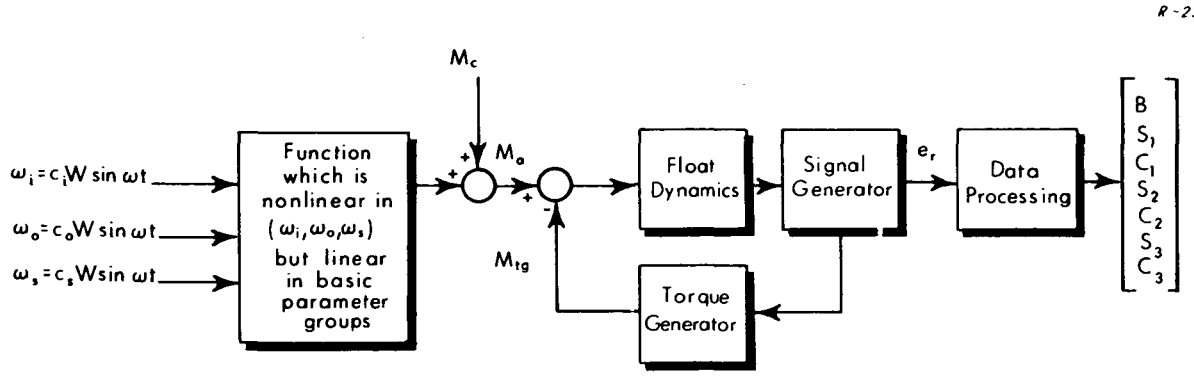

$$M_{tg} \cong M_a = B + S_1 \sin \omega t + C_1 \cos \omega t + S_2 \sin 2\omega t + C_2 \cos 2\omega t + S_3 \sin 3\omega t + C_3 \cos 3\omega t$$

Figure 3.1-1 General Single-Axis Angular Vibration Test

for that particular test. Estimation of these seven quantities requires a more sophisticated data processing procedure than the conventional one of measuring average drift rate over a long period of time (which is simply the measurement of B, the first of the seven coefficients).

Consider now the six test orientations pictured in Fig. 3.1-2. In three cases the sensor is mounted with one of its principal axes coincident with the test motion axis. In the other three cases the sensor is mounted with a line midway between two of its principal axes coincident with the test axis. These pictures apply to a SDF gyro or SDF accelerometer, depending on whether the third principal axis is labeled s or p. Tables 3.1-1 and 3.1-2 present expressions for the seven trigonometric coefficients which correspond to each of these six test axis choices for both instruments. Each Fourier bias coefficient, B, includes a constant torque term, M_c, which represents the disturbance torque which exists in the absence of the test motion. It is a function of orientation, temperature, etc.

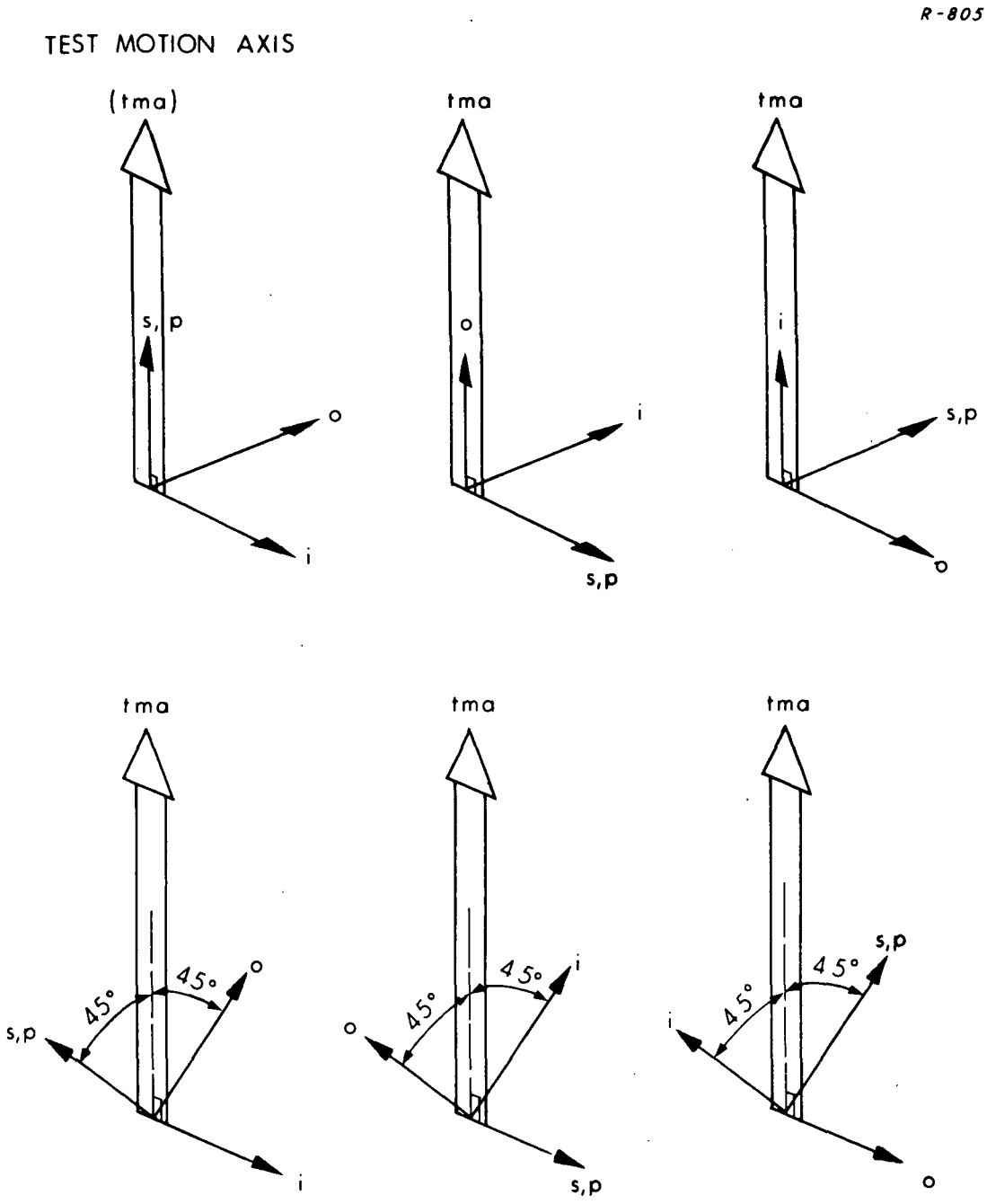

Figure 3.1-2 Six Candidate Test Orientations

TABLE 3.1-1

FOURIER COEFFICIENTS: GYRO ANGULAR VIBRATION TESTS

Test Motion	B $\left(M_c + \frac{\gamma}{2} W^2\right)$	S_1 $\left(\lambda W + \frac{3}{4}\rho W^3\right)$	C_1 $\left(\mu_{C_1}\omega W + \mu_{C_3}\omega W^3\right)$	S_2 $\left(\mu_{S_2}\omega W^2\right)$	C_2 $\left(-\frac{\gamma}{2} W^2\right)$	S_3 $\left(-\frac{1}{4}\rho W^3\right)$	C_3 $\left(\mu_{C_3}\omega W^3\right)$
$\omega_o = W \sin \omega t$	$M_{c_o} + \frac{1}{2}k_8 W^2$	$k_5 W$	$k_2 \omega W$	0	$-\frac{1}{2}k_8 W^2$	0	0
$\omega_s = W \sin \omega t$	$M_{c_s} - \frac{1}{2}k_7 W^2$	$k_6 W$	$k_3 \omega W$	0	$\frac{1}{2}k_7 W^2$	0	0
$\omega_i = W \sin \omega t$	$M_{c_i} + \frac{1}{2}k_7 W^2$	$k_4 W + \frac{3}{4}k_{12} W^3$	$k_1 \omega W$	0	$-\frac{1}{2}k_7 W^2$	$-\frac{1}{4}k_{12} W^3$	0
$\omega_o = \omega_s = \frac{W}{\sqrt{2}} \sin \omega t$	$M_{c_{os}} + \frac{1}{4}\left(-k_7 + k_8 + k_{11}\right) W^2$	$\frac{1}{\sqrt{2}}\left(k_5 + k_6\right) W$	$\frac{1}{\sqrt{2}}\left(k_2 + k_3\right)\omega W - \frac{1}{8\sqrt{2}}k_{14}\omega W^3$	$\frac{1}{4}k_{13}\omega W^2$	$-\frac{1}{4}\left(-k_7 + k_8 + k_{11}\right) W^2$	0	$\frac{1}{8\sqrt{2}}k_{14}\omega W^3$
$\omega_i = \omega_o = \frac{W}{\sqrt{2}} \sin \omega t$	$M_{c_{io}} + \frac{1}{4}\left(k_7 + k_8 + k_9\right) W^2$	$\frac{1}{\sqrt{2}}\left(k_4 + k_5\right) W + \frac{3}{8\sqrt{2}}k_{12} W^3$	$\frac{1}{\sqrt{2}}\left(k_1 + k_2\right)\omega W + \frac{1}{8\sqrt{2}}k_{14}\omega W^3$	0	$-\frac{1}{4}\left(k_7 + k_8 + k_9\right) W^2$	$-\frac{1}{8\sqrt{2}}k_{12} W^3$	$-\frac{1}{8\sqrt{2}}k_{14}\omega W^3$
$\omega_i = \omega_s = \frac{W}{\sqrt{2}} \sin \omega t$	$M_{c_{is}} + \frac{1}{4}k_{10} W^2$	$\frac{1}{\sqrt{2}}\left(k_4 + k_6\right) W$	$\frac{1}{\sqrt{2}}\left(k_1 + k_3\right)\omega W$	0	$-\frac{1}{4}k_{10} W^2$	0	0

Otherwise, all of the coefficients are functions of the test motion quantities and the basic parameter groups only. The bias term, B, is the "dc" level of the output waveform and represents the conventional, average torque measurement. The other coefficients are generated by a harmonic analysis of the "ac" portion. These expressions were obtained by

TABLE 3.1-2

FOURIER COEFFICIENTS: ACCELEROMETER ANGULAR VIBRATION TESTS

Test Motion	B $\left(M_c + \frac{\gamma}{2} W^2\right)$	C_1 $\left(\mu_{C_1} \omega W + \mu_{c_3} \omega W^3\right)$	C_2 $\left(-\frac{\gamma}{2} W^2\right)$	C_3 $\left(\mu_{C_1} \omega W^3\right)$
$\omega_o = W \sin \omega t$	M_{c_o}	$k_2 \omega W$	0	0
$\omega_p = W \sin \omega t$	$M_{c_p} - \frac{1}{2} k_4 W^2$	$k_3 \omega W$	$\frac{1}{2} k_4 W^2$	0
$\omega_i = W \sin \omega t$	$M_{c_i} + \frac{1}{2} k_4 W^2$	$k_1 \omega W$	$-\frac{1}{2} k_4 W^2$	0
$\omega_o = \omega_p = \frac{W}{\sqrt{2}} \sin \omega t$	$M_{c_{op}} - \frac{1}{4}(k_4 - k_7) W^2$	$\frac{1}{\sqrt{2}}(k_2 + k_3) \omega W - \frac{1}{8\sqrt{2}} k_8 \omega W^3$	$\frac{1}{4}(k_4 - k_7) W^2$	$\frac{1}{8\sqrt{2}} k_8 \omega W^3$
$\omega_i = \omega_o = \frac{W}{\sqrt{2}} \sin \omega t$	$M_{c_{io}} - \frac{1}{4}(k_4 - k_5) W^2$	$\frac{1}{\sqrt{2}}(k_1 + k_2) \omega W + \frac{1}{8\sqrt{2}} k_8 \omega W^3$	$\frac{1}{4}(k_4 - k_5) W^2$	$-\frac{1}{8\sqrt{2}} k_8 \omega W^3$
$\omega_i = \omega_p = \frac{W}{\sqrt{2}} \sin \omega t$	$M_{c_{ip}} + \frac{1}{4} k_6 W^2$	$\frac{1}{\sqrt{2}}(k_1 + k_3) \omega W$	$-\frac{1}{4} k_6 W^2$	0

specializing the general expressions derived in Appendix A. For example, for a test motion axis midway between the input and output axes we have:

$$c_i = 1/\sqrt{2}$$

$$c_o = 1/\sqrt{2}$$

$$c_s = 0 \qquad (3.1\text{-}5)$$

Therefore, in the case of the gyro, the expression for the coefficient of the sin $3\omega t$ term [Eq. (A-5(f)] becomes

$$S_3 = -\frac{1}{4} k_{12} W^3 \left(c_i^3 - c_i c_s^2\right)$$

$$= -\frac{\sqrt{2}}{8} k_{12} W^3 \qquad (3.1\text{-}6)$$

The output data from a sequence of six tests on a given instrument can be processed to yield an array of 42 observable quantities. If the six test axes are those pictured in Fig. 3.1-2, the 42 quantities correspond to the expressions given in Table 3.1-1. Examination of this array of expressions shows that, for a given test amplitude and frequency, knowledge of these 42 quantities is more than enough to determine all of the basic parameter groups, k_1 through k_{14}. All six tests are required, but the complete set of 42 observables provides a considerable amount of redundant information. The testing concept outlined in Section 2.4 can now be made more definite as shown in Fig. 3.1-3. The gyro data may be processed (stage Ia) on-line to produce the seven observable quantities (Fourier coefficients) during each test or it may be recorded for subsequent off-line processing. In either case, the next data processing stage, Ib, is an off-line stage in which 42 linear algebraic equations are to be solved for 20 unknowns; 14 basic parameter groups and 6 constant torques, M_c. Approaches to the solution of this over-specified problem are discussed briefly in Section 3.4. The final data processing stage, II, is the purely algebraic problem of solving for individual parameters, given values for the basic parameter groups.

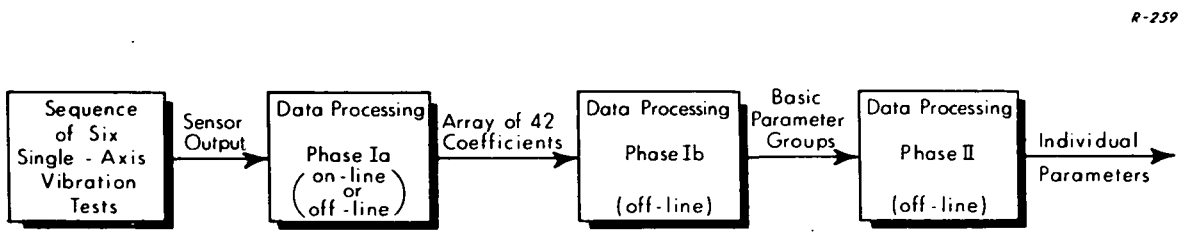

Figure 3.1-3 Data Processing Phases: Single-Axis Vibration Testing

Table 3.1-3 presents expressions for the observable quantities (Fourier coefficients) which correspond to linear vibration tests in which the vibration axis has the same relationship to the sensor axes as in the six angular vibration tests described above.* For these linear vibration tests the test axis is chosen to be horizontal so that the specific force along the test axis has a sinusoidal form with zero average. The constant torque, M_c, includes the usual bias term, M_{bias}, a small term, M_{ang}, associated with the constant earth rate and a term associated with the constant gravitational field. The number of observable quantities for each test is three, corresponding to three-term trigonometric functions which are derived in Appendix A for single-axis linear vibration tests. In both cases (gyro and accelerometer) the set of 18 observable quantities is more than enough to determine all basic parameter groups.

Inspection of the expressions tabulated in Tables 3.1-1 through 3.1-3 reveals that, for both SDF gyros and SDF accelerometers, complete sets of basic parameter groups may theoretically be extracted from a sequence of six angular and six linear vibration tests. The angular

*In the case of the gyro it will be extremely difficult in practice to measure the mass unbalance terms (k_1, k_2, k_3) because of the small angular motions which must inevitably be present. Extraction of these coefficients is performed quite satisfactorily during simple tumble tests.

TABLE 3.1-3

FOURIER COEFFICIENTS: GYRO AND ACCELEROMETER LINEAR VIBRATION TESTS

Test Motion	B $\left(M_c + \frac{\gamma}{2} A^2\right)$	S_1 (λA)	C_2 $\left(-\frac{\gamma}{2} A^2\right)$
$a_o = A \sin \omega t$	M_{c_o}	$k_2 A$	0
$a_{s,p} = A \sin \omega t$	$M_{c_s} + \frac{1}{2} k_5 A^2$	$k_3 A$	$-\frac{1}{2} k_5 A^2$
$a_i = A \sin \omega t$	$M_{c_i} + \frac{1}{2} k_4 A^2$	$k_1 A$	$-\frac{1}{2} k_4 A^2$
$a_o = a_{s,p} = \frac{A}{\sqrt{2}} \sin \omega t$	$M_{c_{os}} + \frac{1}{4}(k_5 + k_8) A^2$	$\frac{1}{\sqrt{2}}(k_2 + k_3) A$	$-\frac{1}{4}(k_5 + k_8) A^2$
$a_i = a_o = \frac{A}{\sqrt{2}} \sin \omega t$	$M_{c_{is}} + \frac{1}{4}(k_4 + k_6) A^2$	$\frac{1}{\sqrt{2}}(k_1 + k_2) A$	$-\frac{1}{4}(k_4 + k_6) A^2$
$a_i = a_s = \frac{A}{\sqrt{2}} \sin \omega t$	$M_{c_{is}} + \frac{1}{4}(k_4 + k_5 + k_7) A^2$	$\frac{1}{\sqrt{2}}(k_1 + k_3) A$	$-\frac{1}{4}(k_4 + k_5 + k_7) A^2$

vibration tests should be conducted with the vibration axis (about which the sensor is rotated) in the vertical direction. The linear vibration tests should be conducted with the vibration axis (along which the sensor is accelerated) in the horizontal plane.

3.1.2 Constant Angular Rate Testing

When a constant angular rate is applied about any axis fixed in the sensor, the resulting applied torque is a constant. A general constant rate of amplitude W can be represented by the equations:

$$\omega_i = c_i W \tag{3.1-7}$$

$$\omega_o = c_o W \tag{3.1-8}$$

$$\omega_{s,p} = c_{s,p} W \tag{3.1-9}$$

For any values of the direction cosines the resulting expression for the applied torque (see Eqs. (2.4-5), (2.4-13) and (2.3-1)) takes the general form:

$$M_a = M_c + \lambda W + \gamma W^2 + \rho W^3 \tag{3.1-10}$$

Table 3.1-4 expresses the coefficients, λ, γ, and ρ, in terms of basic parameter groups for the six test motion axes shown in Fig. 3.1-2. In each case the M_c term represents the constant torque which exists in the absence of an applied angular rate (i.e., when W = 0). For each test axis it is necessary to measure torque for three non-zero values of W in order to separate λ, γ and ρ terms.

Inspection of the left hand (gyro) side of Table 3.1-4 shows that estimates of the λ terms lead directly to estimates of the parameter groups, k_4, k_5 and k_6, and estimates of the γ terms lead to the groups, k_7,k_8,k_9,k_{10} and k_{11}. For accelerometers the λ terms do not appear while the γ terms lead to estimates of the groups, k_4,k_5,k_6 and k_7. (These groups are defined in Table 2.4-1.)

TABLE 3.1-4

APPLIED TORQUE EXPRESSIONS: CONSTANT RATE TESTING

Test Motion	$M_a = M_c + \lambda W + \gamma W^2 + \rho W^3$	
	Gyro	Accelerometer
$\omega_o = W$	$M_{c_o} + k_5 W + k_8 W^2$	M_{c_o}
$\omega_{s,p} = W$	$M_{c_s} + k_6 W - k_7 W^2$	$M_{c_p} - k_4 W^2$
$\omega_i = W$	$M_{c_i} + k_4 W + k_7 W^2 + k_{12} W^3$	$M_{c_i} + k_4 W^2$
$\omega_o = \omega_{s,p} = W/\sqrt{2}$	$M_{c_{os}} + \left[\frac{k_5 + k_6}{\sqrt{2}}\right] W + \left[\frac{-k_7 + k_8 + k_{11}}{2}\right] W^2$	$M_{c_{op}} \left[\frac{-k_4 + k_7}{2}\right] W^2$
$\omega_i = \omega_o = W/\sqrt{2}$	$M_{c_{io}} + \left[\frac{k_4 + k_5}{\sqrt{2}}\right] W + \left[\frac{k_7 + k_8 + k_9}{2}\right] W^2 + \left[\frac{k_{12}}{2\sqrt{2}}\right] W^3$	$M_{c_{io}} + \left[\frac{k_4 + k_5}{2}\right] W^2$
$\omega_i = \omega_{s,p} = W/\sqrt{2}$	$M_{c_{is}} + \left[\frac{k_4 + k_6}{\sqrt{2}}\right] W + \left[\frac{k_{10}}{2}\right] W^2$	$M_{c_{ip}} + \frac{k_6}{2} W^2$

3.1.3 Summary: Angular Motion Test Observables

Table 3.1-5 identifies the gyro parameter groups which may be determined as a result of each type of testing considered. A sequence of constant rate tests is capable of determining all groups except the so-called "μ terms" (k_1, k_2, k_3, k_{13} and k_{14}), which are associated with angular acceleration. A sequence of sinusoidal averaging tests is useful only in determining the "γ terms" (k_7, k_8, k_9, k_{10} and k_{11}). A sequence of sinusoidal harmonic tests is capable of determining the full set of parameter groups, as previously discussed. Thus, a combination of constant rate

TABLE 3.1-5

DETERMINABLE GYRO PARAMETER GROUPS:
ANGULAR MOTION TESTING

	Constant Rate Testing $M_a - M_c = \lambda W + \gamma W^2 + \rho W^3$	Sinusoidal Testing, Averaging $B = M_c + \frac{1}{2}\gamma W^2$	Sinusoidal Testing, Harmonic Extraction $S_1 = \lambda W$ $C_1 = \mu\omega W$ $S_2 = \frac{1}{4}\mu\omega W^2$ $C_2 = -\frac{1}{2}\gamma W^3$ $S_3^* = \frac{1}{4}\rho W^3$ $C_3^* = \frac{1}{4}\mu\omega W^3$
μ terms $k_1, k_2, k_3, k_{13}, k_{14}^*$	No	No	Yes
λ terms k_4, k_5, k_6	Yes	No	Yes
γ terms $k_7, k_8, k_9, k_{10}, k_{11}$	Yes	Yes	Yes
ρ terms k_{12}^*	Yes	No	Yes
Number of runs required	12, (15)	6	6

*Very small: probably unobservable in practice.

tests and sinusoidal averaging tests yields no more groups than those found in constant rate tests alone, but does provide independent measures of the γ, or rectification, terms. Similarly, a combination of sinusoidal harmonic testing with the other types yields no more groups than those found in harmonic testing alone, but does offer the advantage of independent measurements of λ, γ and ρ terms and, therefore, additional cross-checking opportunities. The relative accuracies of the different testing methods are compared in Section 3.2.1.

As illustrated in the numerical examples of Section 3.5, the parameter groups k_{12} and k_{14} are expected to be extremely small. It is, therefore, likely that the cubic terms (ρterms) in constant rate testing and the third harmonic (S_3 and C_3) in sinusoidal testing can be ignored in practice. It is also worth noting that both k_1 and k_{11} are approximately equal to I_{oi_g} and that both k_3 and k_9 are approximately equal to I_{os_g}. Consequently, there may be fewer significant quantities that cannot be measured during constant rate testing than is suggested by Table 3.1-5.

Table 3.1-5 also shows the number of test runs required in each sequence. The constant rate tests will probably require two non-zero rates for each of the six test axes shown in Table 3.1-2 in order to separate the λ and γ terms, making a total of 12 runs. Theoretically, a third rate is required for the three test axes where a cubic (ρ) term appears, making a total of 15 required runs. In practice the cubic terms will probably be ignored. The number of runs listed in Table 3.1-5 under constant rate testing is 24, rather than 12, because each set may be repeated with the sensor re-mounted after a rotation of 180 degrees about the test axis. This would be done in order to correct for a misalignment of the table axis.

Sinusoidal testing entails only one run for each of the six test axes, making a total of six required runs. In practice, for sinusoidal harmonic testing each test will probably be repeated with the sensor re-mounted, as described above. Therefore, the number of required runs is stated as 12. The number 6 is maintained for sinusoidal averaging since table axis misalignment does not cause a constant error torque.

Under the assumptions of our error models (all parameter groups independent of test motion, etc.) no new information is gained by running a sinusoidal test at varying frequencies or amplitudes. In

practice, of course, it would be desirable to vary these test motion quantities in order to check the consistency of the results and to see if and where the error model breaks down.

3.2 SINGLE-AXIS TEST ACCURACY

Procedures which involve sequences of single-axis tests were outlined in the previous section. The objective of these test sequences is to obtain measurements of a set of basic parameter groups which cause motion-induced error torques. The measurements cannot be perfect for a number of reasons. The sources of test errors are analyzed in this section and relationships between error sources and test accuracy are developed.

3.2.1 Overview and Comparison

Test error categories are listed in Table 3.2-1 and discussed briefly below. More detailed discussions are given in following sections. It should be noted that "measurement errors" are associated with the torque rebalance path of the gyro itself, which is used to determine the nature of the applied torque time history. "Motion errors" are associated with imperfections in the motion supplying devices.

Table 3.2-1 indicates which tests are significantly affected by various types of test error. A zero entry in the table implies that the source in question is expected to contribute negligibly small errors to

TABLE 3.2-1

TEST ERROR INFLUENCES

Test Error Categories	Constant Rate Testing	Sinusoidal Averaging	Sinusoidal Harmonic Testing
Test Motion Errors			
Magnitude			
1. Bias	0	γ	μ, λ, γ
2. Waveform Distortion	NA*	0	μ, γ
3. High-Frequency Noise	0	γ	μ, λ, γ
Misalignment			
4. Bias-Fixed	λ	0	λ
5. Run-to-Run Shift	λ, γ	NA	NA
6. Table Wobble	λ, γ	0	μ
Measurement Errors			
7. Quantization	λ, γ	γ	μ, λ, γ
8. Torquer Scale Factor Error	λ, γ	γ	μ, λ, γ
9. Torquer Nonlinearity	λ, γ	γ	μ, λ, γ
10. High-Frequency Noise	λ, γ	γ	μ, λ, γ
Parameter Changes			
11. Run-to-Run Shifts	λ, γ	NA	NA

*NA = Not Applicable.

estimates of the parameters in question. An "NA" entry stands for "not applicable." For example, distortion of the applied test motion waveform is not a problem for constant rate tests. A Greek letter or letters appearing at a particular location in the table indicates which types of coefficients will suffer significant estimation errors due to the error source in question. The following paragraphs provide brief discussions of various test error source categories and references to detailed treatments in succeeding sections.

Test motion bias errors are constant errors in the knowledge of the applied test motion amplitude or of the orientation of the test axis. Test motion bias errors change the values of the observable quantities being measured. Since calculation of sensor parameters is based on assumed test motions which are different, they are in some error. These effects are discussed in detail in Section 3.2.2 and Appendix B. The error in the knowledge of test motion amplitude, in constant rate testing, is expected to be negligibly small because table rate is determined from a measurement of the total time required for an integral number of test table revolutions; this can be done very accurately. The effect of a fixed test axis misalignment error on the μ and γ terms during sinusoidal testing is negligible, as shown in Section 3.2.2. A shift in the misalignment error between two constant rate tests, for a given test axis orientation, affects both the λ and γ estimates, as shown in Section 3.2.2.

Cyclically repeating test motion errors, such as table wobble or distortion of the applied sinusoidal motion, give rise to harmonics in the applied torque time history. In constant rate testing the table-wobble effects may rectify and change the average torque measurement. These errors are discussed in Section 3.2.3. Other examples of cyclic test motion errors are linear vibrations occurring during angular vibration

tests (due to an off-center test axis) and angular vibrations occurring during linear vibration tests (due to unwanted "rocking" motion). The former might be significant when subjecting an accelerometer to angular vibration testing; the latter will be very significant when subjecting a gyro to linear vibration testing.

Errors due to quantization can arise in testing analog-rebalanced sensors as well as pulse-rebalanced sensors. In the first case this will happen whenever the continuously varying torquer input signal is converted into digital form for data processing. As with a pulse-rebalanced sensor, the test data becomes a sequence of integers (pulse counts) which represent the integral of torque over particular time intervals. One count represents the basic quantization interval or data resolution level in units of torque-times-time (e.g. dyne cm sec). All parameter estimates are affected by this quantization. This problem is discussed in detail in Sections 3.2.4 and 3.2.5.

Random high-frequency fluctuations in the applied test motion can be viewed as "process noise" affecting the entire test procedure. This together with similar fluctuations in measurement errors or "measurement noise" places a limit on the achievable parameter estimation accuracies. In some cases the quantization process is effectively a contributor to measurement noise. Besides that contribution there is the difference between the actual physical torque generated (or its integral over an interval) and its indicated value. All Fourier coefficient estimates are affected by these errors. They are discussed in Section 3.2.6 and Appendix C. In the case of constant rate testing, while the applied rate may fluctuate about its average value, the average will be known with negligible error, as discussed above. The first order effect on the estimated parameters will also be negligible since the integrated effect of positive deviations will exactly counteract the integrated effect of negative deviations.

Cyclically repeating measurement errors are the result of fixed rebalance loop errors such as torquer nonlinearity or torquer scale-factor error. The "odd-nonlinearities" affect constant rate testing and the measurement of the μ terms in sinusoidal harmonic testing. The "even nonlinearities" affect sinusoidal averaging and the measurement of the λ and γ terms in sinusoidal harmonic testing. These effects are discussed in Section 3.2.7.

The shift in sensor parameter values between two constant rate tests with a given test axis orientation affects both the λ and γ estimates, in much the same way as a shifted misalignment error affects them. These effects are discussed in Section 3.2.8.

Table 3.2-2 repeats the format of Table 3.2-1, but supplies more detail in the form of error formulas. These formulas express the errors in estimating the μ, λ and γ terms as functions of the error sources, the test motion quantities, the sensor parameters and the test time. For a given test motion axis λ and γ are defined as the coefficients of the W and W^2 terms, respectively, in the appropriate row of Table 3.1-4. Similarly, μ is defined as the coefficient of the appropriate ωW or ωW^2 term in the C_1 or S_2 column of Table 3.1-1. (In some cases alternate expressions, for $\delta\mu_{(C_1)}$ and $\delta\mu_{(S_2)}$, are required.) Some errors are functions of the parameters (μ, λ, γ) themselves; for example, those due to test motion magnitude error (δW) and torquer scale factor error (ϵ_{SC}). Most of the errors are functions of the test motion quantities (W_1 and W_2 for constant rate tests, W and ω for sinusoidal tests). Some errors are functions of the direction cosines (c_i and c_o) relating the test axis to the sensor axes; for example, those due to distortion (Δ), table wobble (ϵ_W) and torquer nonlinearity (ϵ_{NL}).

TABLE 3.2-2

ERROR ANALYSIS SUMMARY

Error Source	Constant Rate Tests $(W_1 >> W_2)$ $M_a - M_c = \lambda W + \gamma W^2$	Sinusoidal Averaging $B = M_c + \frac{1}{2}\gamma W^2$	Sinusoidal Harmonics $C_1 = \mu\omega W,\ S_1 = \lambda W,\ C_2 = -\frac{1}{2}\gamma W^2$ $S_2 = \mu\omega W^2$
1. Magnitude Bias δW	negligible δW	— $\delta\gamma = 2\frac{\gamma}{W}\delta W$	$\delta\mu_{(C_1)} = \frac{\mu}{W}\delta W;\quad \delta\mu_{(S_2)} = 2\frac{\mu}{W}\delta W$ $\delta\lambda = \frac{\lambda}{W}\delta W$ $\delta\gamma = 2\frac{\gamma}{W}\delta W$
2. Distortion Δ	not applicable	— — $\delta\gamma = 0$	$\delta\mu = 0$ $\delta\lambda = 0$ $\delta\gamma = \frac{2}{W} c_i H\Delta;\quad \delta\gamma = \frac{2}{W} c_o I_{oo}\omega\Delta$
3. Magnitude Noise (combined effect with measurement noise, σ_v) σ_W	negligible effect	— — $\sigma_\gamma = \frac{2}{W^2}\sqrt{2\sigma_v\sigma_W\gamma W\sqrt{2\tau_v\tau_u}}$	$\sigma_{\mu_{(C_1)}} = \frac{1}{\omega W}\sqrt{2\sigma_v\sigma_W\omega\mu\sqrt{2\tau_v\tau_u}};\quad \sigma_{\mu_{(S_2)}} = \frac{1}{\omega W^2}\sqrt{2\sigma_v\sigma_W 2\mu\omega W\sqrt{2\tau_v\tau_u}}$ $\sigma_\lambda = \frac{1}{W}\sqrt{2\sigma_v\sigma_W\lambda\sqrt{2\tau_v\tau_u}}$ $\sigma_\gamma = \frac{2}{W^2}\sqrt{2\sigma_v\sigma_W W\gamma\sqrt{2\tau_v\tau_u}}$
4. Misalignment Bias ϵ	$\delta\lambda = \sqrt{1-c_i^2}\,H\epsilon$ $\delta\gamma = 0$	— — $\delta\gamma = 0$	$\delta\mu = 0$ $\delta\lambda = \sqrt{1-c_i^2}\,H\epsilon$ $\delta\gamma = 0$
5. Misalignment Run-to-Run shift ϵ_{SH}	$\delta\lambda = \sqrt{1-c_i^2}\,H\epsilon_{SH}$ $\delta\gamma = -\frac{1}{W_1}\sqrt{1-c_i^2}\,H\epsilon_{SH}$	not applicable	not applicable
6. Table Wobble ϵ_W	$\delta\lambda = \sqrt{1-c_i^2}\,H\epsilon_W$ $\delta\gamma = -\frac{1}{W_1}\sqrt{1-c_i^2}\,H\epsilon_W$	zero average effect	$\delta\mu_{(C_1)} = 0;\quad \delta\mu_{(S_2)} = \frac{2}{W}H\epsilon_W$ $\delta\lambda = 0$ $\delta\gamma = 0$
7. Quantization q	— $\sigma_\lambda = \frac{1}{W_2}\frac{q}{\sqrt{6}}\frac{1}{T}$ $\sigma_\gamma = \frac{1}{W_1 W_2}\frac{q}{\sqrt{6}}\frac{1}{T}$	— — $\sigma_\gamma = \frac{2}{W^2}\frac{q}{\sqrt{6}}\frac{1}{T}$	$\sigma_{\mu_{(C_1)}} = \frac{1}{\omega W}\frac{q}{\sqrt{6}}\omega\sqrt{\frac{2h}{T}};\quad \sigma_{\mu_{(S_2)}} = \frac{1}{\omega W^2}\frac{2}{\sqrt{6}}\omega\sqrt{\frac{2h}{T}}$ $\sigma_\lambda = \frac{1}{W}\frac{q}{\sqrt{6}}\omega\sqrt{\frac{2h}{T}}$ $\sigma_\gamma = \frac{2}{W^2}\frac{q}{\sqrt{6}}\omega\sqrt{\frac{2h}{T}}$
8. Torquer Scale Factor Error ϵ_{SC}	— $\delta\lambda = \lambda\epsilon_{SC}$ $\delta\gamma = \gamma\epsilon_{SC}$	— — $\delta\gamma = \gamma\epsilon_{SC}$	$\delta\mu = \mu\epsilon_{SC}$ $\delta\lambda = \lambda\epsilon_{SC}$ $\delta\gamma = \gamma\epsilon_{SC}$
9. Torquer Nonlinearity $\epsilon_1, \epsilon_2, \epsilon_3$	— $\delta\lambda = \frac{W}{W_1^2}\left(\epsilon_2 M_1^2 + \epsilon_3 M_1^3\right)$ $\delta\gamma = \frac{1}{W_1^2}\left(\epsilon_2 M_1^2 + \epsilon_3 M_1^3\right)$ $M_1 \triangleq \lambda W_1 + \gamma W_1^2$	— — $\delta\gamma = 4\frac{(Hc_i + I_{oo}\omega c_o)}{\pi}\epsilon_1$	$\delta\mu_{(C_1)} = \frac{8}{3}\frac{(I_{oo}\omega c_o)^2}{\pi}W\epsilon_2 + \frac{3}{4}(I_{oo}\omega c_o)^3 W^2\epsilon_3$ $\delta\lambda = \frac{8}{3}\frac{(Hc_i)^2}{\pi}W\epsilon_2 + \frac{3}{4}(Hc_i)^3 W^2\epsilon_3$ $\delta\gamma = \frac{8}{3}\left(\frac{Hc_i - I_{oo}\omega c_o}{\pi W}\right)\epsilon_1$
10. Measurement Noise σ_v	— $\sigma_\lambda = \frac{1}{W_2}\sigma_v\sqrt{2\tau_v}\omega\sqrt{\frac{2h}{T}}$ $\sigma_\gamma = \frac{1}{W_1 W_2}\sigma_v\sqrt{2\tau_v}\omega\sqrt{\frac{2h}{T}}$	— — $\sigma_\gamma = \frac{2}{W^2}\sigma_v\sqrt{2\tau_v}\omega\sqrt{\frac{2h}{T}}$	$\sigma_{\mu_{(C_1)}} = \frac{1}{\omega W}\sigma_v\sqrt{2\tau_v}\omega\sqrt{\frac{2h}{T}};\quad \sigma_{\mu_{(S_2)}} = \frac{1}{\omega W^2}\sigma_v\sqrt{2\tau_v}\omega\sqrt{\frac{2h}{T}}$ $\sigma_\lambda = \frac{1}{W}\sigma_v\sqrt{2\tau_v}\omega\sqrt{\frac{2h}{T}}$ $\sigma_\gamma = \frac{2}{W^2}\sigma_v\sqrt{2\tau_v}\omega\sqrt{\frac{2h}{T}}$
11. Parameter Shifts, Run-to-Run $\lambda_{SH}, \gamma_{SH}, Mc_{SH}$	$\delta\lambda = \lambda_{SH} + W_2\gamma_{SH} + \frac{Mc_{SH}}{W_2}$ $\delta\gamma = -\frac{1}{W_1}(\delta\lambda)$	not applicable	not applicable

The errors due to quantization and measurement noise are functions of test time, T. Note that the errors due to quantization decline faster (as 1/T) for constant rate testing and sinusoidal averaging than for sinusoidal harmonic testing (as $1/\sqrt{T}$). The quantization error formulas are expressed in terms of q, which is normally the single-pulse quantization level. In certain cases of pulse rebalanced sensors, however, a larger "effective" value must be used (see Section 3.2.5).

The effects of measurement noise are actually taken into account twice in Table 3.2-2, in the third and tenth rows. The third row formulas show the combined effect of process noise and measurement noise, assuming that the test has run long enough for a state of equilibrium to have been reached. The tenth row formulas show the transient effect of measurement noise alone, assuming that the equilibrium state has not yet been reached. In performing a numerical error analysis, for a given test time, etc., both sets of formulas should be computed and the larger result used.

The constant rate test error formulas are influenced by the fact that the λ and γ terms must be separated by making two test runs at well-separated test rate magnitudes (W_1 and W_2). The direct result of each run is a measurement of the excess torque above that which exists in the absence of the applied motion. Thus, we have the two equations

$$M_1 = M_{a_1} - M_c = \lambda W_1 + \gamma W_1^2 \qquad (3.2\text{-}1)$$

$$M_2 = M_{a_2} - M_c = \lambda W_2 + \gamma W_2^2 \qquad (3.2\text{-}2)$$

which are linear in λ and γ. Solving Eqs. (3.2-1) and (3.2-2):

$$\lambda = \frac{\frac{W_1}{W_2} M_2 - \frac{W_2}{W_1} M_1}{W_1 - W_2} \tag{3.2-3}$$

$$\gamma = \frac{\frac{1}{W_1} M_1 - \frac{1}{W_2} M_2}{W_1 - W_2} \tag{3.2-4}$$

Considering errors in the two measurements, we can write for estimation errors:

$$\delta\lambda = \frac{\frac{W_1}{W_2} \delta M_2 - \frac{W_2}{W_1} \delta M_1}{W_1 - W_2} \tag{3.2-5}$$

$$\delta\gamma = \frac{\frac{1}{W_1} \delta M_1 - \frac{1}{W_2} \delta M_2}{W_1 - W_2} \tag{3.2-6}$$

If we take W_1 as the larger of the two rates and make it considerably larger than W_2, we can write approximate expressions for $\delta\lambda$ and $\delta\gamma$:

$$\delta\lambda \cong \frac{1}{W_2} \left(\delta M_2 - \frac{W_2^2}{W_1^2} \delta M_1 \right) \tag{3.2-7}$$

$$\delta\gamma \cong \frac{1}{W_1 W_2} \left(\frac{W_2}{W_1} \delta M_1 - \delta M_2 \right) \tag{3.2-8}$$

In the cases where the two measurement errors are expected to be roughly the same size, we can make the further approximation:

$$\delta\lambda \cong \frac{1}{W_2}\,\delta M_2 \qquad (3.2\text{-}9)$$

$$\delta\gamma \cong \frac{-1}{W_1 W_2}\,\delta M_2 \qquad (3.2\text{-}10)$$

Note that various pairs of formulas for λ and γ errors in Table 3.2-2 occur in the same ratio as Eqs. (3.2-9) and (3.2-10).

TABLE 3.2-3

SUMMARY COMPARISON OF SINGLE-AXIS TEST METHODS

	Constant Rate	Sinusoidal Averaging	Constant Rate + Sinusoidal Averaging	Sinusoidal Averaging + Sinusoidal Harmonics	Constant Rate + Sinusoidal Averaging + Sinusoidal Harmonics
Completeness in Finding Sensor Parameters	λ and γ terms	γ terms only	λ and γ terms	all terms (μ, λ, γ)	all terms (μ, λ, γ)
Number of Runs Required	24	6	30	12	42
Redundant Data, Cross-checking Opportunities	Very Little	None	Some (γ terms)	Much (λ and γ terms)	Most (λ and γ terms)
Data Processing Difficulty	Simple (Pulse Count)	Simple (Pulse Count)	Simple (Pulse Count)	More Difficult (Extract Harmonics)	More Difficult (Extract Harmonics)
Quantization Effect Decreases As:	$\frac{1}{T}$	$\frac{1}{T}$	$\frac{1}{T}$ (λ, γ terms)	$\frac{1}{T}$ (γ terms) $\frac{1}{\sqrt{T}}$ (μ, λ, γ terms)	$\frac{1}{T}$ (λ, γ terms) $\frac{1}{\sqrt{T}}$ (μ, λ, γ terms)
Estimation Accuracy Advantages	Negligible δW and $\sigma_W(\lambda, \gamma)$ No $\Delta(\gamma)$	No effects due to $\bar{\epsilon}_{SH}$, β_{SH}, γ_{SH}, $Mc_{SH}(\gamma)$ Negligible Δ effect Negligible ϵ_W effect	Free to choose best of two methods (γ terms)	No effects due to $\bar{\epsilon}_{SH}$, $\lambda_{SH}, \gamma_{SH}, M_{cSH}(\lambda, \gamma$ terms) Negligible ϵ_W effects (λ, γ terms)	Free to choose best of all methods (λ, γ terms)

Table 3.2-3 summarizes a comparison of the various single-axis test methods and meaningful combinations. The first four rows review information already given in Table 3.1-5 and discussed in Section 3.1.3. The last two rows summarize points of significant difference between testing methods shown in the error formulas given in Table 3.2-2.

The major advantages of constant rate testing are:

- The data processing function is simply to count the total number of pulses occurring during each test run and, subsequently, to solve some linear algebraic equations.
- The average applied test rate should be very accurately known since it is given by an integral number of revolutions divided by the total test time. The estimation errors due to both bias (δW) and random fluctuations (σ_W) should both be negligible as a result. This is an advantage in determining both λ and γ terms.
- Distortion (Δ) of the waveform of the applied rate is not a problem.
- Errors due to quantization decrease with $1/T$ rather than $1/\sqrt{T}$ as in sinusoidal harmonic testing. This is an accuracy advantage in estimating the λ terms.

The major advantages of sinusoidal testing are:

- All parameter groups can be found, including the μ terms.
- It is not necessary to make multiple runs for each test axis in order to separate the λ and γ terms. This results in fewer total runs and avoids extra errors due to run-to-run shifts in test axis misalignments (ϵ_{SH}) and parameters ($\lambda_{SH}, \gamma_{SH}, M_{c_{SH}}$).

- There is no average effect of a test axis wobble (ϵ_W) and the effects on most harmonic terms are small. This is an accuracy advantage in estimating the λ and γ terms.

- There is more redundant information in the array of observable quantities extracted from the test sequence and, therefore, more chances for cross-checking results.

Of course by paying the price in time and effort required to perform both types of testing we can achieve the advantages of both, as well as additional cross-checking opportunities.

(Note: the remainder of Section 3.2 explains the origin of the error formulas presented in Table 3.2-2. Those readers not concerned with derivation details may wish to skip directly to Section 3.3. Those interested primarily in quantitative results may wish to skip directly to the numerical examples given in Section 3.5.)

3.2.2 Bias Test Motion Errors

This section summarizes the effects of bias test motion errors on the values of gyro parameters derived from the test results. The test motion errors considered are errors in the knowledge of amplitude and frequency of the applied motions and misalignment of the test motion axes.

A complete set of sinusoidal tests involves the six cases summarized in Table 3.1-1. The data from each test is processed to yield seven Fourier coefficients. From the set of 42 coefficients, the values of 14 basic parameter groups are calculated and from the 14 groups the values of certain individual parameters can be computed. Appendix B presents a complete and detailed error analysis showing the effects of bias

test motion errors on all 42 coefficient values. The 42 coefficients contain much redundant information and many of them will be of relatively little interest except in providing verification of results obtained from a particular subset (discussed below). In practice all 42 values could be used as inputs to a regression analysis in order to make optimal use of all available data. For purposes of producing a straightforward look at the effects on the estimates of individual parameters, however, we will consider only the direct effect of test motion errors on particular Fourier coefficients and the subsequent effects on the particular μ, λ, γ or ρ term associated with each coefficient. In many cases one of these coefficients is directly proportional to one basic parameter group which in turn is equal or approximately equal to one individual parameter. Therefore, in most cases a one percent error in the computed Fourier coefficient results in a one percent error in the corresponding parameter or parameter group. For example, for the test which employs angular vibration about the output axis, the coefficients S_1, C_1 and C_2 lead directly to the parameter groups k_5, k_2 and k_8, respectively. Errors in amplitude, δW, and frequency, $\delta\omega$, lead to errors in the coefficients as follows:

$$\delta S_1 = (k_5)\,\delta W$$

$$\delta C_1 = (k_2\omega)\,\delta W + (k_2 W)\,\delta\omega$$

$$\delta C_2 = -(k_8 W)\,\delta W \qquad (3.2\text{-}11)$$

Since we have:

$$k_5 = \frac{S_1}{W}$$

$$k_2 = \frac{C_1}{\omega W}$$

$$k_8 = -2\frac{C_2}{W^2} \qquad (3.2\text{-}11a)$$

it follows that:

$$\delta k_5 = \frac{1}{W}\,\delta S_1$$

$$= (k_5)\frac{\delta W}{W} + (o)\frac{\delta \omega}{\omega}$$

$$\delta k_2 = \frac{1}{\omega W}\,\delta C_1$$

$$= (k_2)\frac{\delta W}{W} + (k_2)\frac{\delta \omega}{\omega}$$

$$\delta k_8 = -\frac{2}{W^2}\,\delta C_2$$

$$= -2k_8\frac{\delta W}{W} + (o)\frac{\delta \omega}{\omega} \qquad (3.2\text{-}11b)$$

In general we can write:

$$\delta(\ ) = E_W(\ )\frac{\delta W}{W} + E_\omega(\ )\frac{\delta\omega}{\omega} + E_{\bar{\epsilon}}\,H_{\bar{\epsilon}} \qquad (3.2\text{-}12)$$

where the parenthesized term can be any μ, λ, γ or ρ and the E_W, E_ω and $E_{\bar{\epsilon}}$ are normalized error coefficients. Inspection of the results presented in Appendix B leads to the values tabulated in Table 3.2-4 for these quantities. The E_W values show that a 1% error in the amplitude of the applied test vibration results in an error in the estimated parameter group of 1, 2, or 3%. The entries in the E_ω column show that a given percentile frequency error has a 1-to-1 effect on μ terms and no influence on other terms. Most entries in the misalignment error coefficient column, $E_{\bar{\epsilon}}$, are "negligible." The expression in the λ row of the right-hand column is a function of c_i, the direction cosine between the test axis and the gyro input axis; $E_{\bar{\epsilon}}$ varies between zero when $c_i = 1$ and unity when $c_i = 0$. The latter is true when the test axis is the output or spin axis. The fact that $E_{\bar{\epsilon}} = 1$ in these two cases represents the fact that a one $\widehat{\sec}$ misalignment of the test motion axis results in a one $\widehat{\sec}$ error in the derived measures of α_s and β_o.

The test motion magnitude bias error formulas given in Table 3.2-2 represent the fact that E_W is unity for all λ terms and two for all γ terms, etc. The bias misalignment formulas represent the fact that the only significant effect of a test axis misalignment occurs when the angular momentum H is given an undesired component along the test axis. The torque measurement error is, then:

$$\delta M = \sqrt{1 - c_i^2}\ H W \bar{\epsilon} \qquad (3.2\text{-}12a)$$

TABLE 3.2-4

NORMALIZED ERROR COEFFICIENTS:
BIAS TEST MOTION ERRORS

( )	E_W	E_ω	$E_{\bar{\epsilon}}$
μ_{C_1}	1	1	negligible
μ_{S_2}	2	1	negligible
λ	1	0	$\sqrt{1 - c_i^2}$
γ	2	0	negligible
ρ	3	0	negligible

This error effects only the estimation of λ terms (misalignments) in sinusoidal testing. Therefore:

$$\delta\lambda = \frac{1}{W}\,\delta M = \sqrt{1 - c_i^2}\; H\,\bar{\epsilon} \qquad (3.2\text{-}12b)$$

In constant rate testing the torque measurement errors due to a bias misalignment ($\bar{\epsilon}$) and a run-to-run shift ($\Delta\bar{\epsilon}$) are:

$$\delta M_1 = \sqrt{1 - c_i^2}\; H\, W_1\, \bar{\epsilon} \qquad (3.2\text{-}13)$$

$$\delta M_2 = \sqrt{1 - c_i^2}\; H\, W_2\, (\bar{\epsilon} + \Delta\bar{\epsilon}) \qquad (3.2\text{-}14)$$

Substituting Eqs. (3.2-13) and (3.2-14) into Eqs. (3.2-5) and (3.2-6) yields:

$$\delta\lambda = \sqrt{1 - c_i^2}\, H\, (\bar{\epsilon} + \Delta\bar{\epsilon}) \qquad (3.2\text{-}15)$$

$$\delta\gamma = -\sqrt{1 - c_i^2}\, \frac{H}{W_1}\, \Delta\bar{\epsilon} \qquad (3.2\text{-}16)$$

Equations (3.2-11), (3.2-15) and (3.2-16) are the basis for the error formulas appearing in the fourth and fifth rows of Table 3.2-2.

3.2.3 Cyclic Test Motion Errors

This section treats the effects of imperfections in the motion supplying devices which cause cyclically repeating test motion errors. These effects may be studied by considering a single test motion cycle. There is no advantage to be gained by averaging data taken over many cycles since the resulting error torques also repeat in each cycle. Table 3.2-5, which repeats the expressions given in Table 3.1-1, indicates which observable quantities will be affected by various types of cyclic errors.

Distortion of the nominally sinusoidal shape of the applied test motion will seriously affect the harmonic terms (S_2, C_2, S_3 and C_3) in cases where there is a very large input torque, $H\omega_i$, at the fundamental test motion frequency. This occurs when the test axis has a component along the gyro input axis ($c_i = 1$ or $1/\sqrt{2}$). Exaggerated examples of distorted shapes are pictured in Fig. 3.2-1 with the corresponding errors in Fourier coefficients [$E(S_2)$, $E(C_2)$, etc.]. The affected observable

TABLE 3.2-5

SIGNIFICANT CYCLIC ERRORS

Test Axis	c_i	B $\left(M_c+\frac{\gamma}{2}W^2\right)$	S_1 $\left(\lambda W+\frac{3}{4}\rho W^3\right)$	C_1 $\left(\mu_{C_1}\omega W+\mu_{C_3}\omega W^3\right)$	S_2 $\left(\mu_{S_2}\omega W^2\right)$	C_2 $\left(-\frac{\gamma}{2}W^2\right)$	S_3 $\left(-\frac{1}{4}\rho W^3\right)$	C_3 $\left(\mu_{C_3}\omega W^3\right)$
o	0	(NL) $M_{c_o}+\frac{1}{2}k_8W^2$	k_5W	(NL) $k_2\omega W$	(TW) 0	(NL) $-\frac{1}{2}k_8W^2$	(NL) 0	0
s	0	$M_{c_s}-\frac{1}{2}k_7W^2$	k_6W	$k_3\omega W$	(TW) 0	$\frac{1}{2}k_7W^2$	0	0
i	1	(NL) $M_{c_i}+\frac{1}{2}k_7W^2$	(NL) $k_4W+\frac{3}{4}k_{12}W^3$	$k_1\omega W k_1\omega W$	(DN) 0	(NL) (DN) $\frac{1}{2}k_7W^2$	(NL) (DN) $-\frac{1}{4}k_{12}W^3$	(DN) 0
o/s	0	(NL) $M_{c_{os}}+\frac{1}{4}\left(-k_7+k_8+k_{11}\right)W^2$	$\frac{1}{\sqrt{2}}\left(k_5+k_6\right)W$	(NL) $\frac{1}{\sqrt{2}}\left(k_2+k_3\right)\omega W-\frac{1}{8\sqrt{2}}k_{14}\omega W^3$	(TW) (DN) $\frac{1}{4}k_{13}\omega W^2$	(NL) $\frac{1}{4}\left(-k_7+k_8+k_{11}\right)W^2$	(NL) 0	$\frac{1}{8\sqrt{2}}k_{14}\omega W^3$
i/o	$\frac{1}{\sqrt{2}}$	(NL) $M_{c_{io}}+\frac{1}{4}\left(k_7+k_8+k_9\right)W^2$	(NL) $\frac{1}{\sqrt{2}}\left(k_4+k_5\right)W+\frac{3}{8\sqrt{2}}k_{13}W^3$	(NL) $\frac{1}{\sqrt{2}}\left(k_1+k_2\right)\omega W+\frac{1}{8\sqrt{2}}k_{14}\omega W$	(TW) (DN) 0	(NL) (DN) $-\frac{1}{4}\left(k_7+k_8+k_9\right)W^2$	(NL) (DN) $-\frac{1}{8\sqrt{2}}k_{12}W^3$	(DN) $-\frac{1}{8\sqrt{2}}k_{14}\omega W^3$
i/s	$\frac{1}{\sqrt{2}}$	(NL) $M_{c_{is}}+\frac{1}{4}k_{10}W^2$	(NL) $\frac{1}{\sqrt{2}}\left(k_4+k_6\right)W$	$\frac{1}{\sqrt{2}}\left(k_1+k_3\right)\omega W$	(TW) (DN) 0	(NL) (DN) $-\frac{1}{4}k_{10}W^2$	(NL) (DN) 0	(DN) 0

(NL) torquer nonlinearity (TW) table wobble (DN) distortion

quantities are indicated by the symbol (DN) in Table 3.2-5. These quantities will be difficult to measure in the presence of even small distortions of the applied motion. The bias term, B, and the fundamental cosine term, C_1, should be unaffected for the following reasons. The average test angular rate must remain zero or the test table angle would drift away from its zero reference position. A fundamental cosine term error, $E(C_1)$,

R-260

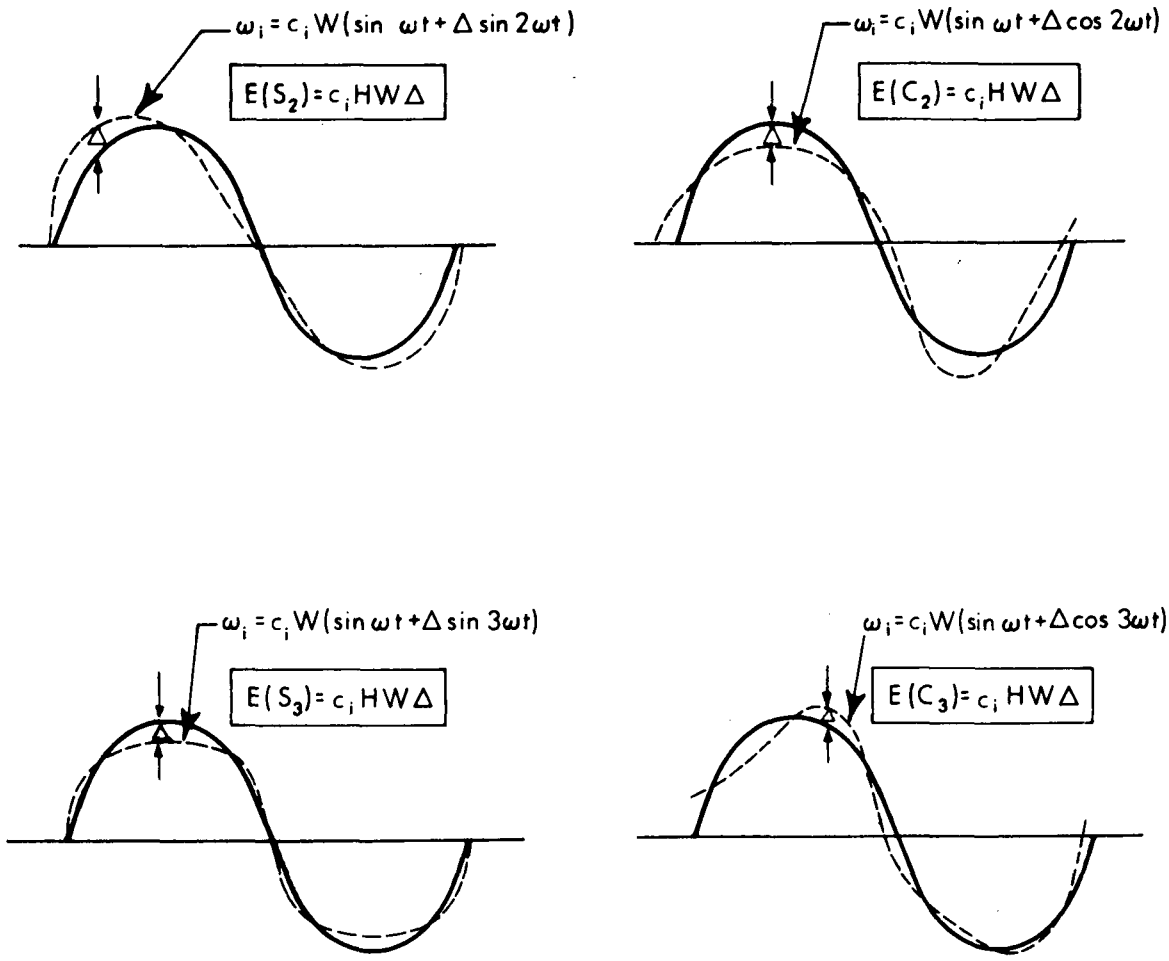

Figure 3.2-1 Distorted Test Motion Sinusoids

would be equivalent to an error in the knowledge of the test motion phase angle, but the phase of the test motion should be known extremely well based on zero-crossings of the table reference position. An error in S_1 is quite possible, but this is completely equivalent to a bias error in the test motion amplitude, W, treated in the previous section.

The first error formula for $\delta\gamma$ in the second row of Table 3.2-2 is obtained by combining the $E(C_2)$ expression in Fig. 3.2-1 with the relation:

$$\delta\gamma = \frac{2}{W^2}\,\delta C_2 \qquad (3.2\text{-}17)$$

The second error formula is obtained by noting that the dominant applied torque in some tests is the output axis inertia term, $c_o I_{oo} \omega W \cos \omega t$.

A table wobble or oscillation of the test axis about a cross axis can significantly affect the term S_2 in five of the six tests outlined in Table 3.2-5. These are indicated by the symbol (TW) . It can also affect the torque measurement during constant rate testing due to the unwanted constant angular rate components associated with the resulting conical motion of the test axis. These effects may be significant whenever the cross axis about which the wobbling takes place is coincident with the gyro input axis, or whenever the direction cosine between the two is large. The angular rate about the input axis includes an undesired (and unknown) component, $\delta\omega_i$, which is proportional to this direction cosine. Since the magnitude of the expected wobbling is of the order of some seconds of arc, the undesired component is extremely small compared to the nominal test angular rate. However, when the motion has a component in the direction of the gyro input axis, the resulting error torque, $H\delta\omega_i$, can be significant in comparison with other torques associated with the desired test motion. Undesired components of ω_o and ω_s, due to the wobbling motion, will also cause unwanted torques, but these will be negligibly small since they are small fractions of terms which are small nominally.

Figure 3.2-2 pictures three Euler angles (ψ, θ, φ) relating a set of base axes (X, Y, Z) to a set of table axes (x, y, z). Nominally x remains coincident with X and the table motion is represented by the angular rate, $\dot{\phi}$, which is oscillatory in sinusoidal testing and steady in constant rate testing. That is:

$$\left.\begin{aligned} \dot{\phi} &= W \sin \omega t \\ \varphi &= -\frac{W}{\omega} \cos \omega t \end{aligned}\right\} \text{ sinusoidal tests} \qquad (3.2\text{-}18a)$$

$$\left.\begin{aligned} \dot{\phi} &= W \\ \varphi &= Wt \end{aligned}\right\} \text{ constant rate tests} \qquad (3.2\text{-}18b)$$

Table wobble is represented by oscillatory small-angle histories for ψ and θ.

The angular rates of the table can be expressed, in table coordinates, in terms of the Euler angle rates by the following standard set of equations:

$$\begin{aligned} \omega_x &= \dot{\phi} - \dot{\psi} \sin \theta \\ \omega_y &= \dot{\theta} \cos \varphi + \dot{\psi} \cos \theta \sin \varphi \\ \omega_z &= \dot{\theta} \sin \varphi + \dot{\psi} \cos \theta \cos \varphi \end{aligned} \qquad (3.2\text{-}19)$$

R-822

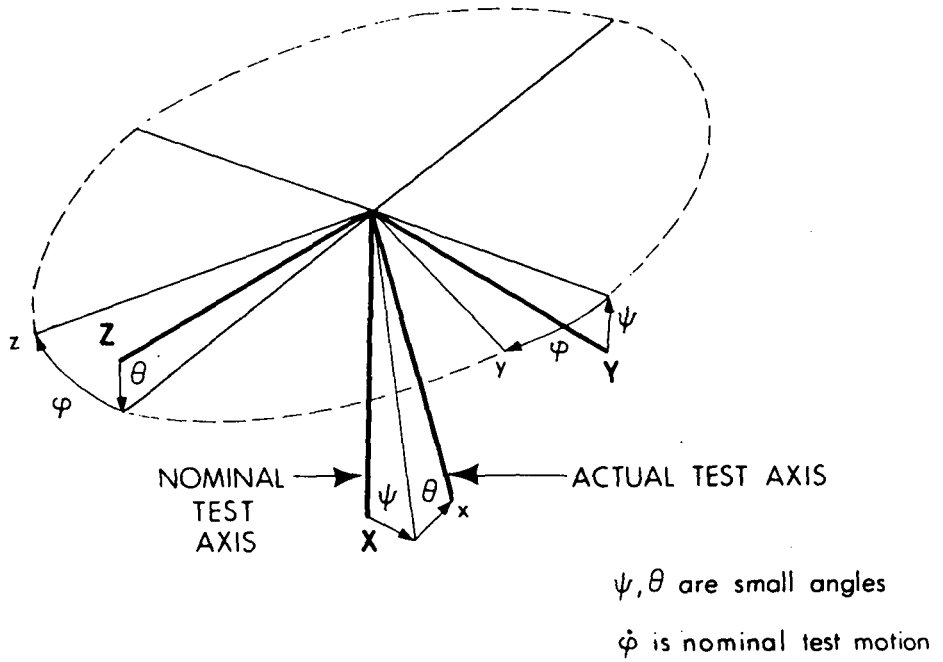

Figure 3.2-2 Euler Angles Relating Base Axes to Table Axes

(See, for example, Ref. 6, p.475.) Since the gyro is rigidly attached to the table, these equations also represent the gyro case angular rates in some case-fixed coordinate frame. Based on small angle assumptions ($\cos\theta \cong \cos\psi \cong 1$, etc.) and the elimination of higher order terms we can write the following expressions.

For low frequency sinusoidal testing:

$$\left.\begin{aligned} \omega_x &\cong W \sin \omega t \\ \omega_y &\cong \dot{\theta} \\ \omega_z &\cong \dot{\psi} \end{aligned}\right\} \qquad (3.2\text{-}19a)$$

For constant rate testing:

$$\left.\begin{aligned} \omega_x &\cong W \\ \omega_y &\cong \dot{\theta} \cos Wt + \dot{\psi} \sin Wt \\ \omega_z &\cong -\dot{\theta} \sin Wt + \dot{\psi} \cos Wt \end{aligned}\right\} \qquad (3.2\text{-}19b)$$

In sinusoidal testing the expected form of table wobbling is a second harmonic oscillation of the test axis due to an offset center of mass of the table and equipment mounted on it. An offset in the y direction (d_y), for example, causes a double frequency acceleration ($d_y W^2 \sin^2 \omega t$), which causes a bearing torque and angular displacement about the z axis. The magnitude of the displacement depends upon the table unbalance and geometry and the bearing stiffness, but its time history should closely follow the forcing acceleration for low frequency test motions. Therefore:

$$\left.\begin{aligned} \psi(t) &\cong \psi_1 \sin^2 \omega t \\ &= \frac{\psi_1}{2} (1 - \cos 2\omega t) \\ &= \psi_{avg} - \epsilon_\psi \cos 2\omega t \end{aligned}\right\} \qquad (3.2\text{-}20a)$$

where ϵ_ψ is the amplitude of the wobble. Differentiating, we obtain:

$$\left.\begin{aligned} \dot{\psi} &\cong 2\omega\, \epsilon_\psi \sin 2\omega t \\ \dot{\theta} &\cong 2\omega\, \epsilon_\theta \sin 2\omega t \end{aligned}\right\} \qquad (3.2\text{-}21a)$$

(The $\dot{\theta}$ equation corresponds to a z axis center of mass offset.) Consideration of Eqs. (3.2-21a) and (3.2-19a) shows that there will be a second harmonic oscillation about some axis in the y - z plane. The resulting error torque depends on the extent to which the gyro input axis coincides with this axis. Assuming a worst-case situation (the wobble axis coincides with the gyro input axis when $c_i = 0$, or with the projection of the gyro input axis onto the y-z plane when $c_i = 1/\sqrt{2}$) the appropriate error formula is:

$$E(S_2) = 2\omega \epsilon_W \sqrt{1 - c_i^2}\, H\, W \qquad (3.2\text{-}22a)$$

where c_i is the direction cosine between the gyro input axis and the test axis and ϵ_W represents the combined effect of ϵ_θ and ϵ_ψ. The other Fourier coefficients, B, S_1, C_1 and C_2, are unaffected. Therefore, the μ, λ and γ terms are all unaffected, except for the μ term, $\frac{1}{4} k_{13}$, which is associated with S_2 in the "o/s" test. In this case:

$$\left.\begin{aligned} \delta\mu &= \frac{1}{\omega W^2} E(S_2) \\ &= \frac{2}{W} H \sqrt{1 - c_i^2}\, \epsilon_W \\ &= \frac{2}{W} H \epsilon_W \end{aligned}\right\} \qquad (3.2\text{-}23)$$

In constant rate testing the expected form of wobble is a conical motion of the test axis, again caused by the net mass unbalance about the axis of rotation. In this case the Euler angles, ψ and θ, oscillate at the

test motion frequency, W, with θ leading ψ by $\pi/2$ radians when the direction of table rotation, φ, is as shown in Fig. 3.2-2. Therefore:

$$\left.\begin{aligned} \psi &= \epsilon_1 \sin Wt + \epsilon_2 \cos Wt \\ \theta &= \epsilon_1 \cos Wt - \epsilon_2 \sin Wt \end{aligned}\right\} \qquad (3.2\text{-}20b)$$

Differentiation of Eq. (3.2-20b) and substitution into Eq. (3.2-19b) leads to expressions for ω_y and ω_z which contain constant and double frequency terms. The latter cancel, leaving:

$$\left.\begin{aligned} \omega_y &\cong -W\epsilon_2 \\ \omega_z &\cong W\epsilon_1 \end{aligned}\right\} \qquad (3.2\text{-}21b)$$

The result is an undesired constant rate about some axis in the y - z plane, leading to the worst-case error torque formula:

$$\delta M = W H \sqrt{1 - c_i^2}\, \epsilon_W \qquad (3.2\text{-}22b)$$

Combination of Eq. (3.2-22b) with Eqs. (3.2-7) and (3.2-8) yields the error formulas for $\delta\lambda$ and $\delta\gamma$ given in Table 3.2-2.

3.2.4 Errors Due to Quantization

When pulse rebalanced sensors are tested, the test data is a sequence of integers which represent the integral of torque over particular time intervals. The same is true in testing analog rebalanced sensors in cases where the torque command signal is integrated and quantized to provide an output pulse sequence. In constant rate testing and sinusoidal average testing the data is simply the total pulse count which, when divided by total test time, represents the average torque level over the duration of the test. In sinusoidal harmonic testing the test time, T, is usually divided into a sequence of equally spaced intervals of length, h. In the limiting case for pulse rebalanced sensors h is a single pulse width, making the test data a sequence of binary or ternary numbers representing the time history of the rebalance torque. However, h can also be chosen as any integral number of pulse widths.

Consider first the case of an analog rebalanced gyro where the outputs appear at varying intervals, not generally occurring exactly at the beginning and end of the counting intervals. The example time-line of Fig. 3.2-3 shows a case where p pulses are counted within the interval (t_i, t_i+h). The error due to quantization depends on the quantities, x_i and x_{i+1}. The error in measuring the integrated torque over the interval is:

$$e \cong q\left(\frac{x_i}{\ell_i} - \frac{x_{i+1}}{\ell_{i+1}}\right) \qquad (3.2\text{-}24)$$

where q is the weight of a single pulse or count (measured in dyne cm sec). If we assume x_i and x_{i+1} to be independent random variables uniformly distributed over the spacing intervals, ℓ_i and ℓ_{i+1}, in which they occur, then the joint distribution of the normalized quantities, x_i/ℓ_i and x_i/ℓ_{i+1}, will be as shown at the left side of Fig. 3.2-4; the resulting density function, p(e),

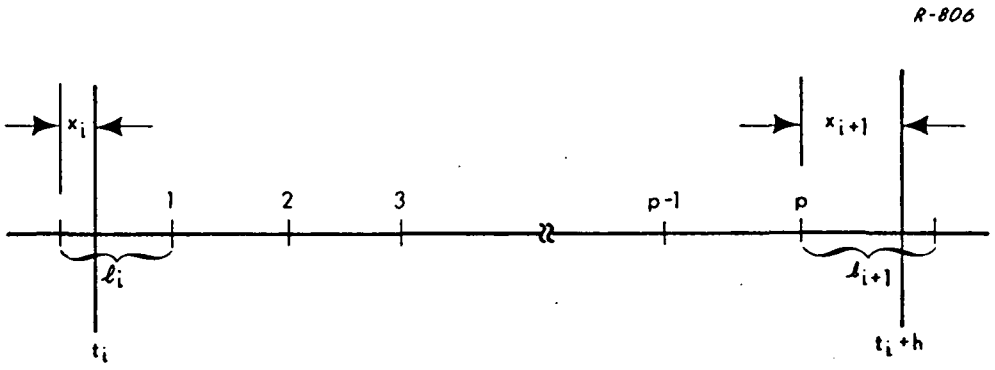

Figure 3.2-3 Pulse Sequence

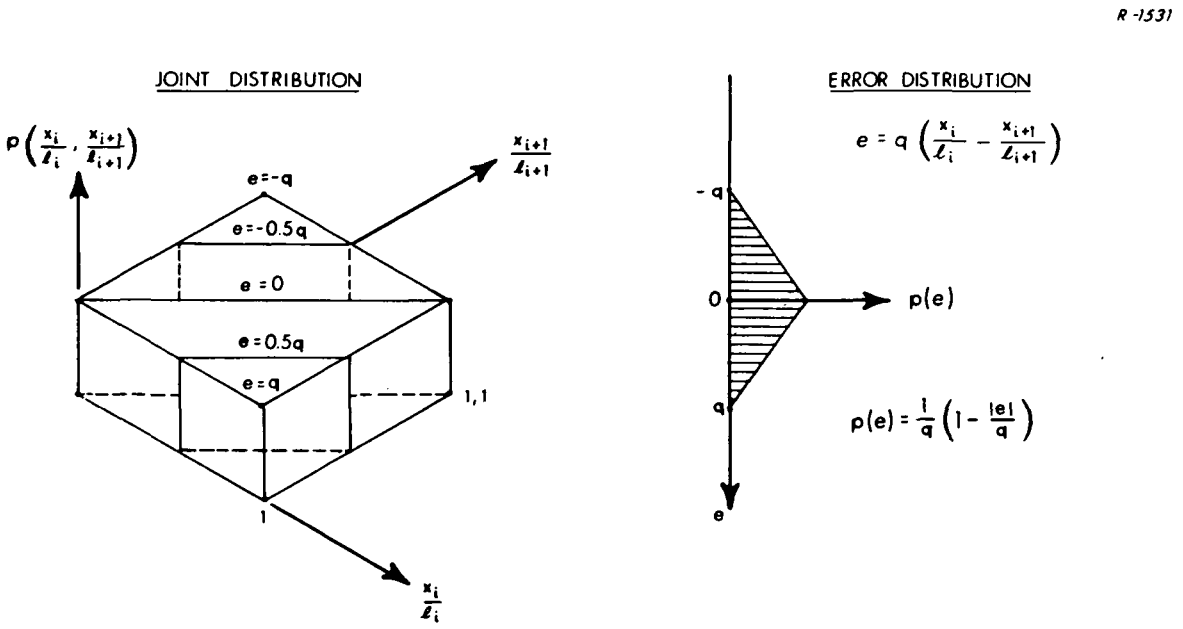

Figure 3.2-4 Distribution of Error Due to Quantization

for the error is illustrated at the right. It has zero mean and variance:

$$\sigma_e^2 = \int_{-q}^{q} e^2 \, p(e) \, de = 2 \int_{o}^{q} \left(\frac{e^2}{q} - \frac{e^3}{q^2} \right) de$$

$$= \frac{1}{6} q^2 \qquad (3.2\text{-}25)$$

Therefore:

$$\sigma_e = \frac{q}{\sqrt{6}} \qquad (3.2\text{-}26)$$

The resulting error in measuring the average torque during a constant rate or sinusoidal test is:

$$\sigma_M = \frac{\sigma_e}{T} = \frac{q}{\sqrt{6}\, T} \qquad (3.2\text{-}27)$$

In sinusoidal harmonic testing, the objective is to estimate the observable quantities, S_1, C_1, S_2 and C_2, after removing the average value, B, from the time varying torque. Thus:

$$M(t) - B = S_1 \sin \omega t + C_1 \cos \omega t + S_2 \sin 2\omega t + C_2 \cos 2\omega t \qquad (3.2\text{-}28)$$

Each integer measurement is given by:

$$z_i = \int_{h(i-1)}^{hi} [M(t) - B]\, dt$$

$$= \frac{S_1}{\omega}\left[-\cos \omega h_i + \cos \omega h(i-1)\right] + \frac{C_1}{\omega}\left[\sin \omega h_i - \sin \omega h(i-1)\right]$$

$$+ \frac{S_2}{2\omega}\left[-\cos 2\omega h_i + \cos 2\omega h(i-1)\right] + \frac{C_2}{2\omega}\left[\sin 2\omega h_i - \sin 2\omega h(i-1)\right] \qquad (3.2\text{-}29)$$

Defining a state vector of quantities to be estimated as:

$$\underline{x} = \begin{bmatrix} S_1 \\ C_1 \\ S_2 \\ C_2 \end{bmatrix} \qquad (3.2\text{-}30)$$

and a j-dimensional vector, $\underline{z}$, of measurements, taken over an interval $T = hj$, we can form the least-squares estimate, $\hat{x}$, as follows:

$$\underline{\hat{x}} = (H^T H)^{-1} H^T \underline{z} \qquad (3.2\text{-}31)$$

where H is the j x 4 measurement matrix:

$$H = \frac{1}{\omega} \begin{bmatrix} f_1 & g_1 & p_1 & q_1 \\ f_2 & g_2 & p_2 & q_2 \\ \vdots & & & \\ f_j & g_j & p_j & q_j \end{bmatrix} \qquad (3.2\text{-}32)$$

where:

$$f_i = -\cos \omega hi + \cos \omega h(i-1) \qquad (3.2\text{-}33)$$

etc. (see Eq. (3.2-29)). Therefore:

$$H^T H = \frac{1}{\omega^2} \begin{bmatrix} \sum_1^j f_i^2 & \Sigma f_i g_i & \Sigma f_i p_i & \Sigma f_i q_i \\ \Sigma g_i f_i & \Sigma g_i^2 & \Sigma g_i p_i & \Sigma g_i q_i \\ \Sigma p_i f_i & \Sigma p_i g_i & \Sigma p_i^2 & \Sigma p_i q_i \\ \Sigma q_i f_i & \Sigma q_i g_i & \Sigma q_i p_i & \Sigma q_i^2 \end{bmatrix} \qquad (3.2\text{-}34)$$

Summing over a full cycle of N points ($N = 2\pi/\omega h$), we find:

$$H^T H = \frac{1}{\omega^2} \begin{bmatrix} N/2 & 0 & 0 & 0 \\ 0 & N/2 & 0 & 0 \\ 0 & 0 & N/2 & 0 \\ 0 & 0 & 0 & N/2 \end{bmatrix} \tag{3.2-34a}$$

Similarly, over an integral number (M) of cycles of N points each:

$$H^T H = \frac{1}{\omega^2} \begin{bmatrix} MN/2 & 0 & 0 & 0 \\ 0 & MN/2 & 0 & 0 \\ 0 & 0 & MN/2 & 0 \\ 0 & 0 & 0 & MN/2 \end{bmatrix} = \frac{1}{\omega^2} \begin{bmatrix} T/2h & 0 & 0 & 0 \\ 0 & T/2h & 0 & 0 \\ 0 & 0 & T/2h & 0 \\ 0 & 0 & 0 & T/2h \end{bmatrix} \tag{3.2-35}$$

Therefore:

$$(H^T H)^{-1} = \omega^2 \begin{bmatrix} 2h/T & 0 & 0 & 0 \\ 0 & 2h/T & 0 & 0 \\ 0 & 0 & 2h/T & 0 \\ 0 & 0 & 0 & 2h/T \end{bmatrix} \tag{3.2-36}$$

For a sequence of independent measurement errors of variance $q^2/6$ [Eq. (3.2-26)], the estimation error covariance can be shown to be:

$$\overline{(\hat{\underline{x}} - \underline{x})(\hat{\underline{x}} - \underline{x})^T} = \frac{q^2}{6} (H^T H)^{-1} \tag{3.2-37}$$

Therefore:

$$\sigma_{S_1} = \sigma_{C_1} = \sigma_{S_2} = \sigma_{C_2} = \frac{q}{\sqrt{6}} \omega \sqrt{\frac{2h}{T}} \qquad (3.2\text{-}38)$$

The error formulas in the seventh row of Table 3.2-2 are based on Eqs. (3.2-27), (3.2-38), (3.2-9) and (3.2-10).

3.2.5 Errors Due to Pulse Rebalancing

In testing pulse rebalanced sensors we must consider additional errors which are attributed to the pulse rebalance scheme itself -- errors which occur even though the rebalance path works in an ideal way -- zero scale factor error, perfectly controlled pulse width, etc. These errors arise in the following two ways:

- Regardless of loop dynamics it is impossible for the feedback torque to be a perfect replica of the applied torque simply because it is quantized. Some integral number of pulses is counted over any given measurement interval, whereas the integrated applied torque may take on a continuum of values.

- The dynamical behavior of the nonlinear loop may lead to still larger errors associated with limit cycles or forced oscillations. Thus, the integral of the rebalance torque may alternately "get ahead of" and "fall behind" the integral of the input torque by an amount which can be much larger than one pulse.

The first of the two effects mentioned above is an "error due to quantization." The preceding analysis for analog rebalanced sensors with

quantized output applies with little change in this case, and the associated rms measurement error is again:

$$\sigma_e = q/\sqrt{6} \tag{3.2-39}$$

where the quantization level is:

$$q \leq M_{tg} T_i \tag{3.2-40}$$

where T_i is the sampling interval built into the rebalance electronics and M_{tg} is the rebalance torque level.

For either of the two effects mentioned above that part of the preceding analysis which relates σ_e to the resulting estimation errors, σ_M, also holds. That is:

$$\sigma_M = \sigma_e /T \tag{3.2-41}$$

for average torque measurements, and:

$$\sigma_M = \sigma_e \omega \sqrt{2h/T} \tag{3.2-42}$$

for harmonic component measurements. The latter equation, (3.2-42), is based on the assumption that the sequence of measurement errors, e, are uncorrelated. This assumption will be discussed subsequently.

In analyzing the effect of the loop dynamics, however, it is necessary to develop new expressions for the individual measurement error statistics. These statistics depend on the specific behavior of the rebalance loop used -- its characteristic modes in the presence of various inputs. Thus, we find different results for binary, ternary and time-modulation

rebalanced sensors and different results within these classifications as well, depending on the choice of parameters.

The first step in deriving the desired expressions is a general one which applies to most pulse rebalanced sensors. Consider the block diagram shown at the top of Fig. 3.2-5 representing a generalized rebalance loop. The actual measurements obtained during a test are net pulse counts over particular time intervals -- the number of positive pulses minus the number of negative pulses occurring in the interval (t_i, t_j), for example. The net count, n_{ij}, multiplied by the individual pulse weight, q, is a measure, ideally, of the integral of the rebalance torque over that interval. In subsequent data processing this measurement is used to represent the integral of the applied torque, M_a, over the same time interval. The measurement error is, therefore, the difference between these two integrals:

$$e_{ij} = \int_{t_i}^{t_j} M_a \, dt - \int_{t_i}^{t_j} M_{tg} \, dt = \int_{t_i}^{t_j} M_o \, dt \qquad (3.2\text{-}43)$$

Consider now the diagram at the bottom of Fig. 3.2-5 in which the float dynamics block has been broken into an equivalent cascade of three separate linear elements with outputs e, α' and α. We can see by comparing Eq. (3.2-43) with the diagram that the change in the quantity e over a measurement interval is equal to the measurement error. Thus:

$$e_j - e_i = e_{ij} \qquad (3.2\text{-}44)$$

Similarly, the change in the quantity α' is proportional to the measurement error. Thus:

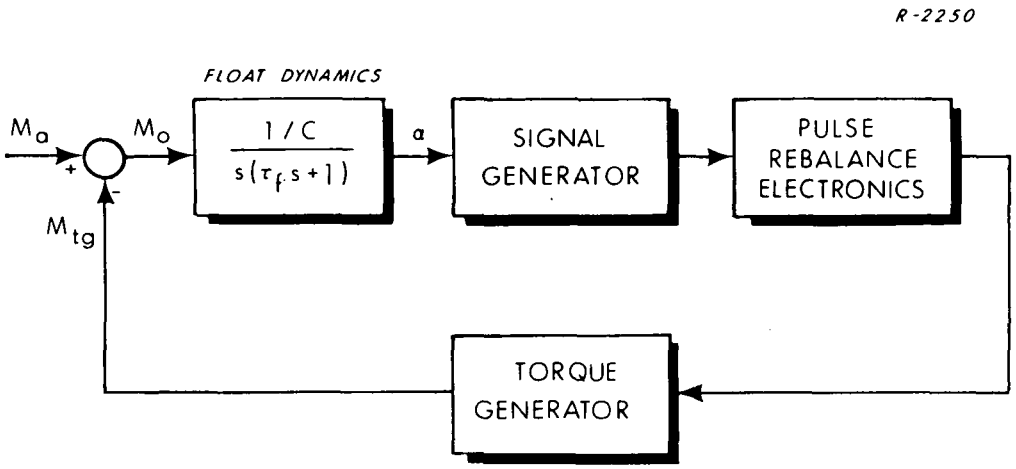

a) COMPLETE LOOP

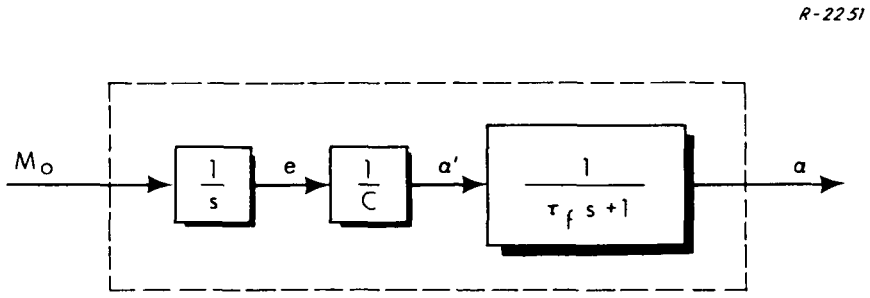

b) EQUIVALENT FLOAT DYNAMICS CASCADE

Figure 3.2-5 **Block Diagram of a Generalized Rebalanced Loop**

$$e_{ij} = C\left(\alpha_j' - \alpha_i'\right) \tag{3.2-45}$$

Further, the quantity α' is linearly related to the float angle, α, by a simple first order lag with unity gain. We can now make the following general statement: the measurement error for a particular time interval is proportional to the change, over that interval, in a fictitious quantity, α', which leads the float angle variation by an amount associated with the float time constant, $\tau_f = I_{oo}/C$, where the factor of proportionality is the float damping coefficient, C.

We assume that the time history of α' over any given measurement interval can be described approximately as an oscillation of amplitude $A_{\alpha'}$ about an average value $\overline{\alpha'}$, with quantities φ_i and φ_j as the phase angles at the start and end of the interval. We can then write:

$$\alpha_i' = \overline{\alpha'} + A_{\alpha'} \sin \varphi_i \tag{3.2-46}$$

$$\alpha_j' = \overline{\alpha'} + A_{\alpha'} \sin \varphi_j \tag{3.2-47}$$

Therefore:

$$\Delta\alpha' = \alpha_j' - \alpha_i' = A_{\alpha'}\left(\sin \varphi_j - \sin \varphi_i\right) \tag{3.2-48}$$

and

$$\overline{\Delta\alpha'^2} = A_{\alpha'}^2\left(\overline{\sin^2 \varphi_j} - 2\,\overline{\sin \varphi_j \sin \varphi_i} + \overline{\sin^2 \varphi_i}\right) \tag{3.2-49}$$

where overbars indicate ensemble averages.

As will be shown subsequently, the characteristic frequency of oscillation in binary and ternary rebalance loops depends on the dynamic properties of the linear elements in the loop and on the applied torque input. The phase angles at the start and end of the clock-controlled measurement intervals will take on a variety of values distributed from zero to 2π. For a large ensemble of measurement intervals we can reasonably assume uniform distributions for both φ_i and φ_j; therefore:

$$\overline{\Delta\alpha'} = \overline{\sin \varphi_i} = \overline{\sin \varphi_j} = 0 \qquad (3.2\text{-}50)$$

and

$$\overline{\sin^2 \varphi_i} = \overline{\sin^2 \varphi_j} = 1/2 \qquad (3.2\text{-}51)$$

On the other hand the phase angle differences, $\Delta\varphi = \varphi_j - \varphi_i$, over single measurement intervals may exhibit considerable regularity for any given test, just because of the coherent characteristic float oscillation associated with a given loop and input magnitude. Some randomness may also be present due to small fluctuations in input or loop parameters and variations in delay due to sampling. So we are dealing with an unknown mixture of regularity and randomness. Consider the following two extreme cases: 1) φ_i and φ_j are statistically independent, and 2) $\Delta\varphi$ is fixed at a particular value. In the first case:

$$\overline{\sin \varphi_j \sin \varphi_i} = 0 \qquad (3.2\text{-}52)$$

and

$$\overline{\Delta\alpha'^2} = A'^2_\alpha, \qquad (3.2\text{-}53)$$

and therefore:

$$\sigma_{\Delta\alpha'} = A_{\alpha'} \tag{3.2-54}$$

In the second case:

$$\begin{aligned} \sin\varphi_j \sin\varphi_i &= \sin\left(\varphi_i + \Delta\varphi\right)\sin\varphi_i \\ &= \left(\sin\varphi_i\cos\Delta\varphi + \cos\varphi_i\sin\Delta\varphi\right)\sin\varphi_i \end{aligned} \tag{3.2-55}$$

therefore:

$$\begin{aligned} \overline{\sin\varphi_j \sin\varphi_i} &= \overline{\sin^2\varphi_i}\cos\Delta\varphi + \overline{\cos\varphi_i \sin\varphi_i}\sin\Delta\varphi \\ &= \frac{1}{2}\cos\Delta\varphi \end{aligned} \tag{3.2-56}$$

Thus, in this case:

$$\overline{\Delta\alpha'^2} = A_{\alpha'}^2\left(1 - \cos\Delta\varphi\right) \tag{3.2-57}$$

and

$$\sigma_{\Delta\alpha'} = A_{\alpha'}\sqrt{1 - \cos\Delta\varphi} \tag{3.2-58}$$

Figure 3.2-6 plots the normalized quantity $\sigma_{\Delta\alpha'}/A_{\alpha'}$ versus all possible values of $\Delta\varphi$. We note for three fourths of all possible values of $\Delta\varphi$ this normalized quantity ranges between 0.54 and 1.414. Therefore, a reasonable typical value is unity, which is identical with the value for the random case, as given by Eq. (3.2-54). Thus, for error analysis purposes we adopt Eq. (3.2-54) as a valid approximation without the need to determine

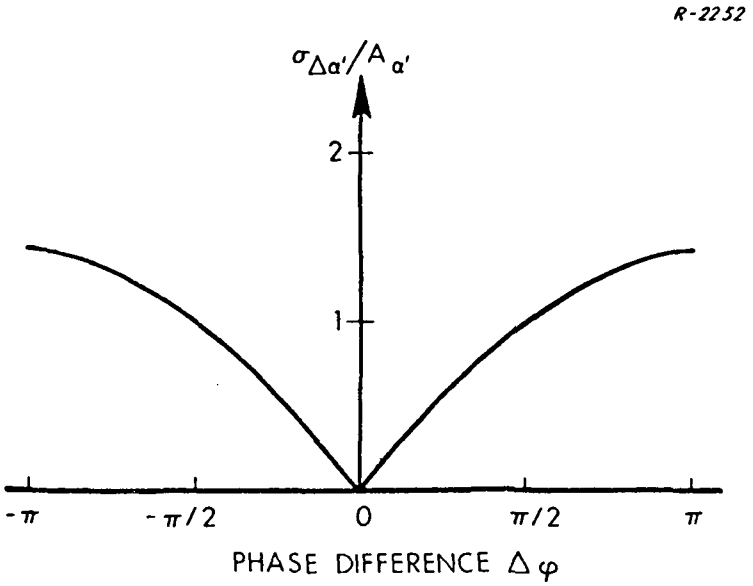

Figure 3.2-6 RMS Change in α' with a Fixed Phase Difference

whether $\Delta\varphi$ is mostly random or regular. This choice is a conservative one since it neglects a substantial improvement which is possible in cases where $\Delta\varphi$ is regular and happens to have a small magnitude (less than $\pm\,\pi/4$).

We now combine Eq. (3.2-54) with Eq. (3.2-45) to obtain the rms measurement error:

$$\sigma_e = C\,A_{\alpha'} \qquad (3.2\text{-}59)$$

Thus, the standard deviation of the individual measurement error, e_{ij}, is proportional to the amplitude of the α' oscillation.* The amplitude of the oscillation of the float angle itself is given by:

$$A_\alpha = \frac{A_{\alpha'}}{\sqrt{\tau_f^2 \nu_\alpha^2 + 1}} \tag{3.2-60}$$

where ν_α is the oscillation frequency. This may be a limit cycle frequency, as in a binary loop; an input-dependent forced oscillation frequency, as in a ternary loop; or a clock-controlled forced oscillation frequency, as in a time-modulation loop. Combining Eqs. (3.2-59) and (3.2-60) we can write:

$$\sigma_e = C A_\alpha \sqrt{\tau_f^2 \nu_\alpha^2 + 1} \tag{3.2-61}$$

Finally, combining Eq. (3.2-62) with Eqs. (3.2-41) and (3.2-42) we can write:

$$\sigma_M = \frac{C A_\alpha}{T} \sqrt{\tau_f^2 \nu_\alpha^2 + 1} \tag{3.2-62}$$

---

*We note also that Eq. (3.2-42) is justified even though the assumption of uncorrelated measurement errors is not strictly correct. When $\Delta\varphi$ is regular, measurement errors in adjacent intervals are highly correlated; but the phase angles φ_i for intervals occupying a particular subdivision in a sequence of test motion cycles (low frequency) can be taken as uncorrelated. Consequently the values of $\Delta\alpha' = A_{\alpha'}(\sin\varphi_j - \sin\varphi_i)$ for this sequence of well-separated intervals are uncorrelated and distributed in accordance with a uniform distribution for φ_i.

for average torque measurements and:

$$\sigma_M = C A_\alpha \sqrt{\tau_f^2 \nu_\alpha^2 + 1} \quad \omega \sqrt{2h/T} \qquad (3.2\text{-}63)$$

for harmonic component measurements. This concludes the first step in the development, which applies to binary and ternary pulse-rebalanced sensors, and relates test accuracy to the amplitude and frequency, A_α and ν_α, of float angle oscillations. Of course these two quantities can depend on the input and the specific pulse rebalance scheme under consideration. (Equation (3.2-62) is also applied below to one version of tests of time-modulation rebalanced sensors. In this version no attempt is made to control the measurement interval to be an integral number of rebalance pulse widths. In this case $\Delta\varphi$ is regular but we consider it a "random constant" and again use Eq. (3.2-54) as a "typical value" approximation to Eq. (3.2-58)).

Some approximate formulas for the characteristic frequency and amplitude and the resulting rms measurement error are assembled in Table 3.2-6. Results are given for binary, ternary and time-modulation rebalancing schemes. In each case the expressions for ν_α and A_α in the first two rows are substituted into Eq. (3.2-61) to yield the expressions for σ_e in the third column.

In a binary rebalance loop the essential nonlinearity is a two-level switch which causes the rebalance torque command to switch between full positive and full negative values. The expressions for ν_α and A_α are based on describing function analysis and are derived in Ref. 2. They represent the limit cycle frequency and amplitude which exist even in the absense of an input. The approximate formulas given for A_α and σ_e are

TABLE 3.2-6

CHARACTERISTIC FREQUENCY AND AMPLITUDE AND TEST MEASUREMENT ERROR IN PULSE REBALANCE LOOPS

	Frequency ν_α	Amplitude A_α	Individual Measurement Error $\sigma_e = C A_\alpha \sqrt{\tau_f^2 \nu_\alpha^2 + 1}$
Binary Loop	$\frac{1}{\sqrt{\tau_f \tau_d}}$	$\frac{4}{\pi} \frac{M_{tg}}{C} \left(\frac{\tau_f \tau_d}{\tau_f + \tau_d}\right)$ $\cong \frac{4}{\pi} \frac{M_{tg}}{C} \tau_d$	$\frac{4}{\pi} M_{tg} \left(\frac{\tau_f \tau_d}{\tau_f + \tau_d}\right) \sqrt{\frac{\tau_f}{\tau_d} + 1}$ $\cong \frac{4}{\pi} M_{tg} \sqrt{\tau_f \tau_d}$
Ternary Loop*	$\frac{\eta}{\sqrt{\tau_f \tau_d}}$	$\frac{2}{\pi} \frac{M_{tg}}{C} \left(\frac{\tau_f \tau_d}{\tau_f + \tau_d}\right)$ $\cong \frac{2}{\pi} \frac{M_{tg}}{C} \tau_d$	$\frac{2}{\pi} M_{tg} \left(\frac{\tau_f \tau_d}{\tau_f + \tau_d}\right) \sqrt{\frac{\tau_f \eta^2}{\tau_d} + 1}$ $\cong \frac{4}{\pi} M_{tg} \frac{\eta}{2} \sqrt{\tau_f \tau_d}$
Time-Modulation Loop	$\frac{2\pi}{T_p}$	$\frac{4}{\pi} \frac{M_{tg}}{C} \frac{T_p}{2\pi} \frac{1}{\sqrt{\left(\frac{2\pi \tau_{tg}}{T_p}\right)^2 + 1}} \frac{1}{\sqrt{\left(\frac{2\pi \tau_f}{T_p}\right)^2 + 1}}$ $\cong \frac{4}{\pi} \frac{M_{tg}}{C} \frac{T_p^2}{4\pi^2 \tau_f}$	[for $h \neq n T_p$] $\frac{4}{\pi} M_{tg} \frac{T_p}{2\pi} \frac{1}{\sqrt{\left(\frac{2\pi \tau_{tg}}{T_p}\right)^2 + 1}}$ $\cong \frac{4}{\pi} M_{tg} \frac{T_p}{2\pi}$
			[for $h = n T_p$] $\sigma_e = M_{tg} \frac{T_i}{\sqrt{6}}$

*See Fig. 3.2-7 for value of η.

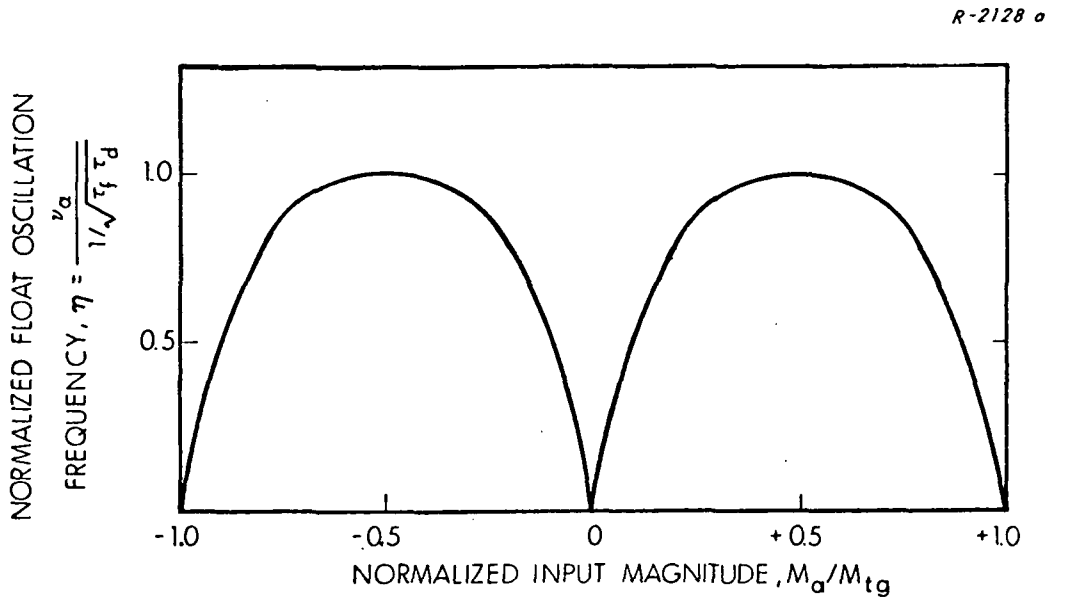

a) TERNARY LOOP

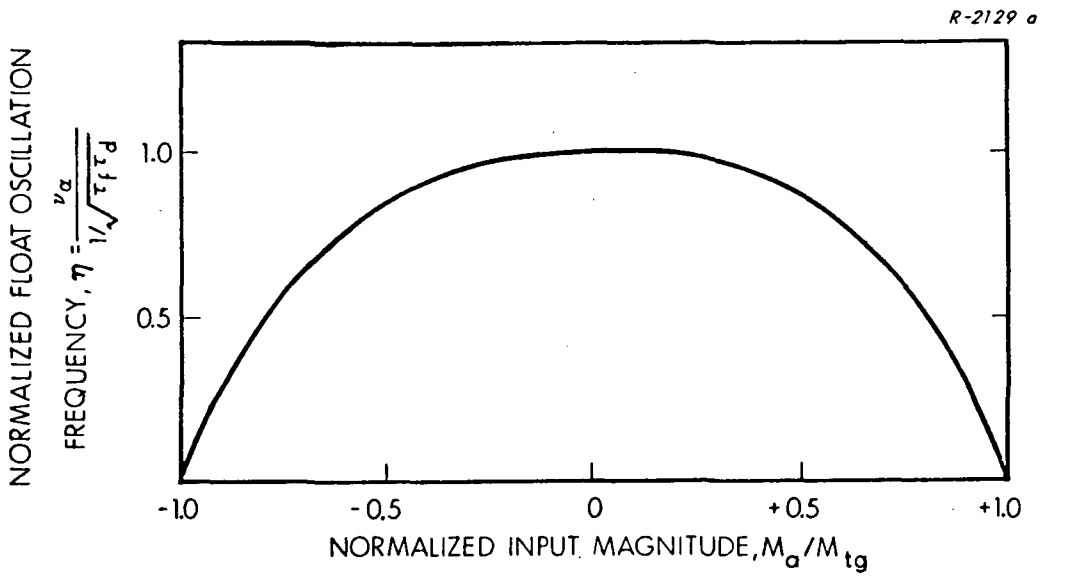

b) BINARY LOOP

Figure 3.2-7 Frequency of Oscillation versus Input Level for Ternary and Binary Rebalance Loops

based on the assumption that the float time constant, τ_f, is much greater than the torque delay time constant, τ_d (see later discussion of relationship of τ_d to τ_{tg}).

In a ternary rebalance loop the essential nonlinearity is a three-level switch with deadzone 2δ. Ref. 2 shows that the ternary loop will not limit cycle in the absense of an input if δ is chosen to satisfy the following inequality:

$$\delta > \frac{2}{\pi} K_{sg} \frac{M_{tg}}{C} \left(\frac{\tau_f \tau_{tg}}{\tau_f + \tau_{tg}} \right) \qquad (3.2\text{-}64)$$

When a non-zero input, $M_a = H \omega_i$, is applied to the loop it causes a torque generator on-time duty cycle which, on the average, balances the input torque. Appendix F develops the characteristic frequency and amplitude of this input-dependent oscillation. This development is based partly on the assumption that Eq. (3.2-64) is satisfied and, therefore, when an input (say a positive value of M_a) is applied, the torque level switches alternately between zero and $+ M_{tg}$. The variation of the frequency of float oscillation (normalized by $1/\sqrt{\tau_f \tau_d}$) with the input torque level (normalized by M_{tg}) is shown at the top of Fig. 3.2-7. The characteristic frequency varies markedly with input in the vicinity of zero and maximum input magnitudes, but is relatively insensitive to input over two broad regions centered at $M_a / M_{tg} = \pm 1/2$. In these mid-regions the frequency is the same as that already given for the binary case and is equally well explained by describing function analysis. The parameter η, which is included in the expression in Table 3.2-6 for the ternary case, is always less than or equal to one. This parameter represents the variation of ν_α from the no-input binary limit cycle frequency (as predicted by describing function theory) for small and large input magnitudes. Actually, a

similar deviation occurs in the binary case for large inputs, as shown at the bottom of Fig. 3.2-7. (The analysis given in Appendix F applies equally well to the binary case.) It is also shown in Appendix F that the amplitude of the float angle oscillations in the ternary case is one half that in the binary case (if both have the same torque level, M_{tg}). Thus, for small to medium inputs the resulting rms measurement error is less in the ternary case by the factor $\eta/2$, which is always less than or equal to one half.

The development in Appendix F does not involve torque lag τ_d directly, but rather uses a fixed delay time, T_D, which is meant to account for the delay in switching from one torque level to another, due to both the sampling of the float angle indication and the lag associated with the torque generator itself. The resulting empirical formula for characteristic frequency, involving T_D, is then shown to be nearly identical to the describing function formula, involving τ_{tg} the time constant associated with torque generator dynamics. (The derivation of the latter formula ignored delays due to sampling.) We have constructed Table 3.2-6 using the new parameter τ_d, which takes both effects into account. For sampling interval T_i the average delay due to sampling is $T_i/2$. Therefore a reasonable expression for the delay time constant is:

$$\tau_d = \tau_{tg} + T_1/2 \qquad (3.2\text{-}65)$$

In a time-modulation rebalance loop the feedback torque is forced to oscillate between $+M_{tg}$ and $-M_{tg}$ with a fixed, clock-controlled period, T_p. The formula for the amplitude of the float angle oscillation given in Table 3.2-6 is obtained by considering the square wave command to the torque generator to be represented by the fundamental of amplitude $4M_{tg}/\pi$ and computing the attenuation of that fundamental after passing it

through an integrator, the two first order lags associated with the time constants τ_f and τ_{tg}, and the gain 1/C. The first formula for σ_e given in Table A corresponds to the situation where the test measurement intervals are controlled by a different clock than that controlling the timing of the rebalance pulses. In this case the phase angle differences, $\Delta\varphi$, between the start and end of each measurement interval are not multiples of 2π. The approximate formulas for A_α and σ_e are based on the assumptions that T_p is much less than $2\pi\tau_f$ and much greater than $2\pi\tau_{tg}$. (That is, the forced oscillation period is assumed to be small compared to float lag but large compared to torquer lag.)

On the other hand, if the measurement intervals were carefully controlled to contain an integral number of torque cycles ($h = n T_p$), then approximately the same phase angle would occur at the end of each measurement interval. In this case the error given by Eq. (3.2-48), is for the most part eliminated, and an appropriate expression for the rms measurement error is the final one given in Table 3.2-6. This is the simple "error due to quantization" formula discussed at the beginning of this section and derived previously for the analog rebalance case with quantized output. In this case the quantization level, q, is given by Eq. (3.2-40) where T_i is the spacing between possible switching times. (For example, $T_i = T_p/64$ in the version of the time-modulation loop used in the Lunar Module Abort Sensor Assembly -- thus, $q = M_{tg} T_p/64$.)

Summary – We have shown how to relate test errors due to quantization to test time and test motion frequency via Eqs. (3.2-41) and (3.2-42) and to rebalance loop parameters by the expressions assembled in Table 3.2-6 for three types of pulse rebalance loops. These formulas

are used in some numerical examples in Section 3.3.2. Test errors of this type in the ternary case are somewhat lower than in the binary case because of a smaller amplitude and (for small inputs) a smaller frequency of float angle oscillation. Two expressions have also been derived for the time-modulation case, their appropriateness depending on how the test measurement intervals are controlled.

3.2.6 Random High Frequency Errors

In Appendix C the first stage (see Fig. 3.1-3, stage Ia) of the the data processing problem is formulated as a problem in linear estimation, for which the Kalman filter is an optimal solution. The "state variables" to be estimated for each single-axis test are the seven Fourier coefficients. That is, the data processing function is to determine sets of Fourier coefficients, but not by Fourier analysis. This formulation is particularly useful in illuminating the effects of random high frequency measurement noise and process noise on the errors in estimating the state variables and on the test durations required to achieve given levels of accuracy.

The development of the first half of Appendix C is somewhat similar to the development of quantization effects for sinusoidal harmonic testing in Section 3.2.4, except that a continuous, rather than discrete, linear estimation formulation is employed. In both cases the estimation errors due to measurement noise decrease as $1/\sqrt{T}$.

Measurement errors are differences between recorded or processed measurements (gyro outputs, table angles, etc.) and the actual quantities they are supposed to represent. In the case at hand the primary measured quantity is torque produced by the torque generator in the rebalance loop of a gyro. Measurement noise refers to random changes or fluctuations in the error in this torque measurement, such that two values of the error a short interval, τ, apart are uncorrelated (or tending so as τ increases). The definition does not include a bias measurement error, nor any cyclicly repeating error such as that due to torquer nonlinearity. Process noise relates to random changes in the state variables (Fourier coefficients) themselves. These can occur because the gyro parameters or the test motion quantities appearing in the state variable definitions are not stationary. In cases where table angle measurements are produced by the test, the errors in these quantities can also be treated as a source of process noise (see Appendix C).

The development of Appendix C leads to some approximate formulas which are useful in predicting achievable estimation error variances. The key parameters are the scalar r and the matrix Q which characterize the measurement noise and process noise, respectively. The random part of the measurement error v(t) is assumed to be Gaussian white noise with zero mean and covariance $r\delta(t-\tau)$ where δ is the Dirac delta function:

$$\overline{v(t)} = 0; \qquad \overline{v(t)\, v(\tau)} = r\delta(t-\tau) \tag{3.2-66}$$

The process noise is a seven-dimensional vector quantity $\underline{u}(t)$ representing the rates of change of the seven Fourier coefficients. It is also assumed to be Gaussian white noise with:

$$\overline{\underline{u}(t)} = 0; \qquad \overline{\underline{u}(t)\,\underline{u}(\tau)^T} = Q\,\delta(t-\tau) \tag{3.2-67}$$

Choosing realistic values for these quantities requires the kind of knowledge expressed in the autocorrelation functions of the random processes involved. Some useful formulas (See page 147 of Ref. 7 or Ref. 8.) are:

$$r = 2\,\sigma_v^2\,\tau_v \tag{3.2-68}$$

$$q_{ii} = 2\,\sigma_{u_i}^2\,\tau_u \tag{3.2-69}$$

where:

σ_v^2 = the measurement noise variance

$\sigma_{u_i}^2$ = the process noise variance of the i^{th} state variable

τ_v = the correlation time of the measurement noise

τ_u = the correlation time of the process noise

The values of the off-diagonal elements of the Q matrix depend on the correlation between changes in the Fourier coefficients. If test motion variations are the major cause of process noise, the several components of the noise vector will be highly correlated. That is, the off-diagonal

elements of the Q matrix will be non-zero and significant. If, on the other hand, gyro parameter changes are the major cause of process noise, we would expect very little correlation between the components of $\underline{u}$. (These comments are discussed in some detail in Appendix C.)

Some time after the start of a test the estimation error variance, σ_i^2, of the i^{th} state variable (Fourier coefficient) reaches an equilibrium condition, in which the information coming in by virtue of new measurements is balanced by the information being lost due to process noise. A conservative formula for the final (equilibrium) value is:

$$\sigma_i^2 = \sqrt{2\, r\, q_{ii}} \tag{3.2-70}$$

The error formulas given in the third row of Table 3.2-2 are based on Eq. (3.2-70) and the assumption that process noise is caused by random fluctuations in the test rate magnitude. Equation (3.2-70) is plotted parametrically in Fig. 3.2-8, along with a companion formula for useful test duration discussed in Section 3.3. A more accurate formula, including the effect of correlated process noise components, is:

$$\sigma_i^2 = \sqrt{2\, r\, q_{ii} \left(1 - c_{ij}^2\right)} \tag{3.2-71}$$

where $i \neq j$. The coefficient c_{ij} is a measure of correlation between the i^{th} and j^{th} components of process noise:

$$c_{ij} = \frac{q_{ij}}{\sqrt{q_{ii}\, q_{jj}}} \tag{3.2-72}$$

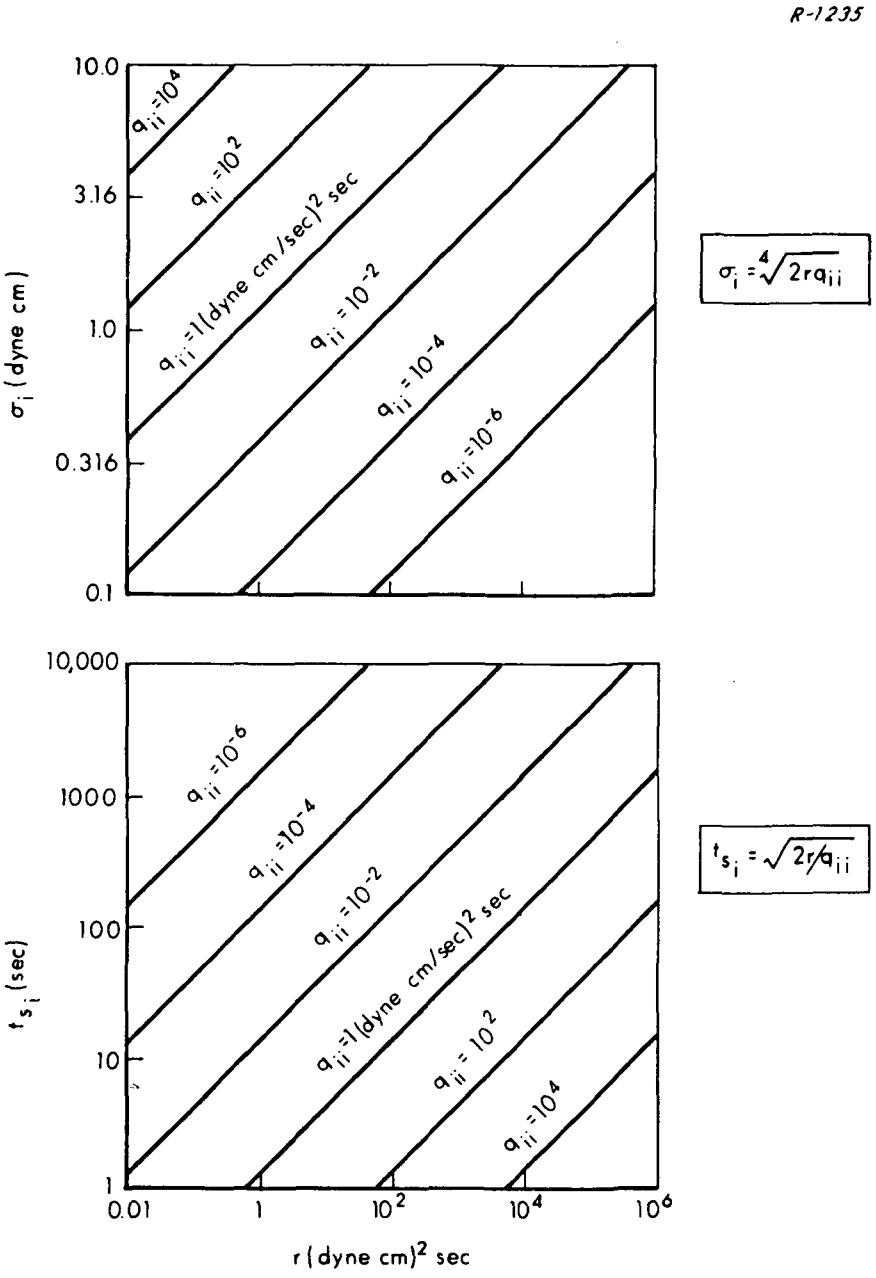

Figure 3.2-8 Final Accuracy and Test Time: Random Errors

and the j^{th} component corresponds to the largest or dominant component of process noise appearing in the test. High correlations between certain process noise components, therefore, helps to reduce certain estimation errors.

Equation (3.2-71) can be combined with Eqs. (3.2-68) and (3.2-69) to yield an expression which is more complicated but which only contains terms which have a physical interpretation. Thus:

$$\sigma_i^2 = 2\,\sigma_v\,\sigma_{u_i}\sqrt{2\,\tau_v\,\tau_u\left(1 - c_{ij}^2\right)} \qquad (3.2\text{-}73)$$

The Kalman filter formulation developed in Appendix C is potentially significant in two ways. First, it provides the above equations, along with related equations presented in Section 3.3, which are useful in predicting the achievable test accuracy and required test duration. Second, it provides a set of optimal data processing equations which could be used for reducing actual test data. A connection between this procedure and Fourier analysis is also developed in Appendix C. The data processing alternatives are discussed further in Section 3.4.

3.2.7 Rebalance Loop Errors

A torquer scale factor error is an error in our knowledge of the linear gain of the rebalance loop. It is usually given as a dimensionless ratio (ϵ_{SC} = so many parts per million). The error formulas in the eighth row of Table 3.2-2 simply express the fact that the resulting errors in all parameter estimates will be equal to their actual values times this ratio.

Torquer nonlinearity causes significant estimation errors for both constant rate and sinusoidal testing in the three cases which involve a large gyroscopic torque, $H\omega_i$ (when $c_i = 1$ or $1/\sqrt{2}$). Noticeable errors may also occur in sinusoidal testing in the three cases which experience a sizeable output axis inertia torque, $I_{oo}\omega_o$ (when $c_o = 1$ or $1/\sqrt{2}$). Observable quantities which may experience significant errors due to these effects are indicated by the symbol (NL) in Table 3.2-5.

Figure 3.2-9 shows two types of nonlinear elements acting on input functions, x(t), and producing output functions, y(t). We consider a nonlinear function, y(x), which combines the two types shown into one equation as follows:

$$y = x + \epsilon_1 |x| - \epsilon_2 |x| x - \epsilon_3 x^3 \qquad (3.2\text{-}74)$$

The first term in Eq. (3.2-74) represents the desired, linear character of the torquer loop. The next term ($\epsilon_1 |x|$) represents a torquer asymmetry which is an example of an "even-valued" nonlinearity. This type of torquer characteristic is most likely to be significant in the pulse rebalanced case. The last two terms ($-\epsilon_2 |x| x$ and $- \epsilon_3 x^3$) represents an "odd-valued" nonlinearity. This type is most likely to characterize an analog rebalance torque loop.

For sinusoidal testing the input function is:

$$x(t) = A \sin \omega t \qquad (3.2\text{-}75)$$

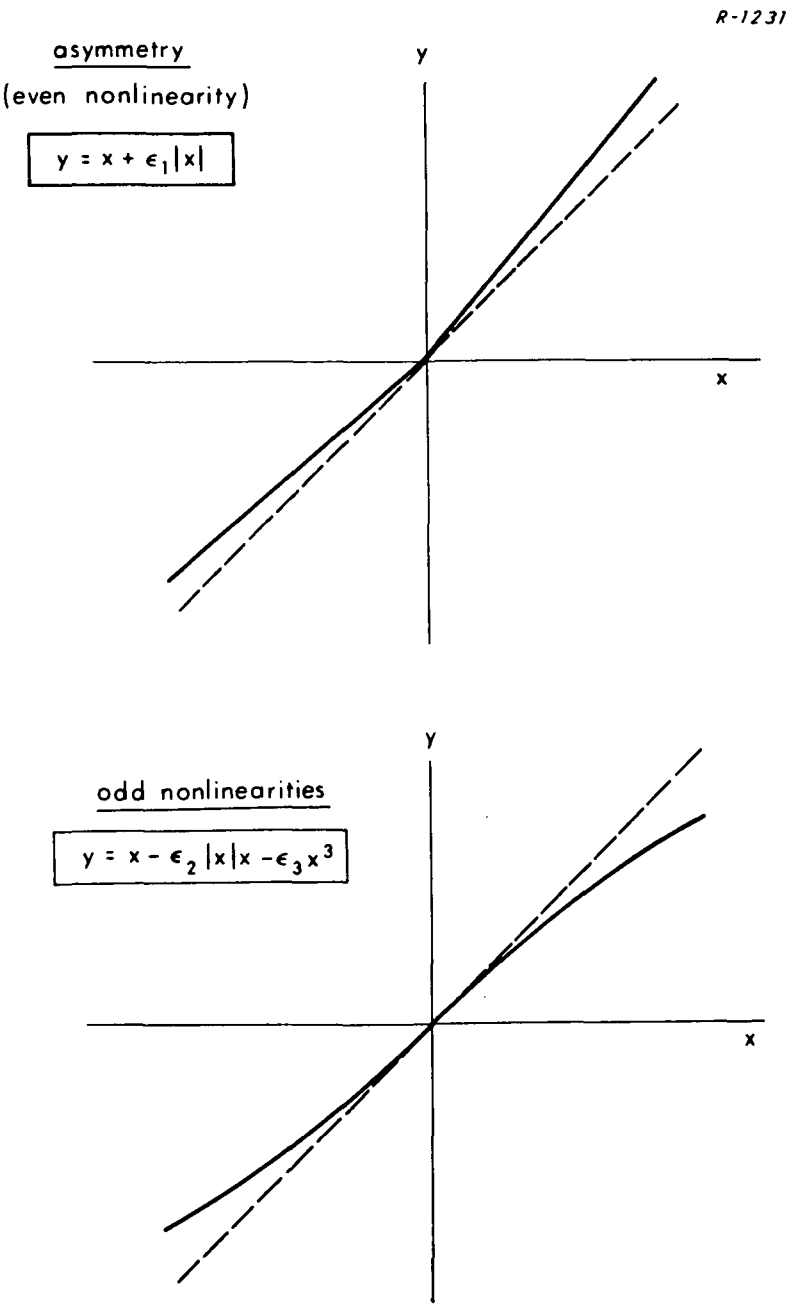

Figure 3.2-9 Torquer Nonlinearities

and the output function, which must also be periodic, can be represented by the trigonometric series:

$$y(t) = b_o + a_1 \sin \omega t + b_1 \cos \omega t + a_2 \sin 2\omega t + b_2 \cos 2\omega t + \ldots \tag{3.2-76}$$

Substitution of Eq. (3.2-75) into Eq. (3.2-74) and Fourier analysis of the resulting expression for y(t) yields the Fourier coefficients given in Table 3.2-7. Thus, the output is equal to the input plus a deviation function, d(t):

$$y(t) = A \sin \omega t + d(t) \tag{3.2-77}$$

where:

$$d(t) = A\left[\frac{2\epsilon_1}{\pi} - \left(\frac{8}{3}\frac{A}{\pi}\epsilon_2 + \frac{3}{4}A^2\epsilon_3\right)\sin \omega t - \frac{4}{3}\frac{\epsilon_1}{\pi}\cos 2\omega t + \left(\frac{8}{15}\frac{A}{\pi}\epsilon_2 + \frac{1}{4}A^2\epsilon_3\right)\sin 3\omega t - \frac{4}{15}\frac{\epsilon_1}{\pi}\cos 4\omega t + \ldots\right] \tag{3.2-78}$$

Figure 3.2-10 shows a linear gyro loop in which the deviation function, d(t), has been added in order to account for the effect of a slightly nonlinear characteristic in the feedback path. The transfer function relating the input $M_a(t)$ to the output, $e_r(t)$ is:

$$\frac{\tilde{e}_r(s)}{\tilde{M}_a(s)} = \frac{K_1\left(\tau_2 s + 1\right)}{s\left(\tau_1 s + 1\right)\left(\tau_2 s + 1\right) + K_1} \tag{3.2-79}$$

TABLE 3.2-7

NONLINEARITY EFFECTS ON SINUSOID

$$x = A \sin \omega t$$

$$y = x + \epsilon_1 |x| - \epsilon_2 |x| \, x - \epsilon_3 x^3$$

$$= b_o + a_1 \sin \omega t + b_1 \cos \omega t$$

$$+ a_2 \sin 2\omega t + b_2 \cos 2\omega t$$

$$+ \ldots$$

	Nominal	ϵ_1 Effect	ϵ_2 Effect	ϵ_3 Effect
$b_o =$	0	$\frac{2A}{\pi} \epsilon_1$	—	—
$a_1 =$	A	—	$-\frac{8}{2} \frac{A^2}{\pi} \epsilon_2$	$-\frac{3}{4} A^3 \epsilon_3$
$b_1 =$	0	—	—	—
$a_2 =$	0	—	—	—
$b_2 =$	0	$-\frac{4}{3} \frac{A}{\pi} \epsilon_1$	—	—
$a_3 =$	0	—	$+\frac{8}{15} \frac{A^2}{\pi} \epsilon_2$	$+\frac{1}{4} A^3 \epsilon_3$
$b_3 =$	0	—	—	—

R-261

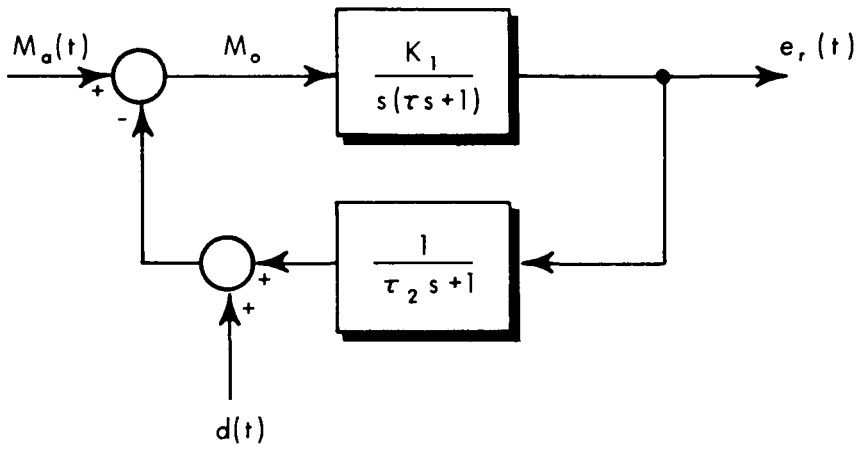

Figure 3.2-10 Linear Sensor Loop with Disturbance Function Added

for low frequencies this becomes:

$$\frac{e_r}{M_a} \cong 1 \qquad (3.2\text{-}80)$$

and, similarly:

$$\frac{e_r}{d} \cong -1 \qquad (3.2\text{-}81)$$

Therefore:

$$e_r(t) \cong M_a(t) - d(t) \qquad (3.2\text{-}82)$$

which simply states that the net torque M_o is kept close to zero by the action of the loop.

For a sinusoidal test motion, W sin ωt, the first approximation to the output (neglecting the effect of the deviation function) is

$$e_r(t) = M_a(t) \cong HWc_i \sin \omega t + I_{oo}\, \omega W\, c_o \cos \omega t \qquad (3.2\text{-}83)$$

and the deviation function is

$$d(t) = HWc_i\left[\frac{2\epsilon_1}{\pi} - \left(\frac{8}{3}\frac{HWc_i}{\pi}\epsilon_2 + \frac{3}{4}H^2W^2c_i^2\epsilon_3\right)\sin \omega t - \frac{4}{3}\frac{\epsilon_1}{\pi}\cos 2\omega t + \ldots\right]$$

$$+ I_{oo}\omega Wc_o\left[\frac{2\epsilon_1}{\pi} - \left(\frac{8}{3}\frac{I_{oo}\omega Wc_o}{\pi}\epsilon_2 + \frac{3}{4}I_{oo}^2\omega^2W^2c_o^2\epsilon_3\right)\cos \omega t\right.$$

$$\left. + \frac{4}{3}\frac{\epsilon_1}{\pi}\cos 2\omega t + \ldots\right] \qquad (3.2\text{-}84)$$

A better approximation to the output is, [using Eq. (3.2-82)]:

$$e_r(t) = -\left[2\frac{HW}{\pi}c_i\epsilon_i + \frac{2I_{oo}\omega W}{\pi}c_0\epsilon_1\right]$$

$$+\left\{HWc_i + \left[\frac{8}{3}\frac{\left(HWc_i\right)^2}{\pi}\epsilon_2 + \frac{3}{4}\left(HWc_i\right)^3\epsilon_3\right]\right\}\sin \omega t$$

$$+\left[\frac{8}{3}\frac{\left(I_{oo}\omega Wc_o\right)^2}{\pi}\epsilon_2 + \frac{3}{4}\left(I_{oo}\omega Wc_o\right)^3\epsilon_3\right]\cos \omega t$$

$$+\left[\frac{4}{3}\frac{HWc_i}{\pi}\epsilon_1 - \frac{4}{3}\frac{I_{oo}\omega Wc_o}{\pi}\epsilon_1\right]\cos 2\omega t$$

$$+ \ldots \qquad (3.2\text{-}85)$$

Since the nominal output is $HWc_i \sin \omega t$, the expressions in the brackets in Eq. (3.2-85) represent the errors in the Fourier coefficient estimates, $E(B)$, $E(S_1)$, $E(C_1)$ and $E(C_2)$, due to torquer nonlinearity.

The error formulas given in the ninth row of Table 3.2-2, for sinusoidal testing, are obtained by substituting the above expressions into the following relations:

$$\left.\begin{aligned} \delta\mu &= \frac{1}{\omega W} E(C_1) \\ \delta\lambda &= \frac{1}{W} E(S_1) \end{aligned}\right\} \text{sinusoidal harmonic testing}$$

$$\delta\gamma = \begin{cases} \dfrac{2}{W^2} E(C_2) \\ \dfrac{2}{W^2} E(B) \end{cases} \quad \text{sinusoidal averaging} \qquad (3.2\text{-}86)$$

These formulas can also be used to correct the results of a vibration test if the torquer nonlinearity is calibrated in advance by means of a series of constant angular rate tests. In that case the final test errors are proportional to the error in the knowledge of the nonlinearity, rather than the nonlinearity itself.

The error formulas for constant rate testing are obtained by observing that we are operating at two points on the same side of the nonlinear gain curve. Since W_2 is assumed to be much

smaller than W_1, we take the significant torque measurement error to be:

$$\delta M_1 = - \epsilon_2 M_1^2 - \epsilon_3 M_1^3$$

$$= - \epsilon_2 \left(\lambda W_1 + \gamma W_1^2\right)^2 - \epsilon_3 \left(\lambda W_1 + \gamma W_1^2\right)^3 \qquad (3.2\text{-}87)$$

Substitution of Eq. (3.2-59) into Eqs. (3.2-7) and (3.2-8) yields the formulas given in the ninth row of Table 3.2-2 for constant rate testing.

3.2.8 Errors Due to Parameter Changes

Error formulas showing the effect of run-to-run shifts in parameter values during constant rate testing are obtained by letting λ and γ take on different values during the runs (W_1 and W_2) and using Eqs. (3.2-3) and (3.2-4) to form estimates, $\hat{\lambda}$ and $\hat{\gamma}$. Thus:

$$\lambda_2 = \lambda_1 + \lambda_{SH} \qquad (3.2\text{-}88)$$

$$\gamma_2 = \gamma_1 + \gamma_{SH} \qquad (3.2\text{-}89)$$

and

$$\left(M_a - M_c\right)_1 = M_1 = \lambda_1 W_1 + \gamma_1 W_1^2 \qquad (3.2\text{-}90)$$

$$\left(M_a - M_c\right)_2 = M_2 = \lambda_2 W_2 + \gamma_2 W_2^2 \qquad (3.2\text{-}91)$$

Therefore:

$$\hat{\lambda} = \frac{\left(\lambda_2 W_2 + \gamma_2 W_2^2\right)\frac{W_1}{W_2} - \left(\lambda_1 W_1 + \gamma_1 W_1^2\right)\frac{W_2}{W_1}}{W_1 - W_2}$$

$$= \lambda_1 + \left(\frac{W_1}{W_1 - W_2}\right)\lambda_{SH} + \left(\frac{W_1 W_2}{W_1 - W_2}\right)\gamma_{SH} \qquad (3.2\text{-}92)$$

and

$$\hat{\gamma} = \frac{\left(\lambda_1 W_1 + \gamma_1 W_1^2\right)\frac{1}{W_1} - \left(\lambda_2 W_2 + \gamma_2 W_2^2\right)\frac{1}{W_2}}{W_1 - W_2}$$

$$= \gamma_1 - \left(\frac{1}{W_1 - W_2}\right)\lambda_{SH} - \left(\frac{W_2}{W_1 - W_2}\right)\gamma_{SH} \qquad (3.2\text{-}93)$$

With $W_1 >> W_2$, we can write the approximate formulas:

$$\delta\lambda = \hat{\lambda} - \lambda_1 \cong \lambda_{SH} + W_2\,\gamma_{SH} \qquad (3.2\text{-}94)$$

$$\delta\gamma = \hat{\gamma} - \gamma_1 \cong -\frac{1}{W_1}\lambda_{SH} - \frac{W_2}{W_1}\gamma_{SH} \qquad (3.2\text{-}95)$$

A shift, M_{cSH}, in the constant (zero input rate) torque between runs has the same effect as a measurement error, δM_2. Thus we can use Eqs. (3.2-9) and (3.2-10) to obtain:

$$\delta\lambda = \frac{1}{W_2} M_{cSH} \tag{3.2-96}$$

$$\delta\gamma = \frac{-1}{W_1 W_2} M_{cSH} \tag{3.2-97}$$

The error formulas in the last row of Table 3.2-2 are obtained by combining Eqs. (3.2-94) and (3.2-95) with Eqs. (3.2-96) and (3.2-97), respectively.

3.3 TEST DURATION

The determination of an appropriate test time, T, is governed by the estimation error components which vary with T. These are primarily the error due to quantization and the error due to measurement noise (see the seventh and tenth rows of Table 3.2-2). We recall that errors due to quantization decrease as 1/T for constant rate testing and sinusoidal averaging, and as $1/\sqrt{T}$ for sinusoidal harmonic testing; errors due to measurement noise decrease, initially, as $1/\sqrt{T}$ in all three cases. For sinusoidal harmonic testing the quantization effect can be considered as a component of measurement noise. The measurement noise effect does not continue to decrease as $1/\sqrt{T}$ without limit, but reaches a state of equilibrium where measurement noise and process noise are in balance (see the third row of Table 3.2-2).

In general all errors can be grouped into three classes, as illustrated in Fig. 3.3-1 where σ is the one-sigma estimation error corresponding to the observable quantity in question. The constant term, k_b, represents the sum of all stationary components, such as the effects of bias errors, cyclic errors and run-to-run shifts. The curve labeled $k_r/\sqrt{T}$ represents the combined effect of measurement noise and process noise. The curve labeled k_q/T represents the effect of quantization during constant rate testing and sinusoidal averaging; this curve is not present for sinusoidal harmonic testing. A reasonable rule for selecting T is to choose a large enough value so that either:

1) Both kinds of time-dependent esimation errors are less than the stationary errors.

or:

2) The equilibrium level has been reached for estimation errors due to measurement-noise/process-noise and that level exceeds the remaining time-dependent term (k_q/T) as well as the stationary term (k_b).

If more than one observable quantity is to be estimated, as in sinusoidal harmonic testing, the above rule should be applied to each of them in turn, and the largest resulting value for T used as the test time.

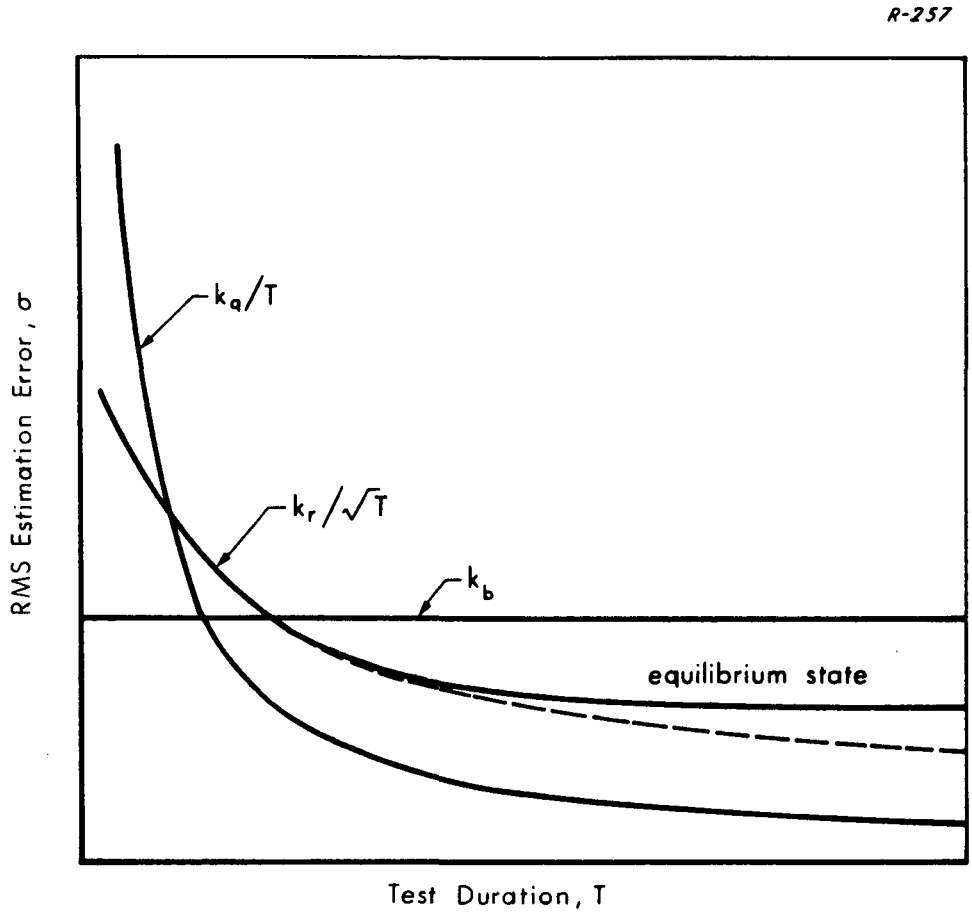

Figure 3.3-1 Time-Dependent Test Errors

3.3.1 Choice of Sample Interval

The effect of the size of the sample interval, h, or number of samples per cycle, $N = 2\pi/\omega h$, for sinusoidal harmonic testing is suggested by the form of the quantization error formulas derived in Section 3.2.4. The standard deviation of the estimate of each observable quantity is given by:

$$\sigma_M = \frac{q}{\sqrt{6}} \omega \sqrt{\frac{2h}{T}} \qquad (3.3\text{-}1)$$

Note that $q/\sqrt{6}$ is the rms error in each sample count and T/h is the total number of data samples taken. Thus, the estimation error is directly proportional to the single sample error and inversely proportional to the square root of the number of samples. For a given test time, T, the error is proportional to the square root of h, indicating that h should be selected as small as possible in order to minimize errors due to quantization. On the other hand, in order to ease the data processing task, h should be selected as large as possible. However, it should not be selected so large that it is impossible to extract the harmonics of the signal. For example, if h = T, the total test time, the procedure is reduced to sinusoidal averaging. In conclusion, the number of samples per cycle should be at least enough to define the first two or three harmonics. A larger number (smaller h) than that will decrease the parameter estimation errors due to quantization but increase the data processing requirements. In the numerical examples given in Section 3.5 the values, N = 10 samples per cycle and T = 100 sec., are used. In those examples the error due to quantization is the largest contributor in only two cases (the estimation of the μ terms when the test motion axis is i and i/s).

3.3.2 Effects of Quantization: Examples

This section presents some illustrative numerical examples relating the data resolution or quantization level to total test time and parameter estimation errors. For a given gyro wheel momentum, H, the quantization level, q(dyne cm sec), can be converted to an equivalent gyro output quantization level, $\Delta\theta(\widehat{sec})$. Similarly, the errors in estimating average torque, σ_M (dyne cm), can be converted to an

equivalent gyro drift rate, σ_D(deg/hr). The results are presented in terms of both σ_M and σ_D, assuming a wheel angular momentum H, of 10^5 gm cm^2/sec. The assumed test motions are, for constant rate tests:

$$W_1 = 0.26 \text{ rad/sec} \quad (15 \text{ deg/sec})$$

$$W_2 = 0.017 \text{ rad/sec} \quad (1 \text{ deg/sec})$$

and, for sinusoidal tests:

$$W = 0.26 \text{ rad/sec} \quad (15 \text{ deg/sec})$$

$$\omega = 2\pi \text{ rad/sec} \quad (1 \text{ Hz})$$

Analog Rebalanced Sensors – Consider an analog loop in which the output is quantized with resolution:

$$q = 4.85 \text{ dyne cm sec}$$

This is equivalent to a 10 $\widehat{\text{sec}}$ rotation about the gyro input axis. Table 3.3-1 presents the results of computations based on the quantization error formulas (see Table 3.2-2) for several values of test time. For constant rate and sinusoidal average testing the one-sigma error in the average torque measurement is:

$$\sigma_M = \frac{q}{\sqrt{6}} \frac{1}{T} \text{ dyne cm} \qquad (3.3\text{-}2)$$

TABLE 3.3-1

EXAMPLE ERRORS DUE TO QUANTIZATION: ANALOG REBALANCING

$q = 4.85$ dyne cm

$\Delta\theta = q/H = 10$ $\widehat{sec}$ per pulse

T (sec)	σ_M (dyne cm)	σ_D (deg/hr)	Constant Rate		Sinusoidal Averaging
			σ_λ (dy cm sec)	σ_γ (dy cm sec^2)	σ_γ (dy cm sec^2)
10	0.198	0.41	11.6	44.7	5.86
100	0.0198	0.041	1.16	4.47	0.586
1000	0.00198	0.0041	0.116	0.447	0.0586
Sinusoidal Harmonic Testing					
T (sec)	σ_M (dyne cm)	σ_D (deg/hr)	σ_μ (dy cm sec^2)	σ_λ (dy cm sec)	σ_γ (dy cm sec^2)
10	1.76	3.60	1.08	6.77	52.1
100	0.556	1.14	0.70	2.70	16.45
1000	0.176	0.36	0.108	0.677	5.21
10000	0.0556	0.114	0.07	0.27	1.65

The equivalent gyro drift rate is:

$$\sigma_D = \frac{\sigma_M(57.3)(3600)}{H} \text{ deg/hr} \qquad (3.3\text{-}3)$$

The corresponding parameter estimation errors are:

$$\left.\begin{aligned} \sigma_\lambda &= \frac{1}{W_2}\,\sigma_M \\ \sigma_\gamma &= \frac{1}{W_1 W_2}\,\sigma_M \end{aligned}\right\} \text{constant rate tests} \qquad (3.3\text{-}4),\ (3.3\text{-}5)$$

$$\left.\sigma_\gamma = \frac{2}{W^2}\,\sigma_M\right\} \text{sinusoidal averaging tests} \qquad (3.3\text{-}6)$$

For sinusoidal harmonic testing the rms errors in the Fourier coefficient estimates are:

$$\sigma_M = \frac{q}{\sqrt{6}}\,\omega\,\sqrt{\frac{2h}{T}} \qquad (3.3\text{-}7)$$

The values given in the lower part of Table 3.3-1 are based on the assumption that 10 samples per second are taken; that is, the sample interval h is 0.1 sec. The equivalent drift rate is again given by Eq. (3.3-3). The corresponding parameter estimation errors are:

$$\sigma_\mu = \frac{1}{\omega W}\,\sigma_M \qquad (3.3\text{-}8)$$

$$\sigma_\lambda = \frac{1}{W}\,\sigma_M \qquad (3.3\text{-}9)$$

$$\sigma_\gamma = \frac{2}{W^2}\,\sigma_M \qquad (3.3\text{-}10)$$

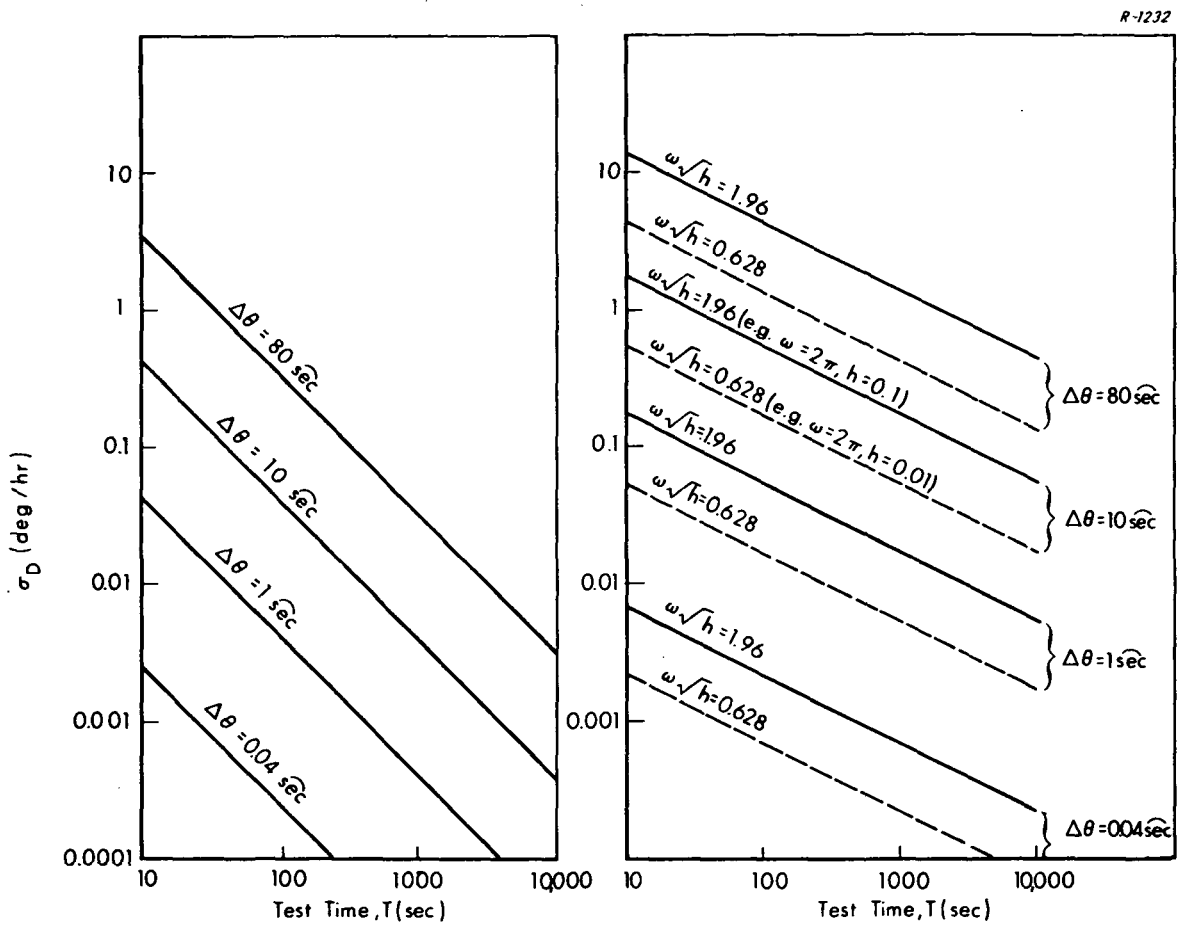

(a) Constant Rate and Sinusoidal Average Testing

(b) Sinusoidal Harmonic Testing

Figure 3.3-2 Effective Drift Rate Due to Quantization

Figure 3.3-2(a) plots σ_D versus test time for four values of quantization level, $\Delta\theta$. The two middle values (1 $\widehat{\text{sec}}$ and 10 $\widehat{\text{sec}}$) are comparable to single-pulse quantization levels for pulse rebalanced sensors. The extreme values (80 $\widehat{\text{sec}}$ and 0.04 $\widehat{\text{sec}}$) represent a range of quantization levels obtainable from an analog rebalanced gyro. For example if a voltage-to-frequency device with a full scale output rate of 5000 counts/sec is used, the high quantization level would be necessary for a maximum applied rate about the gyro input axis of 2 rad/sec, which causes a torque of:

$$M = \omega_i H = 2 \times 105 \text{ dyne cm}$$

Therefore, the device must be scaled to make:

$$q_{max} = \frac{2 \times 10^5}{5000} = 40 \text{ dyne cm sec}$$

and

$$\Delta\theta_{max} = \frac{q}{H} 2.06 \times 10^5 \cong 80 \widehat{\text{sec}}$$

The low quantization level would be possible for a test involving small torques only, such as an applied rate nominally about the gyro spin axis. If the maximum torque expected in this case is 100 dyne cm (see example values in Section 3.5), then the device can be scaled to make $\Delta\theta_{min} \cong 0.04$ sec. This points up a possible advantage in testing analog rebalanced sensors, as opposed to pulse rebalanced instruments. It may be easier, in the analog case, to rescale the data processing electronic equipment to take good advantage of situations involving only low levels of applied output axis torque. By such a rescaling the quantization effect may be reduced, with an attendant possibility of increased error due to torquer nonlinearity and signal generator noise.

For sinusoidal harmonic testing the error in the measurement of drift rate is proportional to the test motion frequency (ω) and to the square root of the sample interval (h). This dependence is shown in Fig. 3.3-2(b) where results are plotted for two values of the parameter, $\omega\sqrt{h}$, for each of the four quantization levels.

Pulse Rebalanced Sensors – It is highly desirable to test entire strapdown instruments, including their rebalance electronics. Since most accurate strapdown gyros and accelerometers are of the pulse rebalanced type, the primary test output will be quantized. The example calculations and curves discussed above apply equally well to testing pulse rebalanced sensors in so far as the "error due to quantization" is concerned. However, as discussed in Section 3.2.5, still larger errors associated with the oscillatory behavior of nonlinear pulse rebalance loops may also occur. Consider, for example, pulse rebalance sensors in which the loop parameters, test motion quantities and test time have the values given at the top of Table 3.3-2. The tabulated values for the characteristic frequency and amplitude of float angle oscillation and for the individual measurement errors are obtained by application of the formulas given in Table 3.2-6. The values for torque estimation errors are obtained via Eqs. (3.2-41) and (3.2-42) for average torque and harmonic component estimates, respectively. These may be related to errors in estimating the λ, γ and μ terms via Eqs. (3.3-4, 5 and 6) and Eqs. (3.3-8, 9 and 10) just as in the analog rebalanced case. The last column in Table 3.3-2 is included in order to relate the error due to loop dynamics to the error associated with the single pulse quantization level. The tabulated quantity is called the "effective loop quantization level;" it is the quantization level which would cause the rms measurement error, σ_e, already computed for a given set of loop parameters, if the two had the same relationship previously derived for the simple error due to quanitzation; namely:

$$\sigma_e = q_{eff} / \sqrt{6} \qquad (3.3\text{-}11)$$

TABLE 3.3-2

EXAMPLE ERRORS DUE TO QUANTIZATION: PULSE REBALANCING

$H = 10^5$ dyne cm sec
$C = 10^5$ dyne cm sec
$I_{oo} = 100$ gm cm^2
$\tau_f = 0.001$ sec
$\tau_{tg} = 0.0001$ sec
$\omega_{i_{max}} = 1$ rad/sec
$M_{tg} = H\,\omega_{i_{max}} = 10^5$ dyne cm
$T = 100$ sec
$h = 0.1$ sec
$\omega = 2\pi$ rad/sec
$W = 0.26$ rad/sec

Type of Rebalance Loop	Frequency ω_α (rad/sec)	Amplitude A_α (mrad)	Individual Measurement Error σ_e (dyne cm sec)	Estimation Error σ_M (dyne cm)		Effective Loop Quantization Level $\Delta\theta_{eff}$ ($\widehat{sec}$)
				Average Torque Estimate	Harmonic Component Estimate	
Binary	3162	0.116	38.5	0.385	10.8	194
Ternary $r = 0.26$ $\eta = 0.85$	2688	0.058	16.6	0.166	4.67	84
Time-Modulation $T_p = 0.001$ $T_i = T_p/64$	6283	0.027	$[h \neq nT_p]$ 17.2	0.172	4.82	87
			$[h = nT_p]$ 0.64	0.0064	0.18	3.2

Thus, converting q_{eff} to angular form:

$$\Delta\theta_{eff} = \sigma_e \sqrt{6}/H \qquad (3.3\text{-}12)$$

This quantity allows us to use the formulas and plots (Fig. 3.3-2) already developed for the analog torquing case. Note that for the binary and ternary loops as well as the time-modulation loop, when $h \neq nT_p$, the effective quantization level is considerably higher than a single pulse weight.

The lowest effective quantization level, by far, occurs in this example for the time-modulation rebalance case when the measurement interval is controlled to be an integral number of pulse widths. Among the other three cases the ternary loop has the lowest effective quantization level, due to its low characteristic frequency of oscillation.

3.3.3 Time to Reach Equilibrium

This section treats the question of how long it takes for estimation errors to reach a state of equilibrium, defined largely by the relative magnitudes of measurement noise and process noise; by filtering data taken over many cycles it is possible to reduce the effects of uncorrelated random errors. The formulation of the first stage of the data processing problem as one of linear estimation (see Appendix C) is useful in indicating the length of time over which it makes sense to filter the data; the state variables to be estimated in each single-axis vibration test are the seven Fourier coefficients.

Figure 3.3-3 is a conceptual plot showing how the estimation error variance σ_i^2 of the i^{th} state variable might change during the course of a test, assuming the use of optimal filtering. The initial value $\sigma_i^2(0)$ is a measure of the uncertainty regarding the variable prior to the start of the test. The final value $\sigma_i^2(\infty)$ represents an equilibrium condition that is reached after sufficient time, in which the information coming in by virtue of new measurements is balanced by the information being lost due to process noise; the final value is independent of the initial value.* The major reduction in σ_i^2 takes place while the curve tends to follow the

*This is only true if certain observability conditions are satisfied. In the problem considered here these conditions are met.

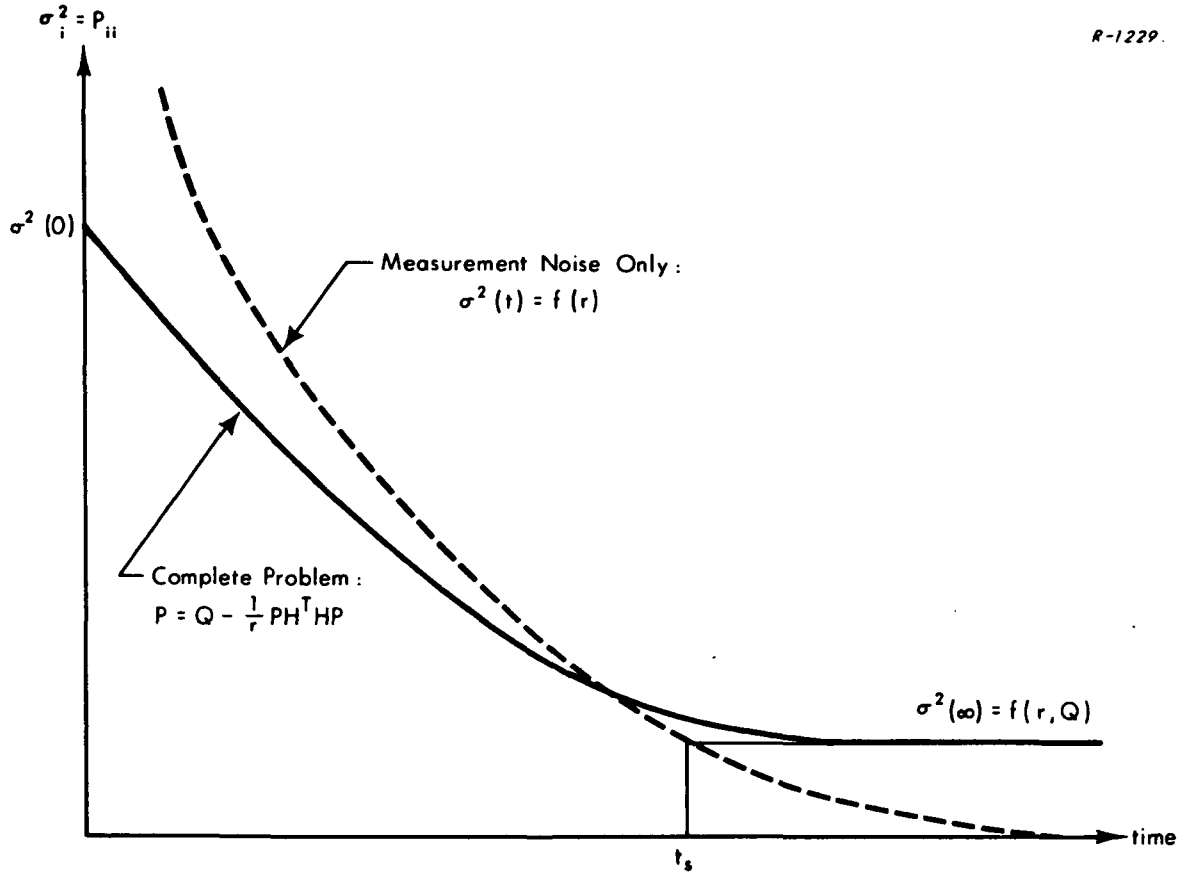

Figure 3.3-3 Estimation Error Variance Time History

dashed line labeled "measurement noise only." This dashed line corresponds to a hypothetical, optimal filtering situation in which there is no process noise and the initial uncertainty is infinite. The dashed curve, therefore, depends on only one parameter, r, which characterizes the measurement noise. It approaches zero asymptotically; by processing noisy measurements of a deterministic quantity the estimation error is made steadily smaller as time progresses.

A "solution time" or "settling time" t_s can be loosely defined as the time it takes the estimation error variance to get "close" to its

final value. The significance of t_s is that a test should be allowed to continue this long in order to get full benefit of the optimal filtering. A useful measure of t_s can be taken as the time at which the dashed line crosses the final value level (see Fig. 3.3-3). This crossing point depends on measurement noise and process noise, but is independent of initial errors. It can be found for any assumed set of measurement noise and process noise statistics by methods developed in Appendix C.

An approximate formula for the settling time in (see Appendix C):

$$t_{s_i} = \sqrt{2 \frac{r}{q_{ii}}} \qquad (3.3\text{-}13)$$

where r and q_{ii} characterize measurement noise and process noise, respectively, as described in Section 3.2.4. Equation (3.3-13) is a companion to Eq. (3.2-70) which gives the final value of the estimation error. Both are plotted parametrically in Fig. 3.2-8.

An alternate expression for the settling time, one which considers the effect of correlated process noise components, is:

$$t_{s_i} = \sqrt{\frac{2r}{q_{ii}}} \frac{1}{\sqrt{1 - c_{ij}^2}} \qquad (3.3\text{-}14)$$

where c_{ij} is a measure of correlation between two components of process noise, the j^{th} component being the one which dominates the problem. Equation (3.3-14) is a companion to Eq. (3.2-71). Together they imply that a high correlation between process noise components sometimes reduces the final estimation error variance, at the same time increasing the time needed to reach the more accurate level.

3.4 TEST DATA PROCESSING

The data processing function, for sinusoidal harmonic testing, can be defined in terms of the procedure pictured in Fig. 3.1-3 which shows three data processing phases: Phase Ia accepts as input the scalar, periodically time-varying sensor output and generates the set of Fourier coefficients for each single-axis test; in phase Ib the complete array of estimated values of the Fourier coefficients for a sequence of six single-axis tests is processed to yield estimates of a complete set of basic parameter groups; in phase II the values of individual parameters are computed.

Phase Ia, in which raw test data is processed, directly influences the choice of laboratory data processing equipment (see Section 4.2). Three candidate types of processing algorithms, Fourier analysis, least squares estimation and Kalman filtering, are considered below. Phase Ib involves the estimation of the basic parameter groups from an array of redundant coefficients. As a practical matter this phase may become a very simple computation based on a subset of "primary" coefficients, as discussed in Section 3.2.2, leaving the redundant information to be used as a cross-check on the operation of the test sequence or as a means to indicate the existence of previously unsuspected error torques. Alternatively, some form of regression analysis may be used to develop an optimum fit to the entire array of redundant data. The possible gain from such a procedure has not been investigated. Phase II, the simple algebraic calculation discussed in Section 2.4, requires no further study. This section will consider in detail the form of the equations to be mechanized in order to perform phase Ia via the three candidate algorithms.

3.4.1 Fourier Analysis

One obvious way to determine the coefficients of a trigonometric series is by Fourier analysis. For two reasons the problem at hand may differ from a classical Fourier analysis problem. These are:

- Because of errors in measurements and test motions we would like to process many cycles of data rather than just one.
- It may be necessary to deal with quantized rather than continuous data. This will certainly be true for a pulse-rebalanced sensor since the data comes naturally in quantized form. It may also be true if data from an analog-rebalanced sensor is to be processed on a digital computer.

The following equations are appropriate for computing Fourier coefficients from a continuous output function $e_r(t)$, taken over a time interval corresponding to m test motion cycles, where the test motion frequency is ω and the cycle period is $T = 2\pi/\omega$:

The rebalance torque is assumed to be the continuous function:

$$M_{tg}(t) = K_{tg}\, e_r(t) \tag{3.4-1}$$

The applied torque is given by:

$$\begin{aligned} M_a = M_{tg} = {} & B + S_1 \sin \omega t + C_1 \cos \omega t \\ & + S_2 \sin 2\omega t + C_2 \cos 2\omega t \\ & + S_3 \sin 3\omega t + C_3 \cos 3\omega t \end{aligned} \tag{3.4-2}$$

The Fourier coefficient estimates are:

$$B = \frac{K_{tg}}{mT} \int_0^{mT} e_r(t)\, dt \qquad (3.4\text{-}3)$$

$$S_n = \frac{2K_{tg}}{mT} \int_0^{mT} e_r(t) \sin n\omega t\, dt \qquad (3.4\text{-}4)$$

$$C_n = \frac{2K_{tg}}{mT} \int_0^{mT} e_r(t) \cos n\omega t\, dt \qquad (3.4\text{-}5)$$

where n = 1, 2 and 3.

Equations (3.4-3), (3.4-4) and (3.4-5) reduce to the classical Fourier analysis equations when m is unity. These equations can be mechanized directly on an analog computer for a sensor which is analog-rebalanced, in which case $e_r(t)$ is produced as an analog signal.

For the pulse rebalanced case, two sets of exact equations which generate the Fourier coefficients corresponding to the square-wave-type torque generator output are developed in Appendix D. For the binary and ternary pulse schemes the equations for the sine and cosine coefficients are:

$$S_n = \frac{1}{mn\pi} \sum_{i=0}^{km-1} M_i \left[(1-\cos n\omega h)\cos n\omega hi + \sin n\omega h \sin n\omega hi\right] \qquad (3.4\text{-}6)$$

$$C_n = \frac{-1}{mn\pi} \sum_{i=0}^{km-1} M_i \left[(1-\cos n\omega h) \sin n\omega hi - \sin n\omega h \cos n\omega hi\right] \quad (3.4\text{-}7)$$

where:

n = 1, 2 and 3

h = pulse width

ω = test motion frequency

m = number of cycles processed

k = number of pulse widths per cycle $(2\pi/\omega h)$

and M_i defines the torque level of the i^{th} pulse according to:

$$M_i = \begin{cases} M & \text{positive torque level} \\ 0 & \text{zero torque level} \\ M & \text{negative torque level} \end{cases}$$

The bias Fourier coefficient is proportional to the net pulse count. That is:

$$B = \frac{1}{mk} \sum_{i=0}^{km-1} M_i \quad (3.4\text{-}8)$$

For the time-modulated pulse torquing scheme the equations for the sine and cosine coefficients are:

$$S_n = \frac{M}{mn\pi} \sum_{i=0}^{km-1} \left[- \left(2 \cos n\omega \ell_i - \cos n\omega h \right) \cos n\omega hi + \left(2 \sin n\omega \ell_i - \sin n\omega h \right) \sin n\omega hi \right] \quad (3.4\text{-}9)$$

$$C_n = \frac{M}{mn\pi} \sum_{i=0}^{km-1} \left[\left(2 \cos n\omega \ell_i - \cos n\omega h \right) \sin n\omega hi + \left(2\sin n\omega \ell_i - \sin n\omega h \right) \cos n\omega hi \right] \quad (3.4\text{-}10)$$

where n, m and k are defined as above; M is the absolute value of the torque level; ℓ_i is the width of the positive torque pulse in the i^{th} interval; each interval has both positive and negative pulses and has the total width, h. The bias Fourier coefficient is given by:

$$B = \frac{M}{mk} \sum_{i=0}^{km-1} \left[2\ell_i - h \right] \quad (3.4\text{-}11)$$

Since h is very small compared to one test motion period, and since ℓ_i is less than h, we can employ the following small angle approximations:

$$\left.\begin{aligned} \cos n\omega h &= \cos n\omega \ell_i = 1 \\ \sin n\omega h &= n\omega h \\ \cos n\omega \ell_i &= n\omega \ell_i \end{aligned}\right\} \quad (3.4\text{-}12)$$

The equations given above reduce to the following set of unified, approximate expressions:

$$B = \frac{hM}{mT} \sum_{i=0}^{km-1} b_i \qquad (3.4\text{-}13)$$

$$S_n \cong \frac{2hM}{mT} \sum_{i=0}^{km-1} b_i \sin(n\omega hi) \qquad (3.4\text{-}14)$$

$$C_n \cong \frac{2hM}{mT} \sum_{i=0}^{km-1} b_i \cos(n\omega hi) \qquad (3.4\text{-}15)$$

where we have used $T = 2\pi/\omega$ and the definitions:

$$b_i = \text{sgn}(M_i) \text{ (binary and ternary)} \qquad (3.4\text{-}16)$$

$$b_i = \frac{\ell_i - h/2}{h/2} \text{ (pulse-width modulation)} \qquad (3.4\text{-}17)$$

Note that Eqs. (3.4-13), (3.4-14) and (3.4-15) look like discrete approximations to Eqs. (3.4-3), (3.4-4) and (3.4-5) for the analog-rebalanced case. In both cases, the sensor output (the continuous signal, e_r, or the sequence, b_i) is multiplied by the "weighting" functions (sin $n\omega t$ or sin $n\omega hi$ and cos $n\omega t$ or cos $n\omega hi$) and integrated or summed to produce the desired Fourier coefficients (S_n and C_n).

3.4.2 Least Squares Estimation

A least squares estimation procedure is outlined in Section 3.2.4. This procedure applies to the case in which the data is a sequence of integers $(z_1, z_2, \ldots z_j)$, each representing the integral of torque over a specified interval of time. The least squares estimate of the vector:

$$\underline{x} = \begin{bmatrix} S_1 \\ C_1 \\ S_2 \\ C_2 \end{bmatrix} \tag{3.4-18}$$

of harmonic coefficients is given by:

$$\hat{\underline{x}} = (H^T H)^{-1} H^T \underline{z} \tag{3.4-19}$$

where the measurement matrix, H, is:

$$H = \frac{1}{\omega} \begin{bmatrix} f_1 & g_1 & p_1 & q_1 \\ f_2 & g_2 & & \\ \cdot & & & \\ \cdot & & & \\ \cdot & & & \\ \cdot & & & \\ f_j & g_j & p_j & q_j \end{bmatrix} \tag{3.4-20}$$

where:

$$f_i = -\cos \omega hi + \cos \omega h(i-1)$$

$$g_i = \sin \omega hi - \sin \omega h(i-1)$$

$$p_i = -\frac{1}{2} \cos 2\omega hi + \frac{1}{2} \cos 2\omega h(i-1)$$

$$q_i = \frac{1}{2} \sin 2\omega hi - \sin 2\omega h(i-1) \qquad (3.4\text{-}21)$$

Processing data by means of Eq. (3.4-19) is essentially similar to Fourier analysis, in that we are multiplying a sequence of measurements by a set of periodically varying weighting functions (the elements of H^T) to obtain estimates of the various harmonic coefficients.

The computation can be simplified in practice if an integral number (say k) of data intervals, h, occur in one test motion period. In this case the elements of each column of H are cyclically repeating:

$$f_i = f_{i+k} = f_{i+2k} = \cdots$$

$$g_i = g_{i+k} = \cdots$$

$$\text{etc.} \qquad (3.4\text{-}22)$$

These sequences of repeating elements multiply the sequence of measurements:

$$z_i, \quad z_{i+k}, \quad z_{i+2k}, \cdots$$

Therefore, we can add up the raw pulse count data in k sections. For example, define the k sums:

$$Z_i = \sum_{\ell=0}^{m-1} z_{i+\ell k} \quad (i=1,2,\ldots k) \tag{3.4-23}$$

where m = j/k, the number of test cycles. Then:

$$H^T_{km \times 4} \, \underline{z}_{km} = \tilde{H}^T_{k \times 4} \, Z_k \tag{3.4-24}$$

where $\tilde{H}^T_{k\times 4}$ is the single-cycle measurement matrix, which repeats itself m times as a partition of H^T, as follows:

$$H^T = \left[\tilde{H}^T \,\vdots\, \tilde{H}^T \,\vdots\, \tilde{H}^T \,\vdots\, \text{------} \,\vdots\, \tilde{H}^T\right] \tag{3.4-25}$$

When this simplified procedure is used, the on-line (real-time) data processing function involves Eq. (3.4-23) only, generating the k outputs, Z_1 through Z_k.

3.4.3 Kalman Filtering

In Appendix C the phase Ia data processing problem is formulated as a problem in linear estimation for which the Kalman filter is an optimal solution. This formulation is a useful analytical device for determining the effects of random process noise and measurement noise on the test accuracy

(Section 3.2-6) and the useful test duration (Section 3.3). This section discusses the advisability of using a Kalman filtering algorithm in processing real test data — the form of the equations to be mechanized and the advantage there might be in using Kalman filtering in preference to Fourier analysis.

The following Kalman filter equations are appropriate for the continuous (analog rebalanced) case:

$$\dot{\underline{\hat{x}}}(t) = K(t)\,[z(t) - H(t)\,\underline{x}(t)] \tag{3.4-26}$$

$$K(t) = \frac{1}{r}\,P(t)\,H^{T}(t) \tag{3.4-27}$$

$$\dot{P}(t) = Q - \frac{1}{r}P(t)H^{T}(t)\,H(t)P(t) \tag{3.4-28}$$

where $\underline{\hat{x}}$ is the optimal estimate of the seven-state (five, if third harmonics are ignored) state vector $\underline{x}$ composed of the set of Fourier coefficients, z is the time-varying scalar measurement (the output of the sensor) and K is the Kalman filter gain matrix which in this case is a 7 x 1 column vector. H is the measurement matrix (in this case a 1 x 7 row vector) with periodically time-varying elements:

$$H(t) = (1,\ \sin \omega t,\ \cos \omega t,\ \sin 2\omega t,\ \cos 2\omega t,\ \sin 2\omega t,\ \cos 3\omega t) \tag{3.4-29}$$

and P is the covariance matrix of the estimation error:

$$P = \overline{(\underline{\hat{x}} - \underline{x})\,(\underline{\hat{x}} - \underline{x})^{T}} \tag{3.4-30}$$

The constant scalar r and the constant matrix Q characterize the measurement noise and process noise, respectively, as discussed in Section 3.2-6. For any given test set-up, Eq. (3.4-28) could be integrated in advance and the result could be substituted into Eq. (3.4-27) to produce a gain matrix with time-varying elements. This function could then be used in real time in Eq. (3.4-26) to process actual test data, z(t). If the actual test is generated in digital form, an alternate expression, based on the discrete form of the Kalman filter, may be used.

Appendix C demonstrates that after some time has elapsed from the start of a test, the Kalman filtering equations above become approximately equivalent to the Fourier analysis procedure in which successive cycles of processed data are averaged together. Therefore, the only obvious difference in the Kalman filter procedure involves the way the data from the first few cycles are processed. The filter estimates in these early cycles should be superior because all available information, including prior estimates, is being used in an optimal way. Since certain sensor parameters should be known accurately prior to the test this advantage may be quite significant, especially if the data processing equipment imposes severe limits on the amount of data which can be handled from a given test.

There is another potential advantage of the Kalman filtering approach which can be significant if some of the sensor parameters undergo significant changes during the course of a particular vibration test. The formulation of the problem can be expanded to take account of such changes (with, for example, a random-walk model) and the changes can be "tracked" during the test, with the result that the optimal estimates produced are significantly more accurate than those generated by Fourier analysis or simple least squares estimation. It is expected, however, that the

parameters under consideration will not change fast enough to make this a strong consideration in choosing a data processing scheme.

In summary, there are two potential advantages of the Kalman filtering approach — the inclusion of prior estimates and the possibility of tracking parameter changes, but more study is required before a definite recommendation concerning its use can be made.

3.5 EXAMPLE CALCULATIONS

This section presents the results of illustrative numerical calculations corresponding to an analog rebalanced single-degree-of-freedom gyro undergoing angular motion tests. The six recommended test motion axes and all three types of testing are included. The calculations include test errors, typical torque levels, and the variation of torque levels with test motion quantities. The test errors are based on the formulas developed in Section 3.2. The error calculations provide a quantitative accuracy comparison of the three types of single axis testing, augmenting the discussion at the end of Section 3.2.1.

3.5.1 Torque Levels

Table 3.5-1 lists the values of the parameter groups used in the example calculations. Table 3.5-2 lists the μ, λ and γ terms corresponding to the given gyro parameters, the assumed test motion quantities W and ω (the same amplitude and frequency are used for all six test axes), and the torque amplitudes (M_μ, M_λ and M_γ) which occur during sinusoidal testing. Note that M_λ is the same as the value, λW, corresponding to a constant rate

TABLE 3.5-1

ASSUMED GYRO PARAMETER VALUES

$k_1 = \alpha_s I_{oo} - I_{oi_g} = 1 \text{ gm cm}^2$

$k_2 = -I_{oo} = -100 \text{ gm cm}^2$

$k_3 = -\alpha_i I_{oo} - I_{os_g} = 1 \text{ gm cm}^2$

$k_4 = H = 10^5 \text{ gm cm}^2/\text{sec}$

$k_5 = \alpha_s H = 5 \text{ gm cm}^2/\text{sec}$ $\quad (\alpha_s \cong 10 \text{ sec})$

$k_6 = -\beta_o H = 5 \text{ gm cm}^2/\text{sec}$ $\quad (\beta_o \cong -10 \text{ sec})$

$k_7 = I_{si_g} + \beta_o \left(I_{ss_r} - I_{ii_r} \right) = 1 \text{ gm cm}^2$

$k_8 = -Q = 10 \text{ gm cm}^2$

$k_9 = I_{os_g} - \alpha_i \left(I_{ss} - I_{ii} \right) - \beta_i \left(I_{ss_r} - I_{oo_r} \right) = 1 \text{ gm cm}^2$

$k_{10} = -H^2/K + \left(I_{ss} - I_{ii} \right) = -50 \text{ gm cm}^2$

$k_{11} = \alpha_s \left(I_{ss} - I_{ii} \right) - I_{ci_g} = 1 \text{ gm cm}^2$

$k_{12} = -H/K \left(I_{ss} - I_{ii} \right) - I_{ii} = -0.05 \text{ gm cm}^2 \text{ sec}$

$k_{13} = \left(I_{oo}/K \right) H = 0.1 \text{ gm cm}^2 \text{ sec}^2$

$k_{14} = -\left(I_{oo}/K \right) \left(I_{ss} - I_{ii} \right) = -5 \times 10^{-5} \text{ gm cm}^2 \text{ sec}^2$

$K = 10^8$ dyne cm/radian

$(I_{ss} - I_{ii}) = 50 \text{ gm cm}^2$

TABLE 3.5-2

ILLUSTRATIVE TORQUE LEVELS

Sinusoidal Test Motion: W = 1 rad/sec, ω = 6.28 rad/sec (1 Hz)

Test Axis	μ (dyne cm sec^2)	$M_\mu = \mu\omega W$ (dyne cm)	λ (dyne cm sec)	$M_\lambda = \lambda W$ (dyne cm)	γ (dyne cm sec^2)	$M_\gamma = \frac{\gamma}{2} W^2$ (dyne cm)
o	$k_2 = -100$	-628.0	$k_5 = 5$	5.0	$k_8 = 10$	5.0
s	$k_3 = 1$	6.28	$k_6 = 5$	5.0	$-k_7 = 1$	0.5
i	$k_1 = 1$	6.28	$k_4 = 10^5$	10^5	$k_7 = 1$	0.5
o/s	$\frac{1}{\sqrt{2}}(k_2 + k_3) = -71.5$ $k_{13} = 0.1$	-449.0 0.16	$\frac{1}{\sqrt{2}}(k_5 + k_6) = 7.07$	7.07	$\frac{1}{2}(-k_7 + k_8 + k_{11}) = 6$	3.0
i/o	$\frac{1}{\sqrt{2}}(k_1 + k_2) = -71.5$	-449.0	$\frac{1}{\sqrt{2}}(k_4 + k_5) = 70,700$	70,700	$\frac{1}{2}(k_7 + k_8 + k_9) = 5$	2.5
i/s	$\frac{1}{\sqrt{2}}(k_1 + k_3) = 1.414$	8.89	$\frac{1}{\sqrt{2}}(k_4 + k_6) = 70,700$	70,700	$\frac{1}{2} k_{10} = -25$	-12.5

test at the rate, W, and M_γ is one half the value, γW^2, corresponding to a constant rate test at the rate, W. The larger torque levels occur as M_λ when the test axis is i, i/o or i/s; these involve gyroscopic terms, $H\omega_i$. The medium-sized levels occur as M_μ when the test axis is o, o/s or i/o; these involve output axis inertia terms, $I_{oo}\omega_o$. All other terms are relatively small. The M_ρ terms, which are not included in the table, are extremely small. For example:

$$M_\rho = \frac{3}{8\sqrt{2}} k_{12} W^3 = 0.013 \text{ dyne cm}$$

Similarly, the μ term involving k_{14} is:

$$M_{\mu_{14}} = \frac{1}{8\sqrt{2}} k_{14} \omega W^3 = 0.000028 \text{ dyne cm}$$

The variation of test torque levels with the magnitude of the applied test motion quantities (W and ω) is illustrated in Figs. 3.5-1 and 3.5-2. The torque levels corresponding to each basic parameter group which contributes torque in the o, s, and i axis tests are plotted versus W in Fig. 3.5-1 and the left hand side of Fig. 3.5-2. The right hand side of Fig. 3.5-2 plots the torques produced in the o/s, i/o and i/s axis tests by those parameter groups (k_9, k_{10}, k_{11} and k_{13}) which do not contribute in the first three tests. The contributions of the parameters already covered in the previous plots are not shown. For example, k_4 produces large torques in both the i/o and i/s axis cases; their magnitudes are $1/\sqrt{2}$ times the value shown (labeled M_{k_4}) for the i axis test.

The M_μ levels (M_{k_1, k_2, k_3}) are linear in both W and ω. The M_λ levels (M_{k_4, k_5, k_6}) are linear in W and independent of ω. The M_γ levels ($M_{k_7, k_8, k_9, k_{10}, k_{11}}$) are proprotional to W^2 and independent of ω. The M_μ term, $M_{k_{13}}$, is proportional to W^2 and linear in ω.

It is worth noting that for a fixed amplitude, A, of angular excursions in a sinusoidal test, all of these quantities vary with frequency. Thus, if:

$$\theta_{test} = A \sin \omega t \qquad (3.5\text{-}1)$$

Then

$$\omega_{test} = \dot{\theta}_{test} = \omega A \cos \omega t \qquad (3.5\text{-}2)$$

Therefore:

$$W = \omega A \qquad (3.5\text{-}3)$$

and:

$$\left.\begin{aligned} M_{\mu} &= \mu \omega W = \mu \omega^2 A \\ M_{\lambda} &= \lambda W = \lambda \omega A \\ M_{\gamma} &= \frac{1}{2} \gamma W^2 = \frac{1}{2} \gamma \omega^2 A^2 \end{aligned}\right\} \qquad (3.5\text{-}4)$$

3.5.2 Test Errors

Table 3.5-3 lists the assumed set of error source values used in the example error calculations which are summarized in Tables 3.5-4 through 3.5-9. The calculations are based on the error formulas given in Table 3.2-2, for the three types of single-axis testing and each of the six test motion axes. For two of the eleven error sources listed in Table 3.5-3 alternate values are given, one for small signal cases (test axes o, s and o/s) and one for large signal cases (test axes i, i/o and i/s). The quantization level, q, is considerably smaller in the small signal cases because of the opportunity for scaling the rebalance loop to take advantage of lower signal levels. It is also assumed that the parameter shifts, λ_{SH}, are larger in

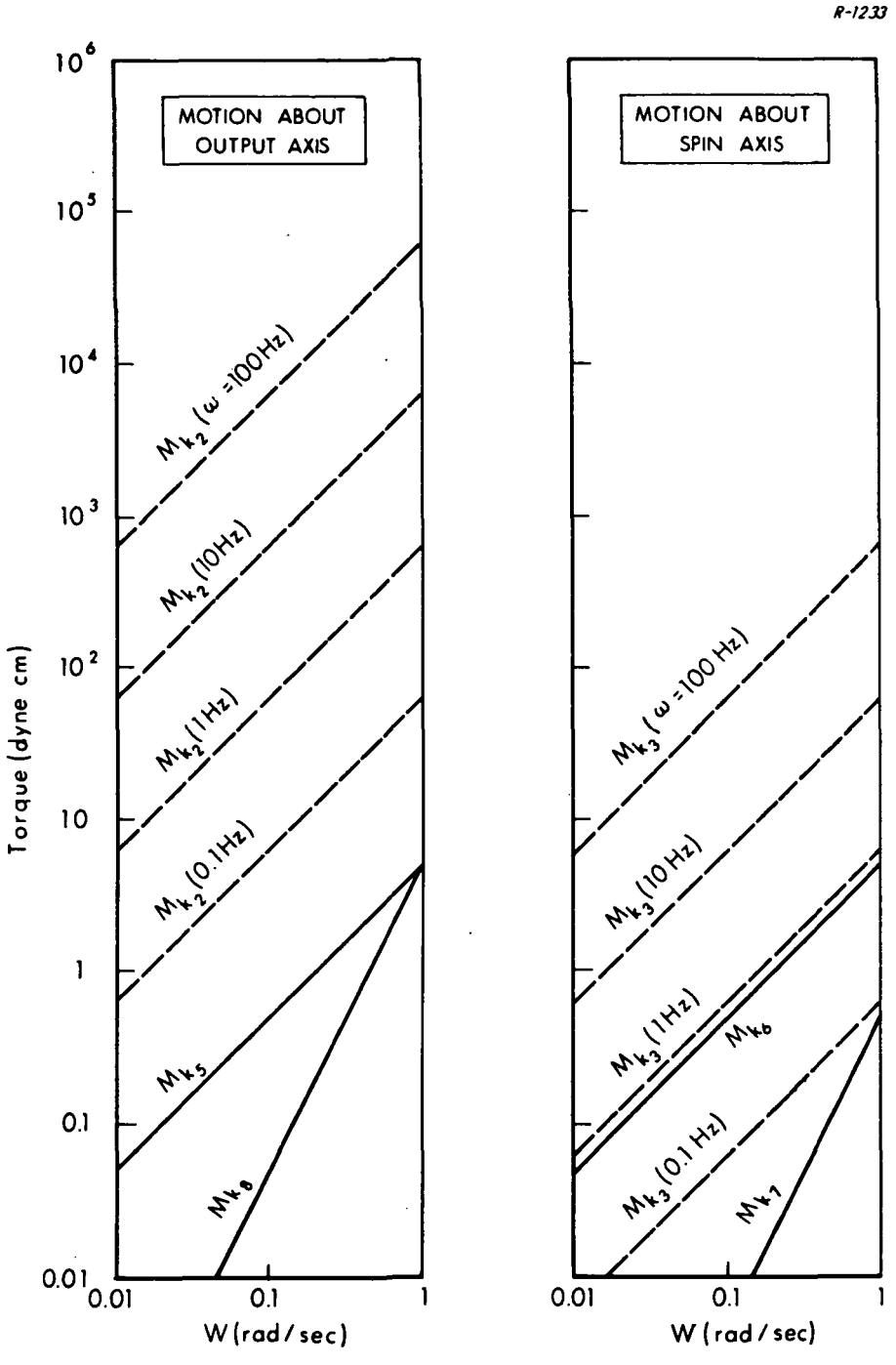

Figure 3.5-1 Variation of Torque Levels With Test Motion Amplitude and Frequency: o and s Test Axes

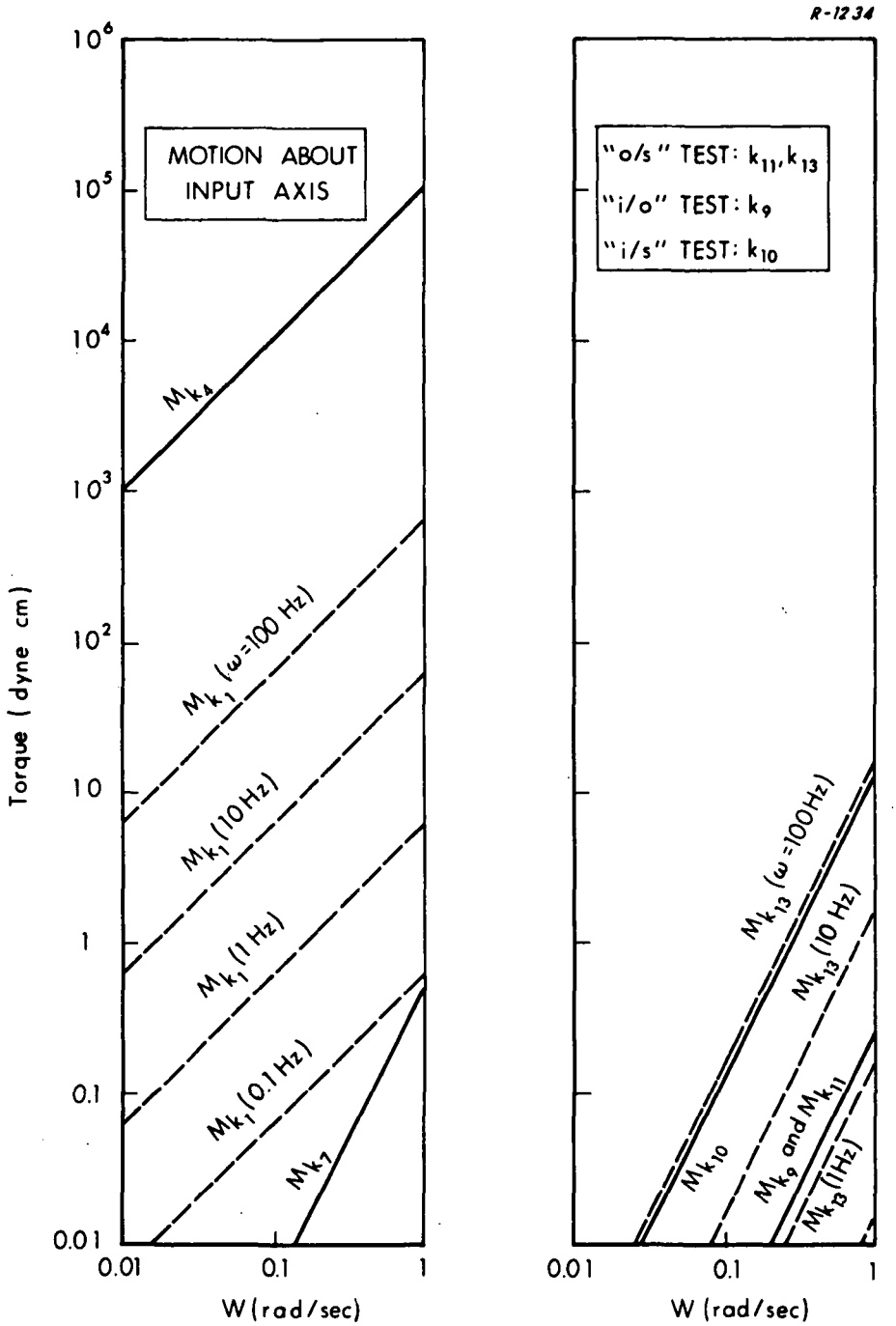

Figure 3.5-2 Variation of Torque Levels With Test Motion Amplitude and Frequency: i, o/s, i/o and i/s Test Axes

TABLE 3.5-3

ASSUMED ERROR SOURCE VALUES

T = 100 sec

h = 0.1 sec (N = 10/cycle)

Error Source		Value
1. Magnitude Bias, (sinusoidal)	δW	0.02 rad/sec
2. Distortion, (sinusoidal)	Δ	1×10^{-3}
3. Magnitude Noise, (sinusoidal)	σ_w, τ_u	0.02 rad/sec, 1 sec
4. Misalignment Bias,	$\bar{\epsilon}$	10.0 $\widehat{\text{sec}}$
5. Misalignment Shift, (constant rate)	$\bar{\epsilon}_{SH}$	5.0 $\widehat{\text{sec}}$
6. Table Wobble,	ϵ_w	1.0 $\widehat{\text{sec}}$
7. Quantization,	q_{sm}/q_{lg}	0.4/40.0 dyne cm sec
8. Torquer Scale Factor,	ϵ_{SC}	2×10^{-4}
9. Torquer Nonlinearity,	$\epsilon_{NL}\begin{cases}\epsilon_1\\ \epsilon_2\\ \epsilon_3\end{cases}$	2×10^{-4} 2×10^{-7} (dyne cm)$^{-1}$ 1×10^{-10} (dyne cm)$^{-2}$
10. Measurement Noise,	σ_v, τ_v	2.0 dyne cm, .01 sec
11. Parameter Shifts, (constant rate)	$\begin{cases}\lambda_{SH_{sm}}/\lambda_{SH_{lg}}\\ \gamma_{SH_{sm}}/\gamma_{SH_{lg}}\\ Mc_{SH}\end{cases}$	0.1/1.0 dyne cm sec 0.1/0.5 dyne cm sec^2 0.01 dyne cm

TABLE 3.5-4

EXAMPLE ERROR SUMMARY: o TEST AXIS

$\mu = k_2$ = 100 dyne cm sec^2 $\quad \lambda = k_5$ = 5 dyne cm sec $\quad \gamma = k_8$ = dyne cm sec^2

		Constant Rate		Sinusoidal Averaging	Sinusoidal Harmonics		
		λ	γ	γ	μ	λ	γ
1. Magnitude Bias	δW				2.0		
		0				0.1	
			0	0.2			0.2
2. Distortion	Δ				0		
		---				0	
			---	0			1.26
3. Magnitude Noise	σ_W				0.42		
		0				0.24	
			0	0.67			0.67
4. Misalignment Bias	$\bar{\epsilon}$				0		
		5.0				5.0	
			0	0			0
5. Misalignment Shift	$\bar{\epsilon}_{SH}$				---		
		2.5				---	
			1.25	---			---
6. Table Wobble,	ϵ_W				0		
		0.5				0	
			0.25	0			0
7. Quantization	q				0.007		
		0.016				0.046	
			0.008	0.003			0.092
8. Torquer Scale Factor	ϵ_{SC}				0.02		
		0.001				0.001	
			0.002	0.002			0.002
9. Torquer Nonlinearity	$\epsilon_{NL}\begin{Bmatrix}\epsilon_1\\ \epsilon_2\\ \epsilon_3\end{Bmatrix}$				0.104		
		0.00001				0	
			0.0001	0.002			0.001
10. Measurement Noise	σ_v				0.013		
		0.79				0.079	
			0.40	0.16			0.16
11. Parameter Shifts	$\begin{Bmatrix}\lambda_{SH}\\ \gamma_{SH}\\ M_{c_{SH}}\end{Bmatrix}$				---		
		0.142				---	
			0.079	---			---
Total (RSS)	σ_μ				2.05		
	σ_λ	5.67				5.01	
	σ_γ		1.34	0.72			1.45

TABLE 3.5-5

EXAMPLE ERROR SUMMARY: s TEST AXIS

$\mu = k_3$ = 1 dyne cm sec^2 $\quad \lambda = k_6$ = 5 dyne cm sec $\quad \gamma = k_7$ = 1 dyne cm sec^2

		Constant Rate		Sinusoidal Averaging	Sinusoidal Harmonics		
		λ	γ	γ	μ	λ	γ
1. Magnitude Bias	δW				0.02		
		0				0.1	
			0	0.02			0.02
2. Distortion	Δ				0		
		---				0	
			---	0			0
3. Magnitude Noise	σ_W				0.04		
		0				0.24	
			0	0.21			0.21
4. Misalignment Bias	$\bar{\epsilon}$				0		
		5.0				5.0	
			0	0			0
5. Misalignment Shift	$\bar{\epsilon}_{SH}$				---		
		2.5				---	
			1.25	---			---
6. Table Wobble	ϵ_W				0		
		0.5				0	
			0.25	0			0
7. Quantization	q				0.007		
		0.016				0.046	
			0.008	0.003			0.092
8. Torquer Scale Factor	ϵ_{SC}				0.0002		
		0.001				0.001	
			0.0002	0.0002			0.0002
9. Torquer Nonlinearity	$\epsilon_{NL}\begin{Bmatrix}\epsilon_1\\ \epsilon_2\\ \epsilon_3\end{Bmatrix}$				0		
		0.000001				0	
			0.00001	0			0
10. Measurement Noise	σ_v				0.013		
		0.79				0.079	
			0.40	0.16			0.16
11. Parameter Shifts	$\begin{Bmatrix}\lambda_{SH}\\ \gamma_{SH}\\ M_{c_{SH}}\end{Bmatrix}$				---		
		0.142				---	
			0.079	---			---
Total (RSS)	σ_μ				0.045		
	σ_λ	5.67				5.01	
	σ_γ		1.34	0.21			0.23

TABLE 3.5-6

EXAMPLE ERROR SUMMARY: i TEST AXIS

$\mu = k_1$ = 1 dyne cm sec^2 $\quad \lambda = k_4$ = 10^5 dyne cm sec $\quad \gamma = k_7$ = 1 dyne cm sec^2

		Constant Rate		Sinusoidal Averaging	Sinusoidal Harmonics		
		λ	γ	γ	μ	λ	γ
1. Magnitude Bias	δW				0.02		
		0				2000	
			0	0.02			0.02
2. Distortion	Δ				0		
		---				0	
			---	0			200
3. Magnitude Noise	σ_W				0.04		
		0				33.5	
			0	0.21			0.21
4. Misalignment Bias	$\bar{\epsilon}$				0		
		0				0	
			0	0			0
5. Misalignment Shift	$\bar{\epsilon}_{SH}$				---		
		0				---	
			0	---			---
6. Table Wobble	ϵ_W				0		
		0				0	
			0	0			0
7. Quantization	q				0.728		
		1.63				4.58	
			0.815	0.326			9.16
8. Torquer Scale Factor	ϵ_{SC}				0.0002		
		20.0				20.0	
			0.0002	0.0002			0.0002
9. Torquer Nonlinearity	$\epsilon_{NL}\begin{Bmatrix}\epsilon_1\\ \epsilon_2\\ \epsilon_3\end{Bmatrix}$				0		
		3.0				16.0	
			30.0	25.5			17.0
10. Measurement Noise	σ_v				0.013		
		0.79				0.079	
			0.40	0.16			0.16
11. Parameter Shifts	$\begin{Bmatrix}\lambda_{SH}\\ \gamma_{SH}\\ M_{cSH}\end{Bmatrix}$				---		
		1.01				---	
			0.50	---			---
Total (RSS)	σ_μ				0.73		
	σ_λ	20.3				2000	
	σ_γ		30.0	25.5			201

TABLE 3.5-7

EXAMPLE ERROR SUMMARY: o/s TEST AXIS

$\mu_{(C_1)} = (k_2+k_3)/\sqrt{2} = 71.3$ dyne cm sec^2 $\quad \lambda = (k_5+k_6)/\sqrt{2} = 7.07$ dyne cm sec $\quad \gamma = (-k_7+k_8+k_{11})/2 = 6$ dyne cm sec^2

$\mu_{(S_2)} = k_{13} = 0.1$ dyne cm sec^3

		Constant Rate		Sinusoidal Averaging	Sinusoidal Harmonics		
		λ	γ	γ	$\mu_{(C_1)}/\mu_{(S_2)}$	λ	γ
1. Magnitude Bias	δW				1.53/0.004		
		0				0.14	
			0	0.12			0.12
2. Distortion	Δ				0		
		---				0	
			---	0			0.89
3. Magnitude Noise	σ_W				0.36/0.084		
		0				0.28	
			0	0.52			0.52
4. Misalignment Bias	$\bar{\epsilon}$				0		
		5.0				5.0	
			0	0			0
5. Misalignment Shift	$\bar{\epsilon}_{SH}$				---		
		2.5				---	
			1.25	---			---
6. Table Wobble	ϵ_W				0/1.0		
		0.5				0	
			0.25	0			0
7. Quantization	q				0.007/0.007		
		0.016				0.046	
			0.008	0.003			0.092
8. Torquer Scale Factor	ϵ_{SC}				0.015/0		
		0.0014				0.0014	
			0.0012	0.0012			0.0012
9. Torquer Nonlinearity	$\epsilon_{NL}\begin{Bmatrix}\epsilon_1\\ \epsilon_2\\ \epsilon_3\end{Bmatrix}$				0.001/0		
		0.00001				0	
			0.0001	0.13			0.001
10. Measurement Noise	σ_v				0.013/0.013		
		0.79				0.079	
			0.40	0.16			0.16
11. Parameter Shifts	$\begin{Bmatrix}\lambda_{SH}\\ \lambda_{SH}\\ M_{c_{SH}}\end{Bmatrix}$				---		
		0.142				---	
			0.079	---			---
Total (RSS)	σ_μ				1.57/1.00		
	σ_λ	5.67				5.01	
	σ_γ		1.34	0.55			1.04

TABLE 3.5-8

EXAMPLE ERROR SUMMARY: i/o TEST AXIS

$\mu = (k_1+k_2)/\sqrt{2}$ = 71.5 dyne cm sec^2 $\quad \lambda = (k_4+k_5)/\sqrt{2}$ = 70,000 dyne cm sec $\quad \gamma = (k_7+k_8+k_9)/2$ = 5 dyne cm sec^2

		Constant Rate		Sinusoidal Averaging	Sinusoidal Harmonics		
		λ	γ	γ	μ	λ	γ
1. Magnitude Bias	δW				1.53		
		0				1414	
			0	0.10			0.10
2. Distortion	Δ				0		
		---				0	
			---	0			142
3. Magnitude Noise	σ_W				0.36		
		0				28.2	
			0	0.47			0.47
4. Misalignment Bias	$\bar{\epsilon}$				0		
		3.53				3.53	
			0	0			0
5. Misalignment Shift	$\bar{\epsilon}_{SH}$				---		
		1.77				---	
			0.88	---			---
6. Table Wobble	ϵ_W				0		
		0.353				0	
			0.177	0			0
7. Quantization	q	1.63			0.728		
						4.58	
			0.815	0.326			9.16
8. Torquer Scale Factor	ϵ_{SC}				0.0153		
		14.1				14.1	
			0.001	0.001			0.001
9. Torquer Nonlinearity	$\epsilon_{NL}\begin{Bmatrix}\epsilon_1\\ \epsilon_2\\ \epsilon_3\end{Bmatrix}$				0.0006		
		1.35				6.9	
			13.53	18.1			12.1
10. Measurement Noise	σ_v				0.013		
		0.79				0.079	
			0.40	0.16			0.16
11. Parameter Shifts	$\begin{Bmatrix}\lambda_{SH}\\ \gamma_{SH}\\ Mc_{SH}\end{Bmatrix}$				---		
		1.01				---	
			0.50	---			---
Total (RSS)	σ_μ				1.73		
	σ_λ	14.8				1414	
	σ_γ		13.6	18.1			143

TABLE 3.5-9

EXAMPLE ERROR SUMMARY: i/s TEST AXIS

$\mu = (k_1+k_3)/\sqrt{2}$ = 1.414 dyne cm sec^2 $\quad \lambda = (k_4+k_6)/\sqrt{2}$ = 70, 7000 dyne cm sec $\quad \gamma = k_{10}/2$ = 25 dyne cm sec^2

		Constant Rate		Sinusoidal Averaging	Sinusoidal Harmonics		
		λ	γ	γ	μ	λ	γ
1. Magnitude Bias	δW				0.028		
		0				1414	
			0	0.50			0.50
2. Distortion	Δ				0		
		---				0	
			---	0			141
3. Magnitude Noise	σ_W				0.05		
		0				28.2	
			0	1.06			1.06
4. Misalignment Bias	ϵ				0		
		3.53				3.53	
			0	0			0
5. Misalignment Shift	$\bar{\epsilon}_{SH}$				---		
		1.77				---	
			0.88	---			---
6. Table Wobble	ϵ_W				0		
		0.353				0	
			0.177	0			0
7. Quantization	q				0.728		
		1.63				4.58	
			0.815	0.326			9.16
8. Torquer Scale Factor	ϵ_{SC}				0.0003		
		14.1				14.1	
			0.005	0.005			0.005
9. Torquer Nonlinearity	$\epsilon_{NL}\begin{Bmatrix}\epsilon_1\\ \epsilon_2\\ \epsilon_3\end{Bmatrix}$				0		
		1.35				6.9	
			13.53	18.0			12.0
10. Measurement Noise	σ_v				0.013		
		0.79				0.079	
			0.40	0.16			0.16
11. Parameter Shifts	$\begin{Bmatrix}\lambda_{SH}\\ \gamma_{SH}\\ M_{c_{SH}}\end{Bmatrix}$				---		
		1.01				---	
			0.50	---			---
Total (RSS)	σ_μ				0.73		
	σ_λ	14.9				1414	
	σ_γ		13.6	18.0			142

in the large signal cases; these shifts represent very small percentage changes in very large quantities (see Table 3.5-2). The assumed test motions are:

$$\left.\begin{aligned} W_1 &= 2 \text{ rad/sec} \\ W_2 &= 0.1 \text{ rad/sec} \end{aligned}\right\} \text{ constant rate tests}$$

$$\left.\begin{aligned} W &= 1 \text{ rad/sec} \\ W &= 2\pi \text{ rad/sec} \end{aligned}\right\} \text{ sinusoidal tests}$$

The calculation of the time-dependent errors is based on the test time:

$$T = 100 \text{ sec.}$$

In each column of Tablse 3.5-4 through 3.5-9 the values in the third and tenth rows have been compared, and the smaller of the two dropped, before combining errors in RSS fashion to calculate the overall one-sigma estimation errors, σ_μ, σ_λ or σ_γ, given at the bottom of the column. (See the discussion in Section 3.2.1.) In each column the one or two largest contributions to the overall error are printed in red.

Table 3.5-10 summarizes selected results from the six preceding tables. For each of the parameter groups, k_1 through k_{11} and k_{13}, the test axis which appears best suited for determining that parameter group is shown in Table 3.5-10, along with the corresponding one-sigma estimation error. For example, $k_7 = \gamma$ for spin axis tests and input axis tests, but the one-sigma estimation error, σ_γ, is much smaller in the former case (compare Tables 3.5-5 and 3.5-6), so the value for the spin axis test is

TABLE 3.5-10

EXAMPLE ERRORS: SUMMARY COMPARISON

Parameter(s)	Basic Parameter Group	Type	Best Test Axis	Nominal Value of Parameter	1σ Error/Largest Contributor		
					Constant Rate	Sinusoidal Average	Sinusoidal Harmonic
$I_{oi_g} \cong$	$-k_1$	μ	i	1 dyne cm sec^2	-----	---	0.73/q
	$-k_{11}$	γ	o/s		$3.28/\bar{\epsilon}_{SH}$	$1.33/\sigma_w$	$2.55/\Delta$
$I_{oo} =$	$-k_2$	μ	o	100 dyne cm sec^2	---	---	$2.05/\delta W$
$I_{os_g} \cong$	$-k_3$	μ	s	1 dyne cm sec^2	---	---	$0.045/\sigma_w$
	k_9	γ	i/o		$27.3/\epsilon_{NL_{2,3}}$	$36.2/\epsilon_{NL_1}$	$143/\Delta$
$I_{si_g} \cong$	k_7	γ	s	1 dyne cm sec^2	$1.34/\bar{\epsilon}_{SH}$	$0.21/\sigma_w$	$0.23/\sigma_w$
$H =$	k_4	λ	i	10^5 dyne cm sec	$20.3/\epsilon_{SC}$	---	$2000/\delta W$
$\alpha_s H =$	k_5	λ	o	5 dyne cm sec	$5.67/\bar{\epsilon}$	---	$5.01/\bar{\epsilon}$
$\beta_o H =$	$-k_6$	λ	s	5 dyne cm sec	$5.67/\bar{\epsilon}$	---	$5.01/\bar{\epsilon}$
$Q =$	$-k_8$	γ	o	10 dyne cm sec^2	$1.34/\bar{\epsilon}_{SH}$	$0.72/\sigma_w$	$1.45/\Delta$
$\frac{H^2}{K} - \Delta I =$	$-k_{10}$	γ	i/s	50 dyne cm sec^2	$27.2/\epsilon_{NL_{2,3}}$	$36.0/\epsilon_{NL_1}$	$284/\Delta$
$\frac{I_{oo}}{K} H =$	k_{13}	γ	o/s	0.1 dyne cm sec^3	---	---	$1.0/\epsilon_w$

included in Table 3.5-10. With each numerical entry is a symbol indicating which of the eleven error sources contributes the most to that particular estimation error. For example the error in estimating k_8 (which is best determined by one of the o axis tests) is dominated by misalignment shift (ϵ_{SH}), test motion magnitude noise (σ_W) or distortion

(Δ), depending on which of the three types of test is used (refer back to Table 3.5-4). The parameter groups, k_{12} and k_{14}, are not included in the example error calculations because of their extremely small size, (see Section 3.5-1).

With three exceptions (k_9, k_{10} and k_{11}) the one-sigma estimation errors given in Table 3.5-10 are simply the appropriate RSS values ($\sigma_\mu, \sigma_\lambda, \sigma_\gamma$) given at the bottom of Tables 3.5-4 through 3.5-9. For example, the value 0.73 for the k_1 estimation error comes from the value for σ_μ given at the bottom of Table 3.5-6. However, k_9 and k_{11} appear only in combination with k_7 and k_8 in the definition of γ in the o/s and i/o test axis cases, respectively. Therefore, k_7 and k_8 must be estimated first (using s and o axis tests) and subtracted from the current estimate of γ as follows:

$$\hat{k}_9 = 2\hat{\gamma}_{o/s} - \hat{k}_7 - \hat{k}_8$$

$$= 2\hat{\gamma}_{o/s} - \hat{\gamma}_s - \hat{\gamma}_o \qquad (3.5\text{-}7)$$

and

$$\hat{k}_{11} = 2\hat{\gamma}_{i/o} + \hat{k}_7 - \hat{k}_8$$

$$= 2\hat{\gamma}_{i/o} + \hat{\gamma}_s - \hat{\gamma}_o \qquad (3.5\text{-}8)$$

The values shown in Table 3.5-10 for σ_{k_9} and $\sigma_{k_{11}}$ are computed from

$$\sigma_{k_9} = \left[4\,\sigma^2_{\gamma_{o/s}} + \sigma^2_{\gamma_s} + \sigma^2_{\gamma_o} \right]^{1/2} \qquad (3.5\text{-}9)$$

and

$$\sigma_{k_{11}} = \left[4\,\sigma^2_{\gamma_{i/o}} + \sigma^2_{\gamma_s} + \sigma^2_{\gamma_o} \right]^{1/2} \qquad (3.5\text{-}10)$$

In a similar manner:

$$\sigma_{k_{10}} = \left[4\,\sigma^2_{\gamma_{i/s}} \right]^{1/2} \qquad (3.5\text{-}11)$$

Table 3.5-10 is arranged to illustrate the relative difficulty in determining the various individual parameters (I_{oi_g}, I_{oo}, etc) using the several types of single axis testing. For the error source values assumed here, it may be observed that:

- The cross product of inertia, I_{oi_g}, may be determined as k_1 by sinusoidal harmonic testing about the input axis or as k_{11} by any of the three types of testing about the o/s axis. The smallest of the estimation errors shown corresponds to the first method (even though it is a large signal case -- the μ term is not affected by distortion, nonlinearity and magnitude bias the way the λ and γ terms are). However, all four values are of the same order of magnitude and each has a different largest contributor, so the relative estimation errors are very sensitive to the error sources.

- The cross product of inertia, I_{OS_g}, may also be determined in any one of four ways, as k_3 (one way) or as k_9 (three ways). In this case there is a clear preference for finding k_3 using sinusoidal harmonic testing (about the s axis), since nonlinearity and distortion have major effects on the determination of k_9, which requires the large signal test axis i/o.

- The cross product of inertia, I_{Si_g}, may be measured in any one of three ways, with angular motion about the spin axis. Sinusoidal testing (averaging or harmonic) appears significantly more accurate than constant rate testing, although this conclusion depends on the values of the dominant error sources, which are different for the two types of testing.

- The output axis inertia, I_{OO}, appears as a μ term only, and measuring its effect requires the use of sinusoidal harmonic testing about the output axis. The dominant error source appears to be uncertainty in the knowledge of the applied test motion amplitude.

- Measuring the wheel momentum, H, involves rotation about the input axis, using a constant rate on a sinusoidal oscillation. The former is much preferred because the applied constant rate magnitude will be known more accurately than the amplitude of the oscillation.

- The misalignments, α_S and β_O, of the sensitive axis of the gyro may be determined using constant rate or sinusoidal harmonic testing about the output and spin axes, respectively. The two types of tests appear to be approximately equal in accuracy since both are dominated by the bias misalignment, ϵ, of the test axis. However, if the procedure of reversing the sensor on the table top and repeating each run is used, the bias misalignment effect may be largely eliminated. In that case different error sources become dominant in the two cases: misalignment shift for constant rate testing, and test motion magnitude noise for sinusoidal harmonic testing.

- The experimentally observed error term, Q, may be measured in any of the three ways, rotating about the output axis. The smallest estimation error shown in that corresponding to sinusoidal averaging, although all three are roughly equal and each has a different largest contributor.

- The k_{10} parameter group, $H^2/K-(I_{SS}-I_{ii})$, may be measured in any of three ways, rotating about the i/s axis (a large signal case). Sinusoidal harmonic testing appears useless due to the large distortion effect. The estimation errors in constant rate testing and sinusoidal averaging are dominated by torquer nonlinearity, the odd nonlinearities, ϵ_2 and ϵ_3, in the former case and the even nonlinearity, ϵ_1, in the latter case. In actual practice since k_{10} is made up of "desired" or nominal gyro parameters, its value should be known a priori more accurately than it can be determined by either of these i/s axis tests. This suggests that the reason for running such tests may be to compare the indicated and a priori values of k_{10} and to employ the differences as measures of the two types of torquer nonlinearity. The resulting measures of the nonlinear terms can then be used to correct the estimates of k_9 as obtained in the i/o axis tests. A set of input axis tests can also be run to obtain another measure of the nonlinearities.

- The k_{13} parameter group, $I_{oo}H/K$, appears only as a μ term and only in the o/s axis sinusoidal harmonic test. Based on the assumed error source values and parameter values the one-sigma estimation error is considerably larger than the nominal value of k_{13}. The dominant error source is table wobble, ϵ_w. Removal of its contribution reduces the overall error to 0.085 dyne cm sec^3. Since the value of k_{13} is well known a priori, an attempt to measure it in this way might be useful in verifying the accuracy of a sinusoidal harmonic testing set-up.

In summary, the reasons for considering the use of sinusoidal harmonic testing are that it provides the only way to measure the effect of I_{oo}, the best way to estimate I_{os_g} and reasonably good redundant estimates of several other gyro parameters in the small signal cases (test motion axes o, s, and o/s). Sinusoidal averaging does not yield anything that is not provided by constant rate testing, but appears to have better accuracy in several cases.

The example calculations summarized above are based on the error formulas developed in Section 3.2 and tabulated in Table 3.2-2. In this case the formulas are used to compute parameter estimation accuracies for an assumed set of error source values and test motion quantities. The same formulas can also be used, in a less straightforward fashion, to generate test equipment performance specifications for given desired estimation accuracies (see examples in Chapter 4).

Chapter Summary — The information which may be extracted from single-axis vibration tests and constant motion tests is identified. The effects of various test error sources, such as test machinery errors and measurement errors, on the accuracy of estimating various observable quantities are analyzed. The different types of tests are compared on the basis of observable quantities, data redundancy, number of test runs required, data processing difficulty and accuracy.

All basic parameter groups can theoretically be computed from the observable quantities obtained in a sequence of six angular and six linear single-axis vibration tests if the harmonic content of the periodic applied torque function is extracted. The six test vibration axes should be oriented parallel to the three principal sensor axes--input, output and spin (or pendulum)--and to the three axes lying midway between pairs of principal axes. The full array of observable quantities from a complete test sequence provides a considerable amount of redundant data which "overspecifies" the basic parameter groups.

A sequence of sinusoidal vibration tests in which only average torque measurements are made yields only the parameter groups which give torques proportional to the square of angular rate or acceleration, and no redundant data. However, the data processing requirements for determining average torque are considerably simpler than for extracting harmonic terms. Extraction of certain harmonic terms provides redundant measurements of these parameter groups but they are generally less accurate than the measurements based on average torque.

All of the parameter groups except those which generate torques proportional to angular accelerations can theoretically be computed from the data produced in a sequence of constant motion tests. More test runs are required since two or more different magnitudes must be used for each test axis in order to separate the effects of various parameter groups. The data processing function is the same as in sinusoidal averaging, and therefore simple. Parameter estimation errors are more affected by some test error sources and less affected by others, as compared to sinusoidal testing.

The data processing function for sinusoidal harmonic testing consists of three phases. The first phase, in which harmonics are extracted from the sensor output data for each run, directly influences the choice of laboratory data processing equipment. Three candidate types of processing algorithm, Fourier analysis, least squares estimation and Kalman filtering, are considered and developed in some detail. The second phase is the computation of the basic parameter groups from the redundant array of Fourier coefficients. The third phase is the solution for individual sensor parameters.

The choice of test duration, for constant rate tests as well as sinusoidal tests, is governed by the need to reduce the effects of quantization and uncorrelated measurement noise. The Kalman filtering formulation of the data processing problem is useful in deriving relationships between test duration and test accuracy. Similarly the least squares estimation formulation is used to show the effects of total test time and the sample interval size on overall test accuracy.

Detailed numerical results of a set of example calculations, corresponding to a typical SDF gyro undergoing a sequence of six constant rate and six sinusoidal angular motion tests, are presented. These results include the torque levels associated with each basic parameter group and the variation of those levels with test motion quantities. Also illustrated is the application of the entire set of test error formulas (given in Table 3.2-2) for each of the three types of single-axis tests considered and each of the six recommended test axes. A summary comparison of the predicted errors in estimating ten potentially significant quantities is given in Table 3.5-10.

4. IMPLICATIONS FOR TEST LABORATORY EQUIPMENT

The investigations described in the previous two chapters lead to some rather important conclusions and recommendations concerning the choice of laboratory equipment. These recommendations must be considered tentative at the present time since the investigations are incomplete. They are included, however, in the hope of stimulating further discussion and interchange of ideas.

4.1 TEST MOTION MACHINERY

A significant overall recommendation stemming from the study to date is that great stress should be placed on the appropriate use of conventional single-axis devices, together with vibratory and constant motion, for testing strapdown inertial sensors. In order to obtain the maximum usefulness from the test data, careful attention should be given to techniques for controlling and/or measuring the supplied motion and to the means for processing the sensor output data produced during the tests.

The following conclusions pertain specifically to single-axis testing of single-degree-of-freedom sensors, on which the study has thus-far focused attention:

- Since it is essential, in sinusoidal harmonic testing, to time-synchronize the sensor output data with the test motion history (see Section 4.2), the test device must include a means to provide accurate timing signals indicating the time of passing through a zero-reference position. These signals must be merged with the recorded sensor outputs or, in the case of

real-time processing, used to control the computation itself. Of course, other measurements leading to a more accurate knowledge of the applied motion history are highly desirable.

- It is more important to keep the form of the applied motion close to that of a pure sinusoidal oscillation than to accurately control (or know) the amplitude of the oscillation. The example calculations suggest that a bias error on the order of one percent in the applied amplitude does not generate unacceptable test errors, while a distortion of the shape of the applied motion that causes second harmonic terms on the order of one-tenth of one percent of the fundamental motion amplitude leads to very large errors in some cases (when the sensor input axis is along or 45 degrees away from the test axis). In some "small signal" cases (when the gyro input axis is perpendicular to the test motion axis) distortion is also a dominant error source. Table 3.5-10 shows that if distortion were significantly reduced from the assumed value, the estimates of parameter groups k_8 and k_{11} via sinusoidal harmonic testing could be greatly improved.

- The example calculations indicate that a bias misalignment of the table axis is the dominant error is estimating component misalignments. (A 10 $\widehat{\text{sec}}$ table axis misalignment results in a 10 $\widehat{\text{sec}}$ error in measuring α_S or β_O, depending on the test axis.) However, this bias effect can be largely removed by repeating the appropriate tests after a 180 degree rotation of the sensor *with respect to the table. If the sensor is rotated as* described, the effects of run-to-run shifts in the table axis misalignment and of table wobble become more important than the bias for constant motion tests. The example calculations suggest that values on the order of several arc seconds will be acceptable for both of these error sources.

- As a result of satisfying the timing requirement discussed in the first item above, the frequency of the applied test motion will be known very precisely. Therefore, uncertainties in the derived Fourier coefficients caused by errors in knowledge of the applied frequency will be insignificant (for the example calculations show that frequency errors on the order of one percent are acceptable).

Nomographs relating test equipment performance, specifically distortion of sinusoidal test motion and quantization, to test accuracy are presented in Figs. 4.1-1 through 4.1-3. They serve to illustrate practical use of the analytical results developed in Chapter 3. Since many of the error formulas given in Table 3.2-2 involve five or six quantities, it is difficult to represent them in the form of parametric curves which display the effects of changes in all variables of interest. Nomographs, however, provide a convenient method for relating all relevant sensor parameters, test motion quantities and geometry, test time, test equipment performance and test accuracy.

The nomograph of Fig. 4.1-1 is based on the following formula for the effect of distortion of an applied sinusoidal test motion on the estimate of a γ term.

$$\delta\gamma = \frac{2\omega c_o I_{oo} \Delta}{W} \qquad (4.1\text{-}1)$$

This formula applies in small signal cases, where the test motion axis is perpendicular to the gyro input axis ($c_i = 0$). If W, ω, c_o and I_{oo} are fixed and a desired (minimum) test accuracy level, $\delta\gamma$, is chosen, then the allowable (maximum) distortion becomes:

$$\Delta = \frac{W \delta\gamma}{2\omega c_o I_{oo}} \qquad (4.1\text{-}2)$$

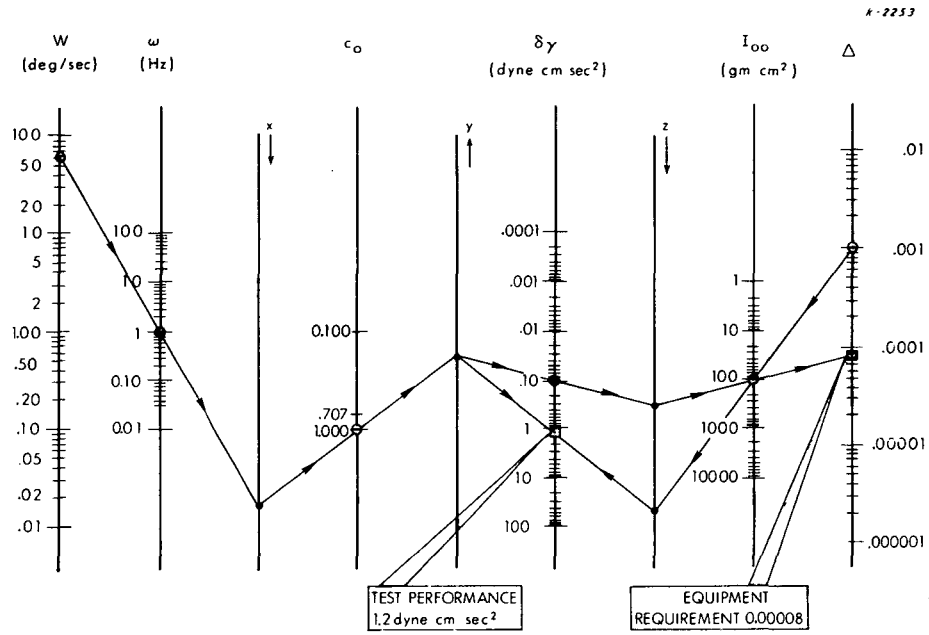

Figure 4.1-1 Nomograph for Distortion Effect - Small Signal Cases

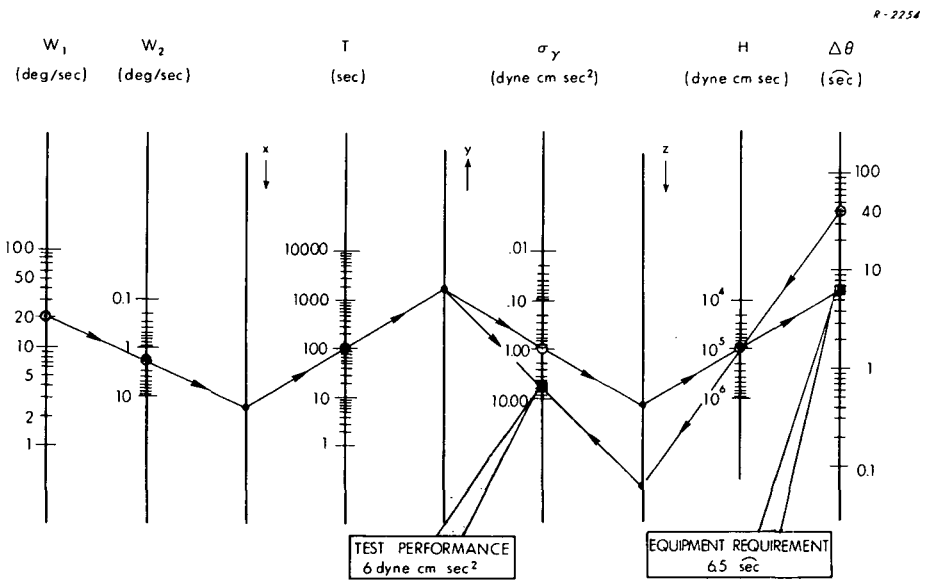

Figure 4.1-2 Nomograph for Quantization Effect - Constant Rate Testing

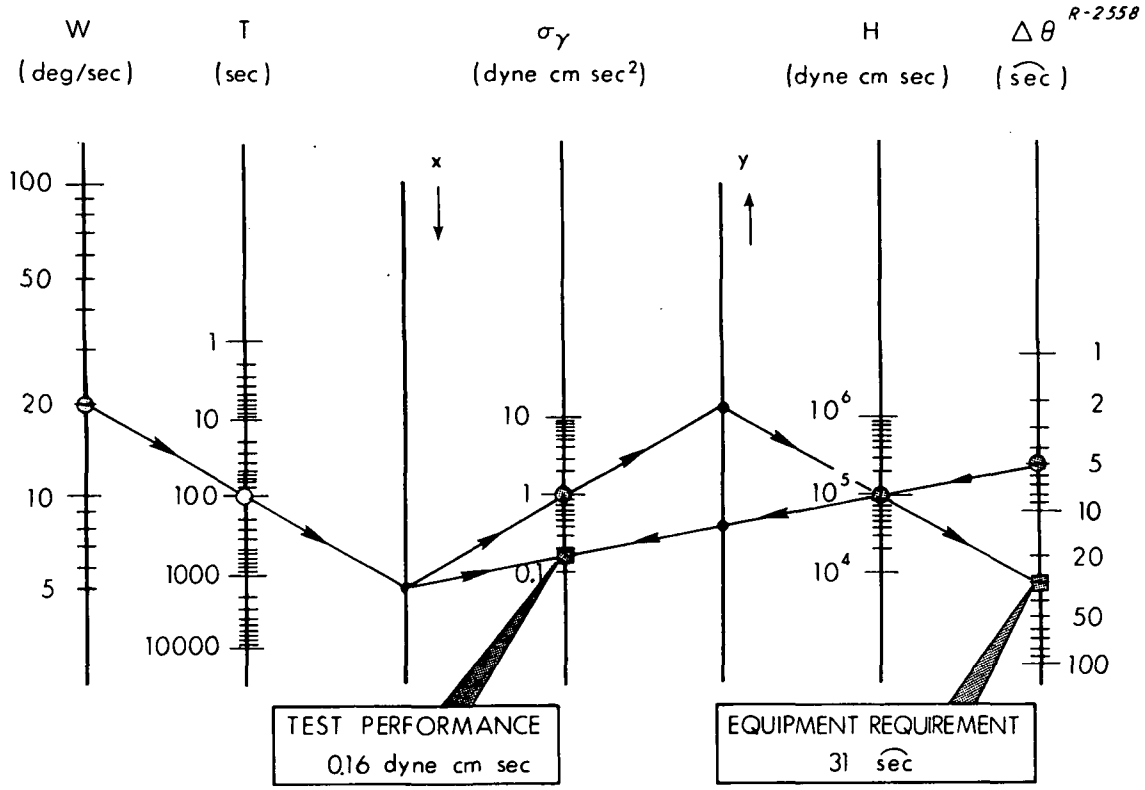

Figure 4.1-3 Nomograph for Quantization Effect - Sinusoidal Averaging

Eq. (4.1-2) is dimensionally correct if, for example, both W and ω are given in rad/sec, $\delta\gamma$ in dyne cm sec^2 and I_{oo} in gm cm^2. For the units indicated at the top of Fig. 4.1-1 the following version applies:

$$\Delta = \frac{W\,\delta\gamma}{\omega c_o I_{oo}} \left[\frac{1}{2(180/\pi)\,2\pi}\right] \qquad (4.1\text{-}3)$$

where the terms in the brackets can be evaluated:

$$\frac{1}{2(180/\pi)\,2\pi} = 0.00139$$

The following formulas, using intermediate variables x, y and z, were used in constructing the nomograph:

$$x = W/\omega \tag{4.1-4}$$

$$y = x/c_o \tag{4.1-5}$$

$$z = y\ \delta\gamma\ 0.00139 \tag{4.1-6}$$

$$\Delta = z/I_{oo} \tag{4.1-7}$$

The sequence of line segments with right-pointing arrows illustrate how the nomograph may be used to determine the equipment performance requirement. In this case the given values:

$$W = 60 \text{ deg/sec}$$

$$\omega = 1 \text{ Hz}$$

$$c_o = 1$$

$$\delta\gamma = 0.1 \text{ dyne cm sec}^2$$

$$I_{oo} = 100 \text{ gm cm}^2$$

lead to the maximum allowable distortion level:

$$\Delta \cong 0.000083$$

Also illustrated is an alternate procedure in which a given distortion level ($\Delta = 0.001$) is assumed, along with the same values for W, ω, c_o and I_{oo} given above. In this case the resulting test error ($\delta_\gamma \cong 1.0$ dyne cm sec^2) is determined by working from both edges of the graph toward a crossing-point on the δ_γ scale.

Figures 4.1-2 and 4.1-3 present nomographs which are based on the following formulas for error due to quantization in constant rate testing and sinusoidal averaging, respectively:

$$\sigma_\gamma = \frac{1}{W_1 W_2} \frac{1}{T} \frac{H \Delta\theta}{\sqrt{6}} \tag{4.1-8}$$

$$\sigma_\gamma = \frac{2}{W^2} \frac{1}{T} \frac{H \Delta\theta}{\sqrt{6}} \tag{4.1-9}$$

Construction of the nomograph for the constant rate case with the units given at the top of Fig. 4.1-2 is based on the following formulas:

$$\Delta\theta = W_1 W_2 T \sigma_\gamma \left[\frac{3600(180/\pi)\sqrt{6}}{(180/\pi)^2} \right] \frac{1}{H} \tag{4.1-10}$$

$$x = W_1 W_2 \tag{4.1-11}$$

$$y = xT \tag{4.1-12}$$

$$z = y \sigma_\gamma 154 \tag{4.1-13}$$

$$\Delta\theta = z/H \tag{4.1-14}$$

where the term in brackets can be evaluated:

$$\frac{3600\sqrt{6}}{180/\pi} = 20\sqrt{6\pi} \cong 154$$

Construction of the nomograph for the sinusoidal averaging case with the units given at the top of Fig. 4.1-3 is based on the following formulas:

$$\Delta\theta = W^2 T \sigma_\gamma \left[\frac{\sqrt{6}\ 3600(180/\pi)}{2(180/\pi)^2} \right] \frac{1}{H} \qquad (4.1\text{-}15)$$

$$x = W^2 T \qquad (4.1\text{-}16)$$

$$y = x\, \sigma_\gamma\, 77.0 \qquad (4.1\text{-}17)$$

$$\Delta\theta = y/H \qquad (4.1\text{-}18)$$

where the term in brackets can be evaluated:

$$\frac{3600\sqrt{6}}{2(180/\pi)} = 10\sqrt{6}\pi \cong 77.0$$

Figures 4.1-2 and 4.1-3 illustrate the same two procedures displayed in Fig. 4.1-1 -- working from left to right to determine the required quantization level* -- and working from both edges toward the middle to determine the γ term estimation accuracy resulting from a given set of test and sensor parameters.

The type of nomograph and procedures illustrated in Figs. 4.1-1 through 4.1-3 can be developed and employed for all of the test error formulas appearing in Table 3.2-2. In each case all but one variable can be fixed and a simple graphical procedure used to determine the unspecified quantity.

---

*For binary and ternary rebalance loops the "effective quantization level" is determined rather than the single pulse weight, as explained in Section 3.2.5.

4.2 DATA PROCESSING EQUIPMENT

Constant Motion and Sinusoidal Averaging — If testing is confined to constant motion and averaging measurements made during vibratory motion, the data processing requirements are relatively simple. For each test run the net number of pulses, representing the integrated torque, and the total test time must be recorded. Following a sequence of test runs some linear algebraic equations must be solved to yield estimates of the parameter groups and sensor parameters (see Eqs. (3.2-3) and (3.2-4)).

Sinusoidal Harmonic Testing — For sinusoidal harmonic testing the data processing equipment required in the test laboratory is determined mainly by the data processing phase Ia (see Fig. 3.1-3). The other phases must await the completion of a sequence of single-axis tests and, therefore, will be performed off-line. (To the extent that some of this subsequent processing can lead to a quick determination if a test is successful, there could be a significant operational advantage in having a limited amount of off-line capability readily accessible at the time the tests are being performed.)

From the point of view of laboratory equipment choices there are basically two ways to perform data processing phase Ia:

- Record the sensor output data (and measurements of test motion if desired) for later off-line processing.
- Process the data on-line as it emerges from the test, producing immediately a set of filtered estimates of the observable quantities (Fourier coefficients).

In either case the leading candidates for a processing algorithm are the Fourier analysis, the least squares estimation, and the Kalman filtering procedures outlined in Section 3.4.

If the first method is used, the crucial equipment specifications are those required of the recording equipment. They result chiefly from the high output data rate. For an analog rebalanced sensor feeding an analog recorder, the recorder bandwidth must be higher than the first few harmonics of the maximum applied test motion frequency. It is not possible at the present time to establish a quantitative requirements since high frequency testing has not been investigated. For a pulse rebalanced sensor feeding a digital recorder, it would be desirable to be able to record the complete sequence of pulses in order to make full use of the test data. In this case the required data recording rate is simply the maximum pulse rate used by the strapdown sensors under test. Consider the following numerical example: a maximum test time of 200 seconds and a binary pulsed gyro with a pulse repetition rate of 5000 pulses per second. The recorder must, therefore, have the capacity to store a sequence of one million binary digits at the rate of one every 0.2 milliseconds. Simultaneously it must record "timing marks" in a parallel channel, indicating the zero-reference points in the test motion history.

If on-line processing is used the computer must be able to accept data at the sensor output data rate and simultaneously, process equations like those of Section 3.4 at this same rate. This implies very short operation times for the computer used. The various sets of equations for the sinusoidal coefficients [for example, Eqs. (3.4-4) and (3.4-5)] point up the need for careful time-synchronization between the output data and the applied motion. The "weighting factors," sin $n\omega t$ and

cos $n\omega t$, must be cycled through $2\pi n$ radians for each period of the test motion, without drifting out of phase. Otherwise, the computation will not be one of averaging m sets of properly computed Fourier coefficients. Also, if either the least squares estimation or Kalman filtering equations are used, the time-varying elements of the H matrix [see Eq. (3.4-29)] must be kept in phase with the actual applied motion history.

Chapter Summary — Test motion machinery specifications may be derived from an understanding of the manner in which test motion errors propagate into parameter estimation errors and from the overall test accuracy requirements. The propagation of test motion errors for constant rate testing, sinusoidal averaging and sinusoidal harmonic testing are treated in detail in Section 3.2 Nomographs provide a convenient way to make use of the error formulas summarized in Table 3.2-2. The overall test accuracy requirements depend on the underlying reasons for conducting a specific set of tests — whether they are research oriented or mission oriented, etc. – as discussed in Section 1.1. The data processing functions for constant rate testing and sinusoidal averaging are quite simple. For sinusoidal harmonic testing the data processing equipment specifications depend on whether off-line or on-line processing is used. In the former case the recorder characteristics, which depend on data rate and test time, are crucial. In the latter case the on-line computer characteristics, which are dictated by the data rate and the detailed nature of the estimation equations outlined in Section 3.4, are crucial.

5. CONCLUSION

5.1 SUMMARY OF FINDINGS

The starting point of this effort is a set of equations (derived in Refs. 2 and 3) for motion-induced error torque in single-degree-of-freedom (SDF) sensors. These error models have been manipulated in a way which is valid for closed-loop, low-frequency testing, yielding error torque expressions which are linear functions of a set of "basic parameter groups" defined in Table 2.4-1. All of these basic parameter groups can theoretically be identified and measured by means of a sequence of single-axis vibration tests, including six angular vibration tests, and six linear vibration tests. All but one of them are independent of test motion frequency and magnitude.*

The following three types of single-axis angular-motion tests have been studied in detail:

- Constant Rate Testing
- Sinusoidal Testing, Averaging
- Sinusoidal Testing, Harmonic Extraction

The bases for comparing the three types include the observable quantities (measurable parameter groups), the amount of redundant data provided, the number of test runs required, the degree of difficulty of data processing

*See the discussion in Section 2.4.1 of the effect of rotor speed control loop dynamics on k_{10}.

required and the accuracy with which various parameters can be estimated. (A comparison summary is given in Table 3.2-3.) Constant rate testing is the simplest to perform but does not produce the complete set of basic parameter groups. Sinusoidal averaging is simpler than sinusoidal harmonic testing but yields an even smaller subset of the complete list. Only sinusoidal harmonic testing provides a measure of all the parameter groups.

The principal data processing function for both constant rate testing and sinusoidal averaging is to compute average torque by generating a net pulse count and dividing by the total time of a test run. For a sequence of sinusoidal harmonic tests there are three data processing stages: the computation of Fourier coefficients defining the periodic applied torque function for each test run; the processing of the entire array of coefficients from a complete sequence to produce the basic parameter groups; and the computation of individual sensor parameters. The first stage may be performed by means of Fourier analysis, least squares estimation or Kalman filtering (detailed equations for all three candidates are given in Section 3.4). The second stage is an "overspecified" algebraic problem involving redundant information. The extra data can be used as a cross-check on the operation of the test sequence or as a means to indicate the existence of error torques not included in the model. The third stage is a simple algebraic problem.

Methods have been developed for analyzing the effects of various test error sources and of test duration on the achievable accuracy in estimating sensor parameters. Three classes of test error sources are considered: test motion errors, measurement errors and changes in the sensor parameters. Motion errors and measurement errors have bias, cyclic and high-frequency noise components, including the effects of quantization. The resulting error formulas (summarized in Table 3.2-2) have been used in a set of illustrative numerical calculations based on an

assumed set of typical SDF gyro parameters. In these examples the nominal magnitudes of the coefficients of the third harmonic terms are extremely small, leading to the conclusion that the significant data from each vibration test will be contained in five Fourier coefficients (the bias term, the coefficients of the sine and cosine terms at the fundamental test motion frequency and the coefficients of the second harmonic sine and cosine terms). Constant rate testing or sinusoidal averaging appear to be more accurate than sinusoidal harmonic testing in a number of cases. Sinusoidal harmonic testing provides good redundant measurements in the cases where the sensor input axis is nominally perpendicular to the test motion axis. It also provides good measurements of parameters and parameter groups which cannot be determined by the other types of testing. In two situations sinusoidal harmonic testing appears to yield the most accurate estimates of parameters which can also be measured using one of the other techniques.

5.2 RECOMMENDATIONS

The apparent effectiveness of a combination of vibration testing and constant rate testing leads to a major recommendation of this study--that conventional single-axis devices should be given strong consideration when developing test procedures for strapdown inertial sensors. Some indications of quantitative test equipment specifications can be drawn from the example test error calculations presented (these are summarized in Section 4.1).

While constant rate testing is by far the simplest to perform, it is important that some cross-checking by sinusoidal averaging and probably by harmonic testing as well, be performed. It may be desirable, for example, to develop an operational calibration procedure using constant rate testing to generate coefficients which will compensate for the effects of system vibrations. The appropriateness of compensation so derived should be verified by means of vibration testing, which more closely resembles the dynamic environment to which strapdown sensors will be subjected.

If maximum benefit is to be obtained from harmonic testing, either high speed recording equipment or high speed on-line, real-time data processing equipment will be required in the test laboratory. These would be needed to extract the harmonic content of the rebalance torque, averaging data taken over many test motion cycles. A trade-off between the sophistication of laboratory data processing equipment and the complexity of motion-supplying devices is apparent. For example, a sequence of single-axis vibration tests combined with data processing which extracts harmonics, can substitute for multi-axis tests employing out-of-phase vibrations.

An overall conclusion may be stated as follows: It appears that useful information can be obtained from a sequence of practically achievable single-axis vibration tests. However, the test error analysis is only as good as the assumptions on which it is based, and it is possible that some test error sources will be much larger than those assumed in the example calculations, or that there are other important error sources not included in the analysis. It is therefore recommended that a set of feasibility tests be conducted as soon as possible. These tests would apply low-frequency single-axis angular vibrations to an

analog-rebalanced SDF gyro and use available signal-processing equipment to determine the harmonic content of the gyro output signal. The test results should be used to answer the following questions:

- Do the magnitudes of the output harmonics agree generally with predictions?
- What are the most significant sources of test error?
- What can be done, via test hardware modifications, to reduce these errors?
- After appropriate hardware modifications have been made, what is the "real" data processing problem remaining? That is, what noise sources must be filtered; or what cyclic or bias errors should be calibrated?

Besides verifying the practicality of the proposed type of testing, a series of feasibility tests would provide information which would be useful in guiding the continuing analytic studies discussed below. These, in turn, would become more useful in producing realistic test laboratory equipment specifications and in developing appropriate data processing procedures.

Continuing studies related to low-frequency, single-axis testing of SDF sensors should be broadened in some respects and deepened in others. The test error analyses should be developed into a parametric study, covering a range of sensor parameters and test motion quantities, with the goal of providing approximate indications of the test duration and equipment precision required to extract sensor parameters to specified accuracies. Particular test situations with particular sensors should be analyzed in detail, with the goal of making specific recommendations as to test procedures and data reduction techniques. A generalized simulation

capability would be useful in verifying analyses already performed and in evaluating alternative data processing schemes.

A better understanding of motion-affected errors which are mentioned in Section 1.1 but not included in the present error models, such as those caused by scale factor changes and friction torques, should be developed. These additional error terms will also be considered in devising test procedures.

The potential advantages and difficulties of employing high-frequency, single-axis vibration tests on inertial sensors should be evaluated. An attempt should be made to re-formulate the data processing problem discussed in Section 3.4 in a convenient way which does not depend on the low-frequency assumption. A high-frequency test motion error analysis should, if needed, also be developed. The goal of this investigation would be to indicate if information concerning dynamic instrument errors that is not revealed by well-designed low-frequency tests can be extracted by high frequency tests, and if so, to provide error analyses which can be interpreted in terms of test equipment specifications.

The importance of stability of strapdown sensor parameters suggests that the recommended tests be employed in a sequential fashion, aimed at measuring stability. Strapdown sensors may only be calibrated before installation in a vehicle (since they cannot be isolated from incidental vehicle motions and reoriented relative to gravity and earth rate) and a means must be available to predict, with known confidence limits, the stability of the measured parameters. Stability will be a prime objective of the instrument designer, and tests which relate sensor design features to coefficient stability will be of great value. Prior theoretical work related to this subject should be reviewed and experiments for evaluating mathematical models of parameter variation should be designed.

APPENDIX A

DERIVATION OF TRIGONOMETRIC SERIES COEFFICIENTS: VIBRATION TESTING OF SINGLE-DEGREE-OF-FREEDOM SENSORS

This appendix derives expressions for the Fourier coefficients which are the observable quantities in single-axis angular and linear vibration tests of single-degree-of-freedom (SDF) gyros and accelerometers.

SDF Gyro: Angular Vibration — The general expression for angular motion-induced torque in a SDF gyro is given as Eq. (2.4-5) and is repeated here:

$$\begin{aligned} M_{ang} = {} & k_1\dot{\omega}_i + k_2\dot{\omega}_o + k_3\dot{\omega}_s \\ & + k_4\omega_i + k_5\omega_o + k_6\omega_s \\ & + k_7\omega_i^2 + k_8\omega_o^2 - k_7\omega_s^2 \\ & + k_9\omega_i\omega_o + k_{10}\omega_i\omega_s + k_{11}\omega_o\omega_s \\ & + k_{12}\omega_i^3 - k_{12}\omega_i\omega_s^2 \\ & + k_{13}\dot{\omega}_o\omega_s + k_{14}\dot{\omega}_o\omega_i^2 - k_{14}\dot{\omega}_o\omega_s^2 \end{aligned} \qquad \text{(A-1)}$$

where k_1 through k_{14} are the basic parameter groups defined in Table 2.4-1a.

A general single-axis angular vibration of amplitude W and frequency ω can be represented by:

$$\omega_i = c_i W \sin \omega t = W_i \sin \omega t \tag{A-2a}$$

$$\omega_o = c_o W \sin \omega t = W_o \sin \omega t \tag{A-2b}$$

$$\omega_s = c_s W \sin \omega t = W_s \sin \omega t \tag{A-2c}$$

where c_i, c_o and c_s are direction cosines relating the vibration axis to the gyro principal axes and W_i is defined as $c_i W$, etc.

The derivation consists of substituting Eqs. (A-2a), (A-2b) and (A-2c) into Eq. (A-1), term by term, and applying well known trigonometric identities, as shown by the following examples:

$$k_1 \dot{\omega}_i = k_1 \omega W_i \cos \omega t \tag{A-3a}$$

$$k_9 \omega_i \omega_o = k_9 W_i W_o \sin^2 \omega t = \frac{1}{2} k_9 W_i W_o (1 - \cos 2\omega t) \tag{A-3b}$$

$$k_{12} \omega_i \omega_s^2 = k_{12} W_i W_s^2 \sin^3 \omega t = \frac{1}{4} k_{12} W_i W_s^2 (3 \sin \omega t - \sin 3\omega t) \tag{A-3c}$$

$$\begin{aligned} k_{14} \dot{\omega}_o \omega_s^2 &= \left[k_{14} W_o W_i^2 \omega \right] \cos \omega t \sin^2 \omega t \\ &= \left[k_{14} W_o W_i^2 \omega \right] \cos \omega t (1 - \cos^2 \omega t) \\ &= \left[k_{14} W_o W_i^2 \omega \right] \left[\cos \omega t - \cos^3 \omega t \right] \\ &= \left[k_{14} W_o W_i^2 \omega \right] \left[\cos \omega t - \frac{1}{4} (\cos 3\omega t - 3 \cos \omega t) \right] \\ &= \frac{1}{4} k_{14} W_o W_i^2 \omega (\cos \omega t - \cos 3\omega t) \end{aligned} \tag{A-3d}$$

After treating all terms in Eq. (A-1) in the above fashion and grouping similar terms, we obtain:

$$M_{ang} = B + S_1 \sin \omega t + C_1 \cos \omega t + S_2 \sin 2\omega t + C_2 \cos 2\omega t + S_3 \sin 3\omega t + C_3 \cos 3\omega t \qquad \text{(A-4)}$$

where the seven trigonometric coefficients (Fourier coefficients) are:

$$B = \frac{1}{2}\left[k_7\left(W_i^2 - W_s^2\right) + k_8 W_o^2 + k_9 W_i W_o + k_{10} W_i W_s + k_{11} W_o W_s\right] \qquad \text{(A-5a)}$$

$$S_1 = k_4 W_i + k_5 W_o + k_6 W_s + \frac{3}{4} k_{12}\left(W_i^3 - W_i W_s^2\right) \qquad \text{(A-5b)}$$

$$C_1 = \omega\left[k_1 W_i + k_2 W_o + k_3 W_s + \frac{1}{4} k_{14} W_o\left(W_i^2 - W_s^2\right)\right] \qquad \text{(A-5c)}$$

$$S_2 = \frac{1}{2} k_{13} \omega W_o W_s \qquad \text{(A-5d)}$$

$$C_2 = -\frac{1}{2}\left[k_7\left(W_i^2 - W_s^2\right) + k_8 W_o^2 + k_9 W_i W_o + k_{10} W_i W_s + k_{11} W_o W_s\right] \qquad \text{(A-5e)}$$

$$S_3 = -\frac{1}{4} k_{12}\left(W_i^3 - W_i W_s^2\right) \qquad \text{(A-5f)}$$

$$C_3 = -\frac{1}{4} k_{14} \omega W_o\left(W_i^2 - W_s^2\right) \qquad \text{(A-5g)}$$

SDF Accelerometer: Angular Motion —The general expression for angular motion-induced torque in a SDF accelerometer is given in Eq. (2.4-13) and is repeated here:

$$\begin{aligned} M_{ang} = {} & k_1\dot{\omega}_i + k_2\dot{\omega}_o + k_3\dot{\omega}_p \\ & + k_4\omega_i^2 - k_4\omega_p^2 \\ & + k_5\omega_i\omega_o + k_6\omega_i\omega_p + k_7\omega_o\omega_p \\ & + k_8\dot{\omega}_o\omega_i^2 - k_8\dot{\omega}_o\omega_p^2 \end{aligned} \qquad \text{(A-6)}$$

where k_1 through k_8 are the basic parameter groups defined in Table 2.4-1b.

Equations just like Eqs. (A-2a), (A2-b) and (A-2c), except that ω_p, c_p and W_p are used instead of ω_s, c_s and W_s, are substituted into Eq. (A-6). After applying the same trigonometric identities, illustrated in Eqs. (A-3a) through (A-3d), and grouping similar terms, we obtain:

$$\begin{aligned} M_{ang} = {} & B + C_1 \cos \omega t \\ & + C_2 \cos 2\omega t \\ & + C_3 \cos 3\omega t \end{aligned} \qquad \text{(A-7)}$$

where the four Fourier coefficients are:

$$B = \frac{1}{2}\left[k_4\left(W_i^2 - W_p^2\right) + k_5 W_i W_o + k_6 W_i W_p + k_7 W_o W_p\right] \qquad \text{(A-8a)}$$

$$C_1 = \omega\left[k_1 W_i + k_2 W_o + k_3 W_p + \frac{1}{4}k_8 W_o\left(W_i^2 - W_p^2\right)\right] \qquad \text{(A-8b)}$$

$$C_2 = -\frac{1}{2}\left[k_4\left(W_i^2 - W_p^2\right) + k_5 W_i W_o + k_6 W_i W_p + k_7 W_o W_p\right] \qquad \text{(A-8c)}$$

$$C_3 = -\frac{1}{4}k_8 \omega W_o\left(W_i^2 - W_p^2\right) \qquad \text{(A-8d)}$$

SDF Gyro: Linear Vibration — The general expression for linear motion-induced torque in a SDF gyro is given in Eq. (2.4-15) and is repeated here:

$$\begin{aligned} M_{lin} = {} & k_1 f_i + k_2 f_o + k_3 f_s \\ & + k_4 f_i^2 + k_5 f_s^2 \\ & + k_6 f_i f_o + k_7 f_i f_s + k_8 f_o f_s \end{aligned} \qquad \text{(A-9)}$$

where k_1 through k_8 are the basic parameter groups defined in Table 2.4-1c.

A general single-axis linear vibration of amplitude A and frequency ω can be represented by:

$$f_i = c_i A \sin \omega t = A_i \sin \omega t \qquad \text{(A-10a)}$$

$$f_o = c_o A \sin \omega t = A_o \sin \omega t \qquad \text{(A-10b)}$$

$$f_s = c_s A \sin \omega t = A_s \sin \omega t \qquad \text{(A-10c)}$$

Substituting Eqs. (A-10a), (A-10b) and (A-10c) into Eq. (A-9) and regrouping, we get:

$$M_{lin} = B + S_1 \sin \omega t + C_2 \cos 2\omega t \qquad \text{(A-11)}$$

where the Fourier coefficients are:

$$B = \frac{1}{2}\left[k_4 A_i^2 + k_5 A_s^2 + k_6 A_i A_o + k_7 A_i A_s + k_8 A_o A_s\right] \qquad \text{(A-12a)}$$

$$S_1 = k_1 A_i + k_2 A_o + k_3 A_s \qquad \text{(A-12b)}$$

$$C_2 = -\frac{1}{2}\left[k_4 A_i^2 + k_5 A_s^2 + k_6 A_i A_o + k_7 A_i A_s + k_8 A_o A_s\right] \qquad \text{(A-12c)}$$

SDF Accelerometer: Linear Vibration – The general expression for linear motion-induced torque in a SDF accelerometer is given in Eq. (2.4-16), which is identical in form to that of Eqs. (2.4-15) and (A-9), except that f_p is used in place of f_s. The basic parameter groups k_1 through k_8 are defined in Table 2.4-1d. Equations just like Eqs. (A-10a), (A-10b) and (A-10c) can be substituted into Eq. (A-9) to yield Eq. (A-11), exactly. The three Fourier coefficients, B, S_1 and C_2, are defined exactly as in Eqs. (A-12a), (A-12b) and (A-12c), except that A_p appears in place of A_s. Therefore:

$$B = \frac{1}{2}\left[k_4 A_i^2 + k_5 A_p^2 + k_6 A_i A_o + k_7 A_i A_p + k_8 A_o A_p\right] \qquad \text{(A-13a)}$$

$$S_1 = k_1 A_i + k_2 A_o + k_3 A_p \qquad \text{(A-13b)}$$

$$C_2 = -\frac{1}{2}\left[k_4 A_i^2 + k_5 A_p^2 + k_6 A_i A_o + k_7 A_i A_p + k_8 A_o A_p\right] \qquad \text{(A-13c)}$$

APPENDIX B

TEST MOTION BIAS ERROR ANALYSIS: ANGULAR VIBRATION TESTING OF SINGLE-DEGREE-OF-FREEDOM GYRO

This appendix describes the effects of bias test motion errors on the Fourier coefficients defining the applied torque function during single-axis angular vibration tests. The test motion errors considered are errors in the knowledge of amplitude and frequency of the applied motions and misalignments of the test motion axes.

Derivation Overview – The derivation begins with Eqs. (A-5a) through (A-5g) of Appendix A. These equations relate the 7 Fourier coefficients to the gyro parameters and the test motion quantities for the general in-phase case:

$$\left(B, S_1, C_1, S_2, C_2, S_3, C_3\right) = \underline{f}\left(k_1 \ldots k_{14}, W_i, W_o, W_s, \omega\right) \qquad \text{(B-1)}$$

where $\underline{f}$ represents the seven given functions.

The derivation proceeds in three major steps as follows. First, partial derivatives are taken with respect to the motion quantities to yield 7 perturbation equations which can be expressed in one vector matrix equation:

$$\underline{\Delta} = \begin{bmatrix} \delta B \\ \delta S_1 \\ \delta C_1 \\ \delta S_2 \\ \delta C_2 \\ \delta S_3 \\ \delta C_3 \end{bmatrix} = M_1 \begin{bmatrix} \delta W_i \\ \delta W_o \\ \delta W_s \\ \delta \omega \end{bmatrix} \qquad \text{(B-2)}$$

where the elements of M_1 are expressions involving the k's, W_i, W_o, W_s and ω.

Second, Eq. (B-2) is transformed into the form:

$$\underline{\Delta} = M_2 \begin{bmatrix} \delta W \\ \epsilon_i \\ \epsilon_o \\ \epsilon_s \\ \delta \omega \end{bmatrix} \qquad \text{(B-3)}$$

which relates the Fourier coefficient errors to test motion magnitude and angle errors, rather than component errors.

Finally, Eq. (B-3) is specialized for the six test axis orientations of interest and reduced to the form:

$$\underline{\Delta} = M_3 \begin{bmatrix} \delta W \\ \epsilon_1 \\ \epsilon_2 \\ \delta\omega \end{bmatrix} \qquad \text{(B-4)}$$

The test axis misalignment angles, ϵ_1 and ϵ_2, have different meanings in each case. If the test axis is one of the principle axes (say i), then ϵ_1 and ϵ_2 are simply the misalignments about the other two (o and s). If the test axis lies midway between two principle axes (say i and o), then ϵ_1 is the misalignment about the third (s) and ϵ_2 is the misalignment about the axis perpendicular to both the test axis and the ϵ_2 axis.

These three steps are followed in detail below, concluding with six equations (B-8a) through (B-8f) giving the expressions for the elements of the matrix M_3 for each of the six test motion axes of interest.

Derivation Details — Equations (B-5a) through (B-5g) give the seven perturbation equations obtained by taking partial derivatives of the seven equations, (A-5a) through (A-5g). Equations (B-6a) through (B-6e) develop the relationship of component errors (δW_i, δW_o, δW_s) to magnitude and angle errors (δW, ϵ_i, ϵ_o, ϵ_s). The three relations of Eq. (B-6e) were substituted into the perturbation equations to obtain new perturbation equations, as shown in Eqs. (B-7a) through (B-7g). Table B-1 summarizes facts needed to specialize the perturbation equations to the six tests of interest. Finally, Eqs. (B-8a) through (B-8g) present the seven perturbation equations in vector-matrix form for the six cases.

$$\delta B = \left[k_7 W_i - \frac{1}{2}k_9 W_o + \frac{1}{2}k_{10} W_s\right]\delta W_i + \left[k_8 W_o - \frac{1}{2}k_9 W_i + \frac{1}{2}k_{11} W_s\right]\delta W_o + \left[-k_7 W_s + \frac{1}{2}k_{10} W_i + \frac{1}{2}k_{11} W_o\right]\delta W_s + [0]\,\delta\omega \qquad \text{(B-5a)}$$

$$\delta S_1 = \left[k_4 + \frac{9}{4}k_{12} W_i^2 - \frac{3}{4}k_{12} W_s^2\right]\delta W_i + \left[k_5\right]\delta W_o + \left[k_6 - \frac{3}{2}k_{12} W_i W_s\right]\delta W_s + [0]\,\delta\omega \qquad \text{(B-5b)}$$

$$\delta C_1 = \omega\left[k_1 + \frac{1}{2}k_{14} W_i W_o\right]\delta W_i + \omega\left[k_2 + \frac{1}{4}k_{14}\left(W_i^2 - W_s^2\right)\right]\delta W_o + \omega\left[k_3 - \frac{1}{2}k_{14} W_o W_s\right]\delta W_s + \left[k_1 W_i + k_2 W_o + k_3 W_s + \frac{1}{4}k_{14} W_o\left(W_i^2 - W_s^2\right)\right]\delta\omega \qquad \text{(B-5c)}$$

$$\delta S_2 = [0]\,\delta W_i + \left[\frac{\omega}{2}k_{13} W_s\right]\delta W_o + \left[\frac{\omega}{2}k_{13} W_o\right]\delta W_s + \left[\frac{1}{2}k_{13} W_o W_s\right]\delta\omega \qquad \text{(B-5d)}$$

$$\delta C_2 = \left[-k_7 W_i + \frac{1}{2} k_9 W_o - \frac{1}{2} k_{10} W_s \right] \delta W_i + \left[-k_8 W_o + \frac{1}{2} k_9 W_i - \frac{1}{2} k_{11} W_s \right] \delta W_o + \left[+k_7 W_s - \frac{1}{2} k_{10} W_i - \frac{1}{2} k_{11} W_o \right] \delta W_s + [0] \delta \omega \qquad \text{(B-5e)}$$

$$\delta S_3 = \left[-\frac{3}{4} k_{12} W_i^2 + \frac{1}{4} k_{12} W_s^2 \right] \delta W_i + [0] \delta W_i + \left[\frac{1}{2} k_{12} W_i W_s \right] \delta W_s + [0] \delta \omega \qquad \text{(B-5f)}$$

$$\delta C_3 = \left[-\frac{\omega}{2} k_{14} W_i W_o \right] \delta W_i + \left[-\frac{\omega}{4} k_{14} \; W_i^2 - W_s^2 \; \right] \delta W_o + \left[\frac{\omega}{2} k_{14} W_o W_s \right] \delta W_s + \left[-\frac{1}{4} k_{14} W_o \; W_i^2 - W_s^2 \; \right] \delta \omega \qquad \text{(B-5g)}$$

$$\overline{W} \triangleq W_i \bar{1}_i + W_o \bar{1}_o + W_s \bar{1}_s \qquad \text{(B-6a)}$$

$$\overline{W} = W \, \bar{1}_W = W \left(c_i \bar{1}_i + c_o \bar{1}_o + c_s \bar{1}_s \right) \qquad \text{(B-6b)}$$

$$\delta \overline{W} = W \, \delta \bar{1}_W + \delta W \bar{1}_W = \delta W_i \bar{1}_i + \delta W_o \bar{1}_o + \delta W_s \bar{1}_s$$

$$= W \left(\delta c_i \bar{1}_i + \delta c_o \bar{1}_o + \delta c_s \bar{1}_s \right) + \delta W \left(c_i \bar{1}_i + c_o \bar{1}_o + c_s \bar{1}_s \right) \qquad \text{(B-6c)}$$

R-2618

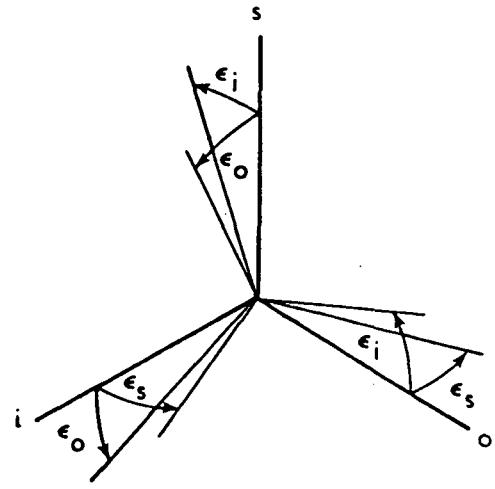

Figure B-1 Test Axis Misalignment Angles

The direction cosine errors are, from Fig. B-1:

$$\delta c_i = c_s \epsilon_o - c_o \epsilon_s$$

$$\delta c_o = c_i \epsilon_s - c_s \epsilon_i$$

$$\delta c_s = c_o \epsilon_i - c_i \epsilon_o \qquad \text{(B-6d)}$$

Therefore:

$$\delta W_i = c_i \delta W + W c_s \epsilon_o - W c_o \epsilon_s$$

$$\delta W_o = c_o \delta W + W c_i \epsilon_s - W c_s \epsilon_i$$

$$\delta W_s = c_s \delta W + W c_o \epsilon_i - W c_i \epsilon_o \qquad \text{(B-6e)}$$

$$\delta B = W\left(k_7 c_i - \frac{1}{2}k_9 c_o + \frac{1}{2}k_{10} c_s\right)\left(c_i \delta W + W c_s \epsilon_o - W c_o \epsilon_s\right)$$
$$+ W\left(-\frac{1}{2}k_9 c_i + k_8 c_o + \frac{1}{2}k_{11} c_s\right)\left(c_o \delta W - W c_s \epsilon_i + W_i \epsilon_s\right)$$
$$+ W\left(\frac{1}{2}k_{10} c_i + \frac{1}{2}k_{11} c_o - k_7 c_s\right)\left(c_s \delta W + W c_o \epsilon_i - W c_i \epsilon_o\right)$$
$$+ (0)\,\delta W$$

$$= W\left[k_7 c_i^2 + k_8 c_o^2 - k_7 c_s^2 - k_9 c_i c_o + k_{10} c_i c_s + k_{11} c_o c_s\right]\delta W$$
$$+ W^2\left[\frac{1}{2}k_{11} c_o^2 + \frac{1}{2}k_{10} c_s^2 - \frac{1}{2}k_{11} c_i c_o + 2k_7 c_i c_s - \left(k_7 - k_8\right) c_o c_s\right]\epsilon_i$$
$$+ W^2\left[\frac{1}{2}k_{10} c_i^2 + \frac{1}{2}k_{10} c_s^2 - \frac{1}{2}k_{11} c_i c_o + 2k_7 c_i c_s - \frac{1}{2}k_9 c_o c_s\right]\epsilon_o$$
$$+ W^2\left[-\frac{1}{2}k_9 c_i^2 + \frac{1}{2}k_9 c_o^2 - \left(k_7 + k_8\right) c_i c_o + \frac{1}{2}k_{11} c_i c_s - \frac{1}{2}k_{10} c_o c_s\right]\epsilon_s \qquad \text{(B-7a)}$$

$$\delta S_1 = \left[k_4 + \left(\frac{9}{4}k_{12} c_i^2 - \frac{3}{4}k_{12} c_s^2\right)W^2\right]\left(c_i \delta W + W c_s \epsilon_o - W c_o \epsilon_s\right)$$
$$+ \left[k_5\right]\left(c_o \delta W - W c_s \epsilon_i + W c_i \epsilon_s\right)$$
$$+ \left[k_6 - \frac{3}{2}k_{12} c_i c_s W^2\right]\left(c_s \delta W + W c_o \epsilon_i - W c_i \epsilon_o\right)$$
$$+ [0]\,\delta\omega$$

$$= \left[k_4 c_i + k_5 c_o + k_6 c_s + \left(\frac{9}{4}k_{12} c_i^3 - \frac{9}{4}k_{12} c_i c_s^2\right)W^2\right]\delta W$$
$$+ \left[\left(k_5 c_s + k_6 c_o\right)W - \frac{3}{2}k_{12} c_i c_o c_s W^3\right]\epsilon_i$$
$$+ \left[\left(k_4 c_s - k_6 c_i\right)W + \left(\frac{3}{4}k_{12} c_i^2 c_s - \frac{3}{4}k_{12} c_s^3\right)W^3\right]\epsilon_o$$
$$+ \left[\left(-k_4 c_o + k_5 c_i\right)W + \left(-\frac{9}{4}k_{12} c_i^2 c_o + \frac{3}{4}k_{12} c_o c_s^2\right)W^3\right]\epsilon_s$$
$$+ [0]\,\delta W \qquad \text{(B-7b)}$$

$$\delta C_1 = \omega\left[k_1 + \frac{1}{2}k_{14}c_i c_o W^2\right]\left(c_i\delta W + Wc_s\epsilon_o - Wc_o\epsilon_s\right)$$
$$+ \omega\left[k_2 + \left(\frac{1}{4}k_{14}c_i^2 - \frac{1}{4}k_{14}c_s^2\right)W^2\right]\left(c_o\delta W - Wc_s\epsilon_i + Wc_i\epsilon_s\right)$$
$$+ \omega\left[k_3 - \frac{1}{2}k_{14}c_o c_s W^2\right]\left(c_s\delta W + Wc_o\epsilon_i - Wc_i\epsilon_o\right)$$
$$+ \left[\left(k_1c_i + k_2c_o + k_3c_s\right)W + \left(\frac{1}{4}k_{14}c_o c_i^2 - \frac{1}{4}k_{14}c_o c_s^2\right)W^3\right]\delta\omega$$
$$= \omega\left[k_1c_i + k_2c_o + k_3c_s + \left(\frac{3}{4}k_{14}c_i^2c_o - \frac{3}{4}k_{14}c_o c_s^2\right)W^2\right]\delta W$$
$$+ \omega\left[\left(k_2c_s + k_3c_o\right)W + \left(-\frac{1}{4}k_{14}c_i^2c_s + \frac{1}{4}k_{14}c_s^3 - \frac{1}{2}k_{14}c_o^2c_s\right)W^3\right]\epsilon_i$$
$$+ \omega\left[\left(k_1c_s - k_3c_i\right)W - \frac{1}{4}k_{14}c_i c_o c_s W^3\right]\epsilon_o$$
$$+ \omega\left[\left(-k_1c_o + k_2c_i\right)W + \left(-\frac{1}{2}k_{14}c_i c_o^2 + \frac{1}{4}k_{14}c_i^3 - \frac{1}{4}k_{14}c_i c_s^2\right)W^3\right]\epsilon_s$$
$$+ \left[\left(k_1c_i + k_2c_o + k_3c_s\right)W + \left(\frac{1}{4}k_{14}c_i^2c_o - \frac{1}{4}k_{14}c_o c_s^2\right)W^3\right]\delta\omega \qquad \text{(B-7c)}$$

$$\delta S_2 = (0)\,\delta W_i$$
$$+ \left(\frac{\omega}{2}k_{13}c_s W\right)\left(c_o\delta W - Wc_s\epsilon_i + Wc_i\epsilon_s\right)$$
$$+ \left(\frac{\omega}{2}k_{13}c_o W\right)\left(c_s\delta W + Wc_o\epsilon_i - Wc_i\epsilon_o\right)$$
$$+ \left(\frac{1}{2}k_{13}c_o c_s W^2\right)\delta\omega$$
$$= \omega\left[k_{13}c_o c_s W\right]\delta W$$
$$+ \omega\left[k_{13}c_o^2\frac{W^2}{2} - k_{13}c_s^2\frac{W^2}{2}\right]\epsilon_i + \omega\left[-k_{13}c_i c_o\frac{W^2}{2}\right]\epsilon_o$$
$$+ \omega\left[k_{13}c_i c_s\frac{W^2}{2}\right]\epsilon_s + \left[k_{13}c_o c_s\frac{W^2}{2}\right]\delta\omega \qquad \text{(B-7d)}$$

$$\delta C_2 = \left[\left(k_7 c_i + k_9 c_o - k_{10} c_s\right) W\right]\left[c_i \delta W + W c_s \epsilon_o - W c_o \epsilon_s\right]$$
$$+ \left[\left(-k_8 c_o + k_9 c_i - k_{11} c_o\right) W\right]\left[c_o \delta W - W c_s \epsilon_i + W c_i \epsilon_s\right]$$
$$+ \left[\left(-k_7 c_s - k_{10} c_i - k_{11} c_o\right) W\right]\left[c_s \delta W + W c_o \epsilon_i - W c_i c_o\right]$$
$$+ [0]\,\delta\omega$$

$$= W\left[k_7 c_i^2 - k_8 c_o^2 - k_7 c_s^2 + k_9 c_i c_o - k_{10} c_i c_s - k_{11} c_o c_s\right]\delta W \;)$$
$$+ W^2\left[-\tfrac{1}{2}k_{11} c_o^2 + \tfrac{1}{2}k_{11} c_s^2 - \tfrac{1}{2}k_{10} c_i c_o - \tfrac{1}{2}k_9 c_i c_s + \left(k_8 - k_7\right) c_o c_s\right]\epsilon_i$$
$$+ W^2\left[+\tfrac{1}{2}k_{10} c_i^2 - \tfrac{1}{2}k_{10} c_s^2 + \tfrac{1}{2}k_{11} c_i c_o + 2k_7 c_i c_s + \tfrac{1}{2}k_9 c_o c_s\right]\epsilon_o$$
$$+ W^2\left[+\tfrac{1}{2}k_9 c_i^2 - \tfrac{1}{2}k_9 c_o^2 - \left(k_7 + k_8\right) c_i c_o - \tfrac{1}{2}k_{11} c_i c_s + \tfrac{1}{2}k_{10} c_o c_s\right]\epsilon_s$$
$$+ [0]\,\delta\omega \qquad \text{(B-7e)}$$

$$\delta S_3 = \left[\left(-\tfrac{3}{4}k_{12} c_i^2 + \tfrac{1}{4}k_{12} c_s^2\right) W^2\right]\left[c_i \delta W + W c_s \epsilon_o - W c_o \epsilon_s\right]$$
$$+ \left[\tfrac{1}{2}k_{12} c_i c_s W^2\right]\left[c_s \delta W + W c_o \epsilon_i - W c_i \epsilon_o\right]$$

$$= W^2\left[-\tfrac{3}{4}k_{12} c_i^3 + \tfrac{3}{4}k_{12} c_i c_s^2\right]\delta W$$
$$+ W^3\left[\tfrac{1}{2}k_{12} c_i^2 c_s\right]\epsilon_i$$
$$+ W^3\left[+\tfrac{1}{4}k_{12} c_s^3 - \tfrac{1}{4}k_{12} c_i^2 c_s\right]\epsilon_o$$
$$+ W^3\left[+\tfrac{3}{4}k_{12} c_o c_i^2 - \tfrac{1}{4}k_{12} c_o c_s^2\right]\epsilon_s$$
$$+ [0]\,\delta\omega \qquad \text{(B-7f)}$$

$$
\begin{aligned}
\delta C_3 = {} & \omega \left[-\frac{1}{2} k_{14} c_i c_o W^2 \right] \left[c_i \delta W + W c_s \epsilon_o - W c_o \epsilon_s \right] \\
& + \omega \left[\left(-\frac{1}{4} k_{14} c_i^2 + \frac{3}{4} k_{14} c_s^2 \right) W^2 \right] \left[c_o \delta W - W c_s \epsilon_i + W c_i \epsilon_s \right] \\
& + \omega \; \frac{1}{2} k_{14} c_o c_s W^2 \quad c_s \delta W + W c_o \epsilon_i - W c_i \epsilon_o \\
& + \quad \left(-\frac{1}{4} k_{14} c_i^2 c_o + \frac{1}{4} k_{14} c_o c_s^2 \right) W^3 \quad \delta\omega \\
= {} & \omega W^2 \left[-\frac{3}{4} k_{14} c_i^2 c_o + \frac{3}{4} c_o c_s^2 \right] \delta W \\
& + \omega W^3 \left[\frac{1}{4} k_{14} c_i^2 c_s - \frac{1}{4} k_{14} c_s^3 + \frac{1}{2} k_{14} c_o^2 c_s \right] \epsilon_i \\
& + \omega W^3 \left[-\frac{1}{2} k_{14} c_i c_o^2 - \frac{1}{2} k_{14} c_i c_o c_s \right] \epsilon_o \\
& + \omega W^3 \left[\frac{1}{2} k_{14} c_i c_o^2 + \frac{1}{4} k_{14} c_i c_s^2 \right] \epsilon_s \\
& + W^3 \left[\frac{1}{4} k_{14} c_i^2 c_o + \frac{1}{4} k_{14} c_o c_s^2 \right] \delta\omega
\end{aligned}
\qquad \text{(B-7g)}
$$

TABLE B-1

SPECIALIZATION TO SIX CASES OF INTEREST

$$(\epsilon_i,\ \epsilon_o,\ \epsilon_s) = f(\epsilon_1,\ \epsilon_2)$$

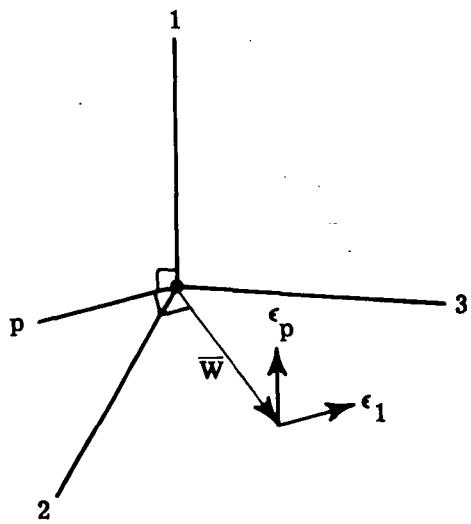

$$\epsilon_1 = \epsilon_1$$
$$\epsilon_2 = \epsilon_p/\sqrt{2}$$
$$\epsilon_3 = -\epsilon_p/\sqrt{2}$$

	c_i	c_o	c_s	ϵ_i	ϵ_o	ϵ_s
$W_i = W$	1	0	0	0	ϵ_1	ϵ_2
$W_o = W$	0	1	0	ϵ_1	0	ϵ_2
$W_s = W$	0	0	1	ϵ_1	ϵ_2	0
$W_i = W_o = \frac{W}{\sqrt{2}}$	$\frac{1}{\sqrt{2}}$	$\frac{1}{\sqrt{2}}$	0	$\frac{\epsilon_p}{\sqrt{2}}$	$-\frac{\epsilon_p}{\sqrt{2}}$	ϵ_1
$W_i = W_s = \frac{W}{\sqrt{2}}$	$\frac{1}{\sqrt{2}}$	0	$\frac{1}{\sqrt{2}}$	$-\frac{\epsilon_p}{\sqrt{2}}$	ϵ_1	$\frac{\epsilon_p}{\sqrt{2}}$
$W_o = W_s = \frac{W}{\sqrt{2}}$	0	$\frac{1}{\sqrt{2}}$	$\frac{1}{\sqrt{2}}$	ϵ_1	$\frac{\epsilon_p}{\sqrt{2}}$	$-\frac{\epsilon_p}{\sqrt{2}}$

Angular Vibration about the Output Axis

$$(W_o = W, \quad c_o = 1)$$

$$\begin{bmatrix} \delta B \\ \delta S_1 \\ \delta C_1 \\ \delta S_2 \\ \delta C_2 \\ \delta S_3 \\ \delta C_3 \end{bmatrix} = \left[\begin{array}{c|c|c|c} k_8 W & \frac{1}{2}k_{11}W^2 & \frac{1}{2}k_9 W^2 & 0 \\ k_5 & k_6 W & -k_4 W & 0 \\ \omega k_2 & \omega k_3 W & -\omega k_1 W & k_2 W \\ 0 & \omega k_{13}\frac{W^2}{2} & 0 & 0 \\ -k_8 W & -\frac{1}{2}k_{11}W^2 & -\frac{1}{2}k_9 W^2 & 0 \\ 0 & 0 & 0 & 0 \\ 0 & 0 & 0 & 0 \end{array}\right] \begin{bmatrix} \delta W \\ \epsilon_i \\ \epsilon_s \\ \delta\omega \end{bmatrix} \qquad \text{(B-8a)}$$

Angular Vibration about the Spin Axis

$$(W_s = W, \quad c_s = 1)$$

$$\begin{bmatrix} \delta B \\ \delta S_1 \\ \delta C_1 \\ \delta S_2 \\ \delta C_2 \\ \delta S_3 \\ \delta C_3 \end{bmatrix} = \left[\begin{array}{c|c|c|c} -k_7 W & -\frac{1}{2}k_{11}W^2 & \frac{1}{2}k_{10}W^2 & 0 \\ k_6 & k_5 W & k_4^* W - \frac{3}{4}k_{12}W^3 & 0 \\ \omega k_3 & \omega\left(k_2^* W + \frac{1}{4}k_{14}W^3\right) & \omega k_1 W & k_3 W \\ 0 & -\omega k_{13}\frac{W^2}{2} & 0 & 0 \\ +k_7 W & +\frac{1}{2}k_{11}W^2 & -\frac{1}{2}k_{10}W^2 & 0 \\ 0 & 0 & \frac{1}{4}k_{12}W^3 & 0 \\ 0 & -\omega\frac{1}{4}k_{14}W^3 & 0 & 0 \end{array}\right] \begin{bmatrix} \delta W \\ \epsilon_i \\ \epsilon_o \\ \delta\omega \end{bmatrix} \qquad \text{*B-8b)}$$

*Dominant Term.

Angular Vibration about the Input Axis

$$(W_i = W, \quad c_i = 1)$$

$$\begin{bmatrix} \delta B \\ \delta S_1 \\ \delta C_1 \\ \delta S_2 \\ \delta C_2 \\ \delta S_3 \\ \delta C_3 \end{bmatrix} = \left[\begin{array}{c|c|c|c} +k_7 W & -\frac{1}{2}k_{10}W^2 & -\frac{1}{2}k_9 W^2 & 0 \\ k_4^* + \frac{9}{4}k_{12}W^2 & -k_6 W & k_5 W & 0 \\ \omega k_1 & -\omega k_3 W & \omega\left(k_2^* W + \frac{1}{4}k_{14}W^3\right) & k_1 W \\ 0 & 0 & 0 & 0 \\ -k_7 W & +\frac{1}{2}k_{10}W^2 & +\frac{1}{2}k_9 W^2 & 0 \\ -\frac{3}{4}k_{12}W^2 & 0 & 0 & 0 \\ 0 & 0 & 0 & \end{array}\right] \begin{bmatrix} \delta W \\ \epsilon_o \\ \epsilon_s \\ \delta\omega \end{bmatrix} \qquad \text{(B-8c)}$$

Angular Vibration about Output and Spin Axes

$$(W_o = W_s = W/\sqrt{2}, \quad c_o = c_s = 1/\sqrt{2})$$

$$\begin{bmatrix} \delta B \\ \delta S_1 \\ \delta C_1 \\ \delta S_2 \\ \delta C_2 \\ \delta S_3 \\ \delta C_3 \end{bmatrix} = \left[\begin{array}{c|c|c|c} (k_8 - k_7 + k_{11})\frac{W}{2} & (-k_7 - k_8)\frac{W^2}{2} & \frac{1}{2}(k_{10}^* - k_9)\frac{W^2}{\sqrt{2}} & 0 \\ (k_5 + k_6)\frac{1}{\sqrt{2}} & (k_5 + k_6)\frac{W}{\sqrt{2}} & k_4^* W - \frac{3}{8}k_{12}W^3 & 0 \\ \omega\left[(k_2^* + k_3)\frac{1}{\sqrt{2}} - \frac{3}{8}k_{14}\frac{W^2}{\sqrt{2}}\right] & \omega\left[(k_2^* + k_3)\frac{W}{\sqrt{2}} - \frac{1}{8}k_{14}\frac{W}{\sqrt{2}}\right] & \omega k_1 W & (k_2^* + k_3)\frac{W}{\sqrt{2}} - \frac{1}{8}k_{14}\frac{W^3}{\sqrt{2}} \\ \omega k_{13}\frac{W}{2} & 0 & 0 & k_{13}\frac{W^2}{4} \\ (-k_8 + k_7 - k_{11})\frac{W}{2} & +(k_7 + k_8)\frac{W^2}{2} & \frac{1}{2}(k_9^* - k_{10})\frac{W^2}{\sqrt{2}} & 0 \\ 0 & 0 & \frac{1}{8}k_{12}W^3 & 0 \\ \omega\frac{3}{8}k_{14}\frac{W^2}{\sqrt{2}} & \omega\frac{1}{4}k_{14}\frac{W^3}{\sqrt{2}} & 0 & \frac{1}{8}k_{14}\frac{W^3}{\sqrt{2}} \end{array}\right] \begin{bmatrix} \delta W \\ \epsilon_i \\ \epsilon_p \\ \delta\omega \end{bmatrix} \qquad \text{(B-8d)}$$

*Dominant Term.

Angular Vibration about Input and Output Axes

$$(W_i = W_o = W/\sqrt{2}, \quad c_i = c_o = 1/\sqrt{2})$$

$$\begin{bmatrix} \delta B \\ \delta S_1 \\ \delta C_1 \\ \delta S_2 \\ \delta C_2 \\ \delta S_3 \\ \delta C_3 \end{bmatrix} = \left[\begin{array}{c|c|c|c} (+k_7+k_8-k_9)\frac{W}{2} & (-k_7+k_8)\frac{W^2}{2} & \frac{1}{2}(k_{11}^*+k_{10})\frac{W^2}{\sqrt{2}} & 0 \\ (k_4^*+k_5)\frac{1}{\sqrt{2}} - \frac{9}{8}k_{12}\frac{W^2}{\sqrt{2}} & (-k_4^*+k_5)\frac{W}{\sqrt{2}} - \frac{9}{8}k_{12}\frac{W^3}{\sqrt{2}} & k_6 W & 0 \\ \omega\left[(k_1+k_2^*)\frac{1}{\sqrt{2}} - \frac{3}{8}k_{14}\frac{W^2}{\sqrt{2}}\right] & \omega\left[(-k_1^*+k_2)\frac{W}{\sqrt{2}} - \frac{1}{8}k_{14}\frac{W^3}{\sqrt{2}}\right] & \omega k_3 W & (k_1+k_2^*)\frac{1}{\sqrt{2}} + \frac{1}{8}\frac{W^3}{\sqrt{2}} \\ 0 & 0 & \frac{1}{2}\omega k_{13}\frac{W^2}{\sqrt{2}} & 0 \\ (-k_7-k_8+k_9)\frac{W}{2} & -(-k_7+k_8)\frac{W^2}{2} & -\frac{1}{2}(k_{11}+k_{10}^*)\frac{W^2}{\sqrt{2}} & 0 \\ -\frac{3}{8}k_{12}\frac{W^2}{\sqrt{2}} & \frac{3}{8}k_{12}\frac{W^3}{\sqrt{2}} & 0 & 0 \\ -\omega\frac{3}{8}k_{14}\frac{W^2}{\sqrt{2}} & \omega\frac{1}{4}k_{14}\frac{W^3}{\sqrt{2}} & \omega\frac{1}{8}k_{14}W^3 & \frac{1}{8}k_{14}\frac{W^3}{\sqrt{2}} \end{array}\right] \begin{bmatrix} \delta W \\ \epsilon_s \\ \epsilon_p \\ \delta\omega \end{bmatrix} \qquad \text{(B-8e)}$$

Angular Vibration about Input and Spin Axes

$$(W_i = W_s = W/\sqrt{2}, \quad c_i = c_s = 1/\sqrt{2})$$

$$\begin{bmatrix} \delta B \\ \delta S_1 \\ \delta C_1 \\ \delta S_2 \\ \delta C_2 \\ \delta S_3 \\ \delta C_3 \end{bmatrix} = \left[\begin{array}{c|c|c|c} \frac{1}{2}k_{10}W & +k_7W^2 & \frac{1}{2}(k_{11}-k_9)\frac{W^2}{\sqrt{2}} & 0 \\ (k_4^*+k_6)\frac{1}{\sqrt{2}} - \frac{9}{8}k_{12}\frac{W^2}{\sqrt{2}} & (k_4^*-k_6)\frac{W}{\sqrt{2}} & 0 & 0 \\ \omega(k_1+k_3)\frac{1}{\sqrt{2}} & \omega(k_1-k_3)\frac{W}{\sqrt{2}} & 0 & (k_1+k_3)\frac{W}{\sqrt{2}} \\ 0 & 0 & \frac{1}{2}\omega k_{13}\frac{W^2}{\sqrt{2}} & 0 \\ -\frac{1}{2}k_{10}W & -k_7W^2 & -\frac{1}{2}(k_{11}-k_9)\frac{W^2}{\sqrt{2}} & 0 \\ 0 & 0 & -\frac{1}{8}k_{12}W^3 & 0 \\ 0 & 0 & \omega\frac{1}{16}k_{14}W^3 & 0 \end{array}\right] \begin{bmatrix} \delta W \\ \epsilon_o \\ \epsilon_p \\ \delta\omega \end{bmatrix} \qquad \text{(B-8f)}$$

*Dominant Term.

APPENDIX C

KALMAN FILTERING FORMULATION

For the single-axis vibration tests described in Chapter 3, the first data processing stage (see phase Ia in Fig. 3.1-3) is one which accepts as input the scalar, periodically time-varying gyro output and produces as output the set of Fourier coefficients defining the applied torque function. This appendix formulates this data processing function as a problem in linear estimation for which the Kalman filter is an optimal solution. The filter equations, which could be used for processing actual test data, are presented. A hypothetical situation in which there is no process noise is used to demonstrate the trade-off between test accuracy and test duration, and to show a connection between this type of processing and classical Fourier analysis. Finally, the full problem, with both measurement noise and process noise is treated and some approximate equations, which are useful in predicting the achievable test accuracy and required test duration, are developed.

C.1 FILTER EQUATIONS

In this section the estimation problem is formulated in mathematical terms and the optimal solution is stated in the form of a set of differential equations, the Kalman filter equations, which can be mechanized to process data. No proof is given here for the optimality of this solution since it is well documented. (See, for example, Ref. 8.)

The problem formulation requires three things: a linear measurement equation, a linear state differential equation and a description of the statistics of the random variables defined in these two equations. A scalar time-varying signal (torquer current) is measured which, except for errors in the measurement process, is proportional to the output of the torque generator. Therefore, the measurement equation is (See App. A.):

$$
\begin{aligned}
z &= M_o + \text{error} \\
&= B + S_1 \sin \omega t + C_1 \cos \omega t \\
&\quad + S_2 \sin 2\,\omega t + C_2 \cos 2\,\omega t \\
&\quad + S_3 \sin 3\,\omega t + C_3 \cos 3\,\omega t \\
&\quad + \text{error}
\end{aligned}
\qquad \text{(C.1-1)}
$$

which can be rewritten:

$$z = x_1 h_1 + x_2 h_2(t) + x_3 h_3(t)$$
$$+ x_4 h_4(t) + x_5 h_5(t)$$
$$+ x_6 h_6(t) + x_7 h_7(t)$$
$$+ v(t)$$
$$= H\underline{x} + v \qquad \text{(C.1-2)}$$

The components of the state vector $\underline{x}$ are the 7 Fourier coefficients. The elements of the measurement matrix H (in this case a row vector) are the set of time-varying functions (1, $\sin \omega t$, $\cos \omega t$, $\sin 2\omega t$, ...). We assume the measurement noise v to be Gaussian white noise with zero mean and covariance $r\delta(t - \tau)$, where δ is the Dirac delta function:

$$\overline{v(t)} = 0; \quad \overline{v(t)\,v(\tau)} = r\delta(t - \tau) \qquad \text{(C.1-3)}$$

Before discussing the state differential equation and process noise we distinguish between the following two test situations. In case a the only data produced by the test is that representing the time history of the gyro torquer output, and it is natural to define measurement noise as above. No measurements of test table angle are generated, and it is also natural to regard fluctuations in the applied test motions as one source of process noise. In case b both gyro rebalance torque and test table angle measurements are generated. In formulating the estimation problem below, however, we continue to treat gyro torque measurement errors as the only source of measurement noise and we regard table angle encoder errors as a source of process noise. This point of view avoids more complex calculations which would arise if we expanded the measurement equation to include table angle measurements.

Case a

The state equation is the seven-dimensional vector differential equation expressing the rates of change of the seven Fourier coefficients. The state equation is:

$$\dot{\underline{x}} = \underline{u} \tag{C.1-4}$$

where the process noise vector $\underline{u}$ is also assumed to be Gaussian white noise with:

$$\overline{\underline{u}(t)} = 0\,; \quad \overline{\underline{u}(t)\underline{u}(\tau)^T} = Q\delta(t-\tau) \tag{C.1-5}$$

There are two ways in which process noise can occur. Consider the following specific example of a single-axis angular vibration test. The test motion axis is midway between the gyro output and spin axes; the applied angular rate is given by:

$$W_o = W_s = \frac{W}{\sqrt{2}} \sin \omega t \tag{C.1-6}$$

Based on the expressions given in Table 3.1-1 we can write for the measurement equation:

$$
\begin{aligned}
z = & \left[M_b + \frac{W^2}{4}\left(k_8 - k_7 + k_{11}\right)\right] \\
& + \left[\frac{W}{\sqrt{2}}\left(k_5 + k_6\right)\right] \sin \omega t \\
& + \left[\frac{\omega W}{\sqrt{2}}\left(k_2 + k_3 - \frac{1}{4}k_4\right)\right] \cos \omega t \\
& + \left[\frac{\omega W^2}{\sqrt{2}} k_{13}\right] \sin 2\,\omega t \\
& + \left[-\frac{W^2}{4}\left(k_8 - k_7 + k_{11}\right)\right] \cos 2\,\omega t \\
& + [0] \sin 3\,\omega t \\
& + \left[\frac{\omega W^3}{8\sqrt{2}}\ k_{14}\right] \cos 3\,\omega t \\
& + v(t) \qquad \text{(C.1-7)}
\end{aligned}
$$

The terms in the brackets are the seven state variables in this example. They can vary either because the basic parameter groups (the k_i's) vary during the test or because the test motion amplitude and frequency (W and ω) vary during the test. If test motion variations are the major cause of process noise, the various components of the noise vector will be highly correlated since W appears in all six non-zero state variable definitions and ω appears in three of them. That is, the off-diagonal elements of the Q matrix will be non-zero and significant. If, on the other hand, gyro parameter changes are the major cause of process noise, we would expect

very little correlation between process noise components; the only exception being a strong correlation between the first and fifth components because both depend on parameter groups k_7, k_8 and k_{11}.

Since both the state equation and the measurement equation are linear (with time-varying coefficients in the latter), and since the process and measurement noises are assumed to be Gaussian, the Kalman filter is the optimal way (minimum variance estimation error) to process the measurement data. The applicable form of these equations may be written:

$$\dot{\hat{\underline{x}}} = K[z - H\hat{\underline{x}}] \tag{C.1-8}$$

$$K = \frac{1}{r}PH^T \tag{C.1-9}$$

$$\dot{P} = Q - \frac{1}{r}PH^THP \tag{C.1-10}$$

where $\hat{\underline{x}}$ is the optimal estimate of the state vector $\underline{x}$, K is the Kalman filter gain matrix (7×1) and P is the covariance matrix of the estimation error:

$$P = \overline{(\hat{\underline{x}} - \underline{x})(\hat{\underline{x}} - \underline{x})^T} \tag{C.1-11}$$

The integration of Eq. (C.1-10) yields curves like that illustrated in Fig. 3.3-3.

Case b

We now consider the situation in which table angle measurements are generated. In the following formulation Eq. (C.1-10) still applies, but with a modified interpretation for the process noise matrix Q. Consider the third state variable in the above example:

$$x_3 = \frac{\omega W}{\sqrt{2}}\left(k_2 + k_3 - \frac{1}{4}k_4\right) \qquad \text{(C.1-12)}$$

Differentiating:

$$\dot{x}_3 = u_3 = \frac{\omega W}{\sqrt{2}}\left(\dot{k}_2 + \dot{k}_3 - \frac{1}{4}\dot{k}_4\right)$$

$$+ \frac{\omega}{\sqrt{2}}\left(k_2 + k_3 - \frac{1}{4}k_4\right)\dot{W}$$

$$+ \frac{W}{\sqrt{2}}\left(k_2 + k_3 - \frac{1}{4}k_4\right)\dot{\omega} \qquad \text{(C.1-13)}$$

We will consider the test motion changes, $\dot{W}$ and $\dot{\omega}$, as control functions which change the values of the state variables (Fourier coefficients). The indicated values of these control functions, which are derived from test table measurements, enter into the filter equations as a control vector. Following the development in Ref. 7, Section 2.2, "State Estimation Without Measurements," we can write for the state equation:

$$\dot{\underline{x}} = \underline{u} = F\underline{x} + G\underline{u}_k + L\underline{p} \qquad \text{(C.1-14)}$$

[See Eq. (2.2-6) in Ref. 7.]

where, in this case:

$F = 0$

$\underline{u}_k$ represents random "system disturbances," or changes in the values of the parameter groups ($\dot{k}_1, \ldots \dot{k}_{14}$).

$\underline{p}$ represents the "control function," or test motion changes ($\dot{W}, \dot{\omega}$).

G is a 7×14 matrix whose elements are terms like $\omega W/\sqrt{2}$

L is a 7×2 matrix whose elements are terms like

$$\frac{\omega}{\sqrt{2}}\left(k_2 + k_3 - \frac{1}{4}k_4\right).$$

Following Eq. (2.2-8) in Ref. 7, we can write:

$$\dot{P} = \cancel{F}^{0} P + P \cancel{F}^{T\,0} + GQ_kG^T + LSL^T \qquad \text{(C.1-15)}$$

where:

$$\overline{\underline{u}_k(t)\,\underline{u}_k(\tau)^T} = Q_k\,\delta(t-\tau) \qquad \text{(C.1-16)}$$

and:

$$\overline{\left[\underline{p}(t) - \underline{p}_{ind}(t)\right]\left[\underline{p}(t) - \underline{p}_{ind}(\tau)\right]^T} = S\,\delta(t-\tau) \qquad \text{(C.1-17)}$$

We define the effective, overall process noise matrix as:

$$Q = GQ_kG^T + LSL^T \qquad \text{(C.1-18)}$$

where GQ_kG^T represents the contribution of random changes in the gyro parameters and LSL^T represents the contribution of "errors in the applied control," i.e., errors in the indicated test motion. We have adopted the following point of view. The indicated history of test motion, derived from the table angle measurements, is regarded as the "desired" control function. The difference between the actual and indicated motion

changes can then be regarded as the error in the applied control. This error is effectively a process noise in this formulation.

Together with the modified interpretation of the process noise matrix Q, Eq. (C.1-10) must be modified to account for the effect of the indicated, or "desired," control:

$$\dot{\underline{\hat{x}}} = K[z - H\underline{\hat{x}}] + L\underline{p}_{ind} \qquad (C.1\text{-}19)$$

C.2 TEST TIME VS ACCURACY

For the hypothetical situation in which there is no process noise (Q = 0) Eq. (C.1-10) reduces to:

$$\dot{P} = -\frac{1}{r} P H^T H P \qquad (C.2\text{-}1)$$

Since the derivative of the inverse matrix can be written:

$$\dot{P}^{-1} = -P^{-1}\dot{P}P^{-1} \qquad (C.2\text{-}2)$$

we can write:

$$\dot{P}^{-1} = \frac{1}{r} P^{-1} P H^T H P P^{-1}$$

$$= \frac{1}{r} H^T H \qquad (C.2\text{-}3)$$

Based on the definition of H we have:

$$H^T H = \begin{bmatrix} 1 & \sin\omega t & \cos\omega t & \sin 2\omega t & \cos 2\omega t & \sin 3\omega t & \cos 3\omega t \\ & \sin^2\omega t & \sin\omega t\cos\omega t & \sin\omega t\sin 2\omega t & \sin\omega t\cos 2\omega t & \sin\omega t\sin 3\omega t & \sin\omega t\cos 3\omega t \\ & & \cos^2\omega t & \cos\omega t\sin 2\omega t & \cos\omega t\cos 2\omega t & \cos\omega t\sin 3\omega t & \cos\omega t\cos 3\omega t \\ & & & \sin^2 2\omega t & \sin 2\omega t\cos 2\omega t & \sin 2\omega t\sin 3\omega t & \sin 2\omega t\cos 2\omega t \\ & & & & \cos^2 2\omega t & \cos 2\omega t\sin 3\omega t & \cos 2\omega t\cos 3\omega t \\ & & \text{symmetric} & & & \sin^2 3\omega t & \sin 3\omega t\cos 3\omega t \\ & & & & & & \cos^2 3\omega t \end{bmatrix}$$

(C.2-4)

Notice that the off-diagonal elements are products of two time functions which are orthogonal over one test motion period, $T = 2\pi/\omega$ (the integral of the product is zero). The integral of the matrix $H^T H$ over exactly one period is, therefore, the diagonal matrix:

$$\int_{t=nT}^{t=(n+1)T} H^T H\, dt = T \begin{bmatrix} 1 & & & & & & \\ & \frac{1}{2} & & & & & \\ & & \frac{1}{2} & & & & \\ & & & \frac{1}{2} & & & \\ & & & & \frac{1}{2} & & \\ & & & & & \frac{1}{2} & \\ & & & & & & \frac{1}{2} \end{bmatrix} \qquad \text{(C.2-5)}$$

Therefore, the change in the inverse covariance matrix over one cycle of the test motion is:

$$\Delta P^{-1} = \frac{T}{r} \begin{bmatrix} 1 & & & & & & \\ & \frac{1}{2} & & & & & \\ & & \frac{1}{2} & & & & \\ & & & \frac{1}{2} & & & \\ & & & & \frac{1}{2} & & \\ & & & & & \frac{1}{2} & \\ & & & & & & \frac{1}{2} \end{bmatrix} \qquad \text{(C.2-6)}$$

and

$$P^{-1}(nT) = P^{-1}(0) + \frac{nT}{r} \begin{bmatrix} 1 & & & & & & \\ & \frac{1}{2} & & & & & \\ & & \frac{1}{2} & & & & \\ & & & \frac{1}{2} & & & \\ & & & & \frac{1}{2} & & \\ & & & & & \frac{1}{2} & \\ & & & & & & \frac{1}{2} \end{bmatrix} \qquad \text{(C.2-7)}$$

where n is the number of cycles since the start of the test. After sufficient time has elapsed the second term of Eq. (C.2-7) dominates the first term, $P^{-1}(0)$, allowing us to write the approximate expression:

$$\underset{t \to \text{large}}{P^{-1}(t)} \approx \frac{t}{r} \begin{bmatrix} 1 & & & & & & \\ & \frac{1}{2} & & & & & \\ & & \frac{1}{2} & & & & \\ & & & \frac{1}{2} & & & \\ & & & & \frac{1}{2} & & \\ & & & & & \frac{1}{2} & \\ & & & & & & \frac{1}{2} \end{bmatrix} \qquad \text{(C.2-8)}$$

The covariance matrix then becomes (taking the inverse of the inverse):

$$\underset{t \to \text{large}}{P(t)} \approx \frac{r}{t} \begin{bmatrix} 1 & & & & & & \\ & 2 & & & & \bigcirc & \\ & & 2 & & & & \\ & & & 2 & & & \\ & & & & 2 & & \\ & \bigcirc & & & & 2 & \\ & & & & & & 2 \end{bmatrix} \qquad \text{(C.2-9)}$$

Thus, for the no-process-noise case, the simultaneous estimation of the seven state variables, x_1 through x_7, separates into seven scalar problems for which the rms estimation errors are:

$$\sigma_1 = \sqrt{P_{11}} = \sqrt{\frac{r}{t}} \qquad \text{(C.2-10)}$$

and

$$\sigma_i = \sqrt{P_{ii}} = \sqrt{\frac{2r}{t}} \qquad (i = 2, 3, \ldots 7) \qquad \text{(C.2-11)}$$

Equation (C.2-11) illustrates the trade-off between test time and test accuracy as a function of the measurement noise.

C.3 CONNECTION WITH FOURIER ANALYSIS

The analysis of the preceding section can be extended slightly to demonstrate an interesting connection between optimal filtering and Fourier analysis techniques.

The combination of Eqs. (C.1-9) and (C.2-9) yields the following approximate expression for the filter gain matrix:

$$\underset{t \to \text{large}}{K} = \frac{1}{r} P H^T \approx \frac{1}{t} \begin{bmatrix} 1 \\ 2\sin \omega t \\ 2\cos \omega t \\ 2\sin 2\omega t \\ 2\cos 2\omega t \\ 2\sin 3\omega t \\ 2\cos 3\omega t \end{bmatrix} \qquad \text{(C.3-1)}$$

Substituting Eq. (C.3-1) into Eq. (C.1-8) yields:

$$\dot{\underline{\hat{x}}} \approx \frac{1}{t} \left\{ \begin{bmatrix} 1 \\ 2\sin \omega t \\ 2\cos \omega t \\ 2\sin 2\omega t \\ \vdots \end{bmatrix} z - \begin{bmatrix} 1 \\ 2\sin \omega t \\ 2\cos \omega t \\ 2\sin 3\omega t \\ \vdots \end{bmatrix} [1 \quad \sin \omega t \quad \cos \omega t \quad \ldots] \underline{\hat{x}} \right\} \qquad \text{(C.3-2)}$$

Integrating Eq. (C.3-2) over one cycle, and treating $\frac{1}{t}$ and $\hat{\underline{x}}$ as constant over this time yields:

$$\Delta\hat{\underline{x}}_{n+1} = \int_{nT}^{(n+1)T} \dot{\underline{x}}\,dt \approx \frac{1}{t}\left\{\int_{nT}^{(n+1)T} \begin{bmatrix} 1 \\ 2\sin\omega t \\ 2\cos\omega t \\ \vdots \end{bmatrix} z\,dt - I\hat{\underline{x}}\,T\right\} \tag{C.3-3}$$

In Fourier analysis the coefficients are determined by:

$$B = \frac{1}{T}\int_0^T z\,dt \tag{C.3-4}$$

$$S_n = \frac{2}{T}\int_0^T z\sin(n\omega t)\,dt \tag{C.3-5}$$

$$C_n = \frac{2}{T}\int_0^T z\cos(n\omega t)\,dt \tag{C.3-6}$$

See, for example Ref. 9. Also $t \cong nT$. Therefore:

$$\Delta\hat{\underline{x}}_{n+1} = \frac{1}{n}\left\{\begin{bmatrix}\text{Fourier estimate of } \underline{x} \\ \text{based on } (n+1)^{st} \text{ cycle} \\ \text{of data.}\end{bmatrix} - \hat{\underline{x}}_n\right\} \tag{C.3-7}$$

and:

$$\hat{\underline{x}}_{n+1} = \hat{\underline{x}}_n + \Delta\hat{\underline{x}}_{n+1} \tag{C.3-8}$$

Thus, after sufficient time has elapsed, the optimal filtering equation becomes approximately Eq. (C.3-8), in which the state vector estimate $\hat{\underline{x}}_n$ based on n cycles of data is adjusted by a weighted (1/n) difference between the Fourier estimate based on the $n+1^{st}$ cycle of data and the previous estimate.

C.4 STEADY STATE SOLUTIONS WITH PROCESS NOISE

We now consider the effects of process noise, represented by the matrix Q in Eq. (C.1-10). The elements of the Q matrix along with the measurement noise r determine the final value of the elements of the P matrix as well as the settling time, t_s. Note that the rms estimation error of the i^{th} state variable is the square root of the i^{th} diagonal element of the covariance matrix:

$$\sigma_i = \sqrt{P_{ii}} \qquad \text{(C.4-1)}$$

Equation (C.1-10) represents $n(n+1)/2$ simultaneous first-order ordinary differential equations which are nonlinear (since P appears twice in one term) and which contain time varying coefficients (the elements of H). The elements of P cannot reach constant values (with $\dot{P} = 0$) since the elements of H change continuously. They can, however, reach a steady-state solution in the form of an oscillation about average values.

The most evident way of investigating these steady-state solutions is to numerically integrate Eq. (C.1-10) via computer, starting from various initial values. Some examples of such integrations for one- and two-dimensional versions of the problem are illustrated in Figs. C-1 and C-2 and discussed below. We can achieve an analytic indication of the final average values by making some simplifying assumptions as follows.

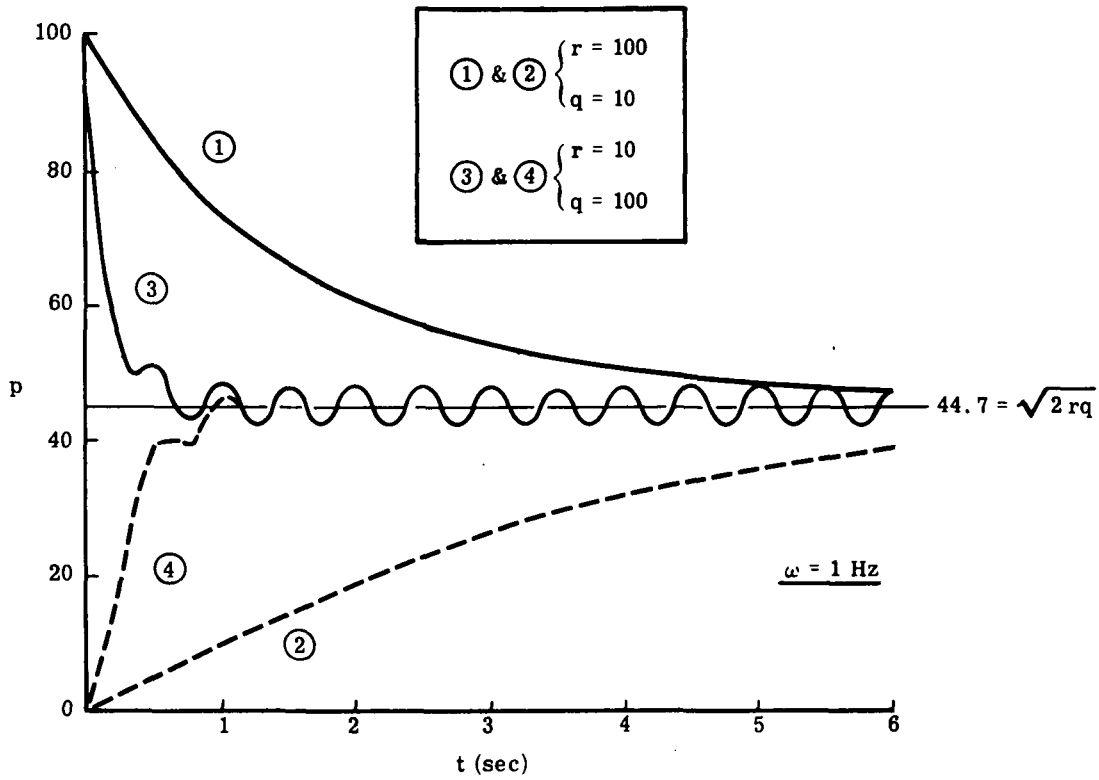

Figure C-1 Numerical Integration Results

Consider, first a one-dimensional version of Eq. (C.1-10) where we are trying to estimate a single variable, the magnitude of a sinusoidal oscillation:

$$\dot{p}(t) = q - \frac{1}{r}h^2(t)p^2(t) \qquad \text{(C.4-2)}$$

where

$$h(t) = \sin \omega t \qquad \text{(C.4-3)}$$

The scalar p is the variance of the estimation error and the scalar q characterizes the process noise. We set h^2 equal to its average value (1/2) and let $\dot{p} = 0$ to obtain the steady-state equation:

$$0 = q - \frac{1}{2r}p_{ss}^2 \qquad \text{(C.4-4)}$$

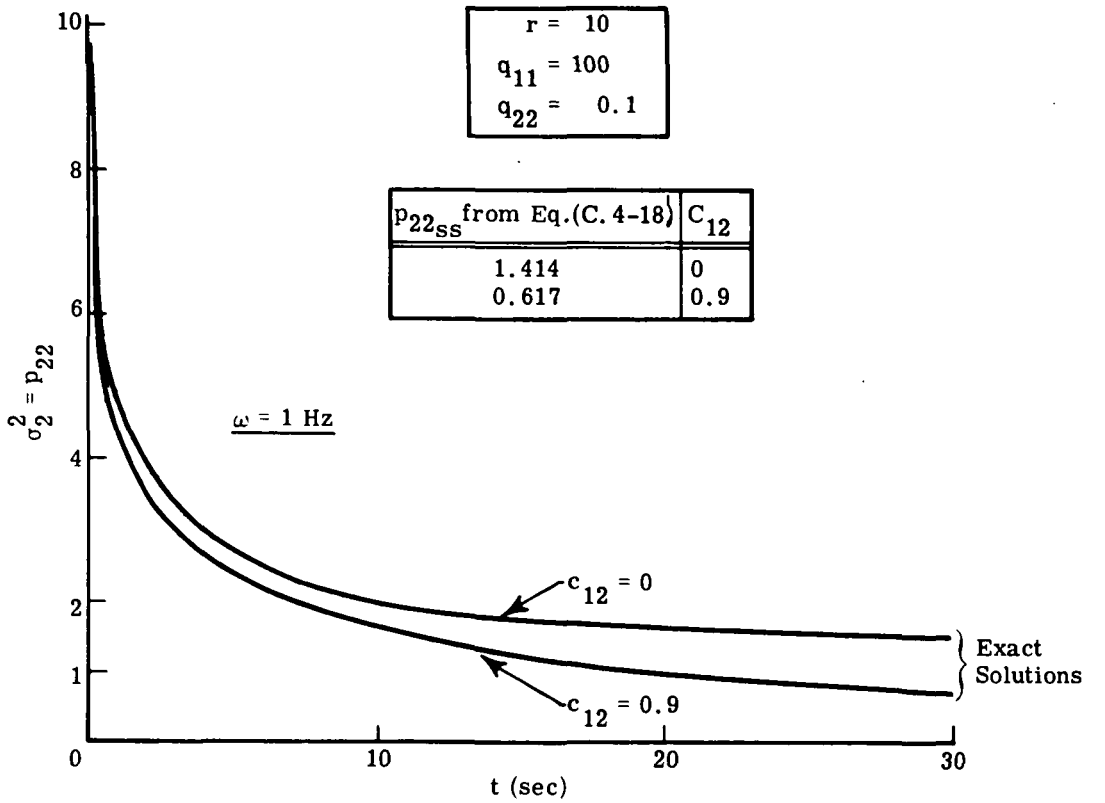

Figure C-2 Improvement in Small Term Estimate Due to Correlation

Therefore:

$$p_{ss} = \sqrt{2qr} \qquad (C.4\text{-}5)$$

The validity of this solution is demonstrated in Fig. C-1 where integrations of the exact equation, Eq. (C.4-2), are plotted for four combinations of r, q and p(0). Note that while the steady-state value is apparently the same in all cases, it is approached much faster with the smaller measurement noise, r. Also note that the true steady-state solution is more oscillatory with the higher ratio of q/r. (Oscillations are also present in cases (1) and (2) but are too small to be seen in the figure.)

Consider next the two-dimensional problem in which a large variable (Fourier coefficient), x_1, is multiplying $\sin \omega t$ and a small variable, x_2 is multiplying $\sin 2\omega t$. We refer to x_1 as the "dominant term" and x_2 as the "nondominant term." In the following development the process noise q_{11} associated with x_1 is assumed to be much larger than the process noise q_{22} associated with x_2. [This would be true whenever test motion amplitude variations are the major cause of process noise; see Eq. (C.1-7).] The off-diagonal element q_{12} of the process noise matrix can take values between zero (no correlation between process noise components) and $\pm\sqrt{q_{11}q_{22}}$ (perfect correlation). Equation (C.1-10) now becomes:

$$\begin{bmatrix} \dot{p}_{11} & \dot{p}_{12} \\ p_{12} & p_{22} \end{bmatrix} = \begin{bmatrix} q_{11} & q_{12} \\ q_{12} & q_{22} \end{bmatrix} - \frac{1}{r} \begin{bmatrix} p_{11} & p_{12} \\ p_{12} & p_{22} \end{bmatrix} \begin{bmatrix} \sin^2 \omega t & \sin \omega t \sin 2\omega t \\ \sin \omega t \sin 2\omega t & \sin^2 2\omega t \end{bmatrix} \begin{bmatrix} p_{11} & p_{12} \\ p_{12} & p_{22} \end{bmatrix} \tag{C.4-6}$$

We let the time varying elements of $H^T H$ take their average values:

$$\sin^2 \omega t = \sin^2 2\omega t = \frac{1}{2} \tag{C.4-7}$$

and

$$\sin \omega t \sin 2\omega t = 0 \tag{C.4-8}$$

We also assume:

$$p_{11_{ss}} \gg p_{22_{ss}} \tag{C.4-9}$$

which is borne out by the results below if $q_{11} \gg q_{22}$. Therefore:

$$p_{11_{ss}} + p_{22_{ss}} \approx p_{11_{ss}} \tag{C.4-10}$$

with the assumptions of Eqs. (C.4-7), (C.4-8) and (C.4-10), Eq. (C.4-6) becomes equivalent to the three scalar equations:

$$\left.\begin{aligned} \dot{p}_{11} &= q_{11} - \frac{1}{2r} p_{11}^2 \\ \dot{p}_{12} &= q_{12} - \frac{1}{2r} p_{11} p_{12} \\ \dot{p}_{22} &= q_{22} - \frac{1}{2r} p_{12}^2 + p_{22}^2 \end{aligned}\right\} \tag{C.4-11}$$

Setting the three left-hand-sides equal to zero yields the steady-state solution:

$$p_{11_{ss}} = \sqrt{2rq_{11}} \tag{C.4-12}$$

$$p_{12_{ss}} = q_{12}\sqrt{\frac{2r}{q_{11}}} \tag{C.4-13}$$

$$p_{22_{ss}} = \sqrt{2r\left(q_{22} - \frac{q_{12}^2}{q_{11}}\right)} \tag{C.4-14}$$

Equation (C.4-12), giving the steady-state variance of the dominant term, is the same as Eq. (C.4-5) for the one-dimensional case. Equation (C.4-16) giving the steady-state variance of the small term, reduces to Eq. (C.4-5) when the cross-correlation term, q_{12}, is zero. Thus, we can write:

$$p_{ii} = \sqrt{2rq_{ii}} - \Delta_i \qquad \text{(C.4-15)}$$

where Δ_i accounts for an improvement due to correlation between the various components of process noise. A conservative formula for the final value of the estimation error for the i^{th} state variable is, therefore:

$$\boxed{\sigma_i^2 = \sqrt{2rq_{ii}}} \qquad \text{(C.4-16)}$$

The settling time (defined in Section 3.3 and illustrated in Fig. 3.3-3) associated with this level of accuracy may be found by setting Eq. (C.2-11) equal to Eq. (C.4-16) and solving for t, yielding

$$\boxed{t_{s_i} = \sqrt{2\frac{r}{q_{ii}}}} \qquad \text{(C.4-17)}$$

Equations (C.4-16) and (C.4-17) are plotted parametrically in Fig. 3.2-5.

An alternate form of Eq. (C.4-14) is:

$$\sigma_2^2 = p_{22_{ss}} = \sqrt{2\,rq_{22}\left(1 - c_{12}^2\right)} \qquad \text{(C.4-18)}$$

where c_{12} is a measure of the correlation between the two components of process noise:

$$c_{12} \triangleq \frac{q_{12}}{\sqrt{q_{11}\,q_{22}}} \qquad \text{(C.4-19)}$$

The corresponding expression for a useful test time is:

$$t_{s_2} = \sqrt{\frac{2\,r}{q_{22}}}\;\frac{1}{\sqrt{1 - c_{12}^2}} \qquad \text{(C.4-20)}$$

The validity of Eq. (C.4-18) is demonstrated in Fig. C-2 where integrations of the exact Eq. (C.4-6) are plotted for two values of the correlation measure (zero and 0.9).

In summary, through the use of simplifying assumptions we have developed a set of formulas which provide useful indications of the final steady-state estimation accuracies, Eqs. (C.4-16) and (C.4-18), and the corresponding settling times, Eqs. (C.4-2) and (C.4-6), for one- and two-dimensional versions of the estimation problem. Comparison of Eqs. (C.4-18) and (C.4-20) with Eqs. (C.4-16) and (C.4-17), respectively,

shows that a strong correlation between process noise components reduces the final estimation error of the nondominant term but increases the time needed to reach the more accurate level. The validity of the above formulas has not been checked for the n-variable case where $n > 2$. It is felt, however, that the formulas will remain valid since the two-dimensional case contains the essential ingredients of the problem.

APPENDIX D

FOURIER ANALYSIS EQUATIONS FOR PULSE REBALANCED TESTING

This appendix derives two sets of exact equations which produce the Fourier coefficients of the torque generator output produced during vibration testing of a pulse rebalanced sensor. The first set corresponds to the binary or ternary pulse-torquing scheme; the second set corresponds to the time modulation scheme. The torque produced by the rebalance loop opposes the total "applied" torque, which is the sum of the desired gyroscopic or pendulous torque and all disturbance torques. Since the applied test motion is periodic and the residual (non-motion-induced) torque is assumed to be constant over the time of the test, the total applied torque is assumed to be a periodic function of time.

D.1 BINARY AND TERNARY PULSE-TORQUING

Figure D-1 pictures typical waveforms of the applied torque, M_a, and the torque generator output, M_{tg}, as well as their integrals, for the binary pulse rebalanced case. The two integral functions are forced, by the action of the closed loop, to have the same low-frequency harmonic content (both consist of the ramp, Bt, plus a periodic function). The two torque functions, M_a and M_{tg}, must also have the same low-frequency description, even though they appear quite different in form. The derivative of the torque generator output, $\dot{M}_{tg}$, consists of a sequence of

R-1230

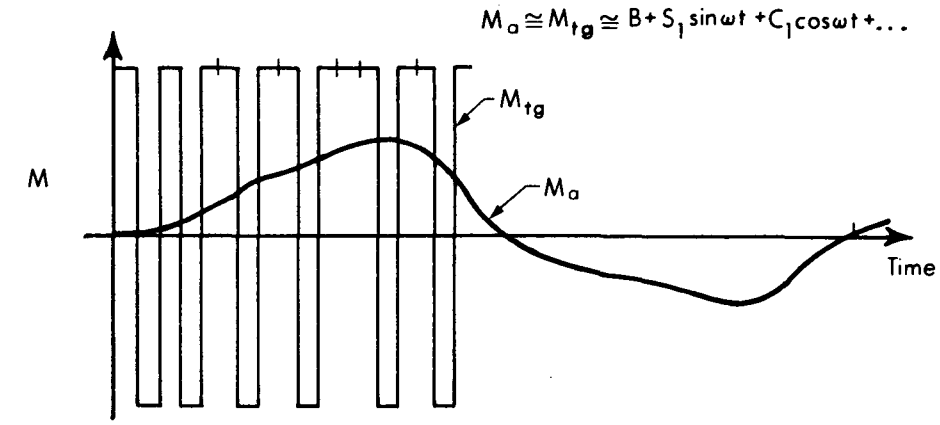

(a) Torque Waveform

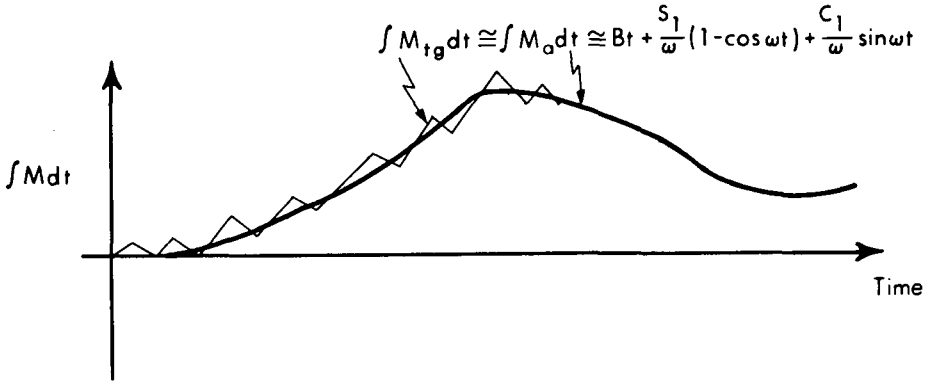

(b) Integral of Torque

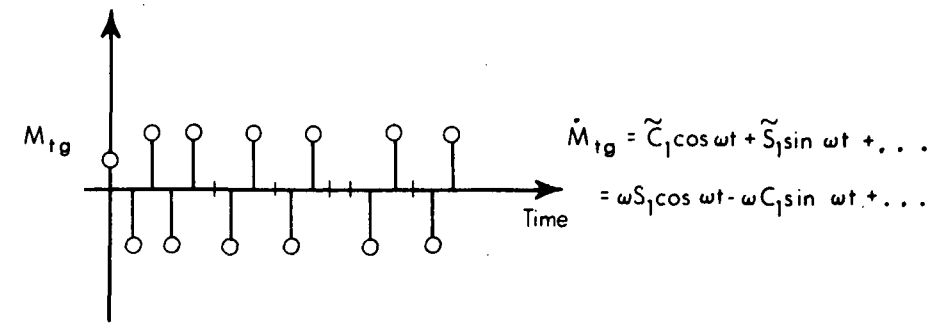

(c) Derivative of Torque

Figure D-1 Binary Pulse Rebalancing Waveforms

impulse functions, as shown at the bottom of the figure. It must also be a periodic function since it is the derivative of a periodic function. Its trigonometric coefficients ($\tilde{S}_1$, $\tilde{C}_1$, etc.) are related to the torque function coefficients as shown. That is,

$$\tilde{S}_n = -\omega n C_n \qquad \text{(D.1-1)}$$

$$\tilde{C}_n = \omega n S_n \qquad \text{(D.1-2)}$$

We can conveniently apply classical Fourier analysis to the derivative function. Thus, looking at one test motion cycle, lasting time, $T = 2\pi/\omega$, we can write:

$$\tilde{S}_n = \frac{2}{T}\int_0^T \dot{M}(t)\sin n\omega t\, dt = \frac{\omega}{\pi}\int_0^T \dot{M}(t)\sin n\omega t\, dt \qquad \text{(D.1-3)}$$

$$\tilde{C}_n = \frac{2}{T}\int_0^T \dot{M}(t)\cos n\omega t\, dt = \frac{\omega}{\pi}\int_0^T \dot{M}(t)\sin n\omega t\, dt \qquad \text{(D.1-4)}$$

A single square pulse, starting at time t_i, lasting one pulse width, h, and of magnitude M_i has the form sketched below.

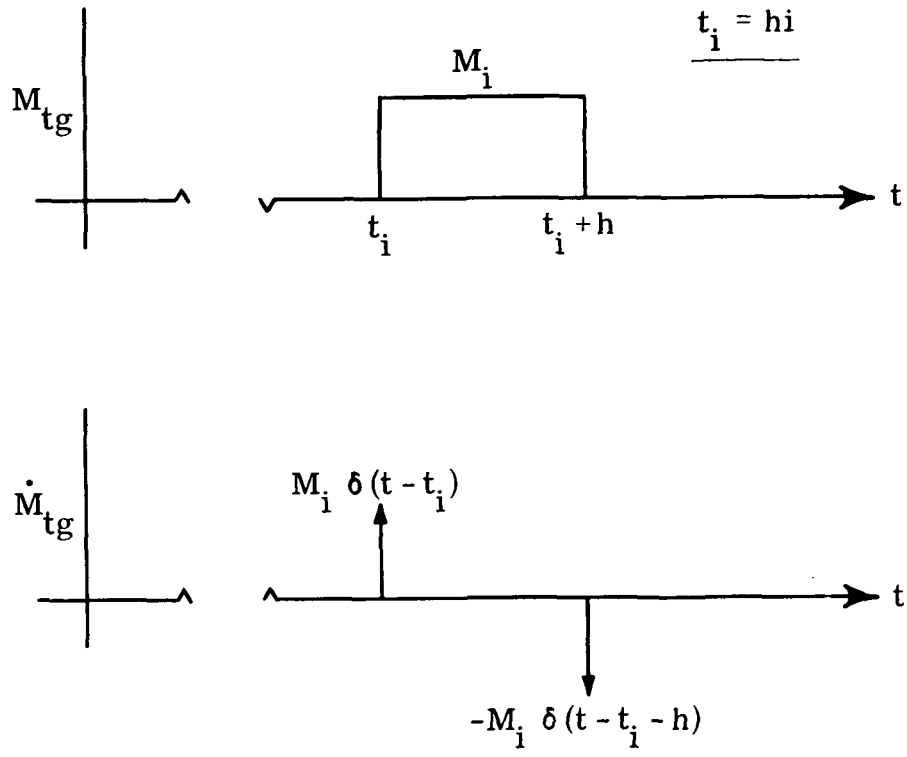

The derivative function consists of equal magnitude positive and negative impulse functions spaced h seconds apart. The contribution of these two impulses to the integral of Eq. (D.1-3) is:

$$\Delta\tilde{S}_{n_i} = \frac{\omega}{\pi}\left[\sin n\omega t_i - \sin n\omega (t_i + h)\right]$$

$$= \frac{\omega}{\pi}\left[\sin n\omega h_i - \sin n\omega h\,(i+1)\right] \qquad \text{(D.1-5)}$$

Note that M_i can take on either of two levels for binary torquing and any of three levels for ternary torquing, according to:

$$M_i = \begin{cases} M \text{ for a positive pulse} \\ 0 \text{ for zero torque} \\ -M \text{ for a negative pulse} \end{cases}$$

Adding up contributions like that of Eq. (D.1-5) over one full cycle of k pulse eidths, where k = T/h, we obtain:

$$\tilde{S}_n = \frac{\omega}{\pi} \sum_{i=0}^{k-1} M_i \left[\sin n\omega hi - \sin n\omega h (i+1) \right] \qquad \text{(D.1-6)}$$

Now, using the identity:

$$\sin(\alpha + \beta) = \sin\alpha \cos\beta + \cos\alpha \sin\beta \qquad \text{(D.1-7)}$$

we obtain:

$$S_n = \frac{\omega}{\pi} \sum_{i=0}^{k-1} M_i \left[(1 - \cos n\omega h) \sin n\omega hi - \sin n\omega h \cos n\omega hi \right] \qquad \text{(D.1-8)}$$

Averaging over m full cycles, or km pulse widths, we obtain:

$$S_n = \frac{1}{m} \frac{\omega}{\pi} \sum_{i=0}^{mk-1} M_i \left[(1 - \cos n\omega h) \sin n\omega hi - \sin n\omega h \cos n\omega hi \right] \qquad \text{(D.1-9)}$$

Similarly:

$$\tilde{C}_n = \frac{1}{m}\frac{\omega}{\pi}\int_0^T \dot{M}(t)\cos n\omega t\, dt$$

$$= \frac{1}{m}\frac{\omega}{\pi}\sum_{i=0}^{km-1} M_i\left[\cos n\omega hi - \cos n\omega h\,(i+1)\right]$$

$$= \frac{1}{m}\frac{\omega}{\pi}\sum_{i=0}^{km-1} M_i\left[(1-\cos n\omega h)\cos n\omega hi + \sin n\omega h \sin n\omega hi\right] \qquad \text{(D.1-10)}$$

where we have used the identity:

$$\cos(\alpha+\beta) = \cos\alpha\cos\beta - \sin\alpha\sin\beta \qquad \text{(D.1-11)}$$

Substituting Eqs. (D.1-9) and (D.1-10) into Eqs. (D.1-1) and (D.1-2) we obtain, finally:

$$S_n = \frac{1}{mn\pi}\sum_{i=0}^{km-1} M_i\left[(1-\cos n\omega h)\cos n\omega hi + \sin n\omega h \sin n\omega hi\right] \qquad \text{(D.1-12)}$$

$$C_n = \frac{1}{mn\pi}\sum_{i=0}^{km-1} M_i\left[(1-\cos n\omega h)\sin n\omega hi - \sin n\omega h \cos n\omega hi\right] \qquad \text{(D.1-13)}$$

Equations (D.1-12) and (D.1-13) are exact expressions for the Fourier coefficients defining the periodic function, $M_{tg}(t)$. These expressions are summations, rather than integrals, because we have chosen to work with the derivative signal, $\dot{M}_{tg}(t)$, which is a sequence of Dirac delta functions. The "input" data consist of the sequence of binary or ternary numbers, M_i, which represent the time history of the sensor rebalance pulses.

D.2 TIME MODULATION TORQUING

In the time modulation scheme (Ref. 2) the torque level switches between +M and -M, just as in the binary scheme, but the pulse widths are varied, as shown in the sketch below.

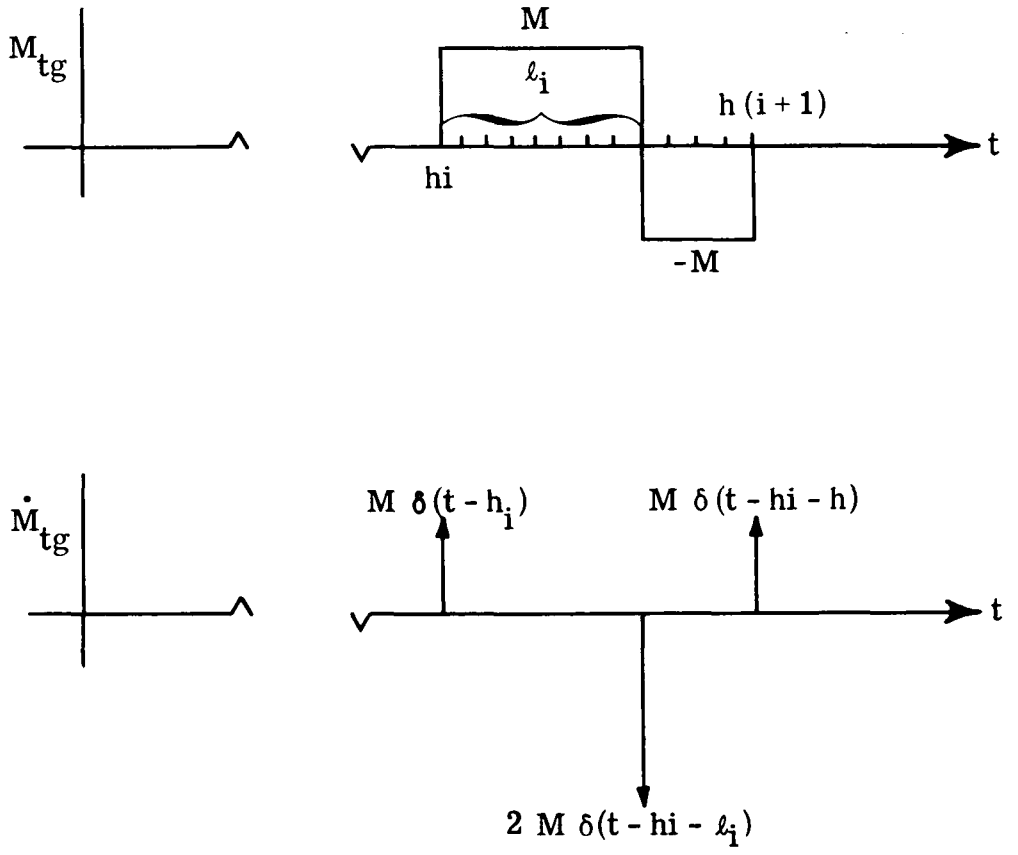

Each time interval of width h is divided between a positive pulse and a following negative pulse. The switch from positive to negative takes place at one of a number of discrete points in the interval. In the i^{th} increment [between t = ih and t = (i+1)h] the switching time is $t = ih + \ell_i$. The net torque is positive if $\ell_i > h/2$.

The contribution of the combined positive and negative pulses during the i^{th} interval to the integral of Eq. (D.1-3) is:

$$\Delta\tilde{S}_n = \frac{\omega}{\pi} M \left[\sin n\omega hi - 2\sin(n\omega hi + n\omega\ell_i) + \sin(n\omega hi + n\omega h)\right] \tag{D.2-1}$$

Adding up contributions like that of Eq. (D.2-1) over m full cycles, or km intervals of width h, we obtain:

$$\tilde{S}_n = \frac{1}{m}\frac{\omega}{\pi} M \sum_{i=0}^{mk-1} \left[\sin n\omega hi - 2\sin(n\omega hi + n\omega\ell_i) + \sin(n\omega hi + n\omega h)\right] \tag{D.2-2}$$

Using the identity given as Eq. (D.1-7) and the fact that, over an integral number of cycles, m:

$$\sum_{i=0}^{mk-1} \sin n\omega hi = 0 \tag{D.2-3}$$

we obtain:

$$\tilde{S}_n = \frac{1}{m}\frac{\omega}{\pi} M \sum_{i=0}^{mk-1} \left[-2\sin n\omega hi \cos n\omega\ell_i - 2\cos n\omega hi \sin n\omega\ell_i + \sin n\omega hi \cos n\omega h + \cos n\omega hi \sin n\omega h\right] \tag{D.2-4}$$

Similarly,

$$\tilde{C}_n = \frac{1}{m}\frac{\omega}{\pi} M \sum_{i=0}^{km-1} \Big[\cos n\omega hi - 2\cos(n\omega hi + n\omega \ell_i) + \cos(n\omega hi + n\omega h \Big]$$

$$= \frac{1}{m}\frac{\omega}{\pi} M \sum_{i=0}^{km-1} \Big[-2\cos n\omega hi \cos n\omega \ell_i + 2\sin n\omega hi \sin n\omega \ell_i + \cos n\omega h_i \cos n\omega h - \sin n\omega hi \sin n\omega h \Big] \qquad \text{(D.2-5)}$$

where we have used the identity given as Eq. (D.1-11).

Substituting Eqs. (D.2-4) and (D.2-5) into Eqs. (D.1-1) and (D.1-2) we obtain, finally:

$$S_n = \frac{M}{mn\pi} \sum_{i=0}^{km-1} \Big[-(2\cos n\omega \ell_i - \cos n\omega h)\cos n\omega hi + (2\sin n\omega \ell_i - \sin n\omega h)\sin n\omega hi \Big] \qquad \text{(D.2-6)}$$

$$C_n = \frac{M}{mn\pi} \sum_{i=0}^{km-1} \Big[(2\cos n\omega \ell_i - \cos n\omega h)\sin n\omega hi + (2\sin n\omega \ell_i - \sin n\omega h)\cos n\omega hi \Big] \qquad \text{(D.2-7)}$$

Equations (D.2-6) and (D.2-7) are exact expressions for the Fourier coefficients defining the periodic rebalance torque when time modulation torquing is used. The input data in this case is the sequence of values, ℓ_i, which represent the widths of successive positive pulses.

APPENDIX E

SURVEY OF STRAPDOWN SENSOR TEST METHODS, 1968

At the commencement of the study reported in this document a survey of contemporary strapdown sensor testing and test equipment was performed. The survey was limited to procedures for determining motion-induced errors in inertial instruments with emphasis on those produced by the angular vibration environment peculiar to strapdown inertial systems. Six facilities – The M.I.T. Instrumentation Laboratory, Cambridge, Massachusetts; TRW Systems, Redondo Beach, California; The Central Inertial Guidance Test Facility, Holloman AFB, New Mexico; The Naval Weapons Center, China Lake, California; Hamilton Standard Systems Center, Farmington, Connecticut; and Honeywell, Inc., Minneapolis, Minnesota – were visited. In addition, Army Missile Command, Huntsville, Alabama and Honeywell, Inc., St. Petersburg, Florida were contacted but visits were not made because no dynamic strapdown test work was being conducted at either of these facilities.

During each visit information was obtained concerning the test equipment available, the error models and data processing employed and tests performed at that particular facility. Attention was also given to the manner in which the actual motion experienced by the test items was determined. No attempt is made here to list the detailed capabilities of each laboratory. Rather, a set of general observations and highlights of the combined test capability of the installations visited are provided.

Angular Vibration Test Equipment — Machinery for subjecting instruments to angular vibrations was available at each of the facilities visited. However, there was a wide variation in the capabilities of different laboratories. The Central Inertial Guidance Test Facility (CIGTF) and the Instrumentation Laboratory were the only two installations capable of providing accurate out-of-phase angular vibrations about a pair of essentially orthogonal axes. The machinery used in both laboratories is essentially identical. The two-axis vibrators are limited to frequencies below about 100 Hz and neither appears capable of testing entire sensor packages of contemporary size and weight.

Both CIGTF and the Hamilton Standard Systems Center (HSSC) had single axis angular vibration machinery capable of applying sinusoidal angular oscillations up to about 1000 Hz to individual sensors. Again, essentially the same device – a torsion table driven by a linear shaker – was found in both locations. The CIGTF, which had been using this device for high frequency testing claimed to have observed bad resonances in the table structure at frequencies above 600 Hz. HSSC had made use of this equipment to study sensor dynamic errors under random angular vibration conditions. TRW Systems' test laboratory has a large angular vibration machine capable of producing single axis oscillations at frequencies up to 2000 Hz with a 500 lb test specimen. However, this device is not capable of the precision inherent in most inertial test machinery.

Most facilities surveyed contained single axis rate tables which could be driven by oscillatory signals to provide a single axis angular vibration testing capability in the frequency range of 100 Hz or less.

Linear Vibration Test Equipment — The best linear vibration capabilities belonged to Honeywell and M.I.T. Both have precision slip tables capable of oscillations in the frequency range of up to 3000 Hz with maximum force of 8,000 – 10,000 lb and displacements up to 1 inch double amplitude. No capability for providing out-of-phase linear vibration along two axes existed in any of the facilities visited.

Test Data Processing – HSSC has a capability for recording the output of a sensor undergoing dynamic testing. About 100 sec of data could be taken this way. In view of the emphasis on recovering harmonic signals during vibration testing which exists in this report, no facility had a satisfactory ability to recover all error parameters from single-axis angular vibration tests.

Both CIGTF and HSSC had a capability for performing spectral density analyses on the applied test motions. In the case of the former facility this was used in conjunction with sinusoidal motion tests on the two-axis angular vibrator while Hamilton Standard performed density analyses to confirm the distribution of random angular rates applied by the single-axis rotary table.

With the exception noted above, all closed loop sensor tests are performed by feeding the instrument output into an up-down counter and only the net pulse count for the duration of the test is available.

Summary — None of the installations visited had either a two-axis vibrator capable of oscillations in the frequency range up to 500 Hz or a capability of recording sensor loop outputs directly while conducting single-axis vibration tests. For this reason, the testing of strapdown sensors for dynamic errors, including those introduced by the rebalance electronics, appears to be in a state of flux. Consequently, the conclusions and recommendations of the study described in part by this document will have a particular impact on the makeup of future inertial sensor test laboratories.

APPENDIX F

ANALYSIS OF OSCILLATIONS IN TERNARY AND BINARY REBALANCE LOOPS

This appendix develops an analysis of the oscillatory behavior of ternary (the nonlinear element is a three-level switch) and binary (the nonlinear element is a two-level switch) rebalance loops. Both are shown to exhibit characteristic frequencies and amplitudes of float angle oscillations which are input-dependent. In the ternary case the frequency of oscillation varies considerably for input rates which are either small (near zero) or large $\left(\text{near } \omega_{i_{max}}\right)$, while it is relatively insensitive for two ranges of input rate centered at $\pm$ 0.5 $\omega_{i_{max}}$. In the binary case the frequency varies considerably for large inputs, while there is a broad insensitive region centered at zero. The characteristic behavior in the insensitive regions is accurately predicted by describing function analysis. The usefulness of the analysis presented below is that it describes the variations in the regions where describing function theory does not apply.

Strictly speaking the following development predicts the response to constant inputs only. The results are felt to be valid, however, for low frequency inputs (when the test motion frequency is low compared to the float angle oscillatory frequency) as well. In fact, the previously published simulation result, which exhibits good agreement with prediction based on this analysis (see Fig. F.1-5), corresponds to a low frequency sinusoidal input.

F.1 ANALYSIS OF OSCILLATIONS IN THE TERNARY LOOP

F.1.1 Problem Formulation

The ternary rebalance loop is represented in block diagram form in Fig. F.1-1. The analysis described below is based on an approximate mathematical model of this loop which includes the following three elements:

- The float dynamics are modeled by a differential equation which corresponds exactly to the transfer function shown in the figure.
- The nonlinear element is modeled exactly as the three-level switch shown; this is a "static nonlinearity" which does not shift the phase of oscillatory signals passing through it.
- The effects of the sampler and the torque generator dynamics are modeled approximately by introducing a fixed "torque switching delay," T_D. That is, for each time the nonlinearity output switches from one level to another, T_D seconds later the torquer output undergoes a corresponding step change.

For a constant, positive input torque, M_a, the resulting dynamic behavior of the loop is described by a sequence of float angle trajectory segments, as illustrated in Fig. F.1-2. These segments are produced by a sequence of alternating constant forcing functions, M_{o_1}, M_{o_2}, M_{o_1}, M_{o_2}, M_{o_1}, etc. where:

$$M_{o_1} = M_a \qquad \text{(F.1-1)}$$

$$M_{o_2} = -M_{t_g} + M_a \qquad \text{(F.1-2)}$$

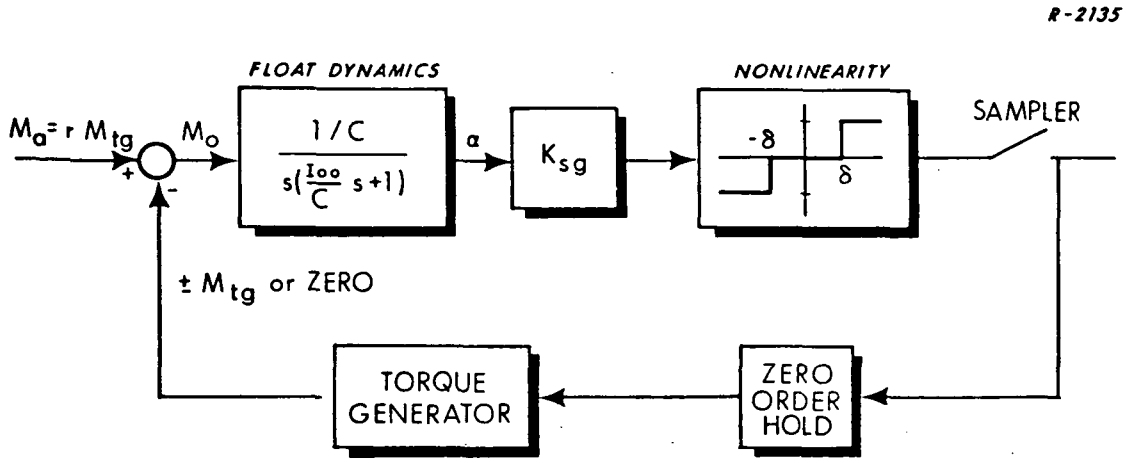

Figure F.1-1 Ternary Rebalance Loop

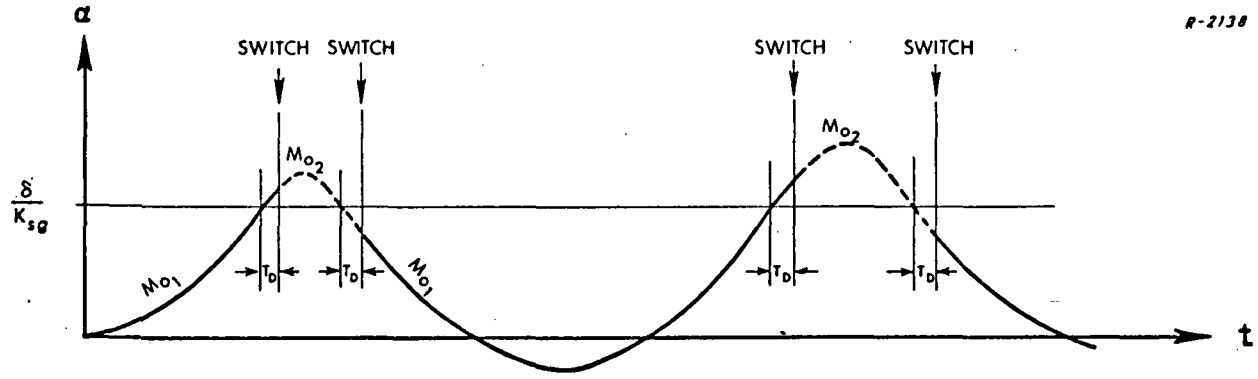

Figure F.1-2 Float Angle Time History Segments

M_{o_1} is a positive torque level, rM_{tg}, and M_{o_2}, is a negative torque level, $-(1-r)M_{tg}$ where r is the ratio of input torque to torquer capacity:

$$r = \frac{M_a}{M_{tg}}; \qquad 0 \leq r \leq 1 \qquad \text{(F.1-3)}$$

(For a negative value of M_a, r lies between zero and minus one and the resulting trajectory segments are a mirror image of those illustrated in Fig. F.1-2.)

The major dynamic element in the loop, the float, is described by the following differential equation:

$$M_{o_i} - C\,\dot{\alpha} = I_{oo}\,\ddot{\alpha} \qquad (i = 1,2) \qquad \text{(F.1-4)}$$

which can be written:

$$\ddot{\alpha} + \frac{C}{I_{oo}}\,\dot{\alpha} = \frac{M_{o_i}}{I_{oo}} \qquad \text{(F.1-5)}$$

or, equivalently:

$$\ddot{\alpha} + \frac{1}{\tau_f}\,\dot{\alpha} = m_i\,G \qquad \text{(F.1-6)}$$

where:

$$\tau_f = I_{oo}/C \qquad \text{(F.1-7)}$$

$$G = M_{tg}/I_{oo} = H\,\omega_{i_{max}}/I_{oo} \qquad \text{(F.1-8)}$$

$$m_1 = r \qquad \text{(F.1-9)}$$

$$m_2 = -(1-r) \qquad \text{(F.1-10)}$$

The shape of the trajectory segments shown in Fig. F.1-2 are determined by solutions to Eq. (F.1-6) for constant values of the forcing functions, $m_1 G$ and $m_2 G$.

Another assumption not explicitly mentioned above is that no "wrong-way" pulses occur. That is, when the input torque is positive,

the rebalance torque level switches between zero and $+M_{tg}$; when the input torque is negative, the rebalance torque switches between zero and $-M_{tg}$.

F.1.2 General Solution and Normalization

The general solution to Eq. (F.1-6) clearly has the following form:

$$\alpha(t) = a + bt + c\,e^{-t/\tau_f} \qquad \text{(F.1-11)}$$

$$\dot{\alpha}(t) = b - \frac{c}{\tau_f}\,e^{-t/\tau_f} \qquad \text{(F.1-12)}$$

$$\ddot{\alpha}(t) = \frac{c}{\tau_f^2}\,e^{-t/\tau_f} \qquad \text{(F.1-13)}$$

The initial conditions must satisfy:

$$\alpha(o) = \alpha_o = a + c \qquad \text{(F.1-14)}$$

$$\dot{\alpha}_o = b - \frac{c}{\tau_f} \qquad \text{(F.1-15)}$$

$$\ddot{\alpha}_o = \frac{c}{\tau_f^2} \qquad \text{(F.1-16)}$$

Substitution of these expressions into Eq. (F.1-6) yields:

$$\frac{c}{\tau_f^2} + \frac{b}{\tau_f} - \frac{c}{\tau_f^2} = m_i\,G \qquad \text{(F.1-17)}$$

Therefore:

$$b = m_i G \tau_f \tag{F.1-18}$$

$$c = \tau_f \left(b - \dot{\alpha}_o\right)$$

$$= m_i G \tau_f^2 - \tau_f \dot{\alpha}_o \tag{F.1-19}$$

$$a = \alpha_o - c$$

$$= \alpha_o + \tau_f \dot{\alpha}_o - m_i G \tau_f^2 \tag{F.1-20}$$

and the general solutions for α and $\dot{\alpha}$ become:

$$\alpha = \left(\alpha_o + \tau_f \dot{\alpha}_o - m_i G \tau_f^2\right) + \left(m_i G \tau_f\right) t + \left(m_i G \tau_f - \tau_f \dot{\alpha}_o\right) e^{-t/\tau_f} \tag{F.1-21}$$

$$\dot{\alpha} = \left(m_i G \tau_f\right) - \left(m_i G \tau_f - \dot{\alpha}_o\right) e^{-t/\tau_f} \tag{F.1-22}$$

An alternative pair of expressions, which display separately the contribution of each initial condition and the forcing function, are:

$$\alpha = \alpha_o + \dot{\alpha}_o \left[\tau_f \left(1 - e^{-t/\tau_f}\right)\right] + m_i G \left[\tau_f t - \tau_f^2 \left(1 - e^{-t/\tau_f}\right)\right] \tag{F.1-23}$$

$$\dot{\alpha} = \dot{\alpha}_o \left[e^{-t/\tau_f}\right] + m_i G \left[\tau_f \left(1 - e^{-t/\tau_f}\right)\right] \tag{F.1-24}$$

We now convert these solutions to a normalized form which will be used in the following sections by defining

$$s \triangleq t/\tau_f, \text{ normalized time}$$

$$x \triangleq \alpha/G\tau_f^2, \text{ normalized float angle}$$

$$x' \triangleq dx/ds, \text{ normalized float angle rate}$$

Therefore, we can write:

$$t = \tau_f s \tag{F.1-25}$$

$$\alpha = G\tau_f^2 x \tag{F.1-26}$$

$$\dot{\alpha} = G\tau_f^2 \dot{x} = G\tau_f x' \tag{F.1-27}$$

Substitution of Eqs. (F.1-25), (F.1-26) and (F.1-27) into Eqs. (F.1-23) and (F.1-24) and division by $G\tau_f^2$ and $G\tau_f$, respectively, yields:

$$x = x_o + x_o'\left(1 - e^{-s}\right) + m_i\left[s - \left(1 - e^{-s}\right)\right] \tag{F.1-28}$$

$$x' = x_o' e^{-s} + m_i\left(1 - e^{-s}\right) \tag{F.1-29}$$

Eqs. (F.1-28) and (F.1-29) are the normalized general solutions describing non-dimensional trajectory segments, x(s), caused by non-dimensional forcing functions, m_i.

F.1.3 Characteristic Frequency and Amplitude

Derivation of Characteristic Frequency – We begin by deriving a relationship between the normalized input level, r, and the normalized period of oscillation, s_p, which is satisfied by a sequence of trajectory segments which periodically repeat themselves. We first define the following non-dimensional quantities:

$$\tilde{\delta} \triangleq \frac{\delta / K_{sg}}{G\tau_f^2}, \text{ normalized switch level}$$

$$\Delta \triangleq T_D/\tau_f, \text{ normalized time delay}$$

$$s_1 \triangleq T_1/\tau_f, \text{ normalized positive torque interval}$$

$$s_2 \triangleq T_2/\tau_f, \text{ normalized negative torque interval}$$

$$s_p \triangleq s_1 + s_2, \text{ normalized period of oscillation}$$

The periodicity conditions on which the analysis is based are indicated graphically by the three examples sketched in Fig. F.1-3. The main idea is that the magnitude and slope, x_1 and x_1', at time t_1 recur at time t_3. The essential conditions are:

$$x_1 = \tilde{\delta} + x_1' \Delta \qquad \text{(F.1-30)}$$

$$x_2 = \tilde{\delta} + x_2' \Delta \qquad \text{(F.1-31)}$$

$$x_3 = \tilde{\delta} + x_3' \Delta = x_1 \qquad \text{(F.1-32)}$$

$$x_3' = x_1' \qquad \text{(F.1-33)}$$

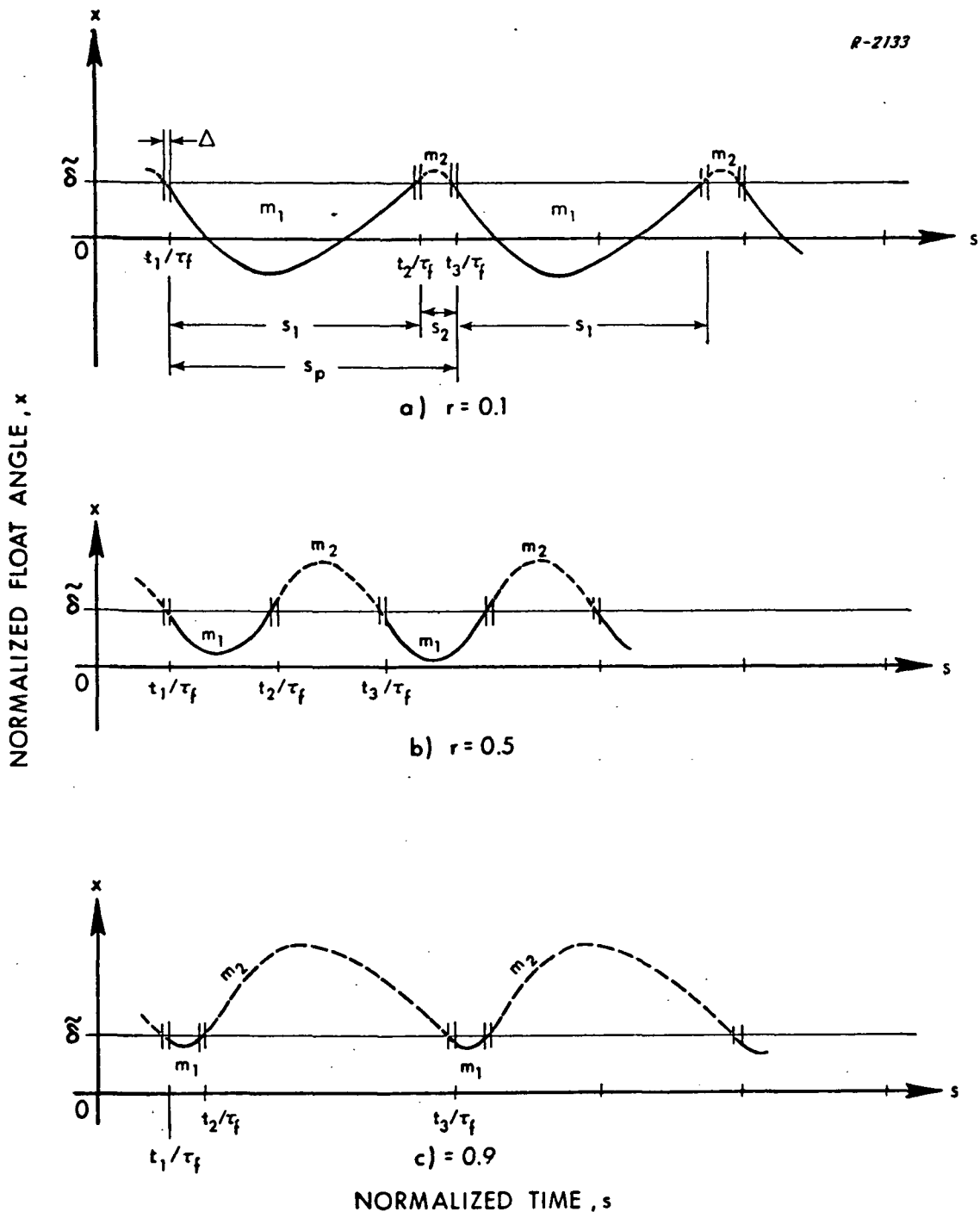

Figure F.1-3 Example Periodic Time Histories

The three cases pictured in Fig. F.1-3 illustrate some general features of the periodic solutions which are worth noting at this point in the development. In the example pictured at the top of the figure -- a small input case (r = 0.1) -- the positive-torque interval is longer than is the negative-torque interval. This makes sense physically since the magnitude of the net negative level, m_2, is larger than the positive level, m_1. (We recall that the positive net torque segment corresponds to zero rebalance torque; the negative net torque segment corresponds to full rebalance torque, $+M_{tg}$.) Just the opposite is true in the large input case (r = 0.9) pictured at the bottom of the figure. In the case shown in the middle (r = 0.5) the positive-torque and negative-torque intervals are equal and the total period is shorter than for the small and large input cases. These example trajectories are discussed again later when analytic results are compared with predictions based on describing function analysis.

Combining the general solutions given in Eqs. (F.1-28) and (F.1-29) with the periodicity conditions of Eqs. (F.1-30) through (F.1-33) the following four equations which characterize periodic solutions are obtained

$$\begin{aligned} x_2 - x_1 &= \tilde{\delta} + x_2'\Delta - \tilde{\delta} - x_1'\Delta \\ &= x_1'\left(1 - e^{-s_1}\right) + m_1\left[s_1 - \left(1 - e^{-s_1}\right)\right] \end{aligned} \qquad \text{(F.1-34a)}$$

$$\begin{aligned} x_1 - x_2 &= x_3 - x_2 \\ &= \tilde{\delta} + x_1'\Delta - \tilde{\delta} - x_2'\Delta \\ &= x_2'\left(1 - e^{-s_2}\right) + m_2\left[s_2 - \left(1 - e^{-s_2}\right)\right] \end{aligned} \qquad \text{(F.1-34b)}$$

$$x_2' = x_1' e^{-s_1} + m_1 \left(1 - e^{-s_1}\right) \qquad \text{(F.1-35a)}$$

$$x_1' = x_3'$$

$$= x_2' e^{-s_2} + m_2 \left(1 - e^{-s_2}\right) \qquad \text{(F.1-35b)}$$

The above four equations, along with Eqs. (F.1-9) and (F.1-10) are manipulated until x_1, x_2, x_1' and x_2' are eliminated and the desired relationship between r and s_p is produced. We start by rewriting Eqs. (F.1-34a) and (F.1-34b):

$$m_1 s_1 - \Delta\left(x_2' - x_1'\right) = \left(m_1 - x_1'\right)\left(1 - e^{-s_2}\right) \qquad \text{(F.1-36a)}$$

$$m_2 s_2 - \Delta\left(x_1' - x_2'\right) = \left(m_2 - x_2'\right)\left(1 - e^{-s_2}\right) \qquad \text{(F.1-36b)}$$

Next, Eqs. (F.1-35a) and (F.1-35b) are rewritten:

$$x_2' - x_1' = \left(m_1 - x_1'\right)\left(1 - e^{-s_1}\right) \qquad \text{(F.1-37a)}$$

$$x_1' - x_2' = \left(m_2 - x_2'\right)\left(1 - e^{-s_2}\right) \qquad \text{(F.1-37b)}$$

Comparison of Eqs. (F.1-36) and (F.1-37) yields:

$$x_2' - x_1' = m_1 s_1 - \Delta\left(x_2' - x_1'\right) \qquad \text{(F.1-38a)}$$

$$x_1' - x_2' = m_2 s_2 - \Delta\left(x_1' - x_2'\right) \qquad \text{(F.1-38b)}$$

Therefore:

$$x_2' = x_1' + \frac{m_1 s_1}{1+\Delta} \qquad \text{(F.1-39a)}$$

$$x_1' = x_2' + \frac{m_2 s_2}{1+\Delta} \qquad \text{(F.1-39b)}$$

When Eqs. (F.1-29a) and (F.1-39b) are added:

$$0 = m_1 s_1 + m_2 s_2 \qquad \text{(F.1-40)}$$

Substituting Eqs. (F.1-9) and (F.1-10):

$$r s_1 - (1 - r) s_2 = 0 \qquad \text{(F.1-41)}$$

This result agrees with physical reasoning -- the average torque applied to the float over each period should be zero. It also follows that:

$$s_1 = \left(\frac{1-r}{r}\right) s_2 = (1-r)\, s_p \qquad \text{(F.1-42)}$$

$$s_2 = \left(\frac{r}{1-r}\right) s_1 = r\, s_p \qquad \text{(F.1-43)}$$

From Eq. (F.1-39a) and (F.1-39b):

$$x_2' - x_1' = \frac{r(1-r)}{1+\Delta}\, s_p \qquad \text{(F.1-44)}$$

Substituting Eq. (F.1-44) into Eqs. (F.1-36):

$$x_1'\left(1 - e^{-s_1}\right) = \Delta\left[\frac{r(1-r)\,s_p}{1+\Delta}\right] - m_1\left[s_1 - \left(1 - e^{-s_1}\right)\right] \qquad \text{(F.1-45a)}$$

$$x_2'\left(1 - e^{-s_2}\right) = \Delta\left[\frac{-r(1-r)\,s_p}{1+\Delta}\right] - m_2\left[s_2 - \left(1 - e^{-s_2}\right)\right] \qquad \text{(F.1-45b)}$$

If we define:

$$E_1 \triangleq 1 - e^{-s_1}$$

$$E_2 \triangleq 1 - e^{-s_2}$$

Eqs. (F.1-45) can be written

$$x_1' = \frac{1}{E_1}\left[\Delta\,\frac{r(1-r)\,s_p}{1+\Delta} - r\left(s_1 - E_1\right)\right] \qquad \text{(F.1-46a)}$$

$$x_2' = \frac{1}{E_2}\left[\Delta\,\frac{-r(1-r)\,s_p}{1+\Delta} + (1-r)\left(s_2 - E_2\right)\right] \qquad \text{(F.1-46b)}$$

Substituting Eqs. (F.1-46) into Eq. (F.1-44):

$$\frac{r(1-r)\,s_p}{1+\Delta} = \frac{1}{E_2}\left[\Delta\,\frac{-r(1-r)\,s_p}{\Delta} + (1-r)\left(s_2 - E_2\right)\right] - \frac{1}{E_1}\left[\Delta\,\frac{r(1-r)\,s_p}{1+\Delta} - r\left(s_1 - E_2\right)\right] \qquad \text{(F.1-47)}$$

and

$$\frac{r(1-r)s_p}{1+\Delta}\left[1+\frac{\Delta}{E_2}+\frac{\Delta}{E_1}\right] = (1-r)\left(\frac{s_2-E_2}{E_2}\right) + r\left(\frac{s_1-E_1}{E_1}\right)$$

$$= (1-r)\frac{s_2}{E_2} - (1-\cancel{r}) + r\frac{s_1}{E_1} - \cancel{r} \qquad \text{(F.1-48)}$$

Dividing Eq. (F.1-48) by r and using Eqs. (F.1-42) and (F.1-43):

$$\frac{s_1}{1+\Delta}\left[1+\frac{\Delta}{E_2}+\frac{\Delta}{E_1}\right] = \frac{s_1}{E_2} - \frac{1}{r} + \frac{s_1}{E_1} \qquad \text{(F.1-49)}$$

giving

$$\frac{1}{r} = s_1\left\{\frac{1}{E_1}+\frac{1}{E_2} - \left[\frac{1+\Delta\left(\frac{1}{E_1}+\frac{1}{E_2}\right)}{1+\Delta}\right]\right\} \qquad \text{(F.1-50)}$$

which simplifies to:

$$\frac{1}{r} = \frac{s_1}{1+\Delta}\left[\frac{1}{E_1}+\frac{1}{E_2} - 1\right] \qquad \text{(F.1-51)}$$

Eq. (F.1-51) is easily shown to be equivalent to:

$$\frac{1}{r} = \frac{s_1}{1+\Delta}\left[\frac{E_p}{E_1 E_2}\right] \qquad \text{(F.1-52)}$$

where:

$$s_1 = (1 - r)\, s_p$$

$$s_2 = r\, s_p$$

$$E_1 = 1 - e^{-s_1}$$

$$E_2 = 1 - e^{-s_2}$$

$$E_p = 1 - e^{-s_p}$$

Eqs. (F.1-51) and (F.1-52) are equivalent forms of the desired relation between the normalized input r and the normalized period s_p. Solutions may be found by fixing r and Δ (normalized delay time), then trying values of s_p until the right hand side is made equal to 1/r.

Proof of Uniqueness of Solution – We now consider the right hand side of Eq. (F.1-51) and show that the quantity $s_1 [1/E_1 + 1/E_2 - 1]$ is a monotonically increasing function of s_p with value 1/r at $s_p = 0$. Therefore, the introduction of the factor $1/1 + \Delta$ provides a unique solution at $s_p = \hat{s}_p$, as illustrated in Fig. F.1-4.

Define:

$$Q \triangleq \frac{s_1}{E_1} + \frac{s_1}{E_2} - s_1$$

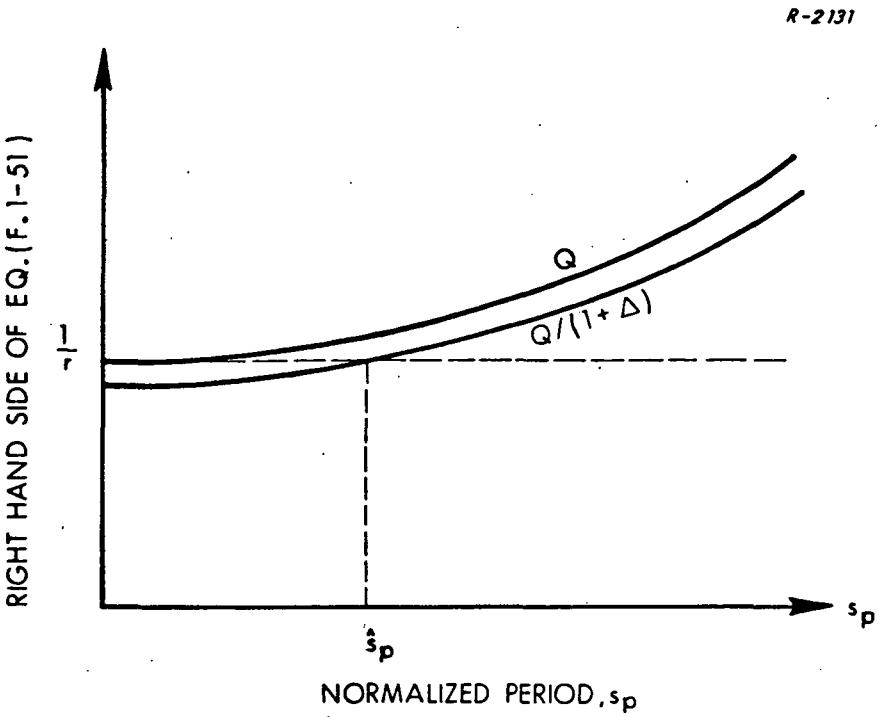

Figure F.1-4 Solution for Normalized Period

which is the right hand side of Eq. (F.1-51) when $\Delta = 0$. Clearly, the limit of:

$$\frac{s_1}{E_1} = \frac{s_1}{1 - e^{-s_1}}$$

equals one (using L'Hospital's Rule) as s_1 tends to zero. Similarly, the limit of:

$$\frac{s_1}{E_2} = \frac{s_1}{1 - e^{-\left(\frac{r}{1-r}\right) s_1}}$$

equals $(1 - r)/r$ as s_1 tends to zero. Therefore:

$$\lim_{s_1 \to 0} Q = 1 + \frac{1 - r}{r} - 0 = \frac{1}{r}$$

This concludes the first part of the proof.

To prove that Q increases monotonically consider its derivative:

$$Q' = \frac{dQ}{ds_1} = \frac{\left(1 - e^{-s_1}\right) - s_1 e^{-s_1}}{\left(1 - e^{-s_1}\right)^2} + \frac{\left(1 - e^{-\left(\frac{r}{1-r}\right)s_1}\right) - s_1 \left(\frac{r}{1-r}\right) e^{-\left(\frac{r}{1-r}\right)s_1}}{\left(1 - e^{-\left(\frac{r}{1-r}\right)s_1}\right)^2} - 1 \qquad \text{(F.1-53)}$$

Q' is clearly positive for any s_1 if:

$$\frac{1 - e^{-x} - x e^{-x}}{\left(1 - e^{-x}\right)^2} \geq \frac{1}{2} \text{ (for any x)} \qquad \text{(F.1-54)}$$

Let:

$$R = \frac{1 - e^{-x} - xe^{-x}}{\left(1 - e^{-x}\right)^2}$$

$$= \frac{1 - e^{-x} - xe^{-x}}{1 - 2e^{-x} + e^{-2x}}$$

$$= \frac{1 - e^{-x} - xe^{-x}}{2 - 2e^{-x} - 2xe^{-x} - 1 + 2xe^{-x} + e^{-2x}}$$

$$= \frac{\alpha}{2\alpha - \beta} \qquad \text{(F.1-55)}$$

where:

$$\beta = 1 - 2xe^{-x} - e^{-2x} \qquad \text{(F.1-56)}$$

We note that $\beta = 0$ when $x = 0$. Furthermore:

$$\frac{d\beta}{dx} = 2xe^{-x} - 2e^{-x} + 2e^{-2x}$$

$$= \left[2e^{-x}\right]\left[x - 1 - e^{-x}\right] \qquad \text{(F.1-57)}$$

Both factors on the right hand side of Eq. (F.1-57) are positive. Therefore:

$$\beta \geq 0$$

$$R \geq 1/2$$

$$Q' \geq 0$$

and Q is monotonically increasing. This concludes the proof that Eq. (F.1-51) or (F.1-52) has a unique non-trivial solution for any non-zero values of r and Δ. Thus, there is one and only one oscillation period which satisfies the periodicity conditions for a given input level and switching delay.

Comparison with Describing Function Analysis – A family of solutions to Eq. (F.1-52) are plotted in Fig. F.1-5. Note that the curves are symmetrical about the mid-line, r = 0.5, and also exhibit minima (maximum frequencies of oscillation) at this point. This behavior was illustrated in the example float angle histories pictured in Fig. F.1-3. Note also that the curves are quite flat across a relatively wide mid-region, and that the period of oscillation appears to be proportional to the square root of Δ. Inspection of the family of curves leads to the following empirical formula, which is approximately correct in this mid-region:

$$P/\tau_f \cong 7.0\sqrt{\Delta} = 7.0\sqrt{T_D/\tau_f} \qquad \text{(F.1-58)}$$

Therefore:

$$P \cong 7.0\sqrt{\tau_f T_D} \qquad \text{(F.1-59)}$$

We now compare Eq. (F.1-59) with a result obtained using describing function analysis. The following formula for a limit cycle frequency of oscillation in a binary or ternary rebalance loop was derived in Ref. 2.

$$\omega_\ell = \sqrt{\frac{1}{\tau_f \tau_{tg}}} \qquad \text{(F.1-60)}$$

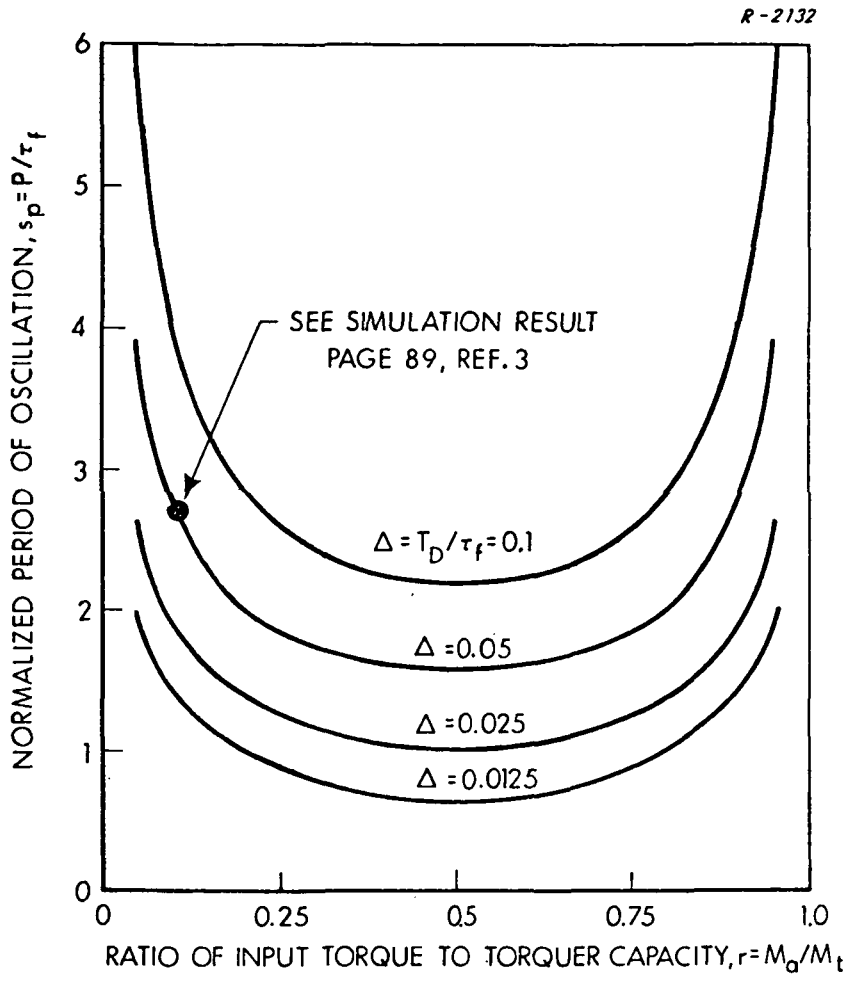

Figure F.1-5 Normalized Period Versus Normalized Input

This is the frequency at which the two linear loop elements cause a combined phase lag of π radians. The corresponding period of oscillation is:

$$P_\ell = 2\pi \sqrt{\tau_f \tau_{tg}} \qquad \text{(F.1-61)}$$

Eqs. (F.1-59) and (F.1-61) are nearly identical if the torque switching delay of the present model is equated with the torque generator time constant, τ_{tg}. Note the point corresponding to $\Delta = 0.05$ and $r = 0.1$

circled in Fig. F.1-5. This point agrees very well with a simulated response time history previously published in Ref. 3. The analysis developed in this Appendix involves considerably more effort than describing function analysis, but it provides the ability to predict the variation in the oscillation period with input magnitude. Describing function analysis cannot predict this type of result accurately because the input to the nonlinearity is not very well represented by its fundamental component alone in the case of small or large inputs to a ternary loop.

Derivation of Characteristic Amplitude – The previous analysis can be extended in order to derive an expression for the peak-to-peak amplitude of oscillation in the float angle. This amplitude is the difference between the minimum float angle which occurs during the positive-torque segment, and the maximum float angle, which occurs during the negative torque segment. (Recall the assumption that the float angle does not go too far in the "wrong" direction; there are no "wrong-way pulses.")

The minimum float angle occurs at normalized time, s_{min}, when the normalized rate of change, as given by Eq. (F.1-29), equals zero. Thus:

$$x' = x_1' e^{-s_{min}} + m_1 \left(1 - e^{-s_{min}}\right) = 0 \qquad \text{(F.1-62)}$$

Therefore

$$e^{-s_{min}} = \frac{m_1}{m_1 - x_1'} \qquad \text{(F.1-63)}$$

and

$$s_{min} = \ell n \left(1 - x_1'/m_1\right) \qquad \text{(F.1-64)}$$

Substitution of Eqs. (F.1-63), (F.1-64) and (F.1-30) into Eq. (F.1-28) yields:

$$x_{min} = \tilde{\delta} + x_1' \left[\Delta + \frac{1}{1 - m_1/x_1'}\right] + m_1 \left[\ell n \left(1 - x_1'/m_1\right) - \frac{1}{1 - m_1/x_1'}\right] \qquad \text{(F.1-65)}$$

Similarly

$$s_{max} = \ell n \left(1 - x_2'/m_2\right) \qquad \text{(F.1-66)}$$

and:

$$x_{max} = \tilde{\delta} + x_2' \left[\Delta + \frac{1}{\left(1 - m_2/x_2'\right)}\right] + m_2 \left[\ell n \left(1 - x_2'/m_2\right) - \frac{1}{\left(1 - m_2/x_2'\right)}\right] \qquad \text{(F.1-67)}$$

Recalling that $r = m_1$ and $-(1 - r) = m_2$, we can rewrite Eqs. (F.1-46) in the form:

$$\frac{x_1'}{m_1} = \frac{1}{E_1}\left[E_1 - s_1\left(1 - \frac{\Delta}{1+\Delta}\right)\right]$$

$$= 1 - \frac{s_1}{E_1(1+\Delta)} \qquad \text{(F.1-68a)}$$

$$\frac{x_2'}{m_2} = \frac{1}{E_2}\left[E_2 - s_2\left(1 - \frac{\Delta}{1+\Delta}\right)\right]$$

$$= 1 - \frac{s_2}{E_2(1+\Delta)} \qquad \text{(F.1-68b)}$$

Therefore:

$$x_1' = m_1\left(1 - w_1\right) = -r\left(w_1 - 1\right) \qquad \text{(F.1-69a)}$$

$$x_2' = m_2\left(1 - w_2\right) = (1 - r)\left(w_2 - 1\right) \qquad \text{(F.1-69b)}$$

where:

$$w_1 \triangleq \frac{s_1}{E_1(1+\Delta)}$$

$$w_2 \triangleq \frac{s_2}{E_2(1+\Delta)}$$

Also:

$$1 - x_1'/m_1 = 1 - \left(1 - w_1\right) = w_1 \qquad \text{(F.1-70a)}$$

$$1 - x_2'/m_2 = 1 - \left(1 - w_2\right) = w_2 \qquad \text{(F.1-70b)}$$

$$1 - m_1/x_1' = 1 - \frac{1}{1 - w_1} = \frac{1}{1 - 1/w_1} \qquad \text{(F.1-71a)}$$

$$1 - m_2/x_2' = 1 - \frac{1}{1 - w_2} = \frac{1}{1 - 1/w_2} \qquad \text{(F.1-71b)}$$

Now, using the above relations in Eqs. (F.1-65) and (F.1-67) we can write for the peak-to-peak amplitude:

$$\Delta x_{pp} = x_{max} - x_{min}$$

$$= \tilde{\delta} - (1-r)\left(1 - w_2\right)\left[\Delta + 1 - 1/w_2\right] - (1-r)\left[\ell n\, w_2 - \left(1 - 1/w_2\right)\right]$$

$$- \tilde{\delta} - r\left(1 - w_1\right)\left[\Delta + 1 - 1/w_1\right] - r\left[\ell n w_1 - \left(1 - 1/w_1\right)\right] \qquad (F.1\text{-}72)$$

Simplifying, we obtain:

$$\Delta x_{pp} = r\left[\left(w_1 - 1\right)\left(\Delta + 1 - 1/w_1\right) - \ell n\, w_1 + \left(1 - 1/w_1\right)\right]$$

$$+ (1-r)\left[\left(w_2 - 1\right)\left(\Delta + 1 - 1/w_2\right) - \ell_n w_2 + \left(1 - 1/w_2\right)\right] \qquad (F.1\text{-}73)$$

Solutions to Eq. (F.1-73) are plotted in Fig. F.1-6. These are based on combinations of r, Δ and s_1 (normalized input, time delay and positive torque interval) which were previously found to satisfy the periodicity condition, Eq. (F.1-52). The amplitude of oscillation appears to be insensitive to input magnitude, even in the small and large input regions where the frequency decreases markedly. Inspection of the curves leads to the following empirical formula:

$$\frac{\Delta\alpha_{pp}}{G\tau_f^2} \cong 1.45\,\Delta = 1.45\,\frac{T_D}{\tau_f} \qquad (F.1\text{-}74)$$

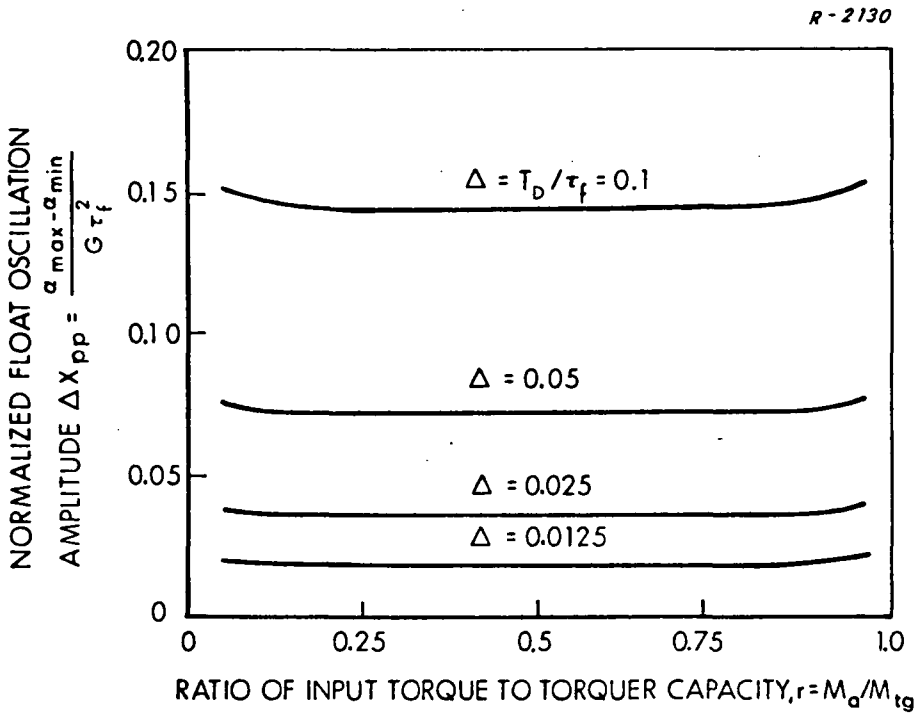

Figure F.1-6 Normalized Amplitude Versus Normalized Input

Therefore, the half amplitude is:

$$A_\alpha = \frac{\Delta\alpha_{pp}}{2} \cong .725 \frac{M_{tg}}{I_{oo}} \tau_f T_D$$

$$= .725 \frac{M_{tg}}{C} \frac{\tau_f T_D}{\tau_f} \qquad \text{(F.1-75)}$$

The result predicted by describing function analysis, for a ternary loop switching between zero and $+ M_{tg}$, is:

$$A_\alpha = \frac{2}{\pi} \frac{M_{tg}}{C} \frac{\tau_f \tau_{tg}}{(\tau_f + \tau_{tg})} \qquad \text{(F.1-76)}$$

The similarity between Eqs. (F.1-75) and (F.1-76) should be noted.

Summary – A convenient summary of all results for the ternary rebalance loop is given in Fig. F.1-7. In constructing this figure we have accepted the describing function results in the vicinity of $r = \pm 0.5$ and used the preceding analysis to treat inputs of large and small magnitudes.

R-2128

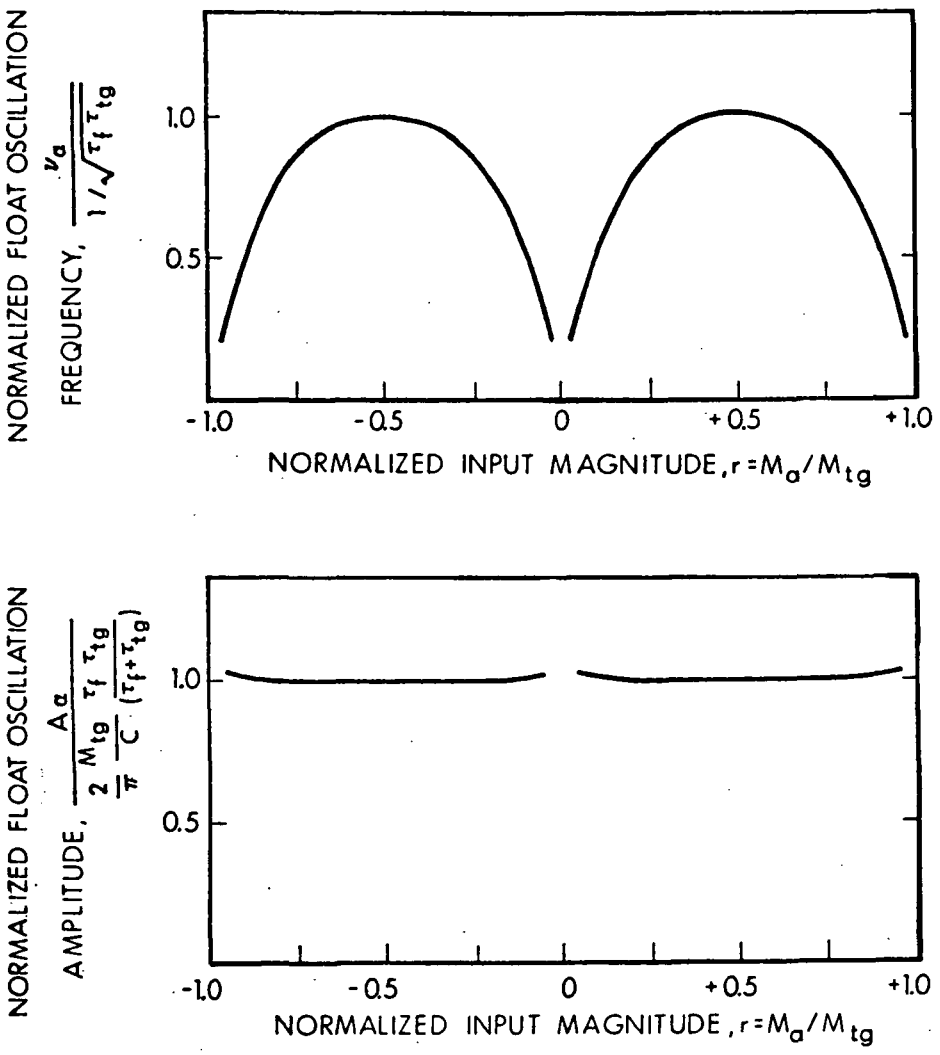

Figure F.1-7 Summary of Results - Ternary Loop

F.2 ANALYSIS OF OSCILLATIONS IN THE BINARY LOOP

The analysis of ternary loop oscillations presented in the preceding section may be applied directly to the binary loop. In this case the rebalance torque switches between $+M_{tg}$ and $-M_{tg}$ rather than $+M_{tg}$ and zero. Therefore, the positive and negative net torque values, respectively, are:

$$M_{o_1} = M_a + M_{t_g} \tag{F.2-1}$$

$$M_{o_2} = M_a - M_{tg} \tag{F.2-2}$$

After defining:

$$\tilde{r} \triangleq 0.5 + r/2$$

$$\tilde{G} \triangleq 2G = 2\,M_{tg}\,/I_{oo}$$

we can write:

$$m_1 = M_{o_1}\,/I_{oo} = \tilde{r}\,\tilde{G} \tag{F.2-3}$$

$$m_2 = M_{o_2}\,/I_{oo} = -(1-\tilde{r})\,\tilde{G} \tag{F.2-4}$$

The entire analysis then proceeds identically, except that $\tilde{r}$ and $\tilde{G}$ appear in place of r and G. The non-dimensional results plotted in Figs. F.1-5 and F.1-6 are also correct if the abscissa is labeled $\tilde{r}$ and the float angle excursion normalized by $\tilde{G}\,\tau_f^2$.

The describing function results for the binary gyro with no input (see Ref. 2) are:

$$\omega_{\ell} = 1/\sqrt{\tau_f \tau_{tg}} \qquad \text{(F.2-5)}$$

$$A_{\ell} = \frac{4}{\pi} \frac{M_{tg}}{C} \frac{\tau_f \tau_{tg}}{(\tau_f + \tau_{tg})} \qquad \text{(F.2-6)}$$

These, again, agree with the plotted results in the mid-region, centered around $\tilde{r} = 0.5$. However, the value $\tilde{r} = 0.5$ corresponds to $r = 0$. Therefore, describing function theory accurately predicts binary loop behavior in the region where the normalized input r is small. A convenient summary of all results for the binary rebalance loop is given in Fig. F.2-1. Comparison of Figs. F.1-7 and F.2-1 shows that the describing function technique is a good predictor of characteristic loop behavior for half-maximum inputs ($r \cong \pm 0.5$) for ternary loops and for small inputs ($r \cong 0$) for binary loops. Also, the factor-of-two difference in the amplitude normalizing quantities shows that, for the cases treated by this analysis, the float angle oscillation amplitude is twice as large for binary loops as for ternary loops.

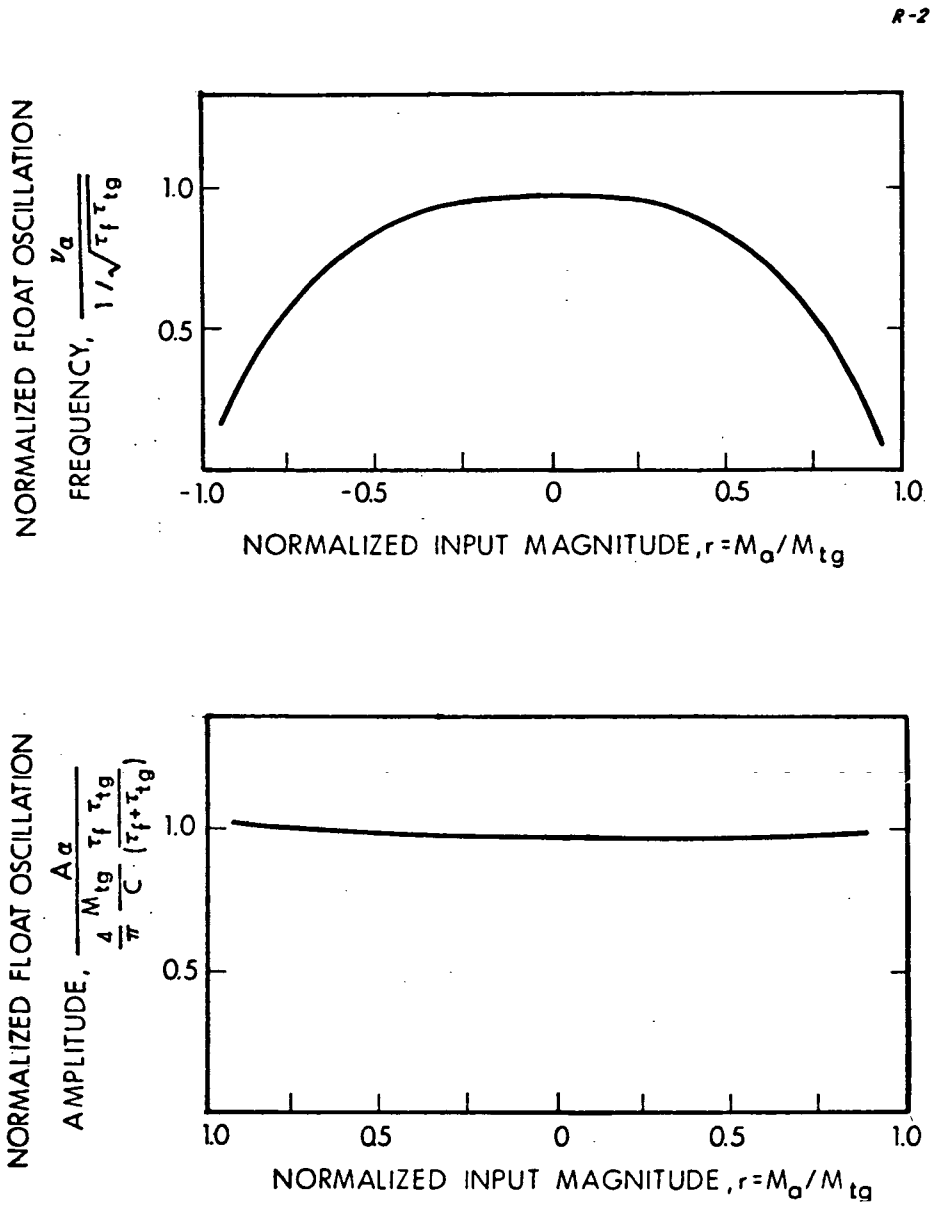

Figure F.2-1 Summary of Results - Binary Loop

Page Intentionally Left Blank

REFERENCES

1. Bumstead, R.M. and Vander Velde, W.E., "Navigation and Guidance Systems Employing a Gimballess IMU," AIAA Preprint No. 63-307, August 1963.

2. Gelb, Arthur, and Sutherland, Arthur A., Jr., "Design of Strapdown Gyroscopes for a Dynamic Environment," TR-101-2, 15 January 1968.

3. Sutherland, Arthur A., Jr., and Beebee, William S., "Design of Strapdown Gyroscopes for a Dynamic Environment," NASA CR-1396, August 1969 (Also TR-101-4, January 1969).

4. Wimber, B.J., "The Apparent Input Axis Misalignment Error Caused by Angular Rotation about the Output Axis of a Single-Degree-of-Freedom, Rate-Integrating Gyro, "Fourth Inertial Guidance Test Symposium Proceedings, MDC TR 68-76, November 1968.

5. Gelb, Arthur and Vander Velde, Wallace E., Multiple-Input Describing Functions and Nonlinear System Design, McGraw-Hill Book Co., August 1968.

6. Rauscher, M., Introduction to Aeronautical Dynamics, John Wiley & Sons, New York, 1953.

7. Gelb, Arthur and Sutherland, Arthur A., Jr., "Application of the Kalman Filter to Aided Inertial Systems," U.S. Naval Weapons Center, China Lake, California, NWC TP 4652, August 1968.

8. Bryson, A.E., and Ho, Y.C., Applied Optimal Control, Blaisdell Company, Waltham, Massachusetts, 1969.

9. Hildebrand, F.B., Advanced Calculus for Engineers, Prentice Hall, New York, 1948.

10. Crawford, B.S., "Strapdown Sensor Tests and Test Data Analysis," TR-147-1, 31 January 1970.

TASC